STUDY OF AN EVAPORATING DROPLET IN AN IMMISCIBLE LIQUID

by

MOHAMMAD-REZA MOKHTARZADEH-DEHGHAN,

B.Sc.(Eng.), M.Sc., D.I.C.

Thesis submitted for the degree of

Doctor of Philosophy

in the Faculty of Engineering of the

University of London

February 1980

Thermal Power Section,
Department of Mechanical Engineering,
Imperial College of Science & Technology,
London SW7 2BX.

ABSTRACT

The secondary refrigerant method of desalination by freezing can be achieved by the evaporation of dispersed droplets of an immiscible refrigerant liquid in direct contact with water. The present study is mainly concerned with an experimental and theoretical investigation into the evaporation of a single droplet in an immiscible liquid.

A theoretical model of the evaporation of a single droplet during its rise in a column of an immiscible liquid is presented. Governing equations are derived and then solved simultaneously applying a numerical method. Results are presented mainly for a butane/distilled water combination. The model is examined for different initial droplet sizes, temperature differences, initial velocities, initial temperatures and materials. Comparisons are made between the predicted and experimental results.

A test rig was designed and built for the experimental study. Butane was used as the dispersed phase and distilled water as the continuous phase. Butane droplets were injected from a submerged orifice at the bottom of the water column. The evaporating bubble-droplet was followed by a ciné camera which recorded its behaviour. Parameters such as growth, rise velocity and heat transfer coefficient are studied. The results are within the range of previous investigators' results.

A new type of experiment was carried out which led to the novel study on the dynamics of non-evaporating (stopped-evaporation) two-phase bubble-droplets. This was achieved by the sudden application of pressure on the surface of the water while the bubble-droplet was rising, which slowed down the evaporation considerably. The rise velocity of stopped-evaporation bubble-droplets are compared with those of evaporating droplets.

Computer programs were developed concerning the theoretical model and to process the experimental data.

An experimental method is presented by which the movement of bubbles is recorded using still photography. Data can be obtained such as path, velocity, indications of surface instabilities, variation of size like growth, and collapse. Results are presented for small and medium size rising air bubbles, spherical cap shape butane bubbles, evaporating butane droplets and condensing butane bubbles in distilled water.

To my Father, Mother, Brother and Sister

ACKNOWLEDGEMENTS

I wish to express my sincere gratitude to my supervisor, Dr A.A. El-Shirbini, for his kind encouragement, guidance and interest throughout the work.

I would like to thank the members of the Steam Laboratory, Messrs N. Wood and J. Martin, and also Mr D. Bloxham of the Engine Laboratory and Mr R. Church of the Fluid Mechanics Laboratory, for their help in setting up the experimental rig. Special thanks are also due to Mr B. King of the Heat Transfer Laboratory for his help whenever possible.

I am grateful to Mrs E. Hall for her excellent and conscientious work in typing the manuscript. Thanks are also extended to Miss E.M. Archer and Mrs S. Boote of the Mechanical Engineering Library for their help in providing the required references.

Finally, I would like to express my deepest gratitude and respect to my parents, who gave me much encouragement, supported me financially and showed great patience throughout the work.

CONTENTS

Note: All computer programs are available at the Imperial College of Science & Technology (Thermal Power Section), London University.

NOMENCLATURE

A	:	area; equivalent spherical area of bubble-droplet (m^2)
$ATMP$	:	atmospheric pressure (N/m^2)
C_D	:	drag coefficient
C_p	:	specific heat (J/kg^oK)
D	:	diameter; equivalent spherical diameter of bubble-droplet (m)
d	:	equivalent spherical diameter of initial droplet (m)
$\underline{e}$	:	unit vector
F	:	force (N/m^2)
f	:	number of bubbles per second
g	:	standard gravitational acceleration (m/s^2)
$\underline{g}$	:	standard gravitational acceleration vector (m/s^2)
h	:	instantaneous heat transfer coefficient ($J/sm^2{}^oK$)
h_{fg}	:	heat of vaporisation (J/kg)
H	:	water column height (m)
k	:	heat conductivity (J/sm^oK)
m	:	mass (kg)
m_{oo}	:	initial mass of droplet (kg)
P	:	vaporisation pressure of the dispersed phase (N/m^2)
$\overline{P}$	:	mean pressure (N/m^2)
$P_{s\infty}$	:	pressure far from the bubble-droplet (N/m^2)
P_c	:	continuous phase liquid pressure (N/m^2)
q	:	rate of heat transfer (J/s)
R	:	radius; equivalent spherical radius of bubble-droplet(m)
T	:	temperature; vaporisation temperature of the dispersed phase (^oC)
T_c	:	temperature of the continuous phase (^oC)
t'	:	time (s)

t : time (s); $t = t' - t''$

t'' : time related to $\xi = 0.005$ (s)

U : rise velocity (m/s)

v : velocity (m/s)

$\underline{v}$: velocity vector (m/s)

V : volume; bubble-droplet volume (m^3)

X : growth rate (m/s)

z : vertical axis

Z : height (m)

r, θ, ϕ : spherical coordinates

ΔT : temperature difference, $\Delta T = T_c - T$ (^oC)

ΔT_0 : overall temperature difference (^oC)

Δt : time between every consecutive shot (s)

Dimensionless Groups

Bo : Bond number, $Bo = (\rho_c - \rho_d)\ g d^2/\sigma$

$E\theta$: Eotvos number, $E\theta = (g D^2 (\rho_c - \rho_d))/\sigma$

Fr : Froude number, $Fr = U/(g\ D_b/2)^{0.5}$

M : dimensionless number, $M = (g\ \mu^4)/(\rho\ \sigma^3)$

Nu : Nusselt number, $Nu = (h\ D)/k$

Pe : Peclet number, $Pe = Re \times Pr$

Pe' : modified Peclet number, $Pe' = Pe/(1 + \mu_l/\mu_c)$

Pr : Prandtl number, $Pr = (\mu\ C_p)/k$

Re : Reynolds number, $Re = (\rho\ U\ D)/\mu$

Ja : Jakob number, $Ja = \rho_c\ C_{p_c}\ (T_\infty - T_{sat})/\rho_v\ h_{fg}$

Greek Letters

α : thermal diffusivity (m^2/s)

β : opening angle (degrees); chemical constant (Appendix C)

ξ : vaporisation ratio, $\xi = m_v/m_{oo}$

μ : viscosity (kg/ms)

ρ : density (kg/m^3)

τ : time period (s)

σ : surface tension; interfacial tension (N/m)

Φ : velocity potential

Subscripts

av : average

b : bubble

c : continuous phase

d : dispersed phase

e : equivalent spherical

i : index

l : dispersed phase liquid

o : overall

sat : saturation

v : vapour

∞ : at infinity

o : initial condition ($t = 0$)

oo : see m_{oo}

CHAPTER 1

INTRODUCTION

1.1 INTRODUCTION

Direct heat and mass transfer between two liquid phases, when one is dispersed into another, is utilised over a wide range of industrial applications. Direct contact heat exchangers have some advantages over the conventional metal to fluid heat exchangers. For example, higher heat transfer area per unit volume can be achieved. The dependence on volume rather than area permits smaller heat exchangers for large scale operations. Costs of maintenance are reduced due to the absence or reduction of fouling compositions on solid surfaces, and uniform driving forces are obtained. This kind of heat exchanger can be further improved if one liquid is evaporated in the other liquid. This makes use of large available heat capacity for heat absorption. In this case, latent heat rather than sensible heat is transferred between the two liquids. Thus, lower mass flow of the coolant can be achieved. Also, larger and more effective heat transfer areas are obtainable. The system can work in a very low temperature difference, as low as $1^{o}C$. Separation of the two liquids is very convenient, and a closed refrigeration cycle can be achieved by condensing the generated vapour. Heat transfer coefficients are higher by one or two orders of magnitude than the two-phase direct contact heat exchangers (75). These advantages apply in general to any pair of fluid systems requiring heat exchange, when a suitable immiscible transfer fluid for the specified case is chosen. Research on direct contact heat exchangers has been stimulated by their application in the process of desalination by freezing (28,80). Considerable research has been supported by the Office of Saline Water (now the Office of Water

Research and Technology) which was set up in the USA in 1952 for research and development in various fields of desalination.

The sea-or-brackish-water conversion processes can be divided into five basic classifications: distillation, membrane, freezing, humidification, and chemical. Freezing techniques have some advantages when compared with other processes. Thermodynamically, freezing appears to be a very economical means of desalting sea water because the latent heat of ice is 335 kJ/kg, whilst the latent heat of vaporisation amounts to 2326 kJ/kg. The process is more suitable for areas with cold sea water, and the low energy consumption potential is important in the areas with high fuel cost. Probably its greatest attraction is that of a pure electrical user, providing independence of siting and integration into a power/water demand pattern (60). Freezing processes escape from scale formation due to the low operating temperatures, which keep the solubility of scale-forming compounds to a minimum. Freezing processes utilise the fact that, when salt water is frozen, fresh water ice crystals are formed, while the salt remains in the unfrozen solution. Ice crystals have very regular and symmetrical structures which cannot accommodate foreign atoms or molecules without severe local strain, and thus salt and every other solute in the water will be rejected by the advancing surface of a growing ice crystal. One of the techniques of freezing processes is the Secondary Refrigerant Method, which utilises direct contact heat transfer between water and a low-boiling-point refrigerant. Pressure in the freezer unit can be adjusted in a way that the liquid refrigerant evaporates and, consequently, part of the water freezes. Ice crystals are collected and washed, and then melted to produce fresh water. For the economical competition with other processes, the freezing system must operate in a closed cycle, integrating the ice-making and ice-melting steps

since this leads to a lower fuel consumption. Low molecular weight hydrocarbons are convenient refrigerants from the point of view of availability, cost and solubility. Butane has been often suggested for this purpose. Butane is soluble to the extent of about 50 to 180 ppm (part per million) at low temperatures in distilled water and salt solutions (62). Butane stripping is then necessary to improve the taste and quality of water, and to recover its economic value. However, the freezing processes encounter some problems. For example, washing ice crystals by desalted water is needed because ice crystals tend to retain a comparatively large volume of the mother liquid in the interstices between the crystals. This is due to the viscous forces which help the brine to adhere to the surfaces of the ice crystals, while capillary forces help to hold it in the interstices. The growth of ice crystals has come under considerable research, since bigger ice crystals may provide more efficient washing methods.

Knowledge of the mechanism of the processes involved is essential for better designing of the freezer. However, the real situation in the freezer is very complicated to be investigated, especially theoretically. The reason is due to the existence of different phases, namely, refrigerant vapour, liquid water and liquid refrigerant, and solid water, while phase changes are taking place. These bring into play at one time problems such as heat and mass transfer, growth of ice crystals, and dynamics of evaporating droplets. Figure 1.1 (85) shows a view of the conditions in the freezer.

To obtain a better understanding of the phenomena involved, the approach has been mainly divided into two categories: the study of evaporating droplets in another immiscible liquid, and the study of the growth of ice crystals. The first category has been further divided into

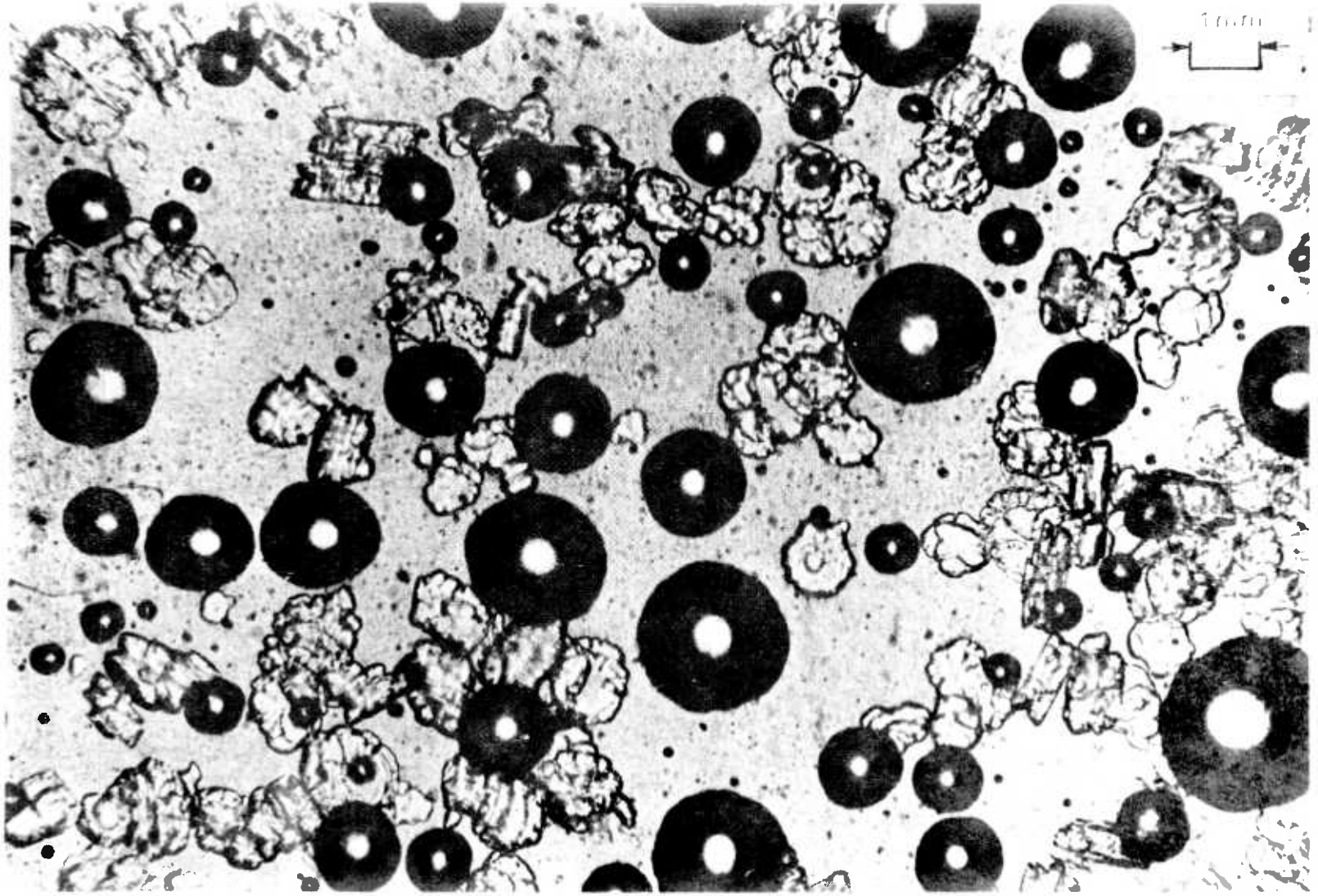

Figure 1.1: Ice crystals and isobutene bubbles in effluent from a well-stirred continuous crystalliser (85)

the study of the evaporation of multiple droplets and the study of the evaporation of a single droplet in another immiscible liquid, which includes the present work.

In the process of evaporation of a droplet in another immiscible liquid from the time of formation and release to ascend, the main problems involved may be divided into formation and release, nucleation, heat transfer, growth, hydrodynamics, and interfacial area. These, and other aspects of bubble and drop phenomena, such as mass transfer, combined heat and mass transfer, collapse, and coalescence, have been encountered in industry. The available literature, which has specifically studied the evaporation of a two-phase bubble-droplet of a refrigerant in another immiscible liquid, is by far much less than the amount of work done on the less complex problem of droplets and bubbles in liquids. Before discussing in more detail the literature available on the evaporation of droplets in immiscible liquids, it is useful to mention in brief the topics outlined above, a knowledge of which would help the understanding of the phenomena involved.

(a) Formation: The formation of bubbles and drops in liquids may be mainly divided into formation from submerged orifices and formation due to the boiling of liquids. The type of formation related to the present work is that from the submerged orifices. A review by Kumar et al (38) discusses this type of formation and the influence of factors on bubble and drop size, and also various models of formation. The important variables which influence the drop size are the velocity and density of the dispersed phase, and the viscosity and density of the continuous phase.

(b) Nucleation: Nucleation in liquids may take place either homogeneously

(that is, freely in the volume of the original phase) or heterogeneously (on the surfaces of the container or foreign particles or structural imperfections). Nucleation on heterogeneities may occur at a smaller motivating potential than that required for homogeneous nucleation. Most nucleation events do take place heterogeneously. Liquid-liquid interfaces are likely places for the initiation of nucleation. However, whether nucleation occurs homogeneously or heterogeneously at liquid-liquid interfaces depends on the values of surface tensions and interfacial tension of the liquids (32,50). Although nucleation in processes like direct contact heat transfer between two liquids with simultaneous change of phase is desirable, it can be undesirable in other cases. For example, the formation of vapour bubbles as a result of pressure reduction (cavitation) can be damaging in the hydraulic machinery, valves, fittings, etc. (37). Moore (49) and Jarvis et al (32) discussed the mechanism of nucleation of superheated drops in liquids. Boiling modes of superheated drops in an immiscible liquid are examined by Mori et al (51,52) using high speed photography. Various aspects of boiling nucleation have been discussed in a review by Cole (8).

(c) Heat Transfer: A number of engineering operations involve the transfer of heat and mass between a continuous fluid phase and a second phase, such as gas bubbles, and liquid drops moving relative to the continuous phase. In a review by Sideman (75), three basic physical models have been discussed for heat transfer to liquid drops in a constant temperature field. These are: rigid drop, completely mixed drop, and drop with internal circulation. The rigid drop model assumes that the liquid in the drop is stagnant and radial conduction controls the rate of heat transfer beneath the drop surface. In the completely mixed drop

model, both liquids have uniform temperatures. In the third model, circulation within the drop develops due to the shear stress applied at the interface because of the viscosity of the surrounding liquid. Some of the experimental and theoretical formulae for these models are summarised and compared in reference (75). Heat transfer to growing bubbles formed from boiling liquids has also been the topic of considerable research (64).

(d) Growth: The work on bubble growth might fall under two main regions (42); growth rates controlled by the inertia forces and growth rates controlled by heat diffusion. An example for the first case is the Rayleigh (61) solution for bubble growth, which leads to:

$$R = C\,t \tag{1.1}$$

where:
$$C = \left[\frac{2}{3}\,\frac{(T_\infty - T_{sat})}{T_{sat}\,\rho_c}\,h_{fg}\,\rho_v\right]^{\frac{1}{2}} \tag{1.2}$$

while the Plesset & Zwick (57) solution for bubble growth in a uniformly superheated liquid, where heat diffusion effects are dominant, leads to:

$$R = C'\sqrt{t} \tag{1.3}$$

where:
$$C' = \left(\frac{12}{\pi}\,Ja^2\,\alpha_c\right)^{\frac{1}{2}} \tag{1.4}$$

Mikic et al (42) derived another solution to be applicable for the entire range of bubble growth, including the above two cases.

(e) Hydrodynamics: Studies on the movement of bubbles and drops in

liquids required studies such as path, terminal velocity, oscillation, wake, distortion, drag, boundary layer, circulation, acceleration, interaction, etc. A review by Harper (26) discusses some of the problems involving bubble and drop movement through liquids. The behaviour of droplets or bubbles moving in another liquid is different from the solid body because of movability of the interface. Droplets deform under the action of hydrodynamic forces, and momentum is transferred across the interface and causes the liquid circulation within the fluid body. The flow pattern inside and outside of the bubbles and droplets can be analysed using Navier-Stokes equations. Non-linearity of these equations necessitates some simplifications. For example, when Stokes flow is present, the inertia term is neglected. The potential flow condition has been widely used in cases where viscous terms may be neglected in comparison with the inertia terms. Another method is the use of boundary layer theory. In this method, the flow is divided into flow far from the body, where potential flow may be assumed, and flow close to the boundary, where the full Navier-Stokes equation is valid. In this case, assuming a thin boundary layer simiplifies the equation of motion (20).

Among the data used on the drag coefficients of bubbles are those of Haberman & Morton (24), and for drops are those of Winnikow et al (89) and Thorsen et al (81).

(f) Interfacial Phenomena: In the hydrodynamics of two-phase systems, one encounters the effect of interfacial tension. The existence of surface tension causes phenomena called the capillary phenomena. These include, for example, the retardation of the movement of droplets and bubbles in liquids which contain dissolved surface-active substances, and the formation of surface waves in liquids under the influence of different

kinds of disturbances (40). If the surface tension is uniform along the interface, the tangential stress is continuous across the interface. The presence of surface-active agents in the two-phase boundaries causes non-uniformity of surface tension. In this case, the tangential stress varies accordingly and this causes a convective motion, at least in one of the phases, which affects the transport processes along the interface (33).

1.2 PREVIOUS WORK ON THE EVAPORATING DROPLET IN IMMISCIBLE LIQUIDS

The first detailed exploratory study on the evaporation of a droplet in an immiscible liquid was carried out by Klipstein (36). Since then, most of the work has been on the experimental side and only a few theoretical models for the process have been tried. It may be more advantageous to review the experimental and theoretical work separately.

1.2.1 Experimental Procedures

For a better understanding of the basic phenomena of evaporating droplets, single drop studies have been chosen by most of the investigators (for example, 36,59,68,77). Drops were formed from single submerged orifices in columns of continuous phases. Closer conditions to the real situation in industry were obtained using multiple nozzles (27, 71-73) or a single nozzle (82).

Various combinations of dispersed phase/continuous phase have been used. Dispersed phases having boiling points higher than the atmospheric temperature, such as n-pentane, have been chosen by most of the investigators (for example, 68,58). Butane, which has been used in desalination plants, was chosen by Sideman et al (68), Missirilis (43), Nazir (53), and Simpson et al (77). Filatkin (14) used a mixture of hydrocarbons for this purpose.

The importance of the surface tensions of both the liquids was investigated by Gradon et al (23), using water as the dispersed phase and silicon oil as the continous phase, and Selecki et al (66), who used carbon tetrachloride drops in water and water drops in castor oil.

To achieve a geometrically simple configuration and rectilinear motion of bubble-droplets, Tochitani et al (83,84) used n-pentane and Furan drops in a highly viscous aqueous glycerol solution. This choice enabled them to study the problem in low Reynolds numbers.

All the investigators studied (single drop study) the drop rise in the quiescent continuous phase, except Nene (54,55), who tried to stop the drop in a pipe by flowing the continuous phase in the opposite direction, Missirilis (43), who formed the drop downward at the nozzle, and Simpson et al (79), who studied the nucleation of butane drops in flowing water.

Nucleation of the droplets was done artificially. Klipstein (36) nucleated the drops by discharging a condenser through a nichrome heating wire in contact with the drop before detachment. Tochitani et al (82) placed a tungsten wire in the feeding line of n-pentane. This wire was electrically heated to generate tiny vapour bubbles in the pentane flow. Mori et al (52) also used electrically heated iron/chrome wire to initiate nucleation in superheated drops. Injection of tiny gas bubbles, such as air or nitrogen, into the droplets has been adopted by Sideman et al (68), Prakash et al (58), Tochitani et al (83), and Simpson et al (77). It should be noted that, under normal industrial operating conditions, such induced nucleation is not warranted. Nucleation of a train of butane drops rising through downward flowing cold distilled water was investigated by Simpson et al (79).

Two-dimensional photography of the evaporating drops has been

an important part of the majority of the previous studies. This allows the history of the drop behaviour, from the formation to release and ascent, to be recorded at small time intervals. Two-dimensional photography, however, necessitated the assumption of axial symmetry of the evaporating drops which was not an accurate assumption for the real shape, especially in the case of large drops. But, because of the more difficult task of three-dimensional photography (for example, using two cameras 90^{o} apart), the two-dimensional approach might be satisfactory. The fact that the camera had to be moved and chase the drop at the same level, and in a plane parallel to the drop, made the situation more difficult. Among the previous workers who used this method are references (1,53,58, 68,83). In the study by Tochitani et al (83), this method seemed to be accurate enough because of the symmetrical shape of the evaporating drops in low Reynolds number conditions. In another method, the history of bubble-droplet growth was recorded using a dilatometer technique (1,59, 83). By this method, the increase of bubble-droplet size caused the liquid in a dilatometer to rise in a tube. The amount of rise was recorded using a photoelectric cell and a recorder (1,59) or using a ciné camera (83). The dilatometric method appeared to be more advantageous than the photography method for recording the change of volume. However, it should be noted that this method requires special precautions so that the transfer of the continuous phase medium due to the bubble growth only appears in the dilatometer tube, and also that this be due to the only droplet which is under study. Also, the dilatometer response time becomes more important with an increase of the size of the continuous phase column.

Droplet velocity measurement was achieved using the positions of the bubble-droplet in different shots, when the photography method was

used. An optical method was adopted by Selecki & Gradon (23,67). In this method, the measuring device consisted of a light source photo-tube connected to a recorder. The light beam was interrupted by the passing bubble and the time of interruption was recorded by the recorder. An optical method might be easier and more accurate for the measurement of average velocity between the two light beams. But difficulties might be encountered, such as bubble deviation from the predicted line, as it is seen in the helical movement of rising bubbles, and consequently missing the light beam. This method was previously used by Aybers et al (4) for the measurement of air bubble velocity in water.

A number of spray column studies were carried out by Sideman et al (71-73). Perforated plates were used to form the droplets. Parameters, such as volumetric heat transfer coefficient, hold up, foam height and optimal column height, were considered (72). The effect of initial drop size and mixing on heat transfer between the two phases were studied in (73,71), respectively. A study based on the photographic observations was carried out by Tochitani et al (82). They injected n-pentane drops in water through a single nozzle. The subcool of the drops at the nozzle outlet and the length of the Rayleigh jet were among the parameters of interest. Selecki et al (66) also conducted a multiple drop study in which the importance of the surface tensions of the liquids and the optimal column height were investigated. As a part of an experimental study of counter current heat exchangers, Harriot et al (27) studied the performance of an evaporator by injecting n-pentane through sieve plates into water. In a pilot plant-size study of desalination by freezing, Hubbard et al (29) used methylene chloride as the refrigerant in brine. The report of the study concentrated on the brine freezing side and no detailed information was given on the refrigerant evaporation side of the problem.

1.2.2 Experimental Results

Among the important parameters which were experimentally investigated by the previous workers were: heat transfer coefficient (instantaneous and average), growth rate, rise velocity, droplet size, total evaporation time, height of complete evaporation, temperature driving force, properties of the liquids, effect of surfactant, and liquid-liquid interfacial area.

(a) Heat transfer coefficient: The heat transfer coefficient has been evaluated from the amount of heat transferred to the bubble-droplet system which, by neglecting the sensible heat, could be obtained from the amount of evaporated liquid which, in turn, has been evaluated from the growth rate of the bubble-droplet. The equation which has been used is in the form of:

$$q = h A \Delta T \tag{1.5}$$

where ΔT is taken as the difference between the continuous phase temperature and dispersed phase saturation temperature, and h is the heat transfer coefficient. If the instantaneous values of the above parameters are used, the instantaneous heat transfer coefficient will be obtained. If A is taken as the initial droplet area and q as the average rate of heat transfer during the evaporation time (1), the average heat transfer coefficient would be the result. Area A may be defined as the overall instantaneous area of the bubble-droplet or the instantaneous liquid-liquid interfacial area. Relating the heat transfer coefficient to the Nusselt number and then, for the sake of correlation to the Reynolds number, arose questions (1) such as: On which of the phases' properties should the dimensionless

parameters be based on? This will be mentioned when each of the correlations presented by the previous investigators will be discussed.

The heat transfer to a two-phase evaporating bubble-droplet may be divided into the heat transfer through the continuous phase liquid-dispersed phase vapour and the liquid-liquid interfaces. The latter is much less than the former (36,68,70) because of the low conductivity of the vapour, and the heat transfer may be assumed to take place mainly through the liquid-liquid interface. The overall heat transfer coefficient is usually obtained from the inside and outside coefficients. The outside coefficient is related to the continuous phase liquid surrounding the bubble-droplet system, and the inside transfer coefficient is related to the dispersed phase within the system. Some characteristics of the outside heat transfer coefficient can be realised from the information available on one-phase bubbles or droplets (75), although it may not be directly applicable to the two-phase bubble-droplet. Since the major heat is transferred through the liquid-liquid interface, which is concentrated at the lower part of the system, wakes which develop at high Reynolds numbers at the rear part of the droplet play an important rôle in the heat transfer process. In the dispersed phase liquid, although a complete circulation, as it is realised in drops (34), may not be happening in the case of bubble-droplets due to the discontinuity of the liquid part compared with a complete drop, some kinds of convection or circulation have been realised by Tochitani et al (84). This was said to have been induced by the shear stress or a kind of interfacial turbulence. They experimented with a high viscous continuous phase which resulted in higher shear stresses in the interface than when low viscous continuous phases, such as water, were used. They obtained much lower resistance to heat transfer inside the system than by assuming only pure conduction,

which was the dominant factor if there was not any movement in the liquid part. However, experiments with low viscous liquids like water have shown that sloshing of the unevaporated liquid phase in the system was one of the main factors and played an important rôle in the heat transfer process. Sideman et al (70) introduced a numerical factor to allow for the increase of liquid-liquid area due to this movement.

The inside resistance to heat transfer due to the dispersed phase liquid film thickness is the dominant factor in the early stages of evaporation (36,68,70,78). As the evaporation proceeds, the outside resistance becomes more important. The overall heat transfer coefficient variation versus time showed a maximum in both the results of Sideman et al (68) and Tochitani et al (84). The results of Filatkin et al (14) showed a decrease, and those of Simpson et al (77) increased gradually over the entire range.

Heat transfer coefficients were more or less independent of the temperature difference between the two phases in the range of $5^{o}C$ to $15^{o}C$ (68). At temperature differences below $5^{o}C$, the heat transfer coefficient increased sharply with decrease in temperature difference. This increase was attributed to the possible higher percentage of error in these ranges. However, Tochitani et al (84) mentioned that both the overall and the heat transfer coefficient related to the liquid-liquid interface decreased when the temperature difference increased. But, from their plotted curves, the difference was more evident when temperature differences differed considerably and at lower vaporisation ratios.

The overall instantaneous and the overall average heat transfer coefficients were higher for smaller droplets in the results of Sideman et al (68), while the coefficients in the results of Tochitani et al (84) tended to be lower. The contradiction might be due to the difference of

the systems under study. In the spray column study (73) also, smaller droplets resulted in higher volumetric heat transfer coefficients. Nene (55,63) measured the heat transfer coefficient of evaporating butane drops down to 0.1% evaporation, and found that this parameter did not depend on the initial droplet diameter or the temperature difference. In his results, the heat transfer coefficient increased sharply with evaporation percentage up to 1% and was nearly constant afterwards.

Klipstein (36) presented the following equation for the instantaneous external heat transfer coefficient:

$$Nu = 2 + 0.094\, Re^{0.93}\, Pr^{1/3} \tag{1.6}$$

He carried out his experiments using ethyl-chloride as the dispersed phase and distilled water, 35% and 65% glycerol solutions as the continuous phase.

Sideman et al (68) used pentane and butane drops in distilled water and sea water. The initial diameter of droplets were approximately 3.5 mm and 2.0 mm. They correlated their heat transfer coefficient results related to the instantaneous bubble-droplet area in the form of:

$$h = a \frac{1}{\Delta T} \frac{\xi^b}{c\, \xi^d + 1} \tag{1.7}$$

where ξ is the vaporisation ratio, and a, b, c and d were to be calculated for each individual droplet from the given tables.

Prakash et al (58) presented different correlations for each of the furan, isopentane, cyclopentane/distilled water combinations and gave a correlation for the three systems as:

$$Nu = 0.5\ (Pe')^{0.445}\ \left(\frac{\rho_c - \rho_{av}}{\rho_c}\right)^{1.81} \qquad (1.8)$$

where ρ_{av} is the average density of the dispersed phase. They mentioned that vapour volume measurement from the cine film was only possible up to 10% evaporation, because of the deformation of the bubble-droplet in the later stages of evaporation. However, the above equation was recommended for extrapolation to higher percentages. The modified Peclet number, Pe', was introduced to account for the viscosity of the dispersed phase. The Nusselt number and the modified Peclet number were based on the dispersed phase liquid properties.

Filatkin et al (14) gave the following correlation for evaporation of a mixture of hydrocarbon droplets in water:

$$Nu = 1.45 \times 10^{-4} \left[\frac{0.0575}{((\rho_c - \rho_d)/\rho_d)^2} + 0.0001\right] (Pe')^{2.1} \qquad (1.9)$$

In the majority of their tests, the temperature of the continuous phase was adjusted in such a way that the evaporation did not exceed 10% evaporation.

Adams et al (1), because of uncertainty in the determination of the exact values of the liquid-liquid interfacial area, chose the average heat transfer coefficient to be based on the initial droplet diameter. Using their own, and others, experimental results, they concluded that the dispersed phase Nusselt number, the continuous phase Prandtl number and the liquid phase Bond number were the best for correlating the results. The following correlation was given:

$$Nu_l = 7550\ Pr_c^{-0.75} \left[\frac{\mu_c}{\mu_c + \mu_l}\right]^{4.3} (Bo)^{0.33} \qquad (1.10)$$

The dimensionless viscosity ratio, as in the above equation, appeared to be better than the simple viscosity ratio, μ_d/μ_l.

For butane/water and butane/4% and 8% sodium chloride solution combinations, the overall instantaneous heat transfer coefficient based on the equivalent spherical area of the bubble-droplet is given by Simpson et al (78) as:

$$h_o = \frac{2.57\ (D/d)^{1/6}}{1 + 0.206\ (D/d)^{5/12}} \qquad (1.11)$$

This correlation was obtained using the experimental data for single butane droplets about 3.75 mm in diameter and overall temperature differences of ΔT_o = 2.0°C to 8.0°C, and is given for $D/d > 2.7$ (for the butane/water combination) and $D/d > 2.0$ (for the butane/salt water combination). Equation (1.11) fits the experimental data to within ± 18% up to about 90% evaporation.

In a study by Rice et al (63), the heat transfer in crystallisers was examined and it was found that the main resistance to heat transfer lay in the brine to evaporating drops.

(b) Growth rate: Variation of growth and growth rate related to the equivalent spherical diameter of bubble-droplet has been described in more detail by Nazir (53), Simpson et al (77) and was pointed out by Sideman et al (76), where their theoretical analysis was compared with experimental results. Also, a sample of curves which was obtained by the dilatometric method of Adams et al (1), indicating the variation of voltage against time which was a representative of the increase of bubble-droplet volume, denoted the trend of the growth against time. The same trend, up to the final stages of evaporation, was shown by these workers. In the final stages, the dilatometric curve (1) showed that the growth slowed down.

(c) Rise velocity: For a one-phase bubble or droplet moving in a liquid, the average terminal velocity can be obtained by measuring the required time to travel a specified distance. In such cases, when the droplet or bubble size and forces acting on the droplet do not change, the terminal velocity can be assumed to be constant. But, for a two-phase growing bubble-droplet, the forces like buoyancy and drag vary and thus the velocity of the system changes accordingly. The instantaneous velocity may be determined from the variation of the bubble-droplet position which can be recorded on a ciné film. This procedure was used by Sideman et al (68), Prakash et al (59), Simpson et al (77), and Tochitani et al (83). Sideman et al (68) correlated their results into equations of the form:

$$H - H_o = B\, t^p \qquad (1.12)$$

where H and H_o are the level of drop above the nucleation point and $t = 0$, respectively, and B and p are constants. Instantaneous velocity was then estimated by differentiating this equation. In their results, velocity increased over the entire range of evaporation. In the results of Simpson et al (77), the rise velocity was nearly constant and about 0.25 m/s up to a diameter ratio of 2.7 (for butane/distilled water combination) and 2.0 (for butane/salt solution combination). Above these ratios, the velocity increased as the square root of the diameter ratio increased. Prakash et al (59) calculated the terminal velocities by using drag coefficients on vapour bubbles from the data of Garner et al (19), and compared them with the velocities of evaporating isopentane, cyclopentane, and furan droplets in distilled water. They concluded that the rise velocity

of vaporising droplets was nearly equal to its instantaneous terminal velocity. Klipstein (36) calculated the terminal velocities by using the data of Haberman et al (24) and Harmathy (25) and concluded that the velocities of growing bubble-droplets lagged corresponding terminal velocities by about 10%. The lag was greater for larger drops. The lag apparently did not increase in the case of greater temperature differences, and thus he commented that the important factor in the determination of the lag was mass of the bubble-droplet.

(d) Liquid-liquid interfacial area: The interfacial area between the continuous phase and the unvaporised liquid in the bubble-droplet is one of the most important factors in the process. All the previous workers agreed that heat was transferred mainly through the liquid-liquid interface. But, unfortunately, there is still little known about the actual area. The reason is mainly because of the variation of this area due to evaporation, bubble-droplet deformation, and oscillations and sloshing of the liquid part. Two- or even three-dimensional photography may not be very successful, especially as the unvaporised liquid layer becomes thin and invisible after about 10% evaporation is reached. Klipstein (36) classified the bubble-droplet shape into three basic shapes, namely, sphere, ellipsoid and spherical cap. Then, by assuming that the shape of liquid puddle at the bottom of the bubble could be taken as an inverse cone (for sphere and ellipsoid shape bubble-droplet) and as an annulus surrounding a truncated cone core (for spherical cap shape), he presented formulae for liquid-liquid interfacial areas. The area increased up to about 40% of evaporation and then decreased more gradually afterwards. He mentioned that spreading tendencies and liquid splashing did not increase the liquid-liquid area significantly.

Sideman et al (70), assuming an ellipsoidal shape with constant eccentricity, found an expression for liquid-liquid area which increased throughout the evaporation.

Tochitani et al (83,84) made simplifications in their calculations of the liquid-liquid area (e.g. the two-phase bubble-droplet was taken as a spheroid and the liquid-liquid part as a segment of the sphere). The type of variation of area in their results agreed with those of Klipstein (36). They showed that the area increased up to about 10% evaporation and decreased afterwards. Tochitani's results should have been subjected to less error than other results, because of his experimental conditions (study with small droplets and high viscous continuous phase), which provided bubble-droplets with a better axial symmetry.

(e) Total evaporation time: Sideman et al (68) obtained the time for complete evaporation of a droplet by correlating their experimental data in the form of:

$$Q - Q_o = c\, t^n \qquad (1.13)$$

where Q is the heat input, and Q_o, c and n are constants. By substituting Q by Q_{max} where Q_{max} is the maximum heat absorbed by the droplet, the calculated t was taken as the total evaporation time. Klipstein (36) estimated the total evaporation time from the extrapolation of plotted curves representing the variation of total heat content versus time. Prakash et al (59) commented that neither of these methods were reliable. They conducted a dilatometric method in which the time of complete evaporation could be directly obtained from the variation of voltage versus

time, recorded by a chart recorder. However, their results seem to be longer than the results of other workers, probably due to the subcool drop temperature while entering the continuous phase medium. Corrections to the Prakash data were reported to have been made by Adams et al (1).

(f) Effect of surface tension: The mechanisms of evaporation, according to the surface tensions of the dispersed phase and the continuous phase liquids, were discussed by Gradon & Selecki (23,66) and Mori et al (51,52). In the majority of the combinations used by the previous workers (e.g. 58,68), the dispersed phase had a lower surface tension than the continuous phase (e.g. butane/water combination). In this case, the growing bubble remains attached to the vaporising liquid droplet. In a combination such as water/silicon oil, where the dispersed phase has a higher surface tension than the continuous phase, a different mechanism of evaporation is obtained in which the vapour bubble is separated from the droplet. These mechanisms are shown by Mori et al (51,52) using high speed photography. In the study by Gradon et al (23), a water/silicon oil combination was used, but it mainly concentrated on the theoretical part and less information on the experimental side of the process was given.

(g) Effect of surfactants: Surfactants can have a significant effect on the transport phenomena of drops. Examples are: lowering the interfacial tensions, hindering the internal circulation, increase of drag, and damping of oscillations (34). Surfactants have a tendency to accumulate in interfaces, causing the drop behaviour to approach that of rigid body. Only a very minute amount of surfactants can have considerable changes in the processes involved. In some cases (12), although the presence of surfactant agents could be proved by their effects, they still did not change the physical properties of the liquids

to a measurable degree.

Klipstein (36) studied the effect of surfactants on the evaporation of ethyl-chloride drops in distilled water and 35% and 65% glycerol solutions, although some of his experiments were affected by the dissolution of Aerosol 22 surfactants in glycerol solutions. In his study, the presence of surfactants resulted in smaller drop formation at the nozzle. Results also showed that the heat transfer rate increased for small drops but decreased for large drops. The reason was said to be due to the increase of the oscillation tendency (in contrast to reference (34)) in the case of small drops and the reduction of interfacial rippling for large drops. Drop velocities decreased to a maximum of 11% compared with the velocities of drops in liquids without surfactants.

1.2.3 Theoretical

(a) Heat transfer: There are still very few theoretical models available of the evaporation of droplets in another immiscible liquid. Any theoretical model is mainly dependent on the shape of the bubble-droplet system and the mechanism of heat transfer is particularly related to the interfacial liquid-liquid area and, consequently, to the shape of the unvaporised liquid within the system. A simplification which was often adopted was the assumption of sphericity of the bubble-droplet. This assumption, which might be valid for small drops or in a narrow range of evaporation, greatly simplifies the theoretical analysis. On the other hand, it is more difficult to assume a specific shape for the vaporising liquid in the bubble-droplet. This is due to the continuous change of the liquid mass and phenomena like growth, bubble-droplet deformation and liquid sloshing. Due to this difficulty, assumptions were made which are sometimes difficult to justify.

Sideman et al (68) presented the first theoretical model of the heat transfer mechanism. Among their simplifying assumptions were: sphericity of the bubble-droplet; growth was neglected compared with drop velocity; potential flow around the system; and it was assumed that the system was in steady-state conditions. It was further assumed that the liquid part was located at the bottom of the bubble and bound to an angle of 360 - 2β, where β is defined as the opening angle. They obtained the average instantaneous heat transfer coefficient as:

$$Nu_c = \frac{h\,D}{k} = \left(\frac{3\cos\beta - \cos^3\beta + 2}{\pi}\right)^{0.5} (Pe_c)^{0.5} \qquad (1.14)$$

This equation shows high values of heat transfer coefficient at the early stages of evaporation, which decreases sharply as evaporation proceeds. They suggested that an average value of $\beta = 135^{o}$ might give a good approximation of the maximum heat transfer coefficient, thus simplifying equation (1.14) to:

$$Nu_c = 0.272\ Pe_c^{0.5} \qquad (1.15)$$

More recently, Tochitani et al (84) derived a similar equation for the outside heat transfer coefficient to drops evaporating in a viscous liquid. Among the basic assumptions were: sphericity of the two-phase bubble; axisymmetric distribution of the liquid at the lower part of the system; quasi-steady-state; Stoke flow around the system; and it was further assumed that the surface of the bubble-droplet was rigid. They obtained:

$$Nu_c = 0.463\ Pe_c^{1/3} \left(\pi - \beta + \frac{\sin 2\beta}{2}\right)^{2/3} \qquad (1.16)$$

where β is defined as the same in reference (68). The agreement with

the experimental results was better in the later stages of evaporation.

Another model with a different approach was developed by Simpson et al (78) which, in contrast with Sideman's model, did not restrict the dispersed phase liquid to the bottom of the bubble-droplet. They suggested that, due to the oscillation of the system and sloshing of the unvaporised liquid, the heat was transferred through a thin liquid butane film formed periodically on the inside surface of the bubble. Thus, a relation for the inside heat transfer coefficient was derived which showed a 1/6 power relationship with the diameter ratio, which was in agreement with their experimental results. For the outside heat transfer coefficient, the same heat transfer solution as Sideman's (68) was applied. Combining the inside and outside heat transfer coefficients, they presented a relation for the overall heat transfer coefficient which is given in section 1.2.2 (equation (1.11)).

(b) Dynamics and growth: An evaluation of the equation of motion was tried by Selecki et al (67). They assumed that the vapour part of the bubble-droplet system was spherical and treated the problem as the bubble was moving in a superheated liquid, while evaporation only took place from the layer of suspended liquid, defined by the angle β as in (68). They used the equation of motion of a bubble growth in a non-viscous, incompressible liquid (Rayleigh's equation). Because, in the case of Rayleigh's equation, evaporation takes place uniformly at the whole of the bubble boundary, they made a modification (although not enough explanation was given in the paper presented) to make this equation applicable for the case of evaporating drops in which evaporation takes place from a part of the bubble boundary. They concluded that a solution, such as that used by Plesset (57), could be used to give a relation for the growth as:

$$R = c\, t^{\frac{1}{2}} \tag{1.17}$$

An equation of this form, which was derived for bubble growth in superheated liquids, gives a negative value for d^2R/dt^2 as time proceeds. But the growth curve, as can be seen from the previous experimental results (76,77) and our own, show that d^2R/dt^2 can be positive throughout the evaporation process. The exception can be seen in the dilatometric curve (1), which showed that growth slowed down near the end of evaporation. The contradiction is due to the fact that the drop superheat in the above experimental results have been reduced, or even eliminated, by artificial nucleation. Finally, Selecki et al (67) derived the equation of motion of an evaporating droplet in an immiscible liquid. The model was compared with their own experimental results in the form of position versus time, and the agreement was good.

Using their theory, Simpson et al (78) derived the following equation for the growth rate:

$$\frac{d(D/d)}{dt} = C\, \Delta T_i\, (D/d)^{1/6} \tag{1.18}$$

where C is a constant for a particular combination, and ΔT_i is the temperature difference between the brine-butane interface and the butane saturation temperature.

1.2.4 Condensation of Vapour Bubbles in Immiscible Liquids

The condensation of vapour bubbles in immiscible liquids could be considered as the reverse process of evaporating droplets. In practice, the use of three-phase heat exchangers utilising direct contact heat

transfer to the evaporating drops will reduce costs by recycling the generated vapours. The recycling process may be achieved by the condensation of vapour bubbles in another immiscible liquid. Better understanding of the phenomena involved may also be useful in the study of the reverse process. Here, in brief, some of the previous work on the subject will be mentioned.

The condensation of vapour bubbles in a liquid of the same material (one-component system) is different from the condensation of vapour bubbles in another immiscible liquid (two-component system). In the former, the condensing vapour merges with the continuous phase, while in the latter the condensate remains within the bubble boundary. In a one-component system, the interface is a vapour-liquid interface and the internal circulation may be fully developed, while in the two-component system the condensate forms a thin liquid film on the bubble's wall which hinders the internal circulation. A preliminary study on the condensation of single pentane bubbles in water was conducted by Sideman et al (74). The heat transfer mechanism up to 80% vapour content was condensed and was attributed to the turbulent behaviour of the bubble associated with deformation and oscillation. After that, due to the resistance of the liquid film on the wall, heat transfer dropped sharply and the bubble behaved more or less as a liquid drop. Condensation was not complete, especially in low temperature driving forces (up to $3^{o}C$) which is of more practical interest. Also, no distinction could be observed between the condensed liquid and the vapour in contrast with the evaporating drops. Theoretical and experimental studies were later reported by Isenberg et al (30,31). Further studies were reported on the effect of non-homogeneous distribution of non-condensables (44), the effect of motion on bubble collapse (46), and the condensation of a bubble train (45).

1.3 THE PRESENT WORK

1.3.1 Objectives

The need for further research to improve the knowledge on the phenomena involved in the secondary refrigerant method of desalination by freezing led to the present investigation. The objectives of this work can be summarised by the following points:

1. To develop a theoretical model of the evaporation of a droplet during its rise in a column of an immiscible liquid.
2. To conduct an experimental programme to study the parameters involved in the process of the evaporation of a refrigerant droplet in water and to examine the theoretical model. This led to the following aims:
   (a) To study the evaporation of a butane droplet during its rise in distilled water.
   (b) To stop the evaporation of the bubble-droplet at a certain range in order to study its behaviour and compare it to the evaporating bubble-droplet.
   (c) To develop a technique to record the path of evaporating droplets. However, this step was extended to further work on the different sizes of bubbles and to the condensing bubbles.

1.3.2 Layout of this Thesis

In Chapter 1, the application of the direct contact heat transfer with change of phase in practice and its advantages over the other methods are explained. Then a survey has been carried out on the previous

work which is relevant to this thesis.

Chapter 2 presents the theoretical model of an evaporating droplet in an immiscible liquid, and the results of the prediction.

Chapter 3 includes the description of the experimental rig, preliminary experiments and the experimental procedure. It describes the experimental conditions, the procedure of data collection and data processing.

Chapter 4 presents the experimental results and discussion, and makes a comparison with other investigators' results.

Chapter 5 is concerned with the comparison of the present experimental results with those predicted from the present theoretical model.

Chapter 6 describes the experimental method by which the movement of bubbles and bubble-droplets in liquids can be studied.

Chapter 7 explains about the computer programs which were developed during this study.

Chapter 8 describes the conclusions.

CHAPTER 2

THEORETICAL MODEL OF AN EVAPORATING DROPLET IN AN IMMISCIBLE LIQUID*

2.1 INTRODUCTION

A theoretical analysis is presented for the evaporation of a droplet in another liquid. The model considers a single two-phase bubble-droplet while growing and rising in a column of another immiscible liquid with infinite extents. The problem has been looked upon in a general point of view, rather than concentrating on a specific parameter or phenomenon. The problem is dealt with mainly as a growing bubble. The model is given for low viscous liquids and is more suitable for higher Reynolds numbers. After making the simplifying assumptions, the governing equations, namely, momentum equation, energy equation, equation of motion, equation of conservation of mass, and equation of state, are derived. The process is time-dependent and so are the governing equations. The equations are written in the form of a set of first order ordinary differential equations, and by specifying the initial conditions, they are solved simultaneously using a numerical method.

The model requires the knowledge of the instantaneous heat transfer coefficient which is an important factor in the process.

The model is examined for different droplet sizes and temperature differences, initial velocities and initial temperatures. Results are presented for butane/ and pentane/distilled water combinations, but the

---

* A paper entitled "A Theoretical Analysis of Evaporating Droplets in an Immiscible Liquid", published in the International Journal of Heat & Mass Transfer (47), was based on the work presented in this chapter.

model can be applied to the other combinations once the properties of the liquids are set.

Comparisons of the predicted results with those from the experiments are made in Chapter 5.

2.2 THE MODEL

2.2.1 Assumptions

The following assumptions are made:

(a) Single bubble-droplet system.

(b) The system boundary is spherical.

(c) The surrounding liquid has a constant temperature throughout, which is incompressible, infinite in extent and quiescent.

(d) The system boundary is impermeable to substances but permeable to heat.

(e) Movement of the bubble-droplet during its ascent is rectilinear.

(f) Both liquids are pure.

2.2.2 Coordinate System

The coordinate system moves with the bubble-droplet and its origin is located at the centre of a sphere (Figure 2.1). Because of assumption (b), the flow around the system is axisymmetric and every point in the field can be specified by r, θ and t. The position of the centre of the sphere is specified by Z which is a function of time.

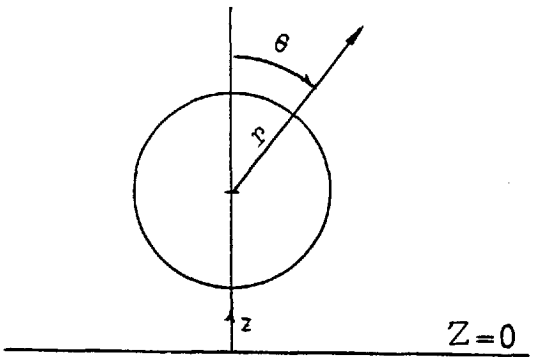

Figure 2.1: Coordinate system

2.2.3 Governing Equations

2.2.3.1 Momentum equation

The Navier-Stokes equations of motion in the spherical coordinates are (6):

r-component:

$$\rho_c \left(\frac{\partial v_r}{\partial t} + v_r \frac{\partial v_r}{\partial r} + \frac{v_\theta}{r}\frac{\partial v_r}{\partial \theta} + \frac{v_\phi}{r \sin\theta}\frac{\partial v_r}{\partial \phi} - \frac{v_\theta^2 + v_\phi^2}{r}\right) =$$

$$-\frac{\partial P_c}{\partial r} + \mu_c \left(\nabla^2 v_r - \frac{2}{r^2} v_r - \frac{2}{r^2}\frac{\partial v_\theta}{\partial \theta} - \frac{2}{r^2} v_\theta \cot\theta - \frac{2}{r^2 \sin\theta}\frac{\partial v_\phi}{\partial \phi}\right) + \rho_c g_r \qquad (2.1)$$

θ-component:

$$\rho_c \left(\frac{\partial v_\theta}{\partial t} + v_r \frac{\partial v_\theta}{\partial r} + \frac{v_\theta}{r}\frac{\partial v_\theta}{\partial \theta} + \frac{v_\phi}{r \sin\theta}\frac{\partial v_\theta}{\partial \phi} + \frac{v_r v_\theta}{r} - \frac{v_\phi^2 \cot\theta}{r}\right) =$$

$$-\frac{1}{r}\frac{\partial P_c}{\partial \theta} + \mu_c \left(\nabla^2 v_\theta + \frac{2}{r^2}\frac{\partial v_r}{\partial \theta} - \frac{v_\theta}{r^2 \sin^2\theta} - \frac{2\cos\theta}{r^2 \sin^2\theta}\frac{\partial v_\phi}{\partial \phi}\right) + \rho_c g_\theta \qquad (2.2)$$

ϕ-component:

$$\rho_c \left(\frac{\partial v_\phi}{\partial t} + v_r \frac{\partial v_\phi}{\partial r} + \frac{v_\theta}{r} \frac{\partial v_\phi}{\partial \theta} + \frac{v_\phi}{r \sin\theta} \frac{\partial v_\phi}{\partial \phi} + \frac{v_\phi v_r}{r} + \frac{v_\theta v_\phi}{r} \cot\theta\right) =$$

$$-\frac{1}{r \sin\theta} \frac{\partial P_c}{\partial \phi} + \mu_c \left(\nabla^2 v_\phi - \frac{v_\phi}{r^2 \sin^2\theta} + \frac{2}{r^2 \sin\theta} \frac{\partial v_r}{\partial \phi} + \frac{2 \cos\theta}{r^2 \sin^2\theta} \frac{\partial v_\theta}{\partial \phi}\right) + \rho_c g_\phi \qquad (2.3)$$

where:

$$\nabla^2 = \frac{1}{r^2} \frac{\partial}{\partial r} \left(r^2 \frac{\partial}{\partial r}\right) + \frac{1}{r^2 \sin\theta} \frac{\partial}{\partial \theta} \left(\sin\theta \frac{\partial}{\partial \theta}\right) + \frac{1}{r^2 \sin^2\theta} \left(\frac{\partial^2}{\partial \phi^2}\right) \qquad (2.4)$$

Using vector notation, equations (2.1) to (2.3) can be written as:

$$\rho_c \frac{D\underline{v}}{Dt} = -\underline{\nabla} P_c + \mu_c \nabla^2 \underline{v} + \rho_c \underline{g} \qquad (2.5)$$

where:
$$\underline{\nabla} = \frac{\partial}{\partial r} \underline{e}_r + \frac{1}{r} \frac{\partial}{\partial \theta} \underline{e}_\theta + \frac{1}{r \sin\theta} \frac{\partial}{\partial \phi} \underline{e}_\phi \qquad (2.6)$$

$$\frac{D}{Dt} = \frac{\partial}{\partial t} + (\underline{v} \cdot \underline{\nabla}) \qquad (2.7)$$

If the flow is assumed to be non-viscous, the term $\mu_c \nabla^2 \underline{v}$ in equation (2.5), which is due to the viscosity of the surrounding liquid, may be neglected. Thus, equation (2.5) reduces to:

$$\rho_c \frac{D\underline{v}}{Dt} = -\underline{\nabla} P_c + \rho_c \underline{g} \qquad (2.8)$$

where:
$$\underline{v} = \underline{v}(r, \theta, t)$$
$$P_c = P_c(r, \theta, t)$$

Since the fluid is assumed to be inviscid, the irrotational flow assumption

is permissible which leads to the potential flow assumption and the velocity can be obtained as:

$$\underline{v} = -\underline{\nabla}\,\Phi \tag{2.9}$$

where: $\Phi = \Phi(r, \theta, t)$

The continuity equation in spherical coordinates is:

$$\frac{\partial \rho_c}{\partial t} + \frac{1}{r^2}\frac{\partial}{\partial r}(\rho_c r^2 v_r) + \frac{1}{r \sin\theta}\frac{\partial}{\partial \theta}(\rho_c v_\theta \sin\theta) + \frac{1}{r \sin\theta}\frac{\partial}{\partial \theta}(\rho_c v_\phi) = 0 \tag{2.10}$$

Since the flow is incompressible:

$$\frac{\partial \rho_c}{\partial t} = 0 \tag{2.11}$$

and using vector notation, equation (2.10) can be written as:

$$\underline{\nabla}.\underline{v} = 0 \tag{2.12}$$

Using equation (2.9) in equation (2.12), we obtain:

$$\nabla^2 \Phi = 0 \tag{2.13}$$

which is the Laplace equation. Equation (2.13) can be solved for an expanding and translating boundary motion separately, and superposition of the two solutions gives the solution for the simultaneous motions. This approach was used by L'Ecuyer (39) for the growing bubble at a submerged orifice. First we consider an expanding spherical boundary. Solution

of equation (2.13), in this case, is in the form of:

$$\Phi_1(r, t) = \frac{a_1}{r} + b_1 \tag{2.14}$$

The boundary conditions are:

$$\left.\begin{aligned} r &= R \quad , \quad v_r = \frac{dR}{dt} \\ r &\to \infty \quad , \quad v \to 0 \end{aligned}\right\} \tag{2.15}$$

Using the above conditions in equation (2.14), we obtain:

$$\left.\begin{aligned} a_1 &= R^2 \frac{dR}{dt} \\ \text{and:} \qquad b_1 &= 0 \end{aligned}\right\} \tag{2.16}$$

Substituting in equation (2.14), we obtain:

$$\Phi_1(r, t) = \frac{R^2}{r} \frac{dR}{dt} \tag{2.17}$$

For a translating spherical boundary, solution of equation (2.13) is:

$$\Phi_2(r, \theta, t) = \left(a_2 r + \frac{b_2}{r^2}\right) \cos \theta \tag{2.18}$$

The boundary conditions in this case are:

$$\left.\begin{aligned} r &= R \quad , \quad v_r = U \cos \theta \\ r &\to \infty \quad , \quad v \to 0 \end{aligned}\right\} \tag{2.19}$$

where U is the rise velocity of the system. From equation (2.18), we obtain:

$$v_r = -\frac{\partial \Phi_2}{\partial r} = -\left(a_2 - \frac{2b_2}{r^3}\right) \cos\theta \tag{2.20}$$

$$v_\theta = -\frac{1}{r}\frac{\partial \Phi_2}{\partial \theta} = +\left(a_2 + \frac{b_2}{r^3}\right) \sin\theta \tag{2.21}$$

Considering the boundary conditions (2.19), we obtain:

$$\left.\begin{aligned} a_2 &= 0 \\ \text{and:} \quad b_2 &= \tfrac{1}{2} U R^3 \end{aligned}\right\} \tag{2.22}$$

thus:
$$\Phi_2(r, \theta, t) = \tfrac{1}{2} U \frac{R^3}{r^2} \cos\theta \tag{2.23}$$

Superposition of solutions (2.17) and (2.23) yields:

$$\Phi = \frac{R^2}{r}\frac{dR}{dt} + \tfrac{1}{2} U \frac{R^3}{r^2} \cos\theta \tag{2.24}$$

which is the potential flow field around a translating and expanding spherical boundary in a quiescent medium.

Using the operator defined in equation (2.7), the left hand side of equation (2.8) can be written as:

$$\begin{aligned} \frac{D\underline{v}}{Dt} &= \frac{\partial \underline{v}}{\partial t} + (\underline{v}\cdot\underline{\nabla})\,\underline{v} \\ &= \frac{\partial \underline{v}}{\partial t} + \tfrac{1}{2}\,\underline{\nabla}\,(\underline{v}\cdot\underline{v}) - \underline{v}\times(\underline{\nabla}\times\underline{v}) \end{aligned} \tag{2.25}$$

Since for the irrotational flow, $\underline{v}\times(\underline{\nabla}\times\underline{v}) = 0$, we obtain:

$$\frac{D\underline{v}}{Dt} = \frac{\partial \underline{v}}{\partial t} + \underline{\nabla} \left(\frac{v^2}{2}\right) \tag{2.26}$$

Substituting equation (2.26) in equation (2.8), we obtain:

$$\rho_c \left[\frac{\partial \underline{v}}{\partial t} + \underline{\nabla} \left(\frac{v^2}{2}\right)\right] = - \underline{\nabla} P_c + \rho_c \underline{g} \tag{2.27}$$

Using equation (2.9) in equation (2.27), we obtain:

$$\underline{\nabla} \left[- \frac{\partial \Phi}{\partial t} + \frac{v^2}{2} + \frac{P_c}{\rho_c}\right] = \underline{g} \tag{2.28}$$

Using the following boundary conditions:

$$\text{at } r \to \infty \quad , \quad \left.\begin{array}{l} P_c \to P_{s\infty} \\ v \to 0 \end{array}\right\} \tag{2.29}$$

integration of equation (2.28) yields:

$$- \frac{\partial \Phi}{\partial t} + \frac{v^2}{2} + \frac{P_c - P_{s\infty}}{\rho_c} = 0 \tag{2.30}$$

where $P_{s\infty}$ is the pressure far from the bubble-droplet system and is equal to the hydrostatic pressure at the bubble-droplet level. Since the coordinate system is moving, it can be shown that:

$$\frac{dr}{dt} = - U \cos \theta \tag{2.31}$$

and:

$$\frac{d\theta}{dt} = \frac{U}{r} \sin \theta \tag{2.32}$$

Using these relations, the differentiation of equation (2.24) yields:

$$\frac{\partial \Phi}{\partial t} = \frac{2R}{r}\left(\frac{dR}{dt}\right)^2 + \frac{R^2}{r}\frac{d^2R}{dt^2} + \frac{1}{2}\frac{R^3}{r^2}\frac{dU}{dt}\cos\theta +$$

$$\frac{5}{2}U\frac{R^2}{r^2}\cos\theta\frac{dR}{dt} + \frac{1}{2}U^2\frac{R^3}{r^3}(2\cos^2\theta - \sin^2\theta) \qquad (2.33)$$

The velocity components v_r and v_θ are calculated as:

$$v_r = -\frac{\partial \Phi}{\partial r} = \frac{R^2}{r^2}\frac{dR}{dt} + U\frac{R^3}{r^3}\cos\theta \qquad (2.34)$$

and:
$$v_\theta = -\frac{1}{r}\frac{\partial \Phi}{\partial \theta} = \frac{1}{2}U\frac{R^3}{r^3}\sin\theta \qquad (2.35)$$

The velocity component v is obtained from:

$$v^2 = v_r^2 + v_\theta^2 \qquad (2.36)$$

Substituting equations (2.33) to (2.36) in equation (2.30), we obtain:

$$\frac{P_c - P_{s\infty}}{\rho_c} = \frac{2R}{r}\left(\frac{dR}{dt}\right)^2 + \frac{R^2}{r}\frac{d^2R}{dt^2} + \frac{1}{2}\frac{R^3}{r^2}\frac{dU}{dt}\cos\theta +$$

$$\frac{5}{2}U\frac{R^2}{r^2}\cos\theta\frac{dR}{dt} + \frac{1}{2}U^2\frac{R^3}{r^3}(2\cos^2\theta - \sin^2\theta) -$$

$$\frac{1}{2}\left(\frac{R^2}{r^2}\frac{dR}{dt} + U\frac{R^3}{r^3}\cos\theta\right)^2 - \frac{1}{8}\left(U\frac{R^3}{r^3}\sin\theta\right)^2 \qquad (2.37)$$

At $r = R$, we obtain:

$$\frac{P_c - P_{s\infty}}{\rho_c} = R\frac{d^2R}{dt^2} + \frac{3}{2}\left(\frac{dR}{dt}\right)^2 + \frac{3}{2}U\cos\theta\cdot\frac{dR}{dt} +$$

$$\frac{1}{2}R\frac{dU}{dt}\cos\theta + \frac{U^2}{2}\left(1 - \frac{9}{4}\sin^2\theta\right) \qquad (2.38)$$

The mean pressure around the system may be calculated as:

$$\overline{P}(R, t) = \frac{\int_A P_c(R, \theta, t)\, dA}{\int_A dA} \tag{2.39}$$

where dA is an element of area on the surface of the sphere and is equal to:

$$dA = R^2 \sin\theta\, d\theta\, d\phi \tag{2.40}$$

The results of integration over an area specified by θ is:

$$\frac{\overline{P}(R, t) - P_{s\infty}}{\rho_c} = R\frac{d^2R}{dt^2} + \frac{3}{2}\left(\frac{dR}{dt}\right)^2 + U^2\left(-\frac{1}{4} + \frac{3}{8}\cos\theta + \frac{3}{8}\cos^2\theta\right) +$$

$$\frac{3}{4}U\frac{dR}{dt}(1 + \cos\theta) + \frac{1}{4}R\frac{dU}{dt}(1 + \cos\theta) \tag{2.41}$$

When $\theta = \pi$, we obtain:

$$\frac{\overline{P}(R, t) - P_{s\infty}}{\rho_c} = R\frac{d^2R}{dt^2} + \frac{3}{2}\left(\frac{dR}{dt}\right)^2 - \frac{U^2}{4} \tag{2.42}$$

The mean pressure outside the bubble may be related to the pressure inside as:

$$P - \overline{P} = \frac{2\sigma}{R} + 4\mu_c\frac{1}{R}\frac{dR}{dt} \tag{2.43}$$

where P is the pressure in the bubble-droplet system and is equal to the vaporisation pressure of the dispersed phase liquid. σ is the interfacial tension at the boundary, and μ is the viscosity of the surrounding liquid. It can be seen that, although the viscous terms were neglected in the momentum equation, viscosity appears in the pressure boundary condition (37). A combination of equations (2.42) and (2.43) yields:

$$\frac{P - P_{s\infty}}{\rho_c} = R\frac{d^2R}{dt^2} + \frac{3}{2}\left(\frac{dR}{dt}\right)^2 + \frac{2\sigma}{\rho_c R} + 4\,\mu_c\,\frac{1}{\rho_c R}\frac{dR}{dt} - \frac{U^2}{4} \qquad (2.44)$$

Rearranging equation (2.44), we obtain:

$$\frac{d^2R}{dt^2} = \frac{P - P_{s\infty}}{\rho_c R} - \frac{3}{2R}\left(\frac{dR}{dt}\right)^2 - \frac{2\sigma}{\rho_c R^2} - 4\,\mu_c\,\frac{1}{\rho_c R^2}\frac{dR}{dt} + \frac{U^2}{4R} \qquad (2.45)$$

2.2.3.2 Equation of motion of bubble-droplet system

For a bubble or droplet rising in a liquid with its terminal velocity, the magnitude of the resisting force, F, is obtained from:

$$F = C_D \cdot \tfrac{1}{2}\,\rho_c\,U^2\,A \qquad (2.46)$$

where C_D is the drag coefficient, U is the terminal velocity, and A is the projected area perpendicular to the direction of motion. Other forces acting on the system are the buoyancy and the gravity force, which are given in relation to F as:

$$F = \rho_c\,g\,V - m_{oo}\,g \qquad (2.47)$$

where V is the volume, and m_{oo} is the mass of the system. In the case of a growing and accelerating bubble boundary, extra resisting forces are applied on the system. These may be obtained by integrating equation (2.38) over the surface of the sphere. The force acting on an element of area is:

$$dF = P_c(R, \theta, t)\,dA \qquad (2.48)$$

where dA is given in equation (2.40). The resulting force along the z-axis (Figure 2.1) is calculated from:

$$dF_n = - P_c(R, \theta, t) \cos \theta \cdot dA \tag{2.49}$$

Thus the total force on the system is obtained by integrating over the entire surface. Thus:

$$F_n = \int_{\phi=0}^{2\pi} d\phi \int_{\theta=0}^{\pi} - P_c(R, \theta, t) R^2 \sin \theta \cos \theta \, d\theta \tag{2.50}$$

Substituting equation (2.38) in equation (2.50) and performing the integration, we obtain:

$$F_n = \frac{4}{3} \pi R^3 \rho_c g - 2 \pi \rho_c U R^2 \frac{dR}{dt} - \frac{2}{3} \pi \rho_c R^3 \frac{dU}{dt} \tag{2.51}$$

The first term in equation (2.51) is the buoyancy force and the last two terms are due to the growth and acceleration of the system, respectively. Using equation (2.51), the Newtonian law for the bubble-droplet system can be written as:

$$m_{oo} \frac{dU}{dt} = -m_{oo} g + \frac{4}{3} \pi R^3 \rho_c g - 2 \pi \rho_c U R^2 \frac{dR}{dt} - \frac{2}{3} \pi \rho_c R^3 \frac{dU}{dt} - \frac{\pi}{2} \rho_c R^2 U^2 C_D \tag{2.52}$$

where m_{oo} is equal to the initial mass of the droplet. Rearranging equation (2.52), we obtain:

$$\frac{dU}{dt} = \frac{1}{(m_{oo} + \frac{2\pi}{3} \rho_c R^3)} \left(-m_{oo} g + \frac{4}{3} \pi R^3 \rho_c g - 2 \pi \rho_c U R^2 \frac{dR}{dt} - \frac{\pi}{2} \rho_c R^2 U^2 C_D\right) \tag{2.53}$$

2.2.3.3 Energy equation

Heat transfer to the bubble-droplet system during the interval of time dt is equal to the heat of evaporation. Thus:

$$q = h A (T_c - T) = - h_{fg} \frac{dm_l}{dt} \tag{2.54}$$

where h is the overall instantaneous heat transfer coefficient between the bulk of the surrounding liquid and the vaporising layer of liquid droplet, m_l is the mass of the unevaporated liquid, T is the boiling temperature of the evaporating liquid, and T_c is the temperature of the surrounding liquid. For a spherical system, equation (2.54) can be written as:

$$4 \pi R^2 h (T_c - T) = - h_{fg} \frac{dm_l}{dt} \tag{2.55}$$

If h_{fg} is considered constant during dt, differentiation of equation (2.55) and rearranging yields:

$$\frac{dT}{dt} = \frac{2}{R} (T_c - T) \frac{dR}{dt} + \frac{1}{4\pi} \frac{h_{fg}}{h} \frac{1}{R^2} \frac{d^2 m_l}{dt^2} + (T_c - T) \frac{1}{h} \frac{dh}{dt} \tag{2.56}$$

2.2.3.4 Equation of state

The vapour-pressure relation of the evaporating substance can be used for the determination of pressure at the existing temperature. Here, the following equation is used (13) (see Appendix D):

$$\log_{10} P = \frac{1}{2T} (b_o - b_2) \tag{2.57}$$

where b_o and b_2 can be calculated using the procedure in reference (13).

Differentiation of equation (2.57) yields:

$$\frac{dP}{dt} = \frac{ln\ 10}{2} \frac{P}{T^2} \left[T \left(\frac{db_o}{dt} - \frac{db_2}{dt} \right) - (b_o - b_2) \frac{dT}{dt} \right]$$

$$= f(P, T, \frac{dT}{dt}) \qquad (2.58)$$

2.2.3.5 Equation of conservation of mass

Since the transfer of mass across the system boundary is assumed to be negligible, thus the total mass of the bubble-droplet system can be assumed constant and the same as the initial mass of the droplet, m_{oo}. For the vapour bubble, we can write:

$$\rho_v = \frac{m_v}{V_v} \qquad (2.59)$$

and:

$$m_v = m_{oo} - m_l \qquad (2.60)$$

For the spherical system, we can write:

$$V_v = \frac{4}{3} \pi R^3 - \frac{m_l}{\rho_l} \qquad (2.61)$$

where the index l refers to the liquid. Combining equation (2.59) to equation (2.61), we obtain:

$$m_l = \frac{m_{oo} - \frac{4}{3} \pi R^3 \rho_v}{1 - (\rho_v / \rho_l)} \qquad (2.62)$$

Neglecting changes of ρ_v and ρ_l, differentiation of equation (2.62) and its combination with equation (2.55) yields:

$$\frac{dR}{dt} = \frac{\rho_l - \rho_v}{\rho_l \rho_v h_{fg}} h (T_c - T) \tag{2.63}$$

Also, by differentiation of equation (2.62) twice, we obtain:

$$\frac{d^2 m_l}{dt^2} = - \frac{4 \pi \rho_v \rho_l}{\rho_l - \rho_v} \left[2 R \left(\frac{dR}{dt}\right)^2 + R^2 \frac{d^2 R}{dt^2} \right] \tag{2.64}$$

2.2.4 Set of Equations

Equations (2.45), (2.53), (2.56), (2.58), (2.63) and (2.64) describe the evaporation of an ascending spherical bubble-droplet in an immiscible liquid.

By assuming:

$$\frac{dR}{dt} = X \tag{2.65}$$

equation (2.45) is transformed into a first order ordinary differential equation. In this case, X is calculated from equation (2.63).

Introducing the variable Z for the height of bubble-droplet in the column, we have:

$$\frac{dZ}{dt} = U \tag{2.66}$$

Summing up the governing equations, we get:

$$\frac{dR}{dt} = X \tag{2.65}$$

$$\frac{dZ}{dt} = U \tag{2.66}$$

$$\frac{dX}{dt} = \frac{P - P_{s\infty}}{\rho_c R} - \frac{3}{2R} \left(\frac{dR}{dt}\right)^2 - \frac{2\sigma}{\rho_c R^2} - 4 \mu_c \frac{1}{\rho_c R^2} \frac{dR}{dt} + \frac{U^2}{4R} \tag{2.67}$$

$$\frac{dU}{dt} = \frac{1}{(m_{oo} + \frac{2}{3}\pi \rho_c R^3)} (-m_{oo} g + \frac{4}{3}\pi R^3 \rho_c g - 2\pi \rho_c U R^2 \frac{dR}{dt} - \frac{\pi}{2}\rho_c R^2 U^2 C_D) \quad (2.53)$$

$$\frac{dT}{dt} = \frac{2}{R}(T_c - T)\frac{dR}{dt} + \frac{1}{4\pi}\frac{h_{fg}}{h}\frac{1}{R^2}\frac{d^2m_l}{dt^2} + (T_c - T)\frac{1}{h}\frac{dh}{dt} \quad (2.56)$$

$$\frac{dP}{dt} = f(P, T, \frac{dT}{dt}) \quad (2.58)$$

where:
$$X = \frac{\rho_l - \rho_v}{\rho_l \rho_v h_{fg}} h (T_c - T) \quad (2.68)$$

and:
$$\frac{d^2m_l}{dt^2} = -\frac{4\pi \rho_v \rho_l}{\rho_l - \rho_v}\left[2R(\frac{dR}{dt})^2 + R^2 \frac{d^2R}{dt^2}\right] \quad (2.64)$$

2.3 SOLUTION OF THE GOVERNING EQUATIONS

Equations (2.53), (2.56), (2.58), (2.65), (2.66) and (2.67) are a system of six first order ordinary differential equations with respect to time. These are solved simultaneously by a numerical method using a CDC 6400 computer. A library subroutine which was available in ICCC (see also Section 7.2.1 of Chapter 7) was used to solve the system of equations. The method of solution was based on ideas given by Gear (21). This procedure was primarily intended for a "stiff" system of equations and it was found to be suitable because of a comparatively short computation time. This routine chooses the step size and the order of the method to try to obtain the specified accuracy with minimum computation. The local error is controlled by varying the step-size and order. The maximum order is six, i.e. a local error of order h^6 (h, here, is the step size). Error bounds were set for each variable and an absolute test was made. This subroutine was used as a part of the main computer program which is explained in Chapter 7. The integration was carried out over the specified

step length which was chosen according to the case of study. The result of integration was proved to be not very sensitive to the step length.

Properties of the dispersed phase (which were written as functions of temperature) were calculated at the beginning of each step, dt, and were kept constant during this time.

Computation started from the initial conditions and terminated either when the mass of the liquid in the droplet was all evaporated, or when the bubble-droplet reached the water surface.

2.3.1 Initial Conditions

In order to solve the system of equations, the initial conditions (at $t = 0$) are necessary. These are:

$$\begin{aligned} R(0) &= R_o \\ Z(0) &= Z_o \\ X(0) &= X_o \\ U(0) &= U_o \\ T(0) &= T_o \\ P(0) &= P_o \end{aligned} \tag{2.69}$$

In cases where the experimental data were available, the initial conditions were specified accordingly (Chapter 5); otherwise, as it is the case for the results which follows in this chapter, they were assumed to have a certain value or were calculated from the available formulae as follows. Time zero was assumed as the time when evaporation has already proceeded and the percentage of evaporation is 0.5%. The initial radius, R_o, can be specified from the following relation:

$$R = \left(\frac{d}{2}\right)\left[1 + \xi\left(\frac{\rho_l}{\rho_v} - 1\right)\right]^{1/3} \qquad (2.70)$$

in which ξ is the vaporisation ratio and, in this case, is equal to 0.005. The bubble-droplet is assumed to be at level zero at $t = 0$. The value of initial growth rate (X_o) is calculated from equation (2.68). To obtain the initial velocity (U_o), the bubble-droplet is assumed to have the same velocity as a droplet and its value is obtained from the formula proposed by Klee et al (35). The initial temperature, T_o, is assumed to be 1.0°C and the initial pressure, P_o, is calculated accordingly (for the effect of different values of T_o, see Section 2.4.4).

2.3.2 Additional Information

Additional information was necessary for the solution of the governing equations, e.g. properties of the dispersed phase and of the continuous phase, instantaneous heat transfer coefficient, instantaneous drag coefficient, and interfacial tension between the vapour of the dispersed phase and the liquid of the continuous phase.

(a) Properties of the liquids: Published properties of the dispersed phase and of the continuous phase were used. This information is given in the form of correlations in Appendix C, which includes the procedure adopted for the calculation of the interfacial tension between the dispersed phase vapour and the continuous phase liquid. The vapour density is obtained from a method described in reference (2) (see Appendix B).

(b) Instantaneous heat transfer coefficient: The heat transfer coefficient in equation (2.56) is the overall instantaneous coefficient. This is calculated from the present experimental results, Simpson's model (equation (1.11)) and Sideman's model (equation (1.15)). In equation (2.56), variation of the heat transfer coefficient against time is needed. Equation (1.15) can be written as:

$$h = C_1 \left(\frac{U}{R}\right)^{0.5} \tag{2.71}$$

where:
$$C_1 = 0.192 \left(\rho_c C_{p_c} k_c\right)^{0.5} \tag{2.72}$$

Thus:
$$\frac{dh}{dt} = C_1 \frac{1}{2R} \left[\left(\frac{R}{U}\right)^{0.5} \frac{dU}{dt} - \left(\frac{U}{R}\right)^{0.5} \frac{dR}{dt}\right] \tag{2.73}$$

and for the case when equation (1.11) is used, we have:

$$\frac{dh}{dt} = \frac{1}{G_2} \frac{dG_1}{dt} - \frac{G_1}{G_2^2} \frac{dG_2}{dt} \tag{2.74}$$

where:
$$G_1 = 2.57 \left(\frac{D}{d}\right)^{1/6} \tag{2.75}$$

$$G_2 = 1 + 0.206 \left(\frac{D}{d}\right)^{5/12} \tag{2.76}$$

$$\frac{dG_1}{dt} = 0.4808\, d^{-1/6}\, R^{-5/6} \frac{dR}{dt} \tag{2.77}$$

and:
$$\frac{dG_2}{dt} = 0.1146\, d^{-5/12}\, R^{-7/12} \frac{dR}{dt} \tag{2.78}$$

(c) Drag coefficient: The drag coefficient in equation (2.53) is the instantaneous drag coefficient of a bubble-droplet rising

in an immiscible liquid. Due to the lack of data on drag coefficients for a moving bubble-droplet, we have chosen to use the available data on the motion of gas bubbles in liquids in nearly the same dimensionless number M, which is defined by:

$$M = \frac{g\,\mu^4}{\rho\,\sigma^3} \tag{2.79}$$

For a butane/water combination, and water temperatures of $4^{o}C$ and $10^{o}C$, M_c is about 1.38×10^{-10} and 0.692×10^{-10}, respectively. Thus, the data of Haberman & Morton (24) (Figure 16, curve 11 for air bubbles in filtered cold water for which $M_c = 1.08 \times 10^{-10}$ and curve 12 for air bubbles in methyl alcohol for which $M_c = 0.89 \times 10^{-10}$) were chosen for the butane/water combination. For a pentane/water combination, and water temperatures of $38^{o}C$ and $44^{o}C$, M_c is about 0.08×10^{-10} and 0.06×10^{-10}, respectively. The nearest data for this combination were the ones for air bubbles in filtered water in which $M_c = 0.26 \times 10^{-10}$ (curve 13, Figure 16, reference (24)). For use in the computer program, polynomials of the third to fifth degree were fitted to the above curves. Coefficients of the polynomials and the range of applicability are given in Table 2.1.

For high Reynolds numbers, the drag coefficient becomes constant and equal to 2.6 (24). Thus, when C_D calculated from the above equations reached the value of 2.6, it was taken then equal to 2.6 onwards.

2.4 RESULTS

Results are presented mainly for the butane/distilled water combination.

Two sizes of droplet have been considered; the small size of 1.2 mm and the larger size of 3.5 mm in diameter. In each case, four temperature

TABLE 2.1

Correlations for the Drag Coefficient as a Function of Reynolds Number as Fitted to the Data of Haberman et al (24)

$$C_D = a_1 + a_2 x + a_3 x^2 + a_4 x^3 + a_5 x^4 + a_6 x^5 \quad (2.80)$$

where: $$x = \log_{10} (Re_c/1000) \quad (2.81)$$

Curve Number (Figure 16 (24))	a_1	a_2	a_3	a_4	a_5	a_6	Range
11	0.06361	-0.2125	-0.2749	-0.3579	0	0	$Re_c < 300$
11	1.521	3.882	1.137	-5.789	-5.763	0	$Re_c > 300$ $C_D < 2.6$
12	1.359	3.211	-0.887	-3.235	3.487	0	$Re_c > 300$ $C_D < 2.6$
13	0.2533	0.6269	1.043	-0.07037	0	0	$Re_c < 450$
13	0.9049	3.299	2.978	-0.08157	-3.426	-18.05	$Re_c > 450$ $C_D < 2.6$

differences, namely, ΔT_o = 2°C, 4°C, 6°C and 8°C, have been examined.

The importance of initial velocity and initial temperature has been tested by assuming different values for them. The effect of 5% error on the determination of the drag coefficient has also been studied. The results include a comparison between butane/ and pentane/distilled water combinations.

In the determination of the results, heat transfer coefficients are calculated using the Sideman et al model (68). For the butane/water combination, and water temperatures lower than 6°C, the drag coefficients are obtained from curve 11 (see Table 2.1) and for higher temperatures from curve 12. Since the initial temperature was assumed to be 1°C, the water temperature was then determined using the specified value of the temperature difference ($T_c = T_o + \Delta T_o$). Having the value of initial pressure and neglecting the term $R\,(d^2R/dt^2)$, the hydrostatic head above the droplet was calculated from equation (2.44). Atmospheric pressure was assumed to be 101300 N/m^2.

2.4.1 Effect of Temperature Difference

The results of the evaporation of a small droplet (1.2 mm in diameter) and a larger one (3.5 mm in diameter) for four temperature differences, ΔT_o = 2°C, 4°C, 6°C and 8°C, are shown in Figures 2.2(a) to (1) and 2.3(a) to (1). Figures 2.2(a), (b) and (c) and 2.3(a), (b) and (c), which indicate the variation of diameter ratio, volume and mass ratio versus time, respectively, show that evaporation time is increased with increase of ΔT as was expected. Consequently, the distance travelled by the droplet for the complete evaporation is longer for lower ΔT (Figures 2.2(d) and 2.3(d)). The same trend is predicted for the four cases.

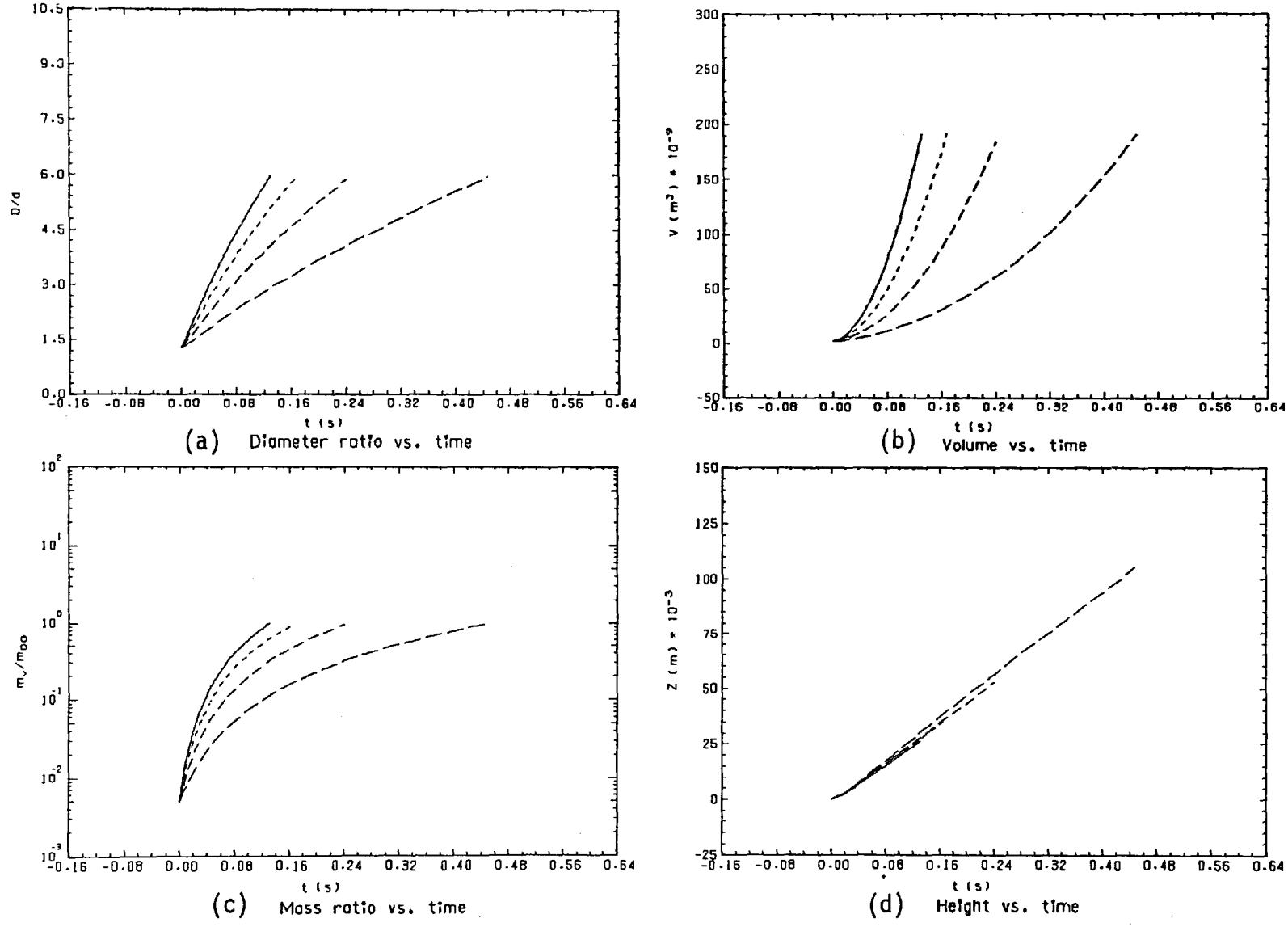

Figure 2.2(a-1): Evaporation of a butane droplet in distilled water, effect of temperature difference, d = 1.2 mm
(——— ΔT_o = 8°C, ------- ΔT_o = 6°C, – – – – ΔT_o = 4°C, — — — ΔT_o = 2°C)

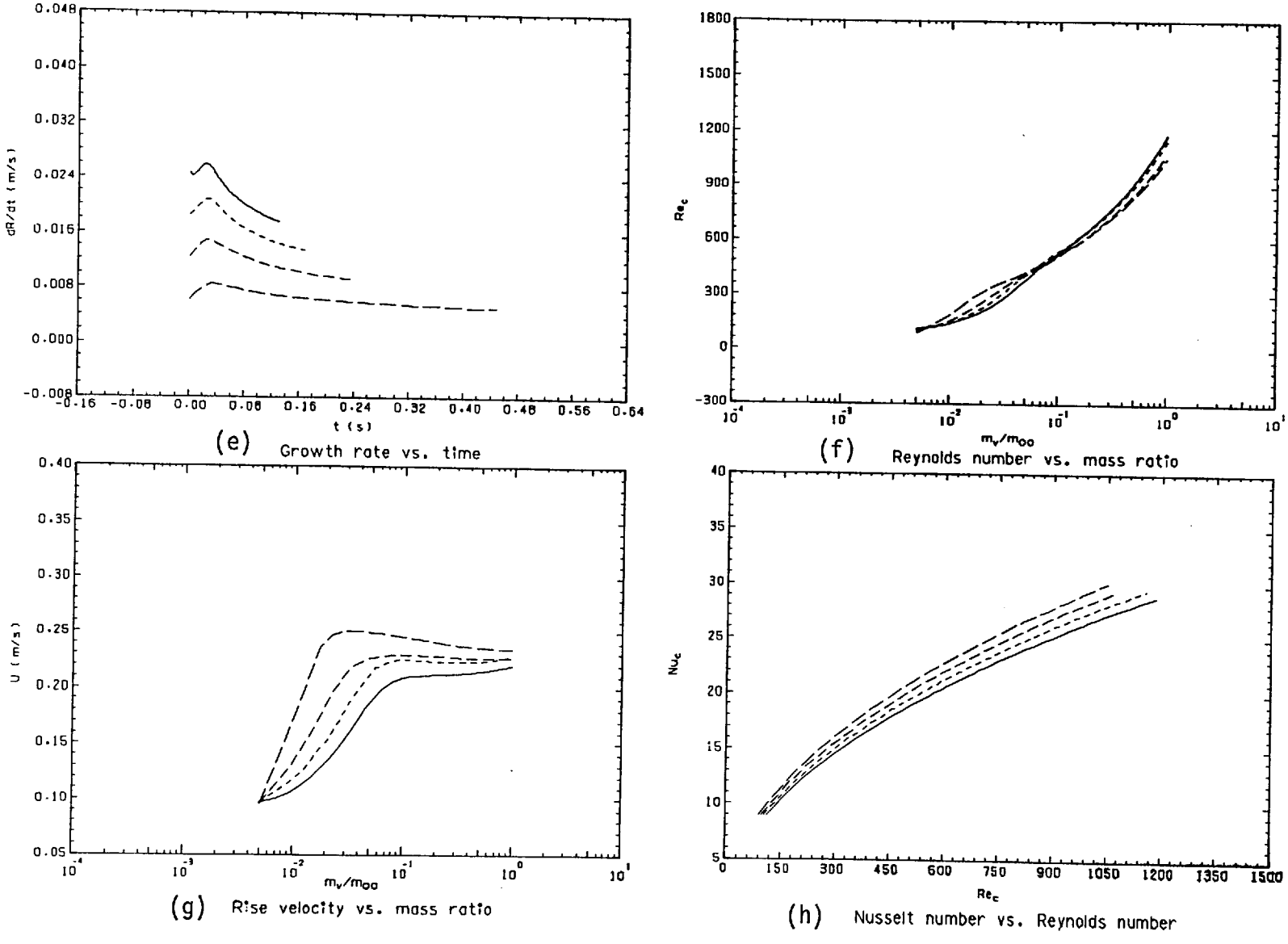

Figure 2.2(a-1) (continued)

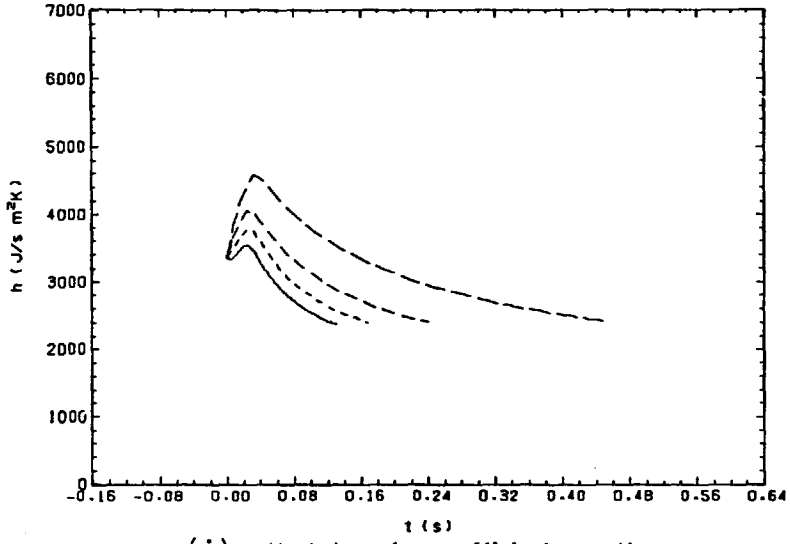

(i) Heat transfer coefficient vs. time

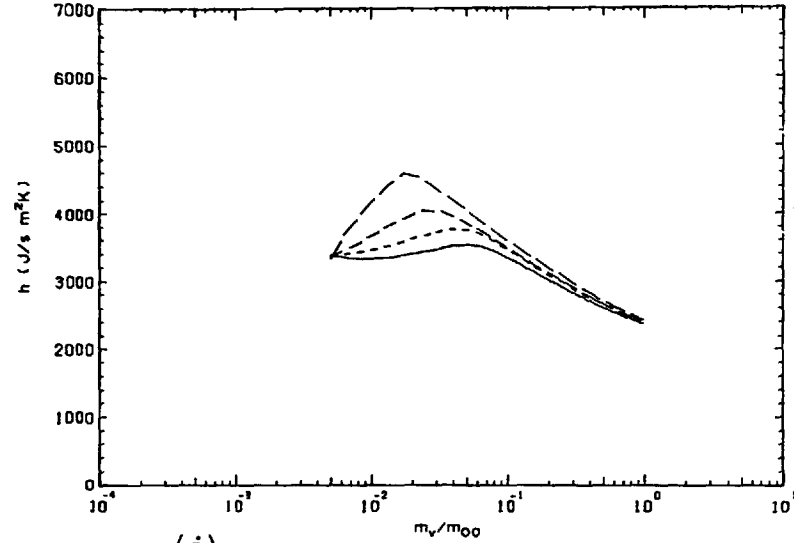

(j) Heat transfer coefficient vs. mass ratio

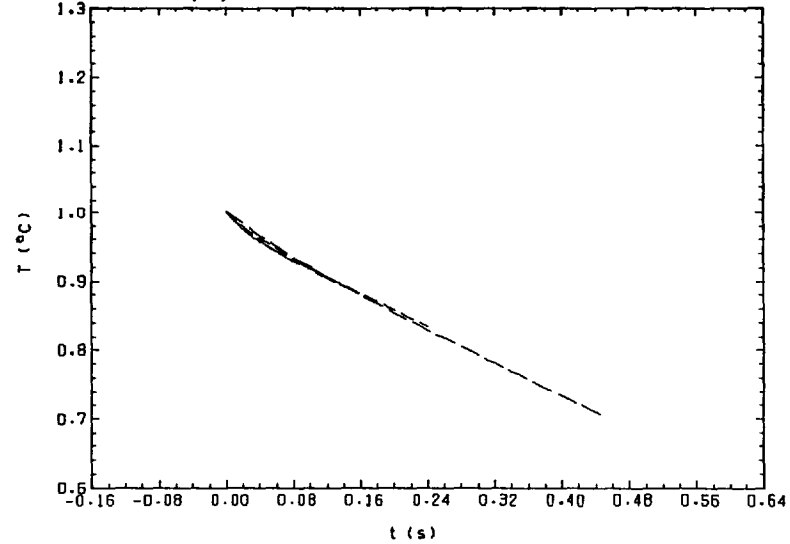

(k) Temperature vs. time

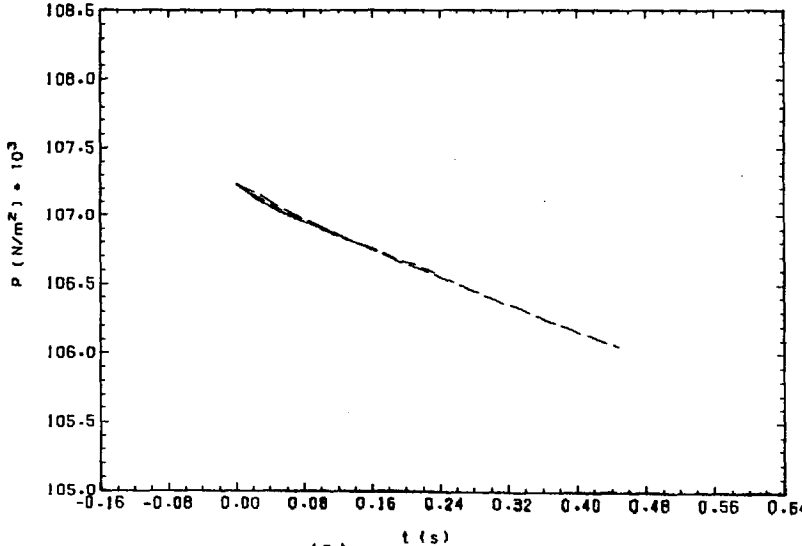

(l) Pressure vs. time

Figure 2.2(a-1) (continued)

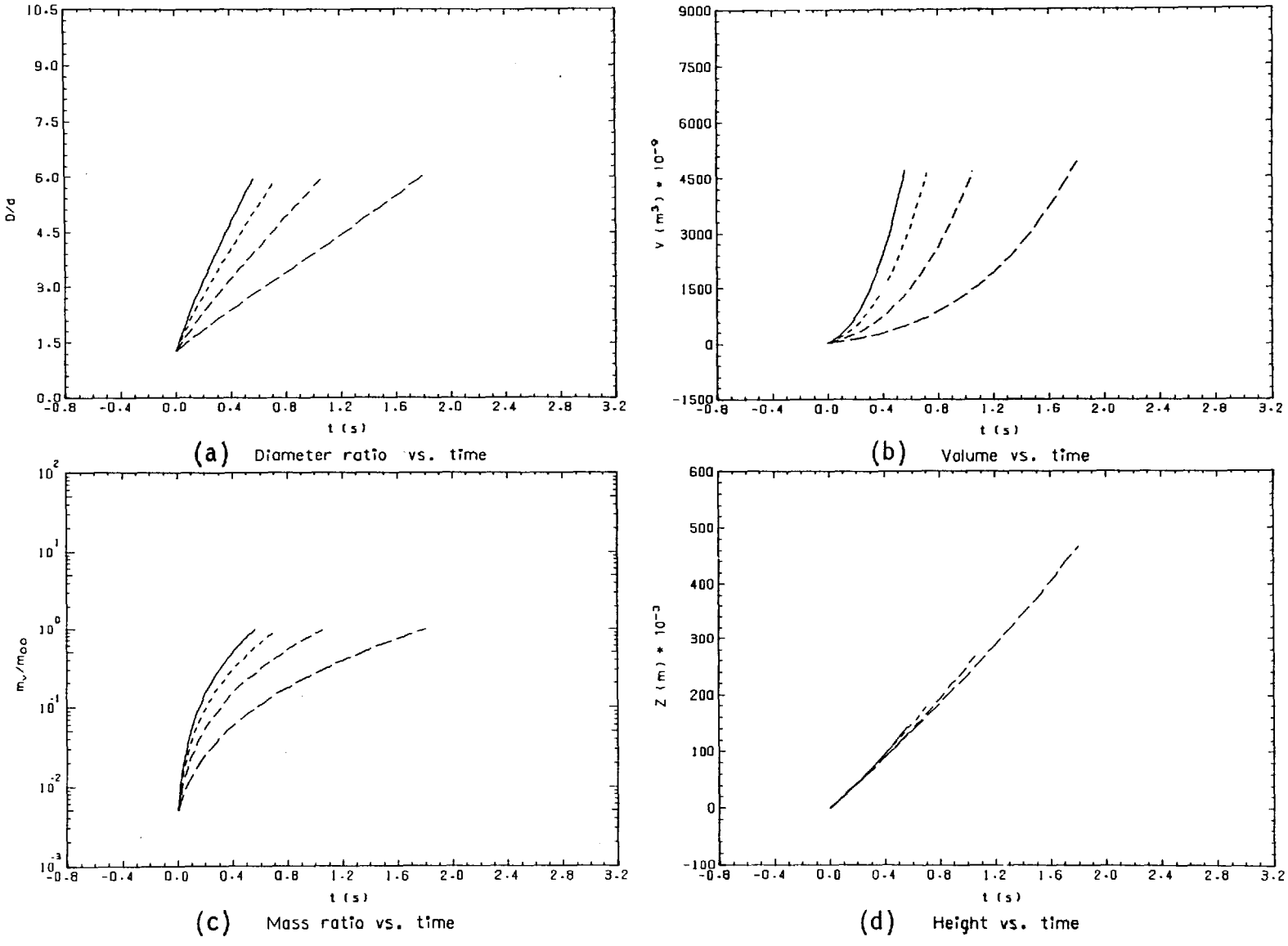

Figure 2.3(a-1): Evaporation of a butane droplet in distilled water, effect of temperature difference, d = 3.5 mm
(——— ΔT_o = 8°C, -------- ΔT_o = 6°C, - - - - - ΔT_o = 4°C, — — — — ΔT_o = 2°C)

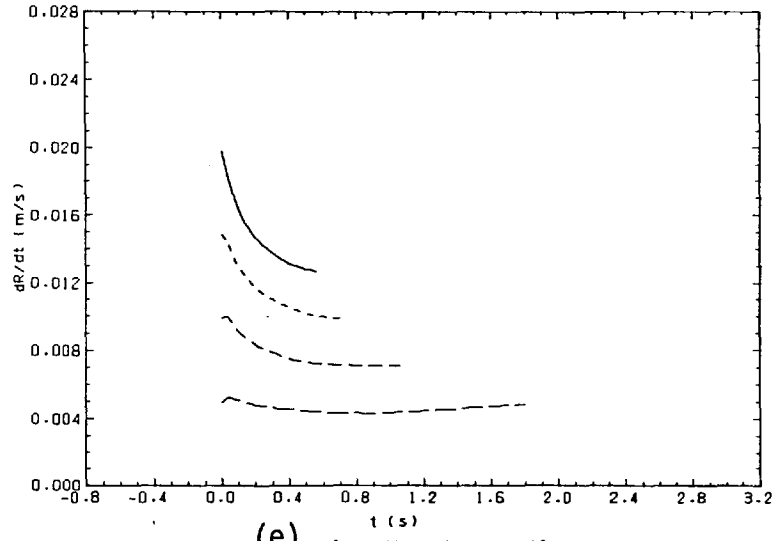

(e) Growth rate vs. time

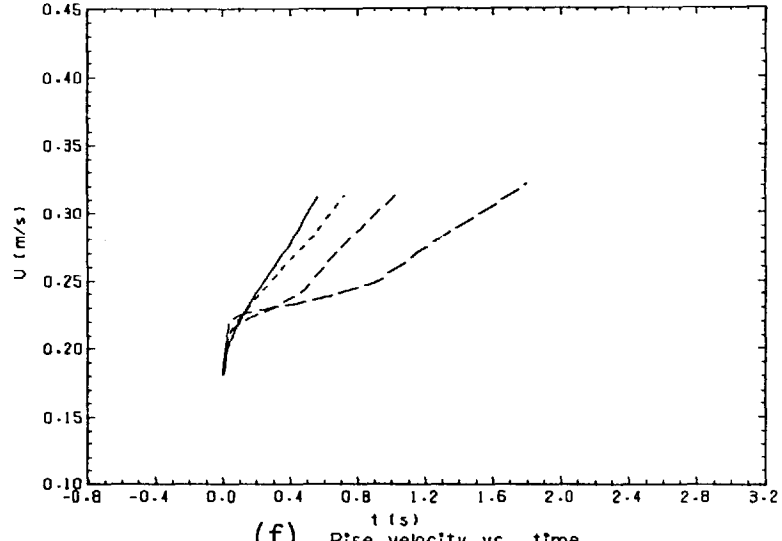

(f) Rise velocity vs. time

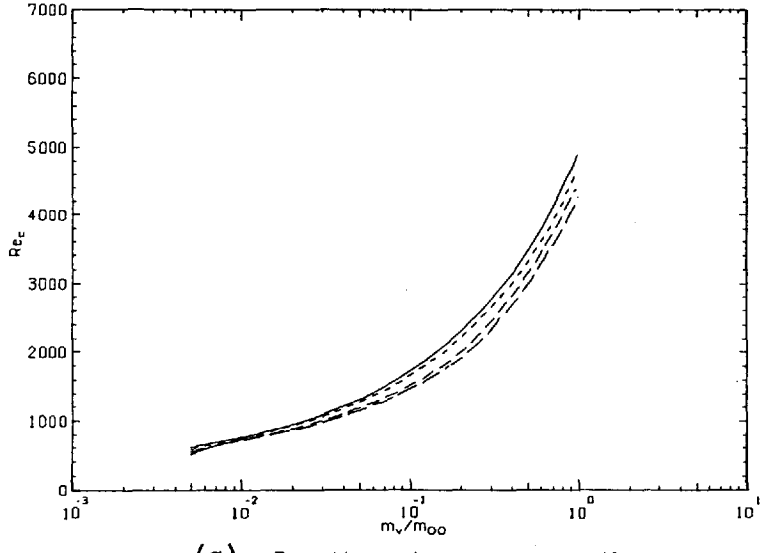

(g) Reynolds number vs. mass ratio

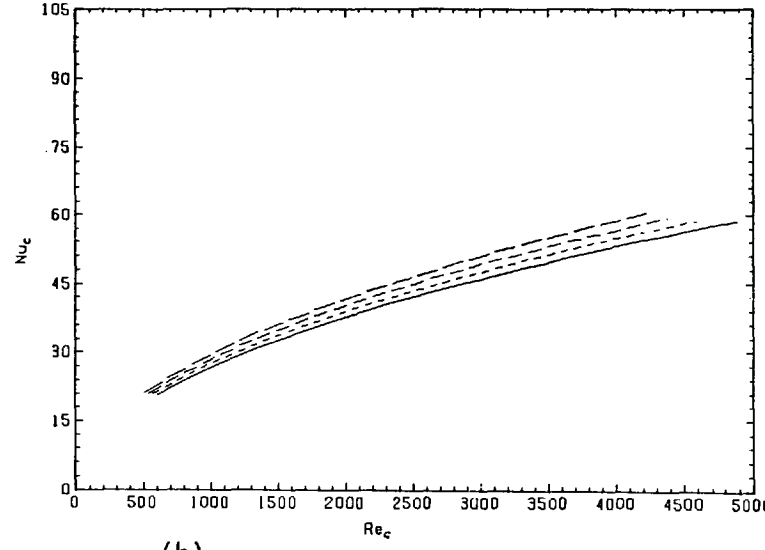

(h) Nusselt number vs. Reynolds number

Figure 2.3(a-l) (continued)

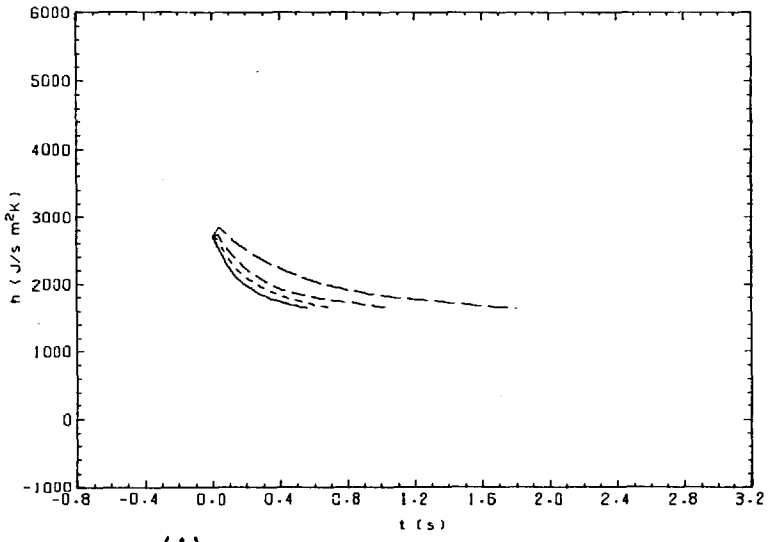

(i) Heat transfer coefficient vs. time

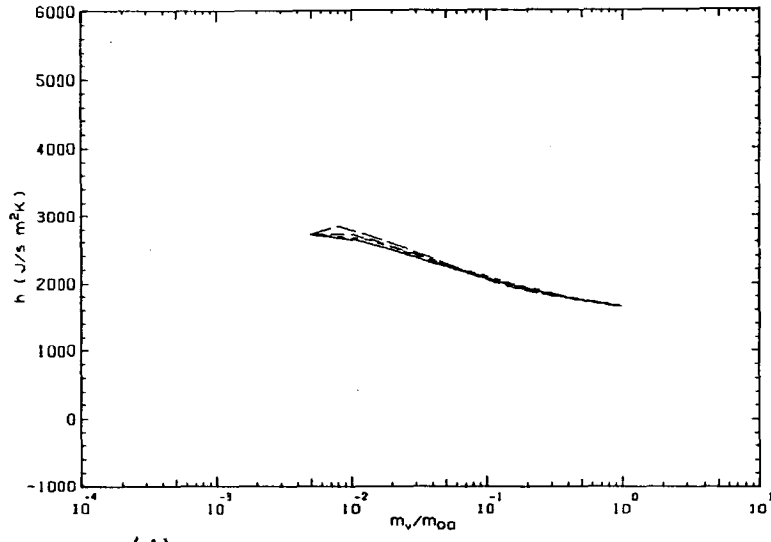

(j) Heat transfer coefficient vs. mass ratio

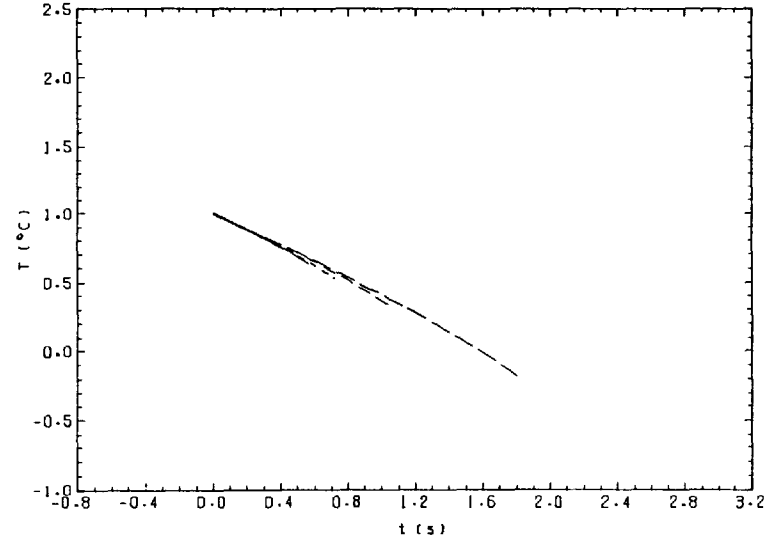

(k) Temperature vs. time

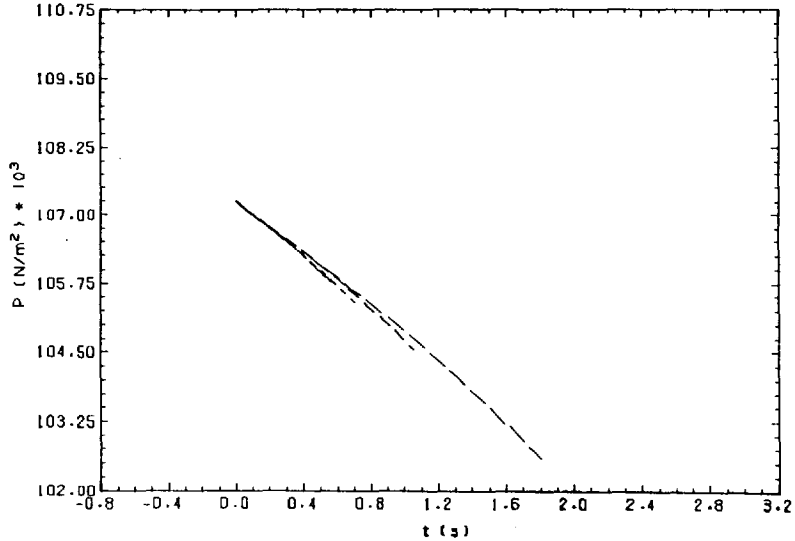

(l) Pressure vs. time

Figure 2.3(a-l) (continued)

Figures 2.2(e) and 2.3(e) show the variation of the growth rate versus time. Higher growth rate has been obtained for higher ΔT. Variation of the growth rate from equation (2.63) depends on the variation of heat transfer coefficient and the temperature difference. Since ΔT increases during the whole process, therefore the heat transfer coefficient is mainly responsible for the type of variation of growth rate. Heat transfer coefficients which are calculated from equation (1.15) is a function of Reynolds number and thus is a function of the rise velocity. Variations of these parameters are shown in Figures 2.2(f) to (j) and 2.3 (f) to (j). Velocity increases sharply in the early stages of evaporation and thus heat transfer coefficient, and consequently the growth rate, behave accordingly. Figure 2.2(e) and 2.3(e) show that the growth rate varies more gradually for lower temperature differences. Nearly the same trend is predicted for smaller and larger droplets. In the former case, rise velocity, after an initial increase, becomes nearly constant (Figure 2.2(g)), while for the latter case slows down after the initial period and, when about 10% evaporation is reached, it continues to rise again (Figure 2.3(f)). A sharp increase of the rise velocity at the beginning should be partly due to the under-estimation of the initial velocity, by assuming the rise velocity of the bubble-droplet to be the same as a droplet having the same dimensions. Lower velocities have been obtained for higher ΔT's due to the higher growth rate. The difference is more distinctive in the early stages and for the case of smaller droplets, since the resisting force due to the growth is comparable to the buoyancy force. The heat transfer coefficient is also lower for higher ΔT and tends to reach the same values in the later stages of evaporation (Figures 2.2(j) and 2.3(j)). In Figures 2.2(h) and 2.3(h), the Nusselt number is plotted against the Reynolds number. Both parameters increase during the whole range. At

the same Reynolds number, lower values are obtained for higher temperature differences. In Figures 2.2(k) and (l) and 2.3(k) and (l), the vaporisation temperature and pressure are plotted against time. As was expected, both parameters decrease as the droplet ascends.

2.4.2 Effect of Initial Droplet Size

The importance of initial droplet size is shown in Figures 2.4(a) to (d), in which three droplet sizes, namely, d = 1.2 mm, 1.6 mm and 2.0 mm, are considered. The temperature difference at t = 0 is assumed to be 2^{o}C. As was expected, longer evaporation time is predicted for larger droplets. The rise velocity increases sharply in the initial period and then flattens. The velocities of the three bubble-droplets coincide in the later stages of evaporation. This is because the dimensions of the bubbles at this stage are in the range where the bubble velocity is independent of the bubble size (86). Since the initial temperature is the same for the three cases, growth rate values and heat transfer coefficients follow the same behaviour (Figures 2.4(b) to (d)).

2.4.3 Effect of Initial Velocity

The effect of initial velocity is tested for a droplet (1.2 mm in diameter and ΔT_o = 2^{o}C) by assuming different initial values, namely, U_o = 0.30 m/s, 0.25 m/s, 0.20 m/s and 0.15 m/s. The results are shown in Figures 2.5(a) to (d). As can be seen, the effect is apparent only in the early period and then the velocities coincide shortly afterwards. The effect on the total evaporation time is insignificant. Growth rate values are also different in the early stages and reach the same values in the later stages of evaporation.

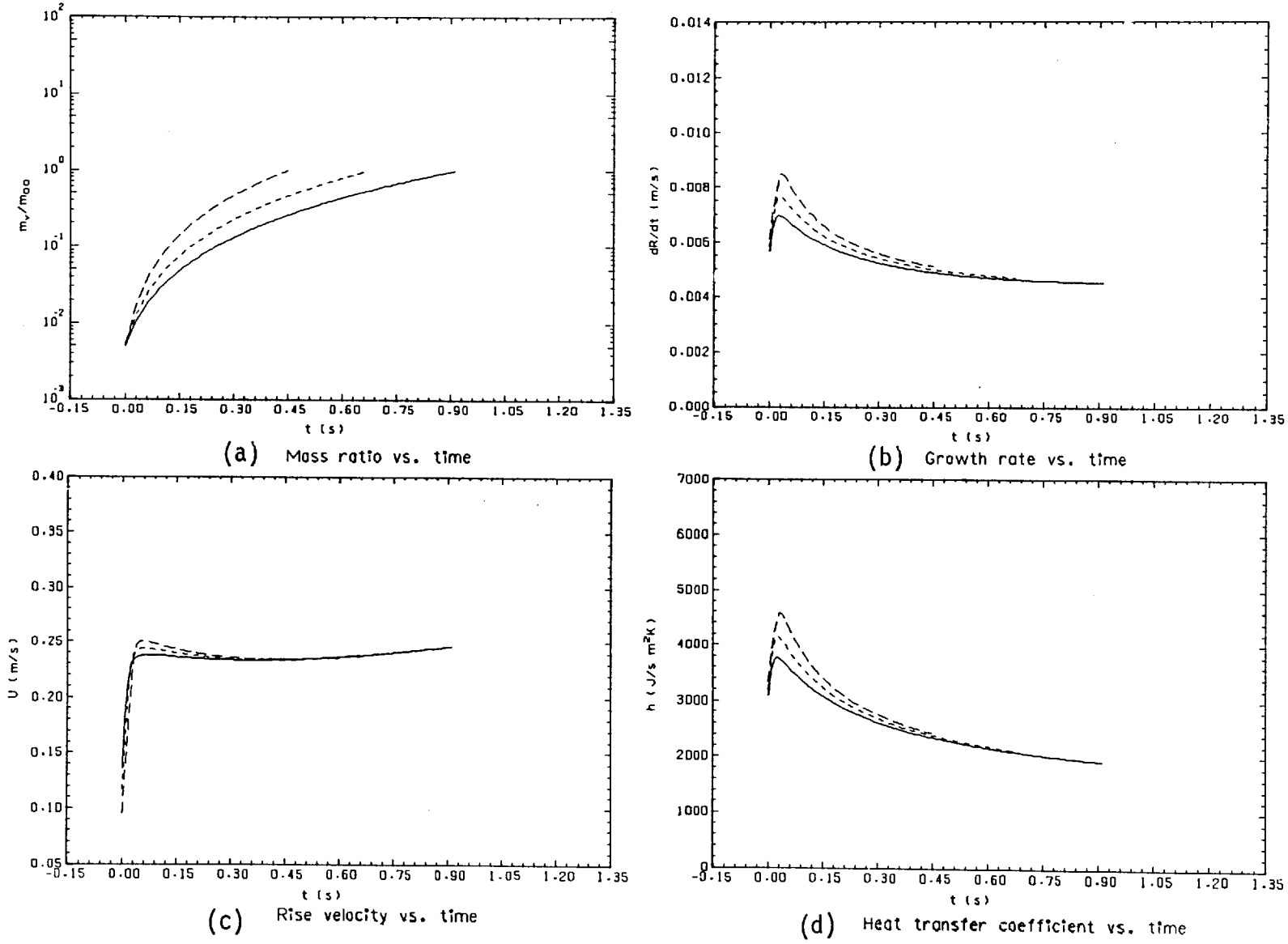

Figure 2.4(a-d): Evaporation of a butane droplet in distilled water, effect of initial droplet size, ΔT_o = 2°C (—— d = 2.0 mm, ------- d = 1.6 mm, – – – – d = 1.2 mm)

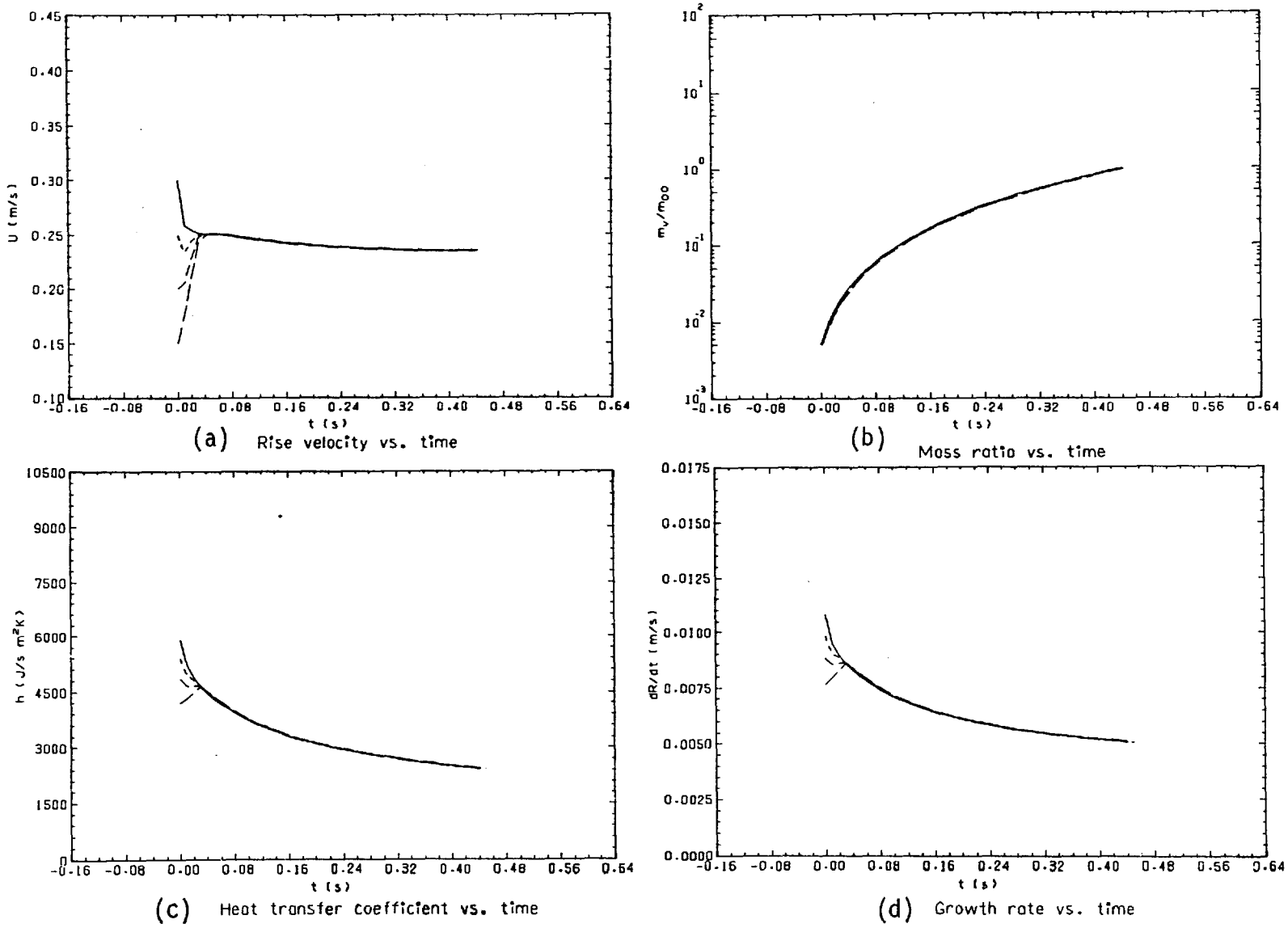

Figure 2.5(a-d): Evaporation of a butane droplet in distilled water, effect of initial velocity, d = 1.2 mm, ΔT_o = 2°C
(——— U_o = 0.30 m/s, ------- U_o = 0.25 m/s, - - - - - U_o = 0.20 m/s, — — — U_o = 0.15 m/s)

2.4.4 Effect of Initial Temperature

Because uncertainty existed in specifying the initial temperature, the effect of this parameter on the others was tested by assuming three values, namely, T_o = 1.5°C, 1.0°C and 0.5°C, while keeping the temperature difference the same and equal to 2.0°C. Consequently, the initial pressure and the hydrostatic head and water temperature were changed accordingly. The results are shown in Figures 2.6(a) to (d). It can be seen that the effect of a change in the initial temperature on the other parameters is insignificant. The variation of temperature against time follows the same trend in the three cases.

2.4.5 Effect of 5% Change in the Drag Coefficient

In order to evaluate the effect of possible error in the determination of the drag coefficient, comparisons were made when this parameter was changed by ± 5%. The results are shown in Figures 2.7(a) to (d). The initial droplet diameter and initial temperature difference in this case are 1.2 mm and 2°C, respectively. Figure 2.7(b) shows that higher velocities are obtained for the lower drag coefficients. Consequently, higher heat transfer coefficients are obtained in this case and the evaporation time is slightly reduced. The effect of a 5% change in the drag coefficients results in a change of about 1.5% in the rise velocity, which may be considered to be small.

2.4.6 Effect of Dispersed Phase Material

Some of the results for the butane/distilled water combination are compared with those for the pentane/distilled water combination (Figures 2.8(a) to (d)). The initial droplet size is the same for the two cases and equal to 1.2 mm in diameter. For each combination, two

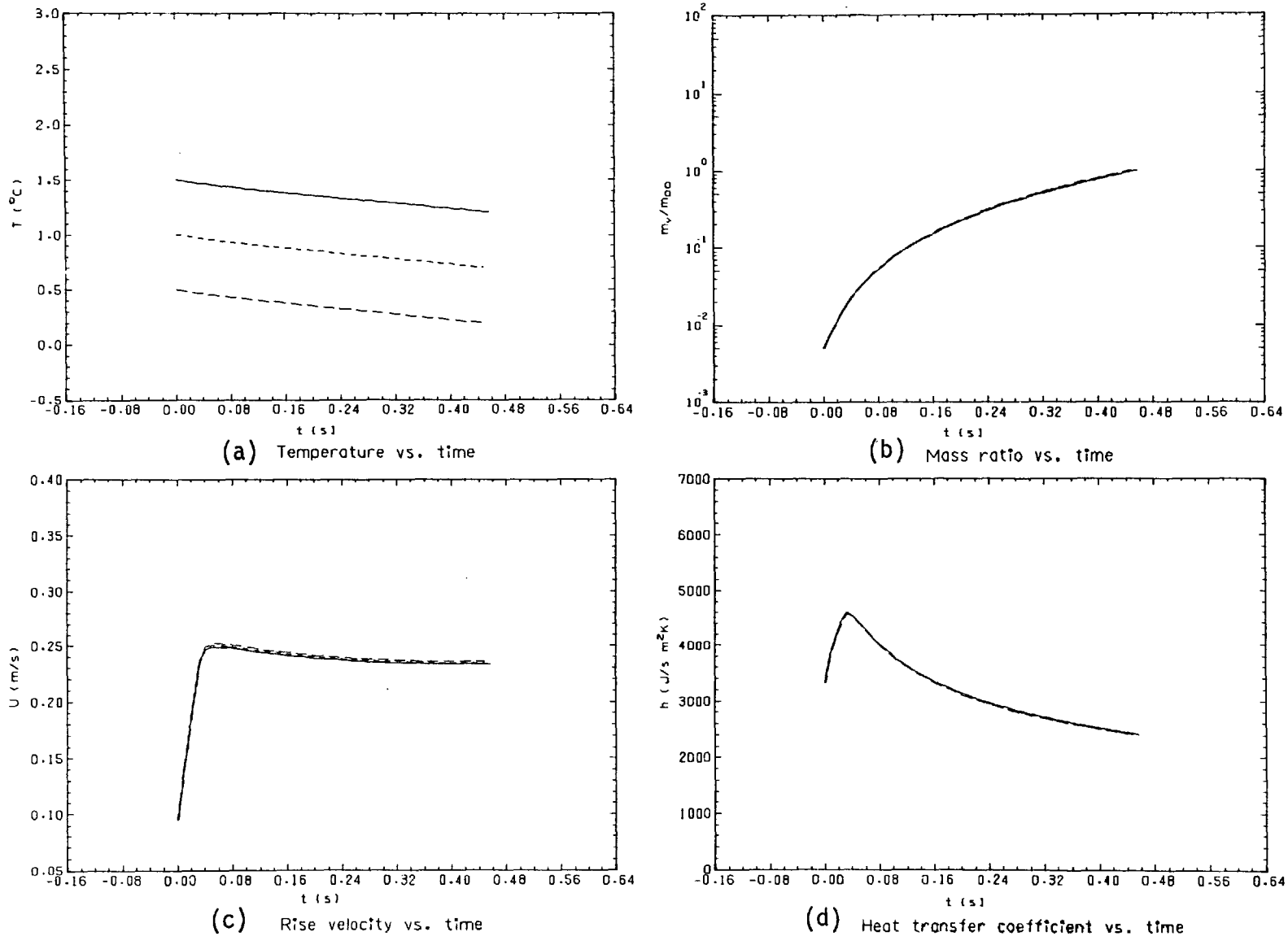

Figure 2.6(a-d): Evaporation of a butane droplet in distilled water, effect of initial temperature, d = 1.2 mm, ΔT_o = 2°C
(——— T_o = 1.5°C, ····· T_o = 1.0°C, - - - - - T_o = 0.5°C)

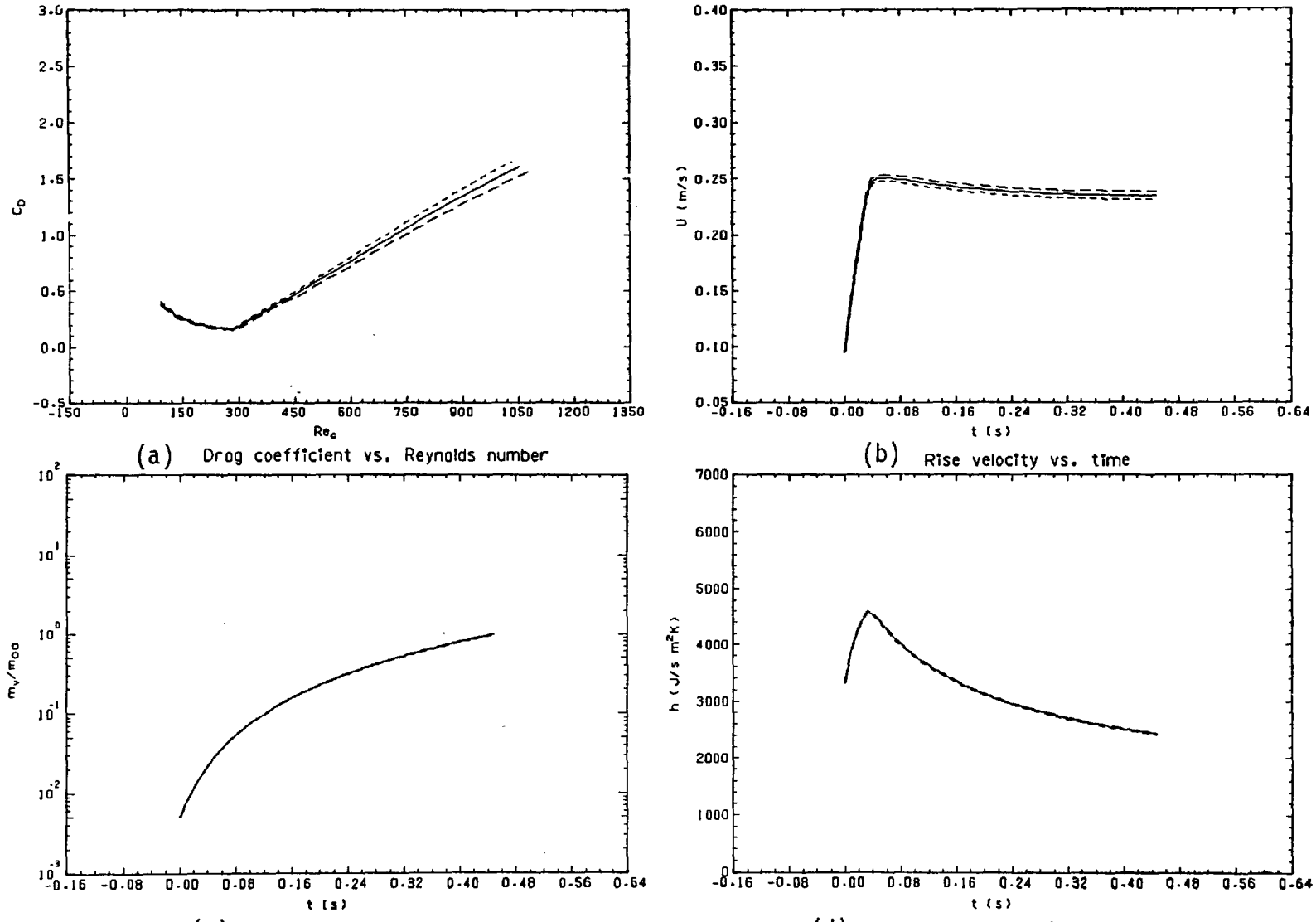

Figure 2.7(a-d): Evaporation of a butane droplet in distilled water, effect of 5% change in drag coefficient, d = 1.2 mm, ΔT_o = 2°C

(——— C_D, ------- 1.05 C_D, – – – – 0.95 C_D)

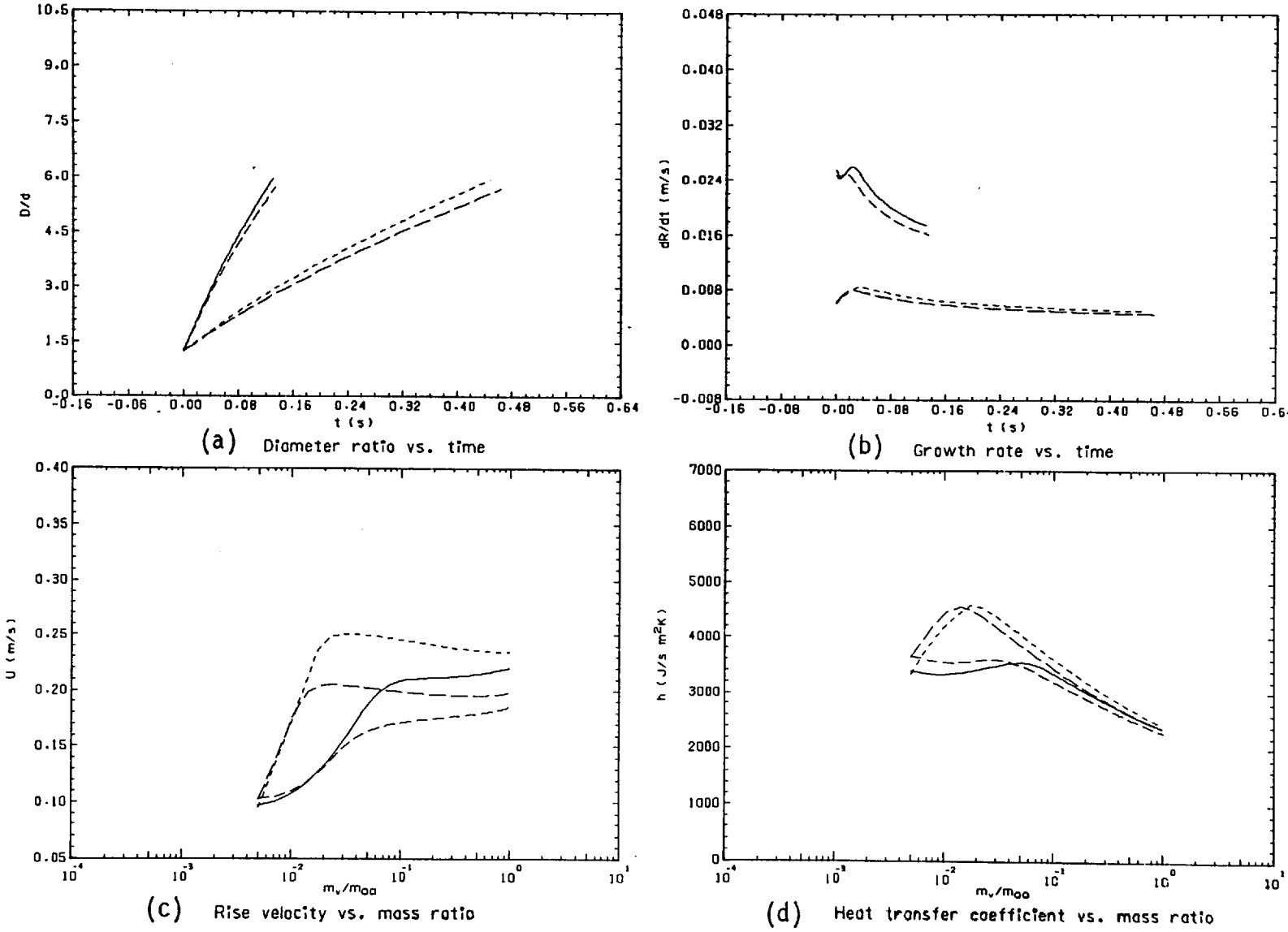

Figure 2.8(a-d): Evaporation of a butane and pentane droplet in distilled water, d = 1.2 mm
(——— butane, ΔT_o = 8°C, ····· butane, ΔT_o = 2°C, – – – – pentane, ΔT_o = 8°C,
– – – pentane, ΔT_o = 2°C)

temperature differences, namely, ΔT_o = 2°C and 8°C, are considered. Since the boiling point of pentane is higher (36.1°C) than that of butane, the water temperature is higher for the former case. Thus, at the same mass ratio, the Reynolds number is higher for the pentane/water combination, which, after the early stages of evaporation, leads to higher drag coefficients. Consequently, lower velocities are obtained, except in the early stages where the difference is very small (Figure 2.8(c)). The reason for the behaviour in the early stages is due to the fact that slightly higher drag coefficients were obtained for the butane/water combination. The variation of the heat transfer coefficient is shown in Figure 2.8(d), which indicates lower values for the pentane/water combination during most of the evaporation process. Therefore, lower growth rates and longer evaporation times are predicted for this combination (Figures 2.8(a) and (b)).

Referring to the data of Haberman & Morton for drag coefficients (Figure 16, reference (24)), since the value of the dimensionless parameter, M, for the pentane/water combination is smaller than the value of M specified for curve 13 of this reference, and if shift of the curves to the right continues for the lower M values, somewhat higher drag coefficients should have been estimated by using curve 13. Thus, the rise velocity of an evaporating pentane droplet may be higher than the one which was predicted here.

2.5 DISCUSSION

To simplify the actual problem concerning the evaporation of a droplet in another liquid, assumptions were made which need some further consideration. The governing equations were derived for a spherical bubble-droplet system, irrespective of the detailed geometry within the

system. Depending on the initial size of the droplet, deviations from the spherical shape occur either in the early stages of evaporation or in the later stages. A butane droplet with an initial diameter of 1.2 mm is transformed into a bubble of about 7.2 mm when its liquid content is fully evaporated. The bubble dimensions at this stage are within the range where the shape could be classified as oblate spheroid. For larger droplets of about 4.0 mm in diameter, the spherical shape is only valid in the very early stages of evaporation and the shape soon transforms to that of a spheroid. The range in which the shape may be considered as spheroid can be extended to about 10% evaporation, after which it is classified as a spherical cap. Thus, the spherical assumption may lead to reasonable results when it is applied for small droplets (e.g. smaller than 1.2 mm in diameter) up to the end of evaporation, and for large droplets (about 4.0 mm in diameter) until about 10% evaporation. However, in the presented results which concern large droplets, a smaller size than 4.0 mm (3.5 mm in diameter) was chosen to avoid similarity to the results in Chapter 5.

Since, in the model introduced here, the boundary conditions are those of growing bubbles and the pressure distribution at the bubble boundary is integrated over the entire surface of the sphere, therefore this model is more accurate when most of the bubble-droplet system is occupied with vapour which is expected to happen when about 1% evaporation is reached. However, in the results presented here, the range was extended to 0.5% and the time zero was assumed to be the time when evaporation has already reached this stage.

The heat transfer coefficient in Sideman's semi-theoretical (equation (1.15)) model represents the outside heat transfer coefficient. Neglecting the inside coefficient leads to the evaluation of higher values of the

overall heat transfer coefficient, especially in the early stages of evaporation when the liquid resistance to heat transfer is significant. Also, by using this model, the heat transfer coefficient decreases during most of the evaporation process and thus the growth rate follows nearly the same behaviour, which is not in agreement with the previous (76,78) and present experimental results. However, since Sideman's model consists of dimensionless groups which enables one to use it in different experimental conditions, bearing in mind the disadvantages of this model, it was chosen to be used in conjunction with the present model for the study of the parameters involved. The effect of using different models of heat transfer coefficient on the other parameters are studied in Chapter 5.

The potential flow assumption, which has been widely used, gives better results in higher Reynolds numbers and when the ratio of the viscosities of the two phases are high. In the cases which were studied here, the Reynolds number varied from about 100 to 5000 (Figures 2.2(h) and 2.3(h)). At high Reynolds numbers in the boundary layer on the bubble, the fluid velocity is only slightly perturbed from that of the irrotational flow (26). Thus, the omission of the viscous terms which leads to irrotational flow and potential flow assumptions can be considered as reasonable.

It was assumed that there was no mass transfer across the boundary of the system. The solubility of butane in distilled water is 50 to 180 ppm, and thus it can be assumed to be negligible. However, some water vapour is present in the bubble-droplet system which depends on the water temperature. Therefore, the actual mass of the system increases as evaporation proceeds. For the butane/water combination, where the water temperature is low, the amount of water vapour may be neglected, while for a combination such as pentane/water it should lead to some discrepancies.

Water vapour lowers the partial pressure and the saturation temperature of the vaporising liquid. Therefore, by omission of this factor, longer evaporation time would be predicted. Thus, the present model should be more suitable for the combinations in which the vapour pressure of the continuous phase is small compared to that of the dispersed phase.

Compared to the published joint paper by the author (47), a modification was made when differentiating equation (2.55). In the previous presentation, the heat transfer coefficient was considered constant during the time dt, and thus the term which includes dh/dt was omitted. In the present presentation, the heat transfer coefficient was specified as a function of time, and its derivative with respect to time was included in equation (2.56). The reason for the change was due to a discrepancy which existed between the growth rate predicted from the integration of equation (2.67) and the one calculated from equation (2.65). For the cases studied, the maximum discrepancy appeared in the case of small droplets and when $\Delta T_o = 8^oC$, where it reached 18% at the end of evaporation. Comparison should be made between Figure 3 of the former results (47) and Figure 2.5(d), where the effect of initial velocity is studied. In the present results, the growth rates coincide after a short time, while in the former the growth rate for the lower initial velocities continued to be lower than those for the higher velocities. Rise velocity was affected by the modification by about 1.5% at the maximum. The effect in the other cases was smaller and on the other parameters, such as the total evaporation time, it was insignificant. Considering equation (2.63), the growth rate is a function of the vapour and liquid densities and the heat of vaporisation. These properties are changing with time as the droplet ascends and evaporation proceeds. In the present results, these properties were calculated at the beginning of each step

and were kept constant during the time dt. Due to this, a discrepancy exists between the growth rate values obtained from equations (2.67) and (2.65), which increases as the evaporation proceeds and reaches a maximum at the end of evaporation. In the presented results, this maximum value varies from about 0.1% (for d = 1.2 mm, $\Delta T_o = 8^oC$) to 1.3% (for d = 3.75 mm, $\Delta T_o = 2^oC$).

2.6 RECOMMENDATIONS

The following recommendations for future work can be made:

(a) It should be possible to modify the model to be applicable for the reverse process, which is the condensation of a vapour bubble in an immiscible liquid.

(b) The presence of water vapour was excluded in the theoretical model. In other combinations which work in high water temperatures, this factor should become more effective. Therefore, an improvement would be made if the effect of the continuous phase vapour is considered.

CHAPTER 3

EXPERIMENTAL INVESTIGATION OF DROPLET EVAPORATION IN AN IMMISCIBLE LIQUID

3.1 INTRODUCTION

The experimental part of the present work was carried out in order to study the basic phenomena involved in the evaporation of a droplet in another liquid. Some of these phenomena have been investigated by previous workers (for example, (58), (68) and (77)). But the investigation was to be carried out to verify the previous results and also to increase our present knowledge on the subject. The theoretical model (Chapter 2) was also to be verified by our own experimental results.

A droplet of butane liquid was injected in a column of distilled water. Due to the higher temperature of the surrounding liquid than that of the dispersed liquid, the droplet evaporated and grew while rising in the column of water. To prevent the droplet from superheating, a tiny air bubble was injected in the droplet during its formation at the nozzle. The air bubble provided suitable conditions for evaporation to start whenever the liquid local saturation temperature was reached. Otherwise, the liquid did not evaporate and rose to the top of the column. The evaporating droplet was followed by a ciné camera which recorded its behaviour at time intervals. Experimenting with butane as the dispersed-phase necessitated working in low temperature and near the freezing point of water. In these conditions, some difficulties were encountered, such as premature evaporation of the butane liquid in the feed line or frozen water in the nozzle. These could have been avoided by using a dispersed-phase/water combination which provided working in temperatures near to the ambient temperature. This was adopted by the majority of previous workers.

But since experimenting with butane could be beneficial because of its application in desalination plants, it was therefore decided to work with a butane/distilled water combination as the first choice. Among the parameters of interest were the growth and rise velocity of the evaporating droplets and heat transfer from water to the droplet. A test rig was desgined and built for this purpose.

The experimental study also included a new type of experiment which has not been reported before. It was realised that it was possible to stop the evaporation of an evaporating bubble-droplet by the application of pressure on the surface of the water column. There is a considerable amount of work on bubbles and droplets, but none has been reported for a non-evaporating two-phase bubble-droplet system. The immediate difference between this kind of system and ordinary bubbles or droplets is that the interfacial tension around a non-evaporating bubble-droplet is not the same and consists of vapour-liquid and liquid-liquid interfacial tensions. Also, the presence and movement of the liquid part within the system is its unique feature. The liquid part is concentrated at the bottom and sloshes from side to side, and its behaviour depends on the size and mass ratio (vapour mass/total mass) of the system. In the present study, as the first step, work was only concentrated on the rise velocity of the stopped-evaporation bubble-droplets and compared with those of evaporating droplets.

The size of the droplets in the present experiments were chosen to be rather large to facilitate the experimental conditions. Droplets of about 4.0 mm in diameter gave more control on the formation and nucleation process, and provided longer available time before evaporation could be stopped.

Droplets, during their formation at the nozzle at the bottom of the

water column, were exposed to the warmer continuous phase. This was probably a disadvantage compared with the other designs, such as the ones adopted by Prakash et al (58,59) or Tochitani et al (83), in which droplets travelled a distance in a lower, colder column before they entered the warm liquid. In the present case, droplets might have been injected with some degree of subcool, or premature evaporation could occur at the nozzle. However, the disadvantages of the present procedure (also adopted by Sideman et al (68) and Simpson et al (77)) may be reduced by the advantage that its features are closer to the practical design in industry.

3.2 APPARATUS

Reference is made to Figures 3.1 to 3.5. The general view of the rig is shown in Figure 3.1, the test section in Figures 3.2(a) and (b), and the schematic diagram of the rig is shown in Figures 3.3(a) and (b). The test section [1] consisted of a double-walled square column. The walls were 12 mm apart and were made of Perspex. The dimensions of the inner column were 150 × 150 × 1500 mm. The gap between the two columns was initially made in order to reduce the heat transfer to the column from the atmosphere by making a partial vacuum in the gap. But it was only used for balancing the pressure at the two sides of the column walls by introducing air in the gap. This reduced water leakage problems and was used as a safety measure during the application of pressure on the water surface when evaporation of the droplets was to be stopped. Water was introduced at the bottom of the column by a PVC tube [9]. A pump [18] circulated the water through the column and the heat exchanger [17]. The water temperature along the column was measured by a Chromel-Alumel thermocouple probe [7]. This thermocouple was carried by a stainless

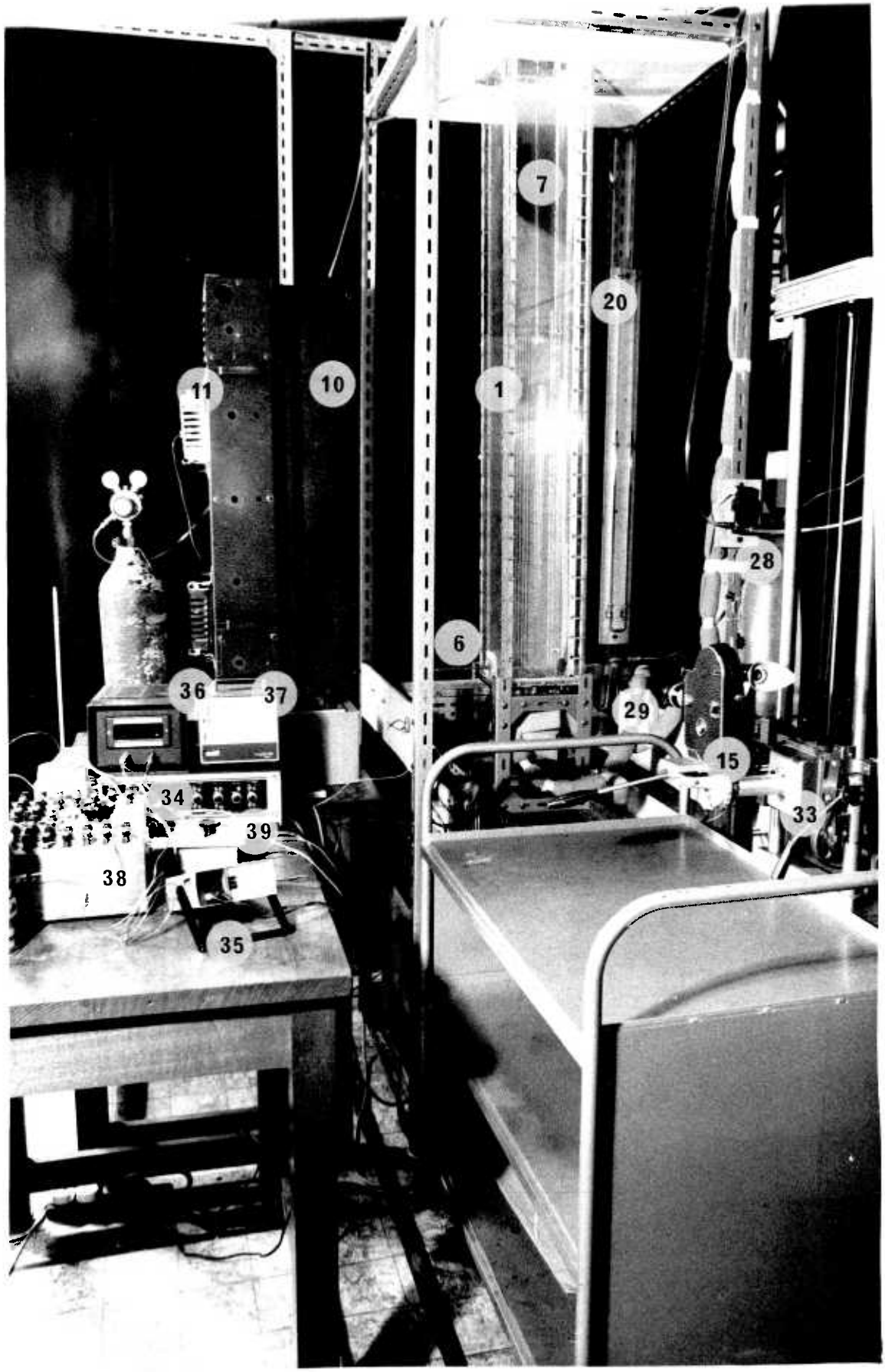

Figure 3.1: General view of the rig

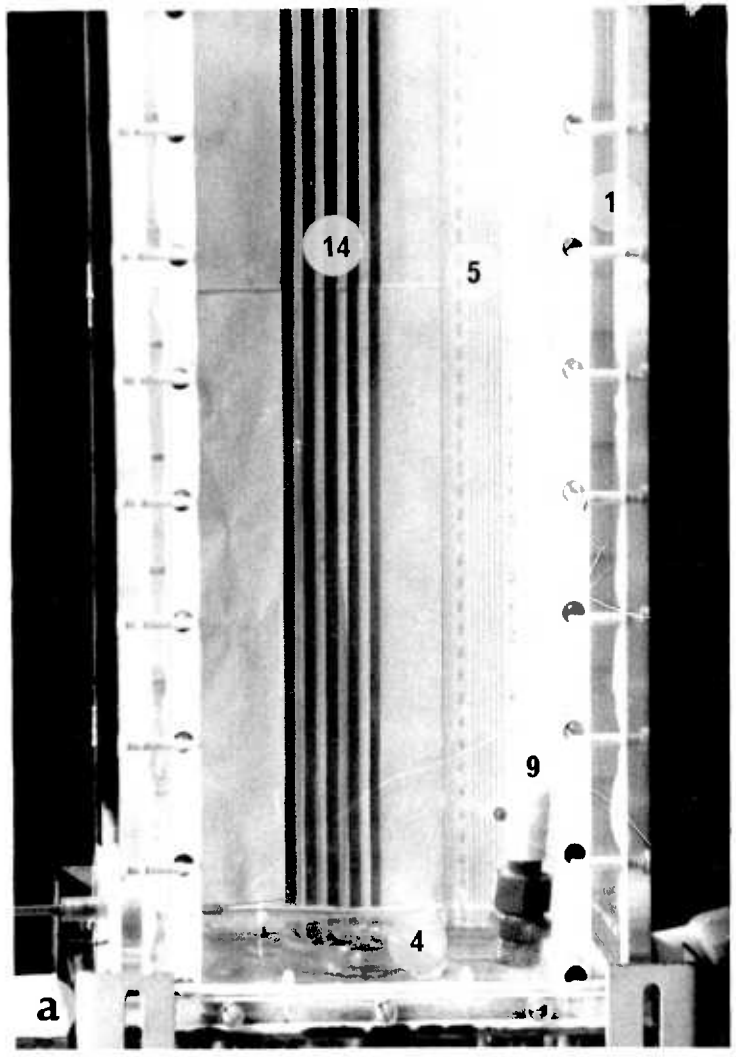

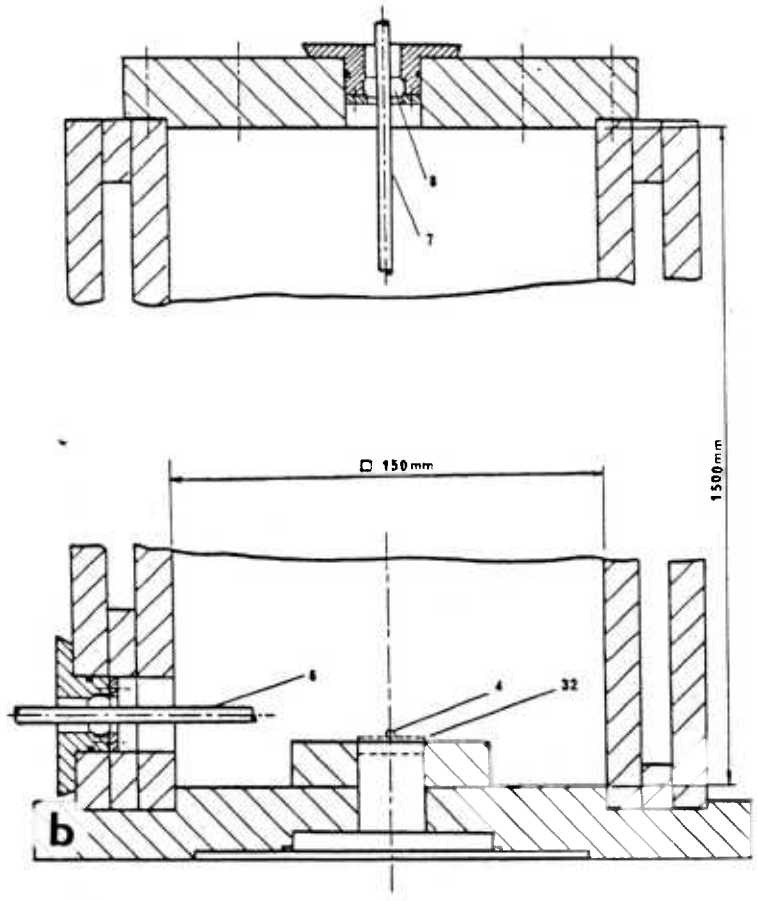

Figure 3.2(a,b): Test section

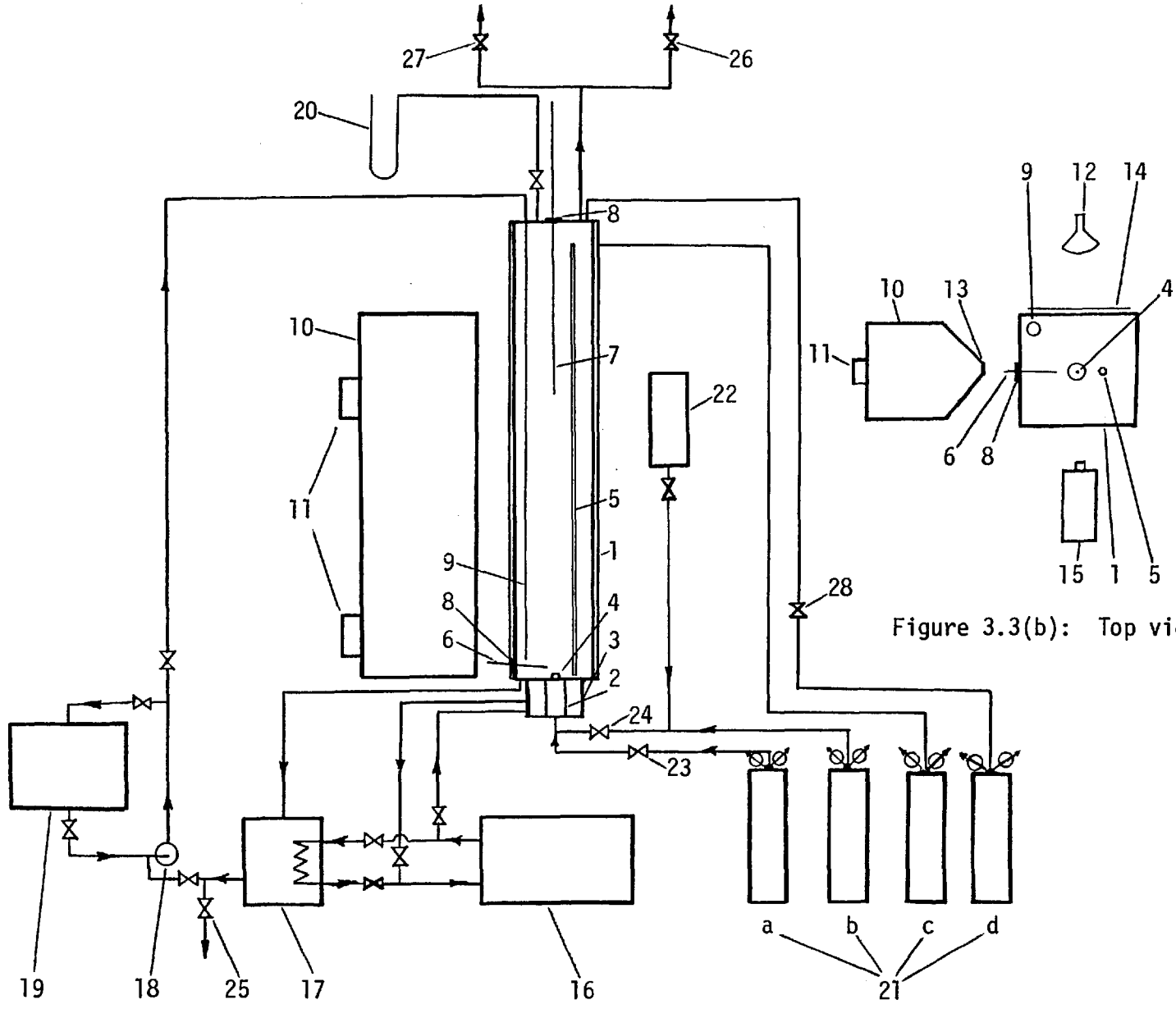

Figure 3.3(b): Top view of the set-up

Figure 3.3(a): Front view of the set-up

Details of the Items Shown in Figures 3.1 to 3.3 and 3.5

1	:	Test section
2	:	Nozzle assembly
3	:	Nozzle assemly jacket
4	:	Nozzle
5	:	Scale
6,7	:	Traversing thermocouple probe
8	:	Spherical bearing
9	:	PVC tubing
10	:	Matt black metal sheet box
11,12	:	Light source
13	:	Slit
14	:	Tracing paper
15	:	Camera
16	:	Refrigerator unit
17	:	Heat exchanger
18	:	Pump
19	:	Water storage tank
20	:	Mercury manometer
21a,b,c,d	:	Air bottle
22	:	Butane bottle
23,24	:	Needle valve
25	:	Drainage for water
26	:	Safety valve
27	:	Throttle valve and drainage for gas
28	:	Electrically actuated valve
29	:	Glass tube
30,31	:	Stainless steel capillary tubing
32	:	Nozzle cap
33	:	Camera support
34	:	Amplifier
35,36	:	Digital voltmeter
37	:	Chart recorder
38,39	:	Selector switch

steel tube which slid in a spherical bearing which was fixed to the column lid. Another Chromel-Alumel thermocouple was fixed to the probe [6] which was attached to the bottom of the side wall of the column (Figure 3.2(b)). By use of this probe, it was possible to measure the droplet temperature and also, by sliding it along the column width, to measure the water temperature at the bottom of the column and near the droplet. Using the spherical bearing, it was possible to move the probes [6] and [7] at an angle, thus giving more manoeuvreability. The lower thermocouple probe included a capillary tube which was used to carry another small diameter capillary close to the drop (when the nucleation procedure was attempted from the side of the droplet) or used for the production of air bubbles, which acted as a kind of agitator if necessary. This capillary was a useful means because it provided an easy way of changing nucleation capillaries without altering or damaging very delicate thermocouple wires. Details of the probe [6] are shown in Figure 3.4. A scale [5] made of a glass tube was used in parts of the tests and later it was replaced by another scale made of two rulers fixed to a support made of a glass tube. The nozzle was made of Perspex of 1 mm diameter. The tip of the nozzle was tapered to reduce spreading of the liquid droplet during formation. The nozzle cap [32] was fixed to the end of the nozzle assembly [2] and could be changed simply. Parts of the nozzle assembly are shown in Figure 3.5(a) and in the assembled form in Figure 3.5(b). The nozzle assembly was fixed in the nozzle jacket [3] which, in turn, was attached to the bottom of the column. Silicon oil from a refrigerator unit [16] (Colora-Kryo-Thermostat, Type WK30) passed through the jacket in order to regulate the dispersed-phase temperature which passed through the nozzle assembly. O-ring connections in the nozzle assembly separated the cooling liquid from the injecting substance. Most parts of the nozzle assembly

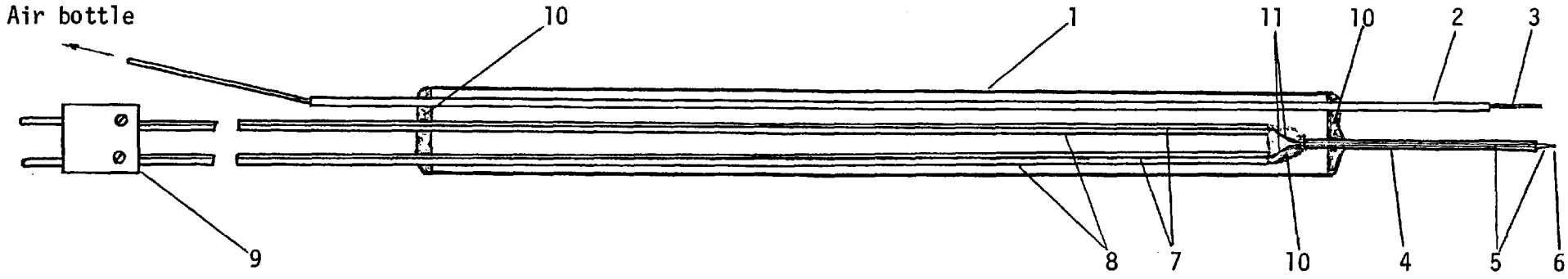

Figure 3.4: Thermocouple probe

Details of the Items Shown in Figure 3.4

1 : Stainless steel tubing, 4.8 mm OD (0.19 in)

2 : Stainless steel tubing, 0.6 mm OD (0.024 in)

3 : Stainless steel tubing, 0.21 mm OD (0.0085 in)

4 : Ceramic tubing (twin bore), 0.86 mm OD (0.034 in)

5 : Chromel-Alumel thermocouple wires, 0.025 mm diameter (0.001 in)

6 : Thermocouple hot junction

7 : Chromel-Alumel wires, 0.15 mm diameter (0.006 in)

8 : Insulated sleeving

9 : Plug

10 : Sealed with epoxy adhesive (Araldite)

11 : Wire connections of items 5 and 7

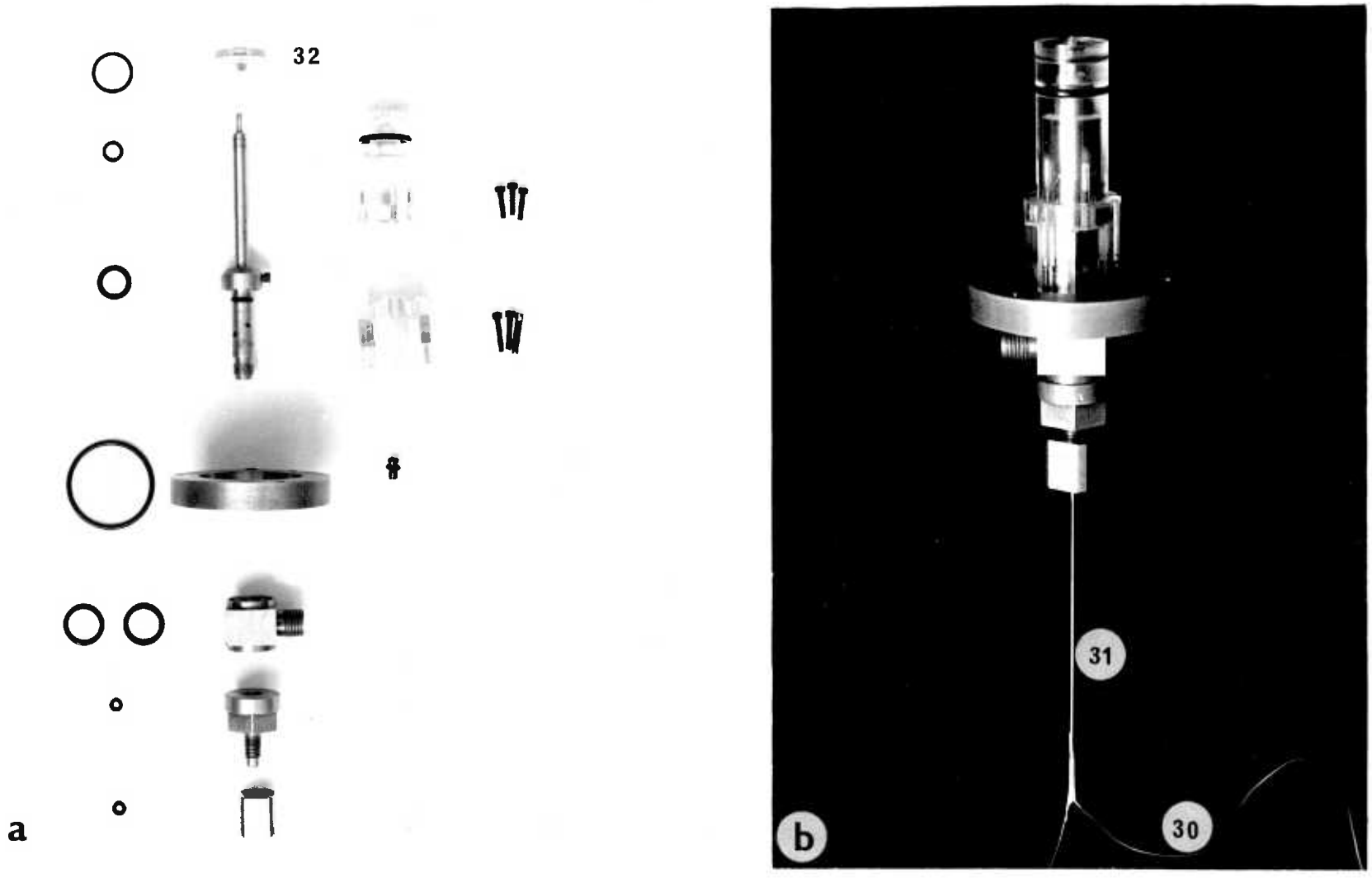

Figure 3.5(a,b): Nozzle assembly

were made of brass to provide good heat transfer. It also carried either a thermocouple (in the butane condensation study (Chapter 6)) or two stainless steel capillary tubes [30] which were used for the production of tiny air bubbles in the butane line. These were carried by another larger diameter tube [31] which entered from the bottom of the assembly (Figure 3.5(b)). These capillaries were connected to two needle valves [23] and [23'] (not shown here). By the use of these valves, the production of air bubbles could be regulated. The outside diameters of these capillaries were 0.21 mm and 0.28 mm. The smaller one was used for nucleation. It produced tiny air bubbles in the stream of butane liquid. The larger capillary was used as an auxiliary to the smaller one and was employed to produce a high flow of air bubbles through the nozzle passage to prevent water penetration into the nozzle (see Section 3.3). The ends of the 0.21 mm and 0.28 mm capillaries were 23 mm and 8 mm below the nozzle tip, respectively.

The column lid was tightly fixed to the top of the column. On the lid, there were connections to the water inlet and mercury manometer [20]. Also, a safety valve [26] plus a throttle valve [27] were connected to the lid, which allowed the regulation of pressure which was applied on the water surface. The throttle valve was also used for the gas drainage. An electrically actuated valve [28] was connected to the air line. This valve was normally closed and was opened by switching it on using a foot switch. The required air pressure was set on the air bottle [21d] which was then transferred through this valve to the water surface. Another air line was connected to the column in order to transfer air from the bottle [21c] to the gap between the columns.

The butane bottle [22] was fixed upside down to provide the feed line with liquid butane. A needle valve [24] was put in the line to regulate

the droplet formation. A glass tube [29] was included in the line before the valve to check the presence and amount of liquid butane.

The matt black metal sheet box [10] had a narrow slit [12], 950 mm long at one of its sides. On the opposite side of the slit, two light sources [11] were attached to the box [10]. The slit allowed a slab of light along the centre of the column. The thickness of the slab was controlled by changing the width of the slit. The relative position of the slit with respect to the column and the camera [15] and the other light source [12] is shown in Figure 3.3(b).

The camera was fixed on a support [33] which was guided on two vertical columns. The surface of the columns were smooth and by use of a reel, it was possible to slide the camera upwards smoothly while it followed the droplet.

3.2.1 Instrumentation

Temperature measurements were done by the thermocouples. The thermocouple which was fixed in the probe [7] was a Chromel-Alumel thermocouple, 1 mm in diameter and manufactured by Gulton. The commercial name was Westmic Mineral Insulated thermocouple, Type G. The conductors were protected within the sheath and the whole thermocouple was flexible. Its hot junction was bonded to the sheath, providing a response time of 0.08-0.15 seconds. The same type of thermocouple was installed in the nozzle assembly when necessary. This type of thermocouple was especially useful and easy to install in places like the nozzle assembly, where the available space was small and the application of conventional thermocouples was limited. Similar thermocouples were used in the measurement of oil and the reference temperature. The very delicate thermocouple which was fixed in the probe [6] was made of Chromel-Alumel thermocouple wires 0.025 mm in

diameter. The manufacturer of the wires was the British Driver Harris Company. The hot junction had a bead about the same size as the wires thus providing a fast response of about 0.04 seconds. The wires were connected at an acute angle, thus enabling the thermocouple junction to pierce the droplet.

The digital voltmeters, which were used in conjunction with the thermocouples, were: a Digital Multimeter, Solartron 7040, made by Schlumberger, with a resolution of 10 μV; and a Digital Panel Meter, DPM 300, made by Advance Instruments, with a resolution of 10 μV.

The chart recorder was called Rustak, and was made by Gulton. The chart speed which was chosen in most tests was 1.42 mm/s. The amplifier was made by Bell & Howell.

The ciné photography was carried out by use of a 16 mm Bolex H16 Reflex ciné camera. The lens used in the majority of cases was 75 mm. Still photography was done by using a Canon FTb camera, and lenses such as a 135 mm, 50 mm and extension tubes, and a +3 close-up lens were used.

The needle valve [24] in the butane line was a Nupro Fine Metering Valve, Size 4MG. The orifice diameter was 0.055 inches. The needle valve [23] was the same type, but had a smaller orifice diameter (Size 2SG, orifice diameter 0.031 in).

The electrically actuated valve [28] which was used in the air pressure line was a Martonair Valve, DM 11400/Y. The valve was normally closed and was opened by switching it on using a foot switch. The response time was 20 milliseconds.

The spherical bearing used in the two probes [6] and [7] was a Glacier Bearing, SE/06/DU3, with a bore of 4.8 mm (0.19 in) in diameter.

The pressure at the top of the column was measured by the mercury manometer [20].

The cold junction of all the thermocouples was kept in a mixture of ice and water.

3.3 APPROACH TO THE FINAL SET-UP AND DIFFICULTIES ENCOUNTERED

Before reaching the final set-up, preliminary experiments were conducted over a relatively long period of time, during which the performance of the rig, especially the parts which were related to formation and nucleation, temperature measurement and photography, was improved. Some of the early experiments were carried out using Sudogaz, which provided some basic information on the various aspects of the study and was also very cheap compared with the instrument-purity butane which was later used. This basic information was needed to improve the nozzle assembly, and the thermocouple probes and nucleation procedures. But not all the experience which was obtained using this gas was directly useful for the time when the much purer gas was used. The Sudogaz was more volatile and consequently more difficult to keep in liquid form in the nozzle assembly passage. The main aim was to discover how to bring the three main steps, namely, droplet formation and release, nucleation and droplet temperature measurement, under control. Butane was sent in to the line in liquid form, and it was important to keep it in this state until it reached the nozzle tip and could be injected as a droplet without having any vapour part. Also, it was intended that the droplet temperature should be slightly lower than the local saturation temperature in order that evaporation did not proceed during droplet formation or while the nucleation step was carried out. Thus, the feed line had to be kept at a lower temperature and this was achieved by circulating cold oil in the nozzle assembly jacket. Usually, liquid butane carried some amount of vapour and it took sometime before droplets could be formed free

of vapour and also be controllable. The vapour seemed to have been formed in the nozzle assembly due to boiling. Insulation around the nozzle assembly was essential to keep the parts cold. When the water temperature was relatively high, droplet formation was more difficult and evaporation could start at the nozzle or just below the nozzle due to the heat transfer from the water to the nozzle parts and liquid gas. In these situations, the temperature of the cooling oil had to be further reduced. On the whole, such problems had been mainly due to the considerable difference between the ambient temperature and the boiling point of butane. Finally, a useful and efficient way was adopted which could lead to a controllable droplet formation free from vapour. The technique was to increase the pressure on the water surface gradually, thus increasing the saturation temperature of the butane. As a result, soon the vapours ceased to appear and only liquid appeared. After a period of time, during which oil was cooling down the butane liquid, the pressure was removed gradually. After that, the appropriate condition was usually reached.

Another main step was to provide each droplet with a tiny nucleus of air in order to initiate evaporation; otherwise, the droplet would rise unevaporated to the water surface. The ideal case was that when the nucleation bubble, of about 0.3 mm diameter or less, joined the droplet just before detachment, thus reducing the probable evaporation at the nozzle. At higher water temperatures, this was especially important because of the higher heat transfer rate to the drop. At first, it was tried to initiate nucleation by a method similar to those which were tried by Nazir (53) and Sideman et al (68). In such a method, nucleation bubbles were injected into the droplet from the side by a capillary. However, we found that this technique was not very successful, although the presence of the probe [6] with the spherical bearing gave good

manoeuvreability in order to move the capillary tip near the droplet. The formation of tiny air bubbles could have been achieved if very thin capillaries were used. Production of only one or a few small bubbles to be added to the droplet was found to be difficult. Also, small bubbles did not immediately separate from the capillary when formed and they stuck to the upper surface of the capillary tip where they were joined by the newly formed bubbles. Therefore, the size of the bubble hanging on the capillary grew until it separated. In such conditions, it was difficult to attach the bubble to the droplet. In some cases, when the production of air bubbles was very slow, and the capillary tip was brought close to the droplet, formation of the droplet actually pushed the air back into the capillary. The bubble appeared again when the droplet went away. Controlling air bubbles in such a low flow rate was difficult, and thus the flow should have been increased, which consequently increased the number of bubbles, which was not intended. Another factor which led us to abandon the nucleation from the side was that it was found to be a big task to push the capillary (0.21 mm in diameter) into the droplet. During their formation, droplets used to avoid the capillary and leaned at every possible angle. They could also have separated before the formation was complete. In cases where the liquid was at the saturation temperature, the touch of the capillary carrying an air bubble caused the evaporation to start before detachment. The ideal case was that when the droplet hit the capillary tip after release and caught a tiny air bubble, but the bubble did not usually attach itself to the droplet. In some cases, evaporation proceeded when the droplet hit the capillary which did not have an air nucleus visible to the naked eye. But this was true when Sudogaz was used, which seemed to be more volatile, or in cases when the droplet temperature had reached the saturation temperature. When instrument-purity

butane was used, this rarely happened. To regulate the nucleation bubble formation, different valves or syringes were fixed in the line, but none was very successful. In any case, it was preferred that the droplet, after separation, travelled a distance before evaporation started, thus reducing the effect of release and intervention by the capillary. Examples of such nucleation procedures are shown in Figures 3.6(a) and (b).

Another alternative was tried. In this procedure, a capillary tube was placed in the butane line. A needle valve [23] was located in the air line to regulate the flow. Air bubbles were continuously formed in the butane liquid flow. By regulation of the air and the butane liquid flow, it was possible to provide each droplet with a small bubble. Compared with the nucleation from the side, there was no intervention by the capillary during the droplet formation or after release. The end of the capillary was placed in different places in the nozzle assembly (for example, Figures 3.7(a) and (b)). It seemed that when the capillary end was very close to the nozzle tip, it somehow disturbed the liquid flow and affected the droplet formation. At the end, it was placed further down in the downstream 23 mm below the nozzle. The size of air bubbles generated by this capillary (0.21 mm OD) was generally smaller than the ones which had been achieved when the capillary approached the droplet from the side. The reason could have been because the capillary was placed nearly vertical. In this situation, the flow of liquid could add an extra force to the buoyancy to separate the bubble from the capillary. This type of nucleation has been attempted by Nazir (53) and Prakash et al (58).

Another task was to design a thermocouple probe to measure the droplet temperature. At first, a Chromel-Alumel thermocouple (Gulton, Type E (see Section 3.2)) was placed in the nozzle assembly. The hot

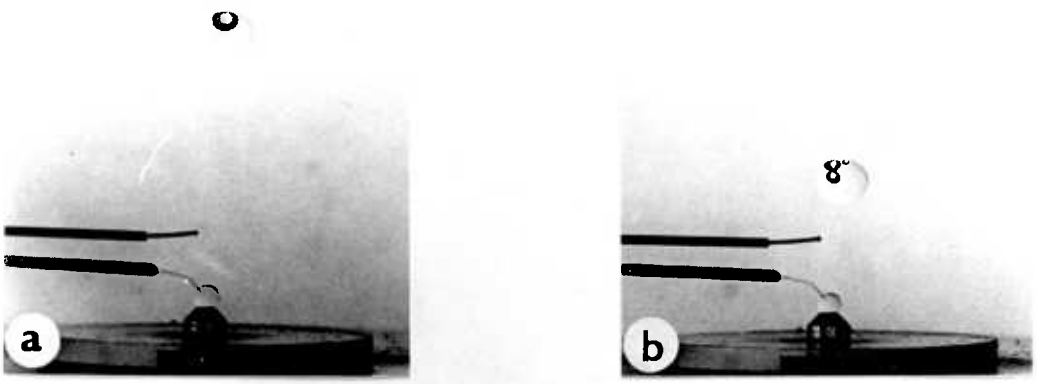

Figure 3.6(a,b): Nucleation procedure from the side

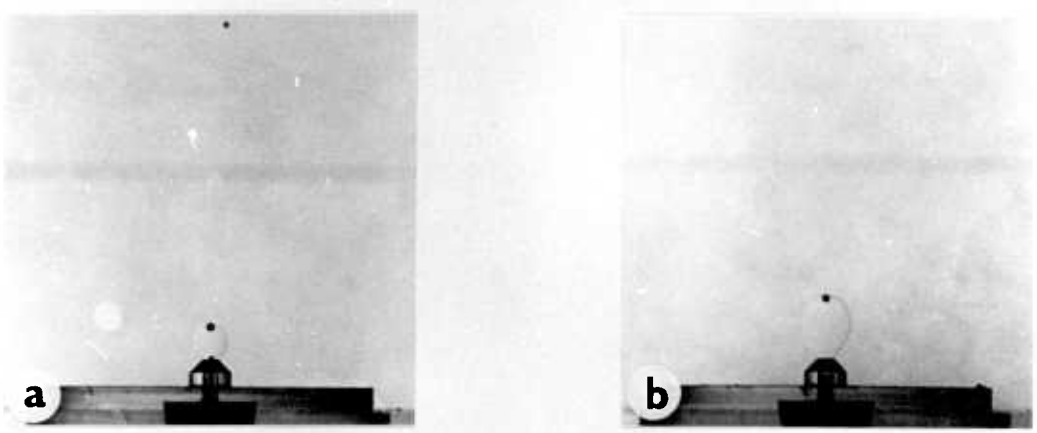

Figure 3.7(a,b): Nucleation procedure from the inside of the nozzle

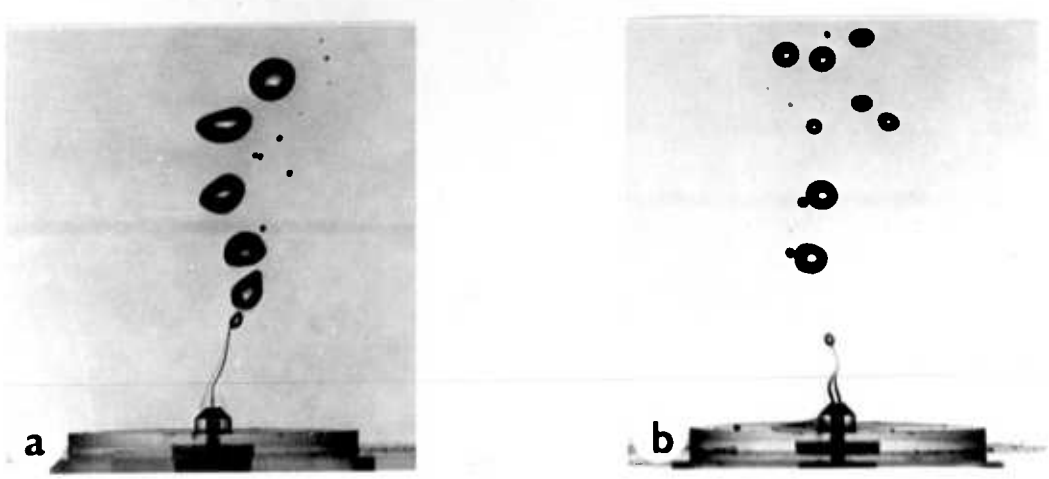

Figure 3.8(a,b): Ice formation at the nozzle

junction was located 3 mm below the nozzle tip in order to measure the liquid flow temperature shortly before droplet formation. This type of indirect measurement was adopted by Sideman et al (68) and Nazir (53), but it was noticed that this might not give an accurate measure of the droplet temperature because the liquid droplet could have warmed up, especially if the formation was slow. However, it could be a sufficient procedure if the droplet formation was relatively fast. In any case, in order to have a better idea of the profile of droplet temperature, and also since the nucleation capillary was to be placed in the nozzle assembly passage, thus leaving little space, it was decided to approach the droplet from the side, using the probe [6]. The use of thermocouples made of relatively thick wires was soon discarded, because the response time was slow and it was also not easy to penetrate into the droplet. Therefore, a very delicate thermocouple wire was essential and it was found that 0.025 mm diameter Chromel-Alumel thermocouple wires were suitable. The shape in which the two wires met was found to be important. The procedure in which the two wires met to make a straight line was found not to be appropriate. In this effort, the wires were stretched and were connected to the ends of a U-shape support which then approached the drop from the side or was placed above it. But the droplet escaped and its movement was slightly disturbed, and the thermocouple junction only touched the droplet surface. Finally, it was found that the only way of pushing the junction into the droplet was when the wires met at a sharp angle. Thus, the probe was designed in this way.

Other problems usually arose during the course of the experiments. The nozzle assembly passage could be blocked by ice due to the presence of water in the nozzle assembly. To prevent this, the butane or air bubble formed at the nozzle while the water was introduced into the column and

during the time it was cooled down. Thus, when one bubble left the nozzle, another one was already forming. The situation was critical when the cold oil was circulated in the nozzle assembly jacket in order to keep the butane in liquid form. At this time, some interruption in the flow occurred due to condensation of vapour flowing through the nozzle passage. In these conditions, water could penetrate more easily. This problem was partly overcome by placing another capillary (0.28 mm OD) in the nozzle passage, whose end was located 8 mm below the nozzle tip. The other end was connected through a needle valve to an air bottle. The task of this capillary was to produce air bubbles continuously at the nozzle while the butane gas flow was being cooled. After a period of time, the air flow was stopped and it made way for the butane liquid flow. Ice formation at the nozzle outlet also occurred and, in some cases, it produced peculiar nozzle-shaped ice blocks, as is shown in Figures 3.8(a) and (b).

The capillaries, especially the smaller one, could easily be blocked or the flow through it could be reduced, possibly due to minute ice particles.

During the tests concerning the stopped-evaporation droplets, these problems increased. The application of pressure pushed some water into the nozzle passage and a blockage could occur. Also, due to low pressure in the capillary line, the nucleation bubbles ceased to form, and so it became more difficult to regulate them. Some instability in the flow and in droplet formation occurred when the pressure was removed. This instability was reduced in time and the conditions were improved.

3.4 EXPERIMENTAL PROCEDURE

The main steps which were taken during the experiments were as follows:

- The air capillaries in the nozzle assembly were slightly open to prevent water penetrating them.
- The column was filled with water to a certain level.
- Butane bubbles were injected in large numbers to saturate the water.
- Water was returned to the storage tank. Air was then blown through the nozzle to clear it from the possible penetrated water.
- The column was filled again with water to the required level. The needle valve [23] was adjusted until butane bubbles form at the nozzle at a small rate, in order to prevent water penetrating the nozzle.
- The pump was switched on to circulate the water through the column and the heat exchanger.
- The specified temperature was set on the thermostat of the refrigerator. The refrigerator was switched on to circulate the oil in the heat exchanger and partially through the nozzle assembly jacket.
- When the water reached the specified temperature, circulation was stopped and the oil was mainly circulated in the nozzle jacket.
- The air flow in the larger capillary (in the nozzle assembly) was increased to prevent water penetrating the nozzle passage during the period of unstable flow conditions.
- When a mixture of evaporating droplets and bubbles appeared, pressure was applied gradually to the top of the water surface in order to increase the boiling temperature of the butane. The air flow through the capillary was reduced.
- After a period of time, the pressure was very gradually removed. If droplets formed properly, the air capillary was closed and the air flow in the nucleation capillary was adjusted.

- Photography and experimental measurements were carried out.

A few additional steps were taken when evaporation of the bubble-droplet was to be stopped. These were as follows:

- Some air pressure was put in the gap between the two columns in order to partially balance the pressure on the water surface.
- The specified pressure was set on the air bottle gauge.
- Pressure was then applied on the water surface by switching on the electrically actuated valve.
- After execution of the run, the valve was switched off to remove the pressure.

During the photography, the droplet was observed through the camera and was followed using the support.

It usually took about four hours before the rig reached the appropriate conditions for data collection.

3.5 PHOTOGRAPHY

Using light on the test column was important in order to obtain a clear image of the bubbles and droplets. Direct lighting from different angles was tried, but was found to be unsuitable. Better results were obtained when back-lighting was used. The light source was placed directly in front of the camera and a white sheet of paper, or tracing paper, was put on the column wall between the camera and the light source (Figure 3.3(b)). This arrangement provided a diffused light on the test column. On a bubble-droplet image, the outline of the bubble part due to the considerable difference between the vapour and water density could be

recognised well (Figure 3.6(a) and (b)), but, since the liquid butane and water were the same colour and also their densities were not very different compared with those of the vapour and liquid, the outline of the liquid part was more difficult to capture. The use of dies to increase the contrast between the two liquids was not recommended (53). Preliminary experiments were accompanied by still photography. In this case, by careful arrangement of the lights and use of a high speed film, it was still possible to capture the outline of the liquid part on the film (Figures 3.6(a) and (b)), but, when 16 mm ciné photography was adopted, the result was not satisfactory. Due to the granular texture of the film, and the relatively small negative size (16 mm compared with 35 mm), the liquid part could not be specified very well. To overcome this problem, as suggested by Sideman (69), black stripes were added to the tracing paper; different widths and angles (vertical, horizontal and crossed) were tried. The arrangement chosen had vertical stripes which were about 5 mm wide and 5 mm apart.

The following arrangements were mainly adopted:

- Ciné camera: Bolex H16 Reflex
  - Speed: 64, 68 frames per second
  - Aperture: 16
  - Lens: 75 mm
- Still camera: Canon FTb
  - Speed: 1/500 second
  - Aperture: 16
  - Lens: 135 mm plus +3 lens
- Ciné film: Ilford Mark V, 400 ASA
  Kodak Tri-X Reversal Film, 400 ASA, 7278

- 35 mm film: Ilford HP5, 400 ASA
  Kodak Tri-X Pan, 400 ASA
- Lights: Wotan, Halogen, Superhot, 1000 W
  Philips, No.2 Photoflood, 500 W

3.6 EXPERIMENTAL CONDITIONS

3.6.1 Materials

Distilled water was used for the continuous phase and n-butane (instrument purity, 99.5% pure) as the dispersed phase. In order to saturate the water with butane, butane bubbles in large numbers were injected into the water prior to each experiment. After the water reached the specified temperature, it was left quiescent during the tests. For the nucleation process, air bubbles were used. Butane was injected in the liquid form at the bottom of the column.

3.6.2 Water Column Height

During the study of evaporating droplets, the water column height above the nozzle tip was mostly 0.90 m. This length covered the required height for the complete evaporation of a butane droplet, although, in some cases, where ΔT was very low, or some height was lost before evaporation started, the droplet reached the water surface before complete evaporation.

In the case of stopped-evaporation droplets, the water height was brought up to near the top of the column, because only a small space was to be left between the water surface and the column lid to allow the pressure to build up quickly. In the majority of the tests, the water head was 1.37 m. Some evaporating droplets were also studied under these conditions.

3.6.3 Temperature Difference

The temperature difference between the water and the droplet is defined as:

$$\Delta T = T_c - T \tag{3.1}$$

where T is the saturation temperature at the corresponding pressure. The water temperature could be considered uniform throughout the water column. A check was made by traversing the thermocouple probe. Along the 0.9 m water height, a maximum difference of $0.25^{o}C$ was realised between the temperature at the top of the water and the temperature near the column base, which was 23 mm below the nozzle level. When the water column was 1.37 m long, a higher temperature difference was realised. However, droplets were mainly studied within a height of about 0.80 m where the water temperature could be considered as uniform. The butane saturation temperature varied along the column height due to the change of hydrostatic head above the droplet.

3.6.4 Droplet Size

The nozzle diameter in all the tests was 1.0 mm, and the size of the generated droplets was about 4.0 mm in diameter. Smaller droplets formed when the nozzle diameter had been reduced by the probable ice formation. Examples of droplet sizes obtained are shown in Figure 3.9.

3.6.5 Pressure on the Water Surface

For the study of evaporating droplets, the column was open to the atmosphere and thus the atmospheric pressure was the only pressure acting on the water surface. In the case of stopped-evaporation droplets, the column lid was tightly shut, and the throttle valve was adjusted and

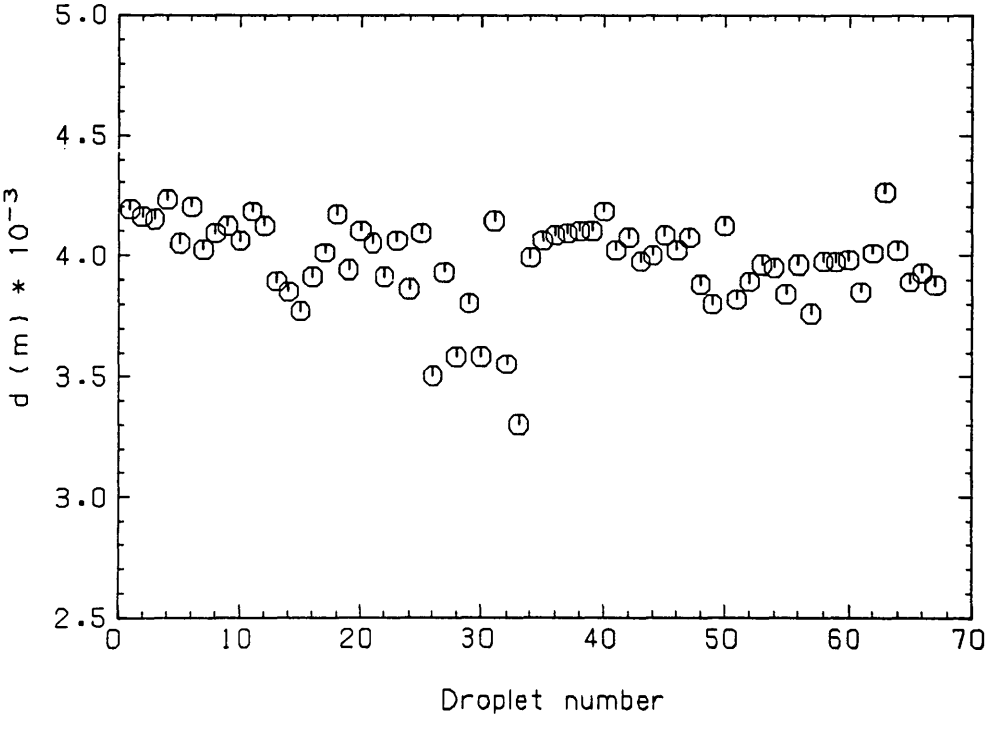

Figure 3.9: Initial droplet size distribution

the air pressure was set. After the application of pressure on the water surface, pressure built up quickly. The pressure shown on the manometer had a short period of fluctuation and then stabilised. This pressure was about 120 mm of mercury in most of the experiments.

3.6.6 Droplet Temperature

The initial droplet temperature was required for the calculation of the initial mass and for taking into consideration of the amount of subcooling of the droplet. This temperature varied according to the experimental conditions. The cooling oil temperature and the frequency of droplet formation, and water temperature, had a direct effect on the droplet temperature. The temperature profile which was recorded by the chart recorder differed according to the position of the thermocouple junction within the droplet. In most cases, it was placed above the nozzle. During formation, the top of the droplet first touched the thermocouple and then the thermocouple penetrated into the drop. During most of the formation time, it measured the liquid droplet temperature along the central axis. Regular and stable formation resulted in a regular pattern of temperature profile for consecutive droplets. When droplet formation was not so stable, an irregular pattern was obtained. Some examples are shown in Figures 3.10(a) to (f). The chart speed was 1.42 mm/s. Figures 3.10(a), (b) and (c) are the result of a uniform droplet formation. Figure 3.10(a) was obtained during very slow formation (f = 0.07). The temperature starts to fall after the thermocouple touches the top of the droplet and continues to decrease until the droplet is released. The period during which the droplet is in touch

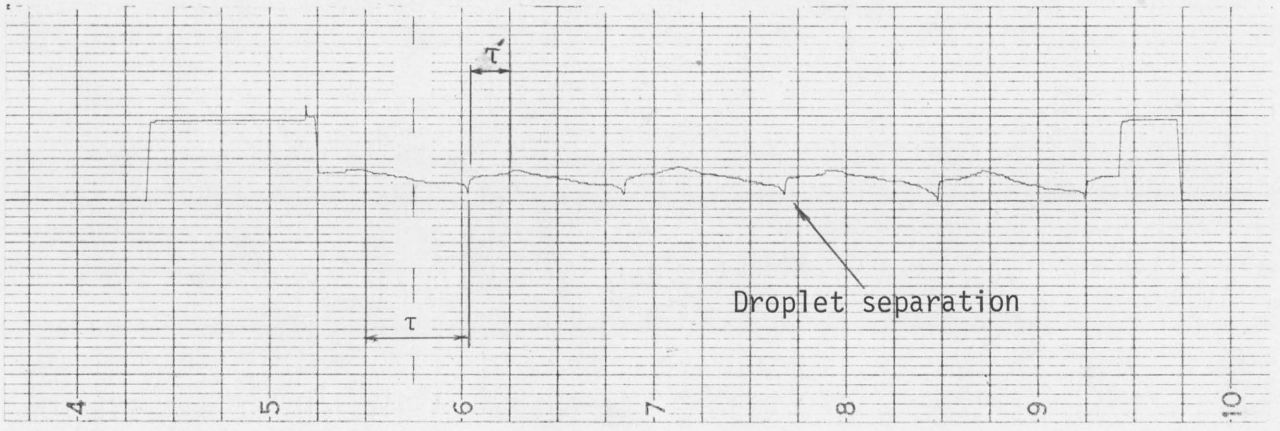

(a)

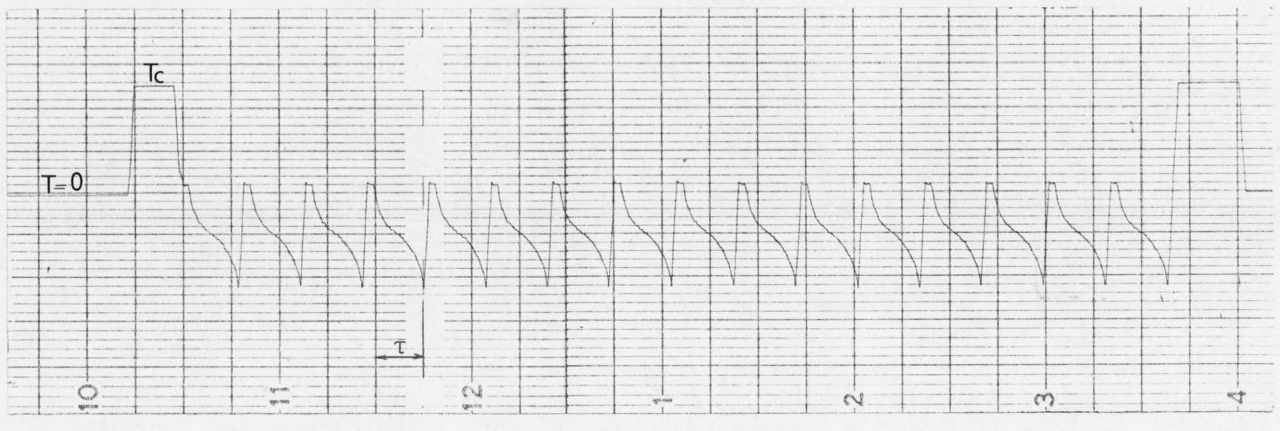

(b)

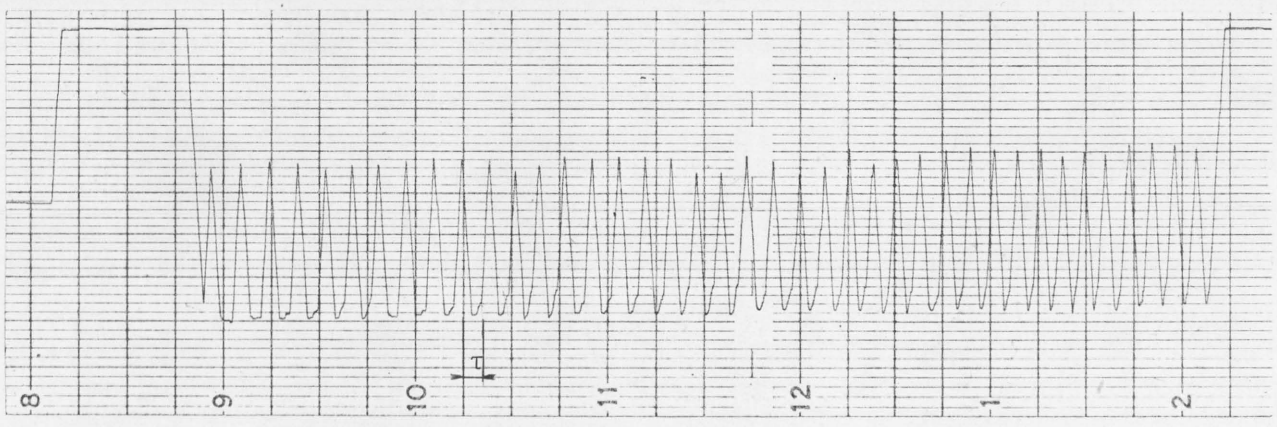

(c)

Figure 3.10(a-f): Droplet temperature during formation

(d)

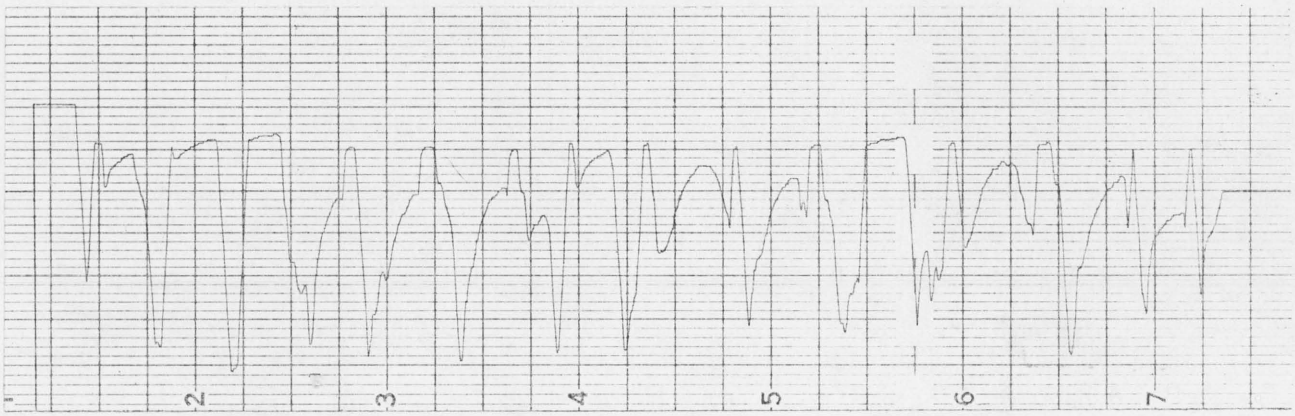

(e)

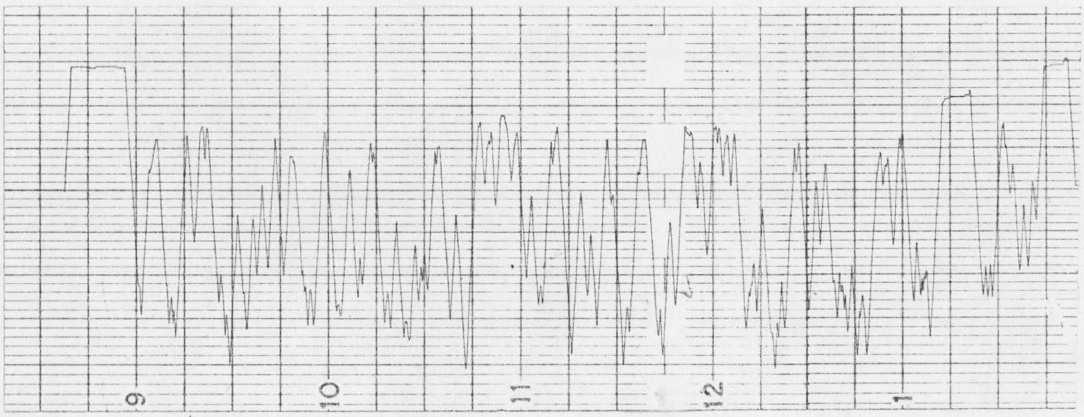

(f)

Figure 3.10(a-f): continued

with the thermocouple is shown by τ. The lowest temperature was obtained at the time of release which could be due to the cold liquid just joining the droplet before it was released. In Figure 3.10(a), because of long contact time, the temperature was close to the surrounding liquid temperature. There was a period of time, τ', when the thermocouple was measuring the water temperature just above the nozzle before it was touched by another new forming droplet. It shows that the water temperature just above the nozzle was cooler than the bulk of water. Figure 3.10(b) shows a quicker droplet formation (f = 0.17). The same pattern as that shown in Figure 3.10(a) can be seen. Due to the shorter formation period, the minimum temperature is lower. Another example is shown in Figure 3.10(d). In this case, the minimum temperature persisted over a longer time due to longer droplet pause at the nozzle, and this indicates some fluctuations. In Figures 3.10(e) and (f), cases are shown where droplets did not form uniformly. Some droplets were released quickly, but some paused at the nozzle. In the latter case, fluctuations can be recognised which seemed to be due to the up and down movement of the droplet during formation, which might be caused by pressure variations or unstable flow conditions in the nozzle assembly.

It was realised that the droplet temperature during formation varied and was not uniform throughout, and near the liquid-liquid interface it was somewhat higher than the middle of the droplet. When formation was slower, the temperature variation was more obvious. Thus, in most cases, an average value could be considered.

In the majority of the tests, the oil temperature passing through the nozzle assembly jacket was set on -10^{o}C.

3.7 DATA COLLECTION

Using cine photography, the behaviour and growth of the bubble-droplet from the time of formation and release to the end of evaporation was recorded. Consequently, dimensions of the bubble-droplet and its position could be measured and, from the knowledge of the camera speed and the number of frames, one could specify the time of each individual shot.

The water temperature, oil temperature (in the refrigerator bath), and reference temperature (in a constant temperature bath) were measured using thermocouples. The resulting voltages and the amplified voltages were noted from the reading of the digital voltmeters. A thermocouple which was placed in the constant temperature bath, provided a constant voltage which was used to obtain the amplification factor of the amplifier. The variation of the liquid droplet temperature was recorded on the chart recorder.

Atmospheric pressure was measured using a barometer. In the case of stopped-evaporation droplets, the pressure was noted by the mercury manometer.

3.8 DATA PROCESSING

3.8.1 Cine Film Analysis

The cine film from each set of experiments was studied at first and the runs with the better conditions were chosen. For example, slow and uniform droplet formation was preferable. Also, droplets having a very small nucleation bubble (about 0.3 mm) were closer to the ideal conditions. Droplets with slight initial subcool had advantage over those which started evaporating just after release, because, in the former case, the droplet travelled a distance before it started evaporation, and

thus its motion became stabilised. In some runs, evaporating droplets behaved differently and deviated considerably from the central line of the column, and thus they were disregarded.

When the proper runs were chosen, each one was studied frame by frame. Due to the large number of frames, it was very laborious and tedious to take the measurements from each frame, and so every few frames were chosen for this purpose. Moreover, this was essential in order to decrease the percentage of error in the vapour volume and height measurements, because, for example, in two consecutive or alternate shots, the bubble growth was within the range of the experimental error. Also, the evaporating bubble-droplet rotated towards the camera in some frames, which made the measurements unreliable. This sort of frame was excluded. In general, the number of frames which were chosen for vapour volume measurement was less than those chosen for height measurement. The height was measured directly from the film, but those frames for vapour volume measurements were first printed on photographic paper. For the time when the vapour volume was not measured, it was obtained by interpolation using the fitted curves to the available data. This will be explained in Section 3.8.8.

3.8.2 Rise Velocity

In order to calculate the velocity of the bubble-droplet, its position was measured directly from the scale which was recorded on the ciné film. The velocity was then calculated using a procedure which is explained in Appendix E. This procedure computes the velocity, U_i, at the point (Z_i, t_i), using a polynomial of degree 2 which passes through the three consecutive points, (Z_{i-1}, t_{i-1}), (Z_i, t_i), (Z_{i+1}, t_{i+1}).

3.8.3 Vapour Volume

Vapour volume was calculated from the dimensions of the bubble, assuming that the bubble shape was axisymmetric. Bubble shapes were approximated as a sphere, an ellipsoid or a spherical cap.

3.8.4 Initial Mass of Droplet

The initial mass of the droplet was calculated having the initial droplet size, which was measured from the ciné film. Usually, the average of the measurements from several frames was taken as the droplet size. Droplet temperature for the calculation of liquid density was not a critical factor, because the variation of liquid density was not sensitive to a few degrees temperature change. Also, as it was explained in Section 3.6.6, the droplet temperature seemed not to be uniform throughout. Considering different tests, it was decided to assume the initial temperature equal to $-1.0^{o}C$ and the liquid density was calculated using this value. The maximum error in the calculation of the initial mass in the case of the minimum measured temperature ($-5.0^{o}C$) was 0.7%.

The total mass of the bubble-droplet system was assumed to be the same as the initial mass throughout the evaporation process. The amount of water vapour in the system due to the low water tempeature and the minute amount of air which was injected into the drop as the nucleus were neglected.

3.8.5 Bubble-Droplet Size

Having the values of the vapour volume and the initial mass of the droplet, the volume of the bubble-droplet was calculated. The total volume is:

$$V = V_l + V_v \tag{3.2}$$

where V_v and V_l are the vapour and liquid volumes, respectively. The latter is obtained from:

$$V_l = \frac{m_l}{\rho_l} \tag{3.3}$$

where m_l is the liquid mass in the system. Since, at any evaporation ratio:

$$m_l = m_{oo} - m_v \tag{3.4}$$

where m_{oo} and m_v are the total mass and vapour mass in the system, and since:

$$m_v = \rho_v V_v \tag{3.5}$$

We obtain:

$$\begin{aligned} V &= \frac{m_{oo} - \rho_v V_v}{\rho_l} + V_v \\ &= \frac{m_{oo}}{\rho_l} + V_v \left(1 - \frac{\rho_v}{\rho_l}\right) \end{aligned} \tag{3.6}$$

In the case of evaporating droplets, ρ_l and ρ_v were calculated assuming that both the liquid and vapour temperatures are that of the saturation temperature corresponding to the local pressure. ρ_v was calculated using a procedure which is explained in Appendix B. The correlation for ρ_l is given in Appendix C. In the case of stopped-evaporation droplets, since the growth was very small, the saturation temperature was close to the water temperature. Thus, in this case, ρ_l and ρ_v were obtained using the value of T_c. The equivalent spherical diameter of the bubble-droplet can then be calculated from equation (3.6). Thus:

$$D = \left(\frac{6V}{\pi}\right)^{1/3} \tag{3.7}$$

3.8.6 Vaporisation Ratio

This was calculated having the vapour mass and the total mass of the bubble-droplet. Thus:

$$\xi = \frac{m_v}{m_{oo}} = 1 - \frac{m_l}{m_{oo}} \tag{3.8}$$

3.8.7 System Pressure

The total pressure in the bubble-droplet system was obtained by adding the atmospheric pressure and the water head pressure at the bubble-droplet level. The pressure due to the interfacial tension under the present experimental conditions was small compared with the total pressure and was therefore neglected. The total pressure in the system is equal to the sum of butane, water and air partial pressures. The amount of air which was injected into the droplet was usually very small, and its effect was more apparent in the very early stages of evaporation when the bubble volume was small, and it decreased quickly as evaporation proceeded; therefore, it was neglected. The water vapour pressure was also neglected and the butane pressure was calculated from the total pressure. A discussion is made in Chapter 4 (Section 4.3.4) on the effect of the exclusion of water vapour pressure on the parameters involved.

3.8.8 Instantaneous Heat Transfer Coefficient

The rate of heat transfer, q, was obtained from:

$$q = h A (T_c - T) \tag{3.9}$$

where h is the overall instantaneous heat transfer coefficient, and A is the heat transfer area and was taken as the equivalent spherical area of the bubble-droplet. The temperature driving force was the difference between the water temperature and the saturation temperature of the dispersed phase. The rate of heat transfer, q, is obtained from the heat required to evaporate a liquid mass of dm_l during the time dt. Thus:

$$q = - h_{fg} \frac{dm_l}{dt} \tag{3.10}$$

Combining equations (3.9) and (3.10), we obtain:

$$h = - \frac{h_{fg}}{A\ (T_c - T)} \frac{dm_l}{dt} \tag{3.11}$$

or:

$$h = \frac{\rho_v\ h_{fg}}{A\ (T_c - T)} \frac{dV_v}{dt} \tag{3.12}$$

The calculation of dV_v/dt directly from the differentiation of the vapour volume/time data lead to a considerable scattering of the heat transfer coefficient values, due to the measurement error which was involved. To overcome this, the data points were smoothed by curve fitting. The fitted curves were polynomials of degree 5. The vapour volume varied from a comparatively small value (e.g. 1 mm^3) at the early stages of evaporation to a large volume (e.g. 7000 mm^3). The procedure for curve fitting was a weight least square method and is explained in Appendix E. In using this method, considerable weight was put on the small values of volume, in order to match them with the large values. The weights were obtained from the following relationship:

$$W_i = \left(\frac{V_{av}}{V_i}\right)^n \tag{3.13}$$

where V_{av} was the average of all the volume values. The power n was given the values 1, 1.5 or 2, where appropriate.

A reasonable maximum degree of polynomials was chosen. The polynomials of the second and third degree did not usually lead to good curve fitting. On the other hand, much higher degrees were not suitable because the fitted curve followed nearly the same variation as that of the data, and thus not much improvement could be expected. Also, the maximum degree of the polynomial was to be chosen in such a way that not much restriction was put on the first and second derivative of the vapour volume. For example, a polynomial of degree 3 restricted the variation of d^2V_v/dt^2 to follow the trend of a first degree line. The minimum suitable degree was 5. In this case, d^2V_v/dt^2 follows the trend of a third degree polynomial. The coefficients of the polynomials are given in Table 4.1 (Chapter 4, Section 4.2.2).

3.8.9 Total Evaporation Time

Estimation of the total evaporation time was made by the extrapolation of the mass ratio values to the complete evaporation ($m_v/m_{oo} = 1$), by using the fitted curves to the vapour volume/time data. The dilatometric method, which was used by Adams et al (1), showed that the evaporation slowed down near the end of evaporation. In the present experimental results, this was not usually realised, probably due to the errors involved in the volume measurement. Thus, if the type of dilatometer chart (representing the variation of total volume versus time), given by Adams et al (1), was the general representative of their experimental results, then the extrapolation to the complete evaporation, which was used here, resulted in a slightly shorter total evaporation time.

3.8.10 Initial Droplet Temperature

Variation of the liquid droplet temperature was recorded by the chart recorder. Using a multiple switch, it was possible to record the temperature of the water and a zero temperature (zero voltage) on the same chart (Figure 3.10). The water temperature was also noted from the reading on the voltmeter. Thus, the droplet temperature was estimated directly from the chart. The linearity of the chart recorder was checked. Known voltages were applied and the displacement of the pen was measured. Then the voltage was plotted versus the displacement. The variation of voltage against displacement was linear over the experimental range.

3.8.11 Temperature Difference

This was defined in Section 3.6.3. In the tabulated results (Tables A.1 to A.18), the overall temperature difference, ΔT_o, is taken as the arithmetic average of the ΔT values at the measured interval times.

3.9 EXPERIMENTAL ERRORS

The main source of error was due to the photography method. Since the column was square, photography through the Perspex walls while the camera followed the droplet parallel to the column axis was not subjected to any significant distortion. Sharp images were obtained on the ciné film. Measurements were made from prints with three times magnification. In these conditions, by using a traversing microscope, the dimensions of the bubble-droplet were measured with an accuracy within ±0.15 mm at the early stages and ±0.6 mm in the later stages of evaporation. In order to estimate the vapour volume, the bubble shape was assumed to be axisymmetric and to have a regular shape. The degree of the error involved could not be specified but, as it was explained in section 3.8.8, the error was

reduced by curve fitting.

The measurement of the bubble-droplet height (taken at the middle of the bubble-droplet) from the scale was liable to some errors. At the early stages of evaporation when the bubble-droplet was relatively small and its shape was regular, the height could be measured within ±0.5 mm which resulted in a maximum of 7% error in velocity (velocity about 0.18 m/s). In the later stages of evaporation when the shape of the system was more irregular or slight rotation existed, the height could be specified within ±1.0 mm. In this case, the time interval chosen for height measurement was longer than that at the early stages of evaporation and the error in velocity was estimated to be less than 4% (velocity about 0.30 m/s). The camera speed was checked by a stroboscope and it was constant. However, examination of the rise velocity variation showed that the data points usually followed the same trend and not considerable scattering occurred. Therefore, the amount of error involved should have been well below the above estimated values.

The digital voltmeters specified the voltages within ±0.01 mV, which corresponded to ±0.25^{o}C, which could result in a high percentage of error at low working temperatures. For example, a 0.10 mV voltage read on the digital voltmeter was subjected to a maximum of 10% error. In order to reduce the error, the signal was amplified, about twenty times. A known reference voltage (about 4.0 mV) was used to calculate the amplification factor after each reading. Then, the maximum error was reduced to 0.7%. In any case, the effect of small differences in temperature did not appear to be distinguishable in the results, such as growth.

In the early stages of evaporation when the liquid volume was significant compared to that of the vapour (e.g. Figure 3.6(a)), the shape of the butane liquid-vapour interface and the size of the bubble as it

appeared in the photographs could have been affected by the curved shape of the liquid-liquid interface. The degree of the effect is not known. To verify this, it can be suggested that an accurately measured vapour volume to be injected into the droplet and then to be compared with its apparent volume while it is within the droplet. The effect of the shape of the bubble may be studied by piercing a well defined shaped object into the droplet and verifying the possible distortion. Attempts were made in this direction but it was not very successful or conclusive. The main problem arose due to the difficult task of penetrating into the droplet. However, it did not seem that, for a butane/water combination and for the droplet sizes under study, the effect would be significant.

In processing the results, the water and butane properties were taken from the published data. Slight variations from these values could not have been the source of significant errors.

Some other factors might have affected the results in a minor way. For example, if the saturation of water has not been achieved sufficiently, some of the dispersed phase has been dissolved in water. However, if it was present, it was not to a degree to be realised. Also, no attempts were made to de-aerate or to purify further the once distilled water.

CHAPTER 4

OBSERVATIONS AND RESULTS

4.1 OBSERVATIONS

The type of droplet formation which was aimed for was that when the droplet grew smoothly and rather slowly at the nozzle. But before reaching this, it could have happened that formation was quick and the growth was not stable. This situation was usually caused by the presence of vapour bubbles in the butane liquid flow. After the butane gas flow was cooled, these bubbles apparently condensed and the situation improved. However, sometimes it was difficult to obtain the conditions when the liquid flow was completely free from the vapour bubbles. Working in higher water temperatures seemed to worsen the situation.

The thermocouple junction was pierced into the droplet during the formation. Due to the small thickness of the thermocouple wires, droplet formation was not apparently affected by its presence and the subsequent release and rise seemed to be the same as the case when the thermocouple was not present. However, in cases when the capillary was in contact with the droplet, due to its relatively large size, it pushed the droplet to the side and with more interference the droplet was released before formation was complete. Also, when the capillary was placed at a higher level above the nozzle (Figure 3.6), it seemed to have a slight effect on the initial rise of the droplet. In the final arrangement, nucleation bubbles formed at the capillary in the nozzle assembly. The generated bubbles in some cases were very small and few of them coalesced at the top of the droplet. It was noticed that these bubbles usually preferred to move along the liquid-liquid interface than to rise straight to the top of the droplet. This might have been due to the flow pattern within the

droplet. The same observation was made when the nucleation was tried from the side of the droplet. In this case, the tip of the capillary was in contact with the droplet surface near the equator plane. Again, the bubbles did not usually rise directly in the water, but they travelled on the droplet surface and at the liquid-liquid interface. When they reached the top of the droplet, they separated and rose in water.

Self-nucleation, i.e. without artificially injected nucleus, did not occur except on rare occasions. Multiple nucleation, i.e. the start of evaporation from different places within the droplet, was also rare, especially when nucleation was made with the help of the capillary in the nozzle assembly. It was more common when the nucleation capillary touched the droplet from the side (Figure 3.6b). In any case, the generated bubbles joined shortly and collected at the top of the droplet.

It seemed that rising droplets were not necessarily sensitive to the air bubbles. In cases when a droplet rose in a train of small air bubbles, evaporation did not start immediately, while a droplet at the same conditions was nucleated by direct touch of the capillary.

When a droplet was not nucleated, it rose to the water surface, where it evaporated shortly afterwards. An example of the rise of such a droplet is shown in Figure 4.1. When the nucleus bubble was present, the droplet evaporated while rising in the column. The vapour part remained at the top and the liquid part seemed to stay at the bottom of the system. The rise of such a system is shown in Figure 4.2. The liquid part could only be recognised up to about 10% evaporation, while after that it occupied a relatively small volume of the bubble-droplet system and was not distinguishable on the film. Before reaching this stage, the system oscillated and the liquid part sloshed from side to side. The liquid sloshing usually started at around 0.1% evaporation fairly slowly and

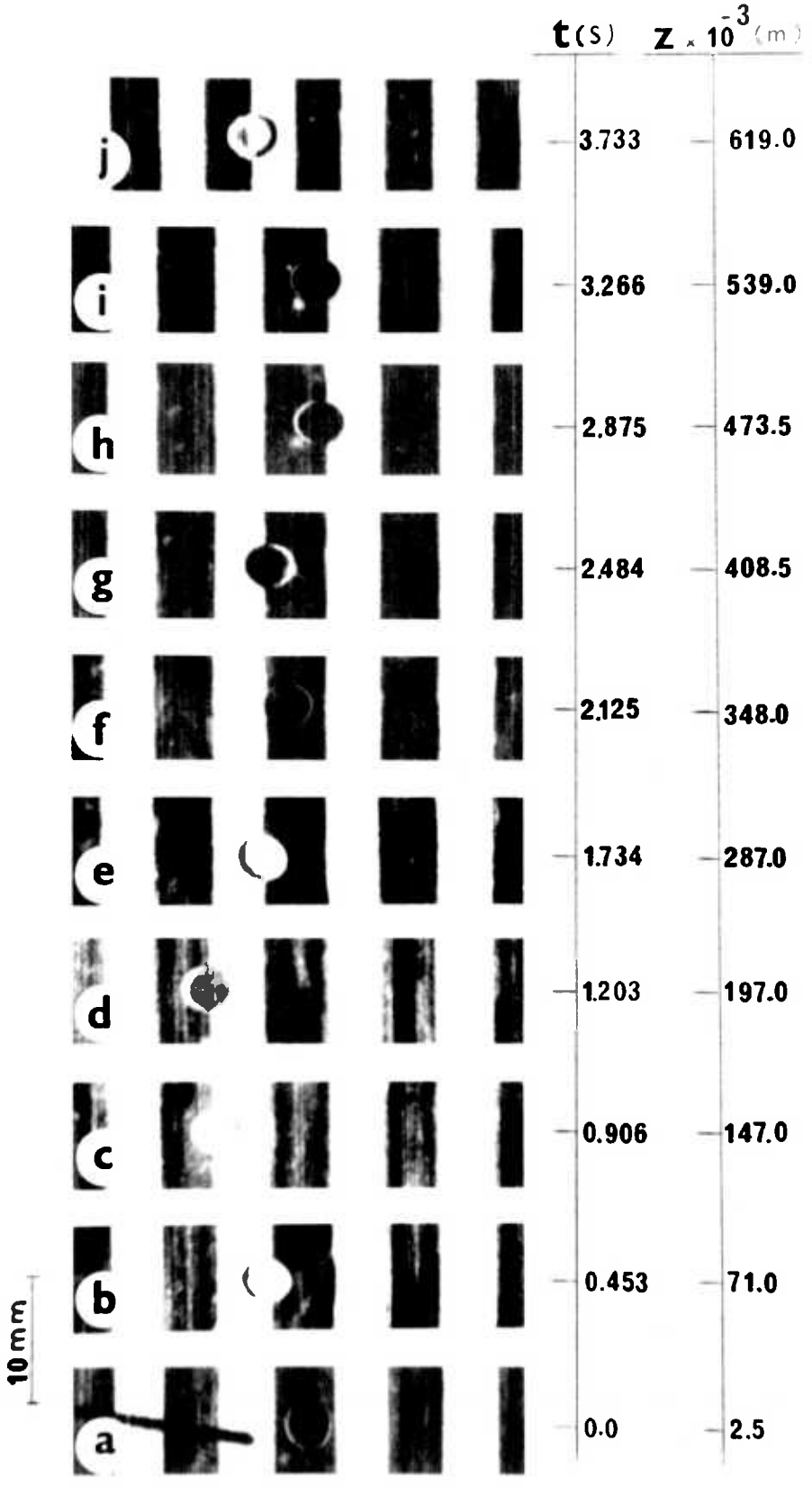

Figure 4.1(a-j): Configurations of a non-evaporating butane droplet rising in water

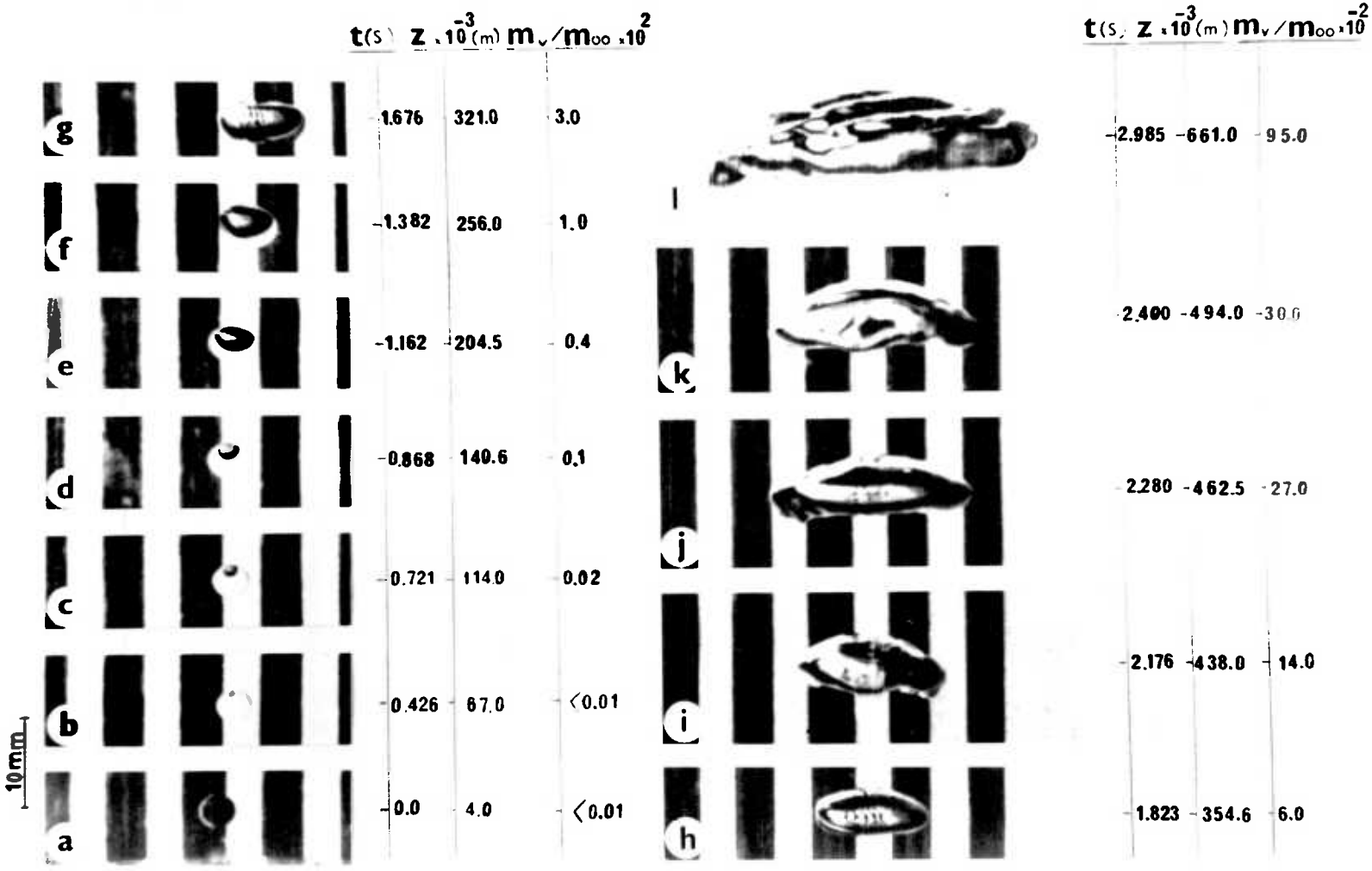

Figure 4.2(a-l): Configurations of an evaporating butane droplet rising in water

gradually increased and became more obvious.

The shapes of the bubble-droplet system in different mass ratios are mainly dependent on the initial size of the droplet. For droplet sizes of around 4.0 mm diameter, the spherical shape changes to spheroidal at about 0.1% and then to spherical cap at around 10% evaporation. For smaller droplets, these percentages are closer to 100%.

The shapes of large bubbles were classified as spherical caps. These bubbles usually seemed to have a concave surface at the bottom. The upper surface was not usually smooth, although in some cases a smooth surface was observed. The irregularities on the bubble surface sometimes appeared to be like waves propagating on the surface which could be seen with the naked eye. The edges of these bubbles also seemed to be rough. The shapes of such bubbles might have been slightly affected by the side walls. Large bubbles did not usually divide except in rare cases, although small bubbles or droplets occasionally separated from the system.

The use of black stripes on the column walls suggests an indirect procedure in order to obtain some information concerning the conditions of a bubble surface. The reflections on the bubble surface took specific shapes according to the curvature of the bubble or the irregularities of the surface in different places. Some examples are given in Figures 4.3(a-f). This kind of information was more difficult to obtain or could not be detected if the stripes were not present. Another example is given in Figures 4.4(a-d), which show the deformation of a bubble, together with slight rotation in four consecutive shots. The change in the shapes of the reflections on the bubble is due to the variation of the surface conditions. More examples are given in Figures 4.5(a-g), where one bubble is being separated from the large bubble. The apparent tension on the bubble surface is especially recognisable on the shots (d), (e) and (f).

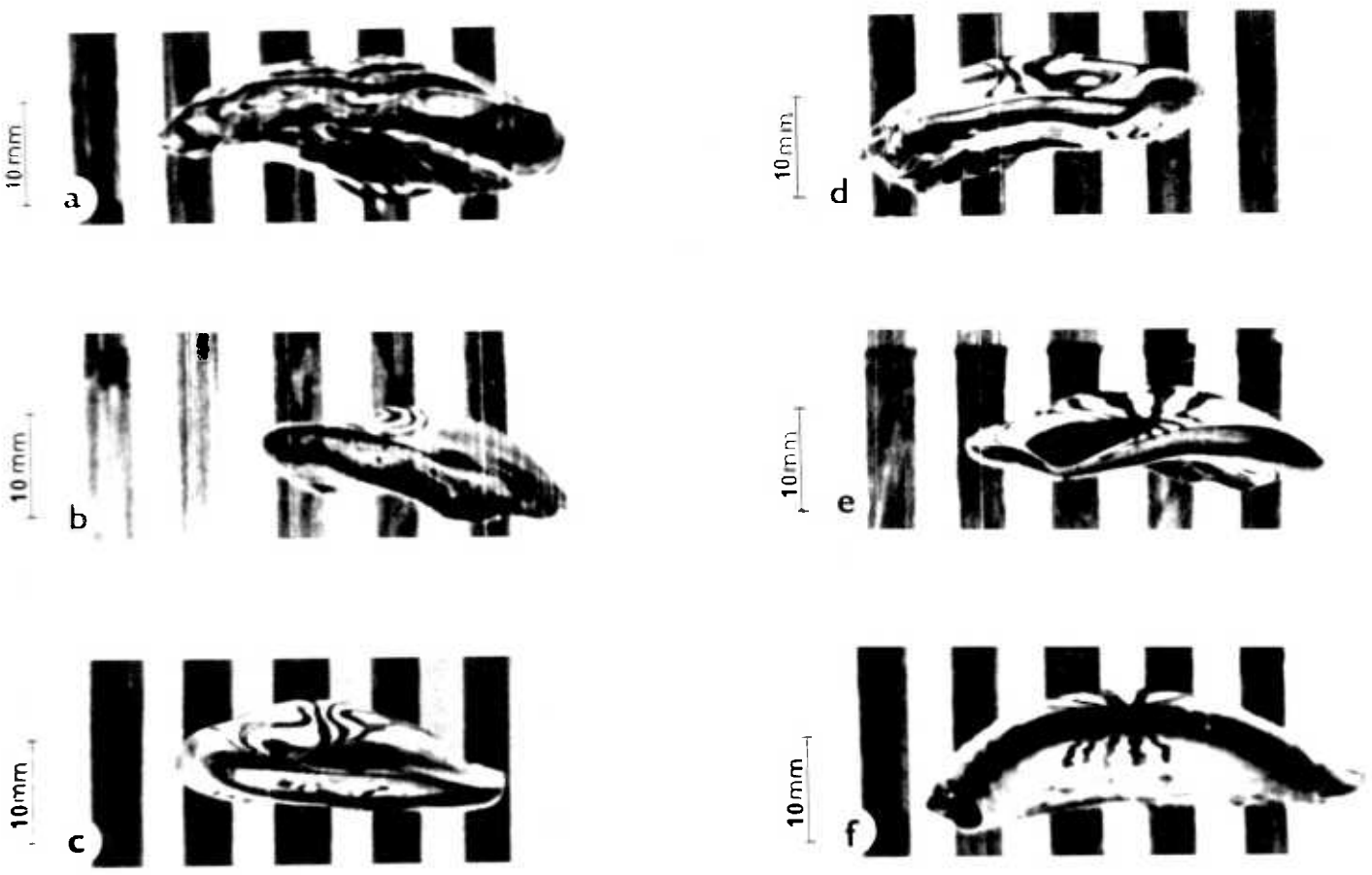

Figure 4.3(a-f): Reflections on the surface of butane bubbles rising in water

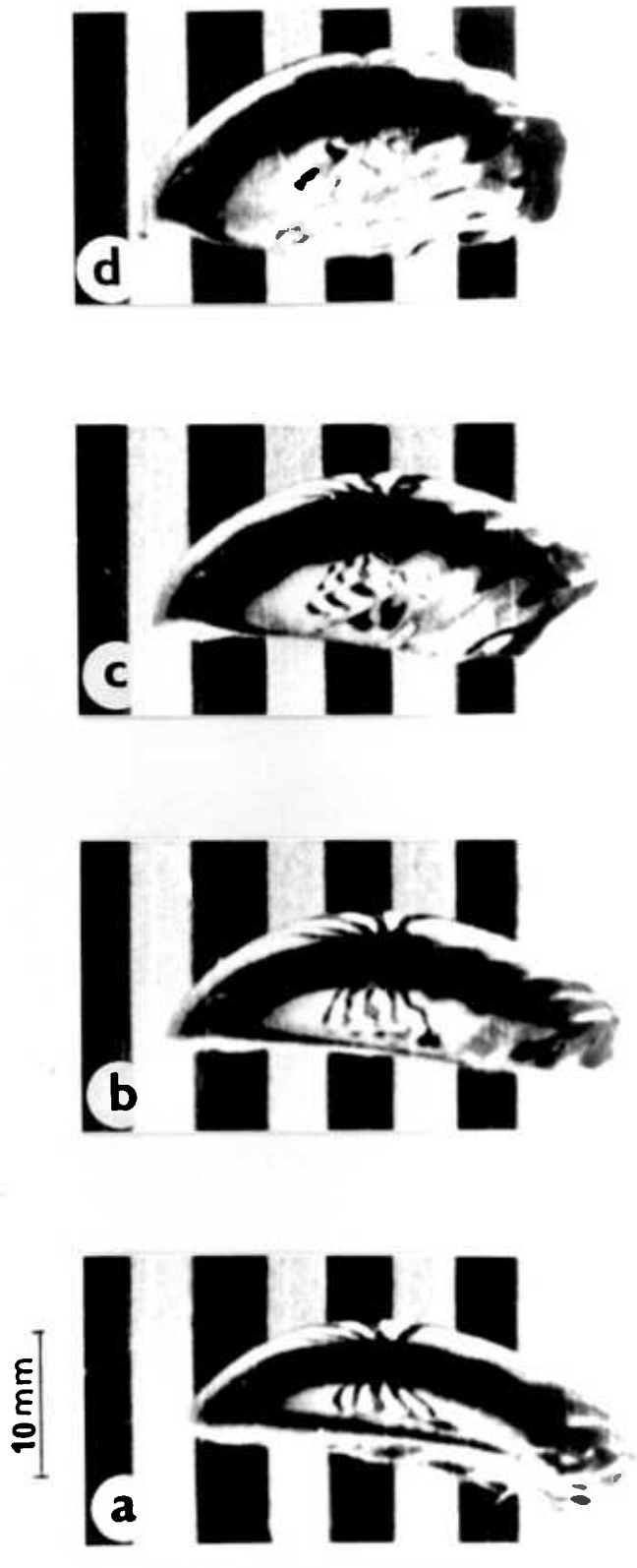

Figure 4.4(a-d): Reflections on the surface of a bubble rising in water (Δt = 1/64 s)

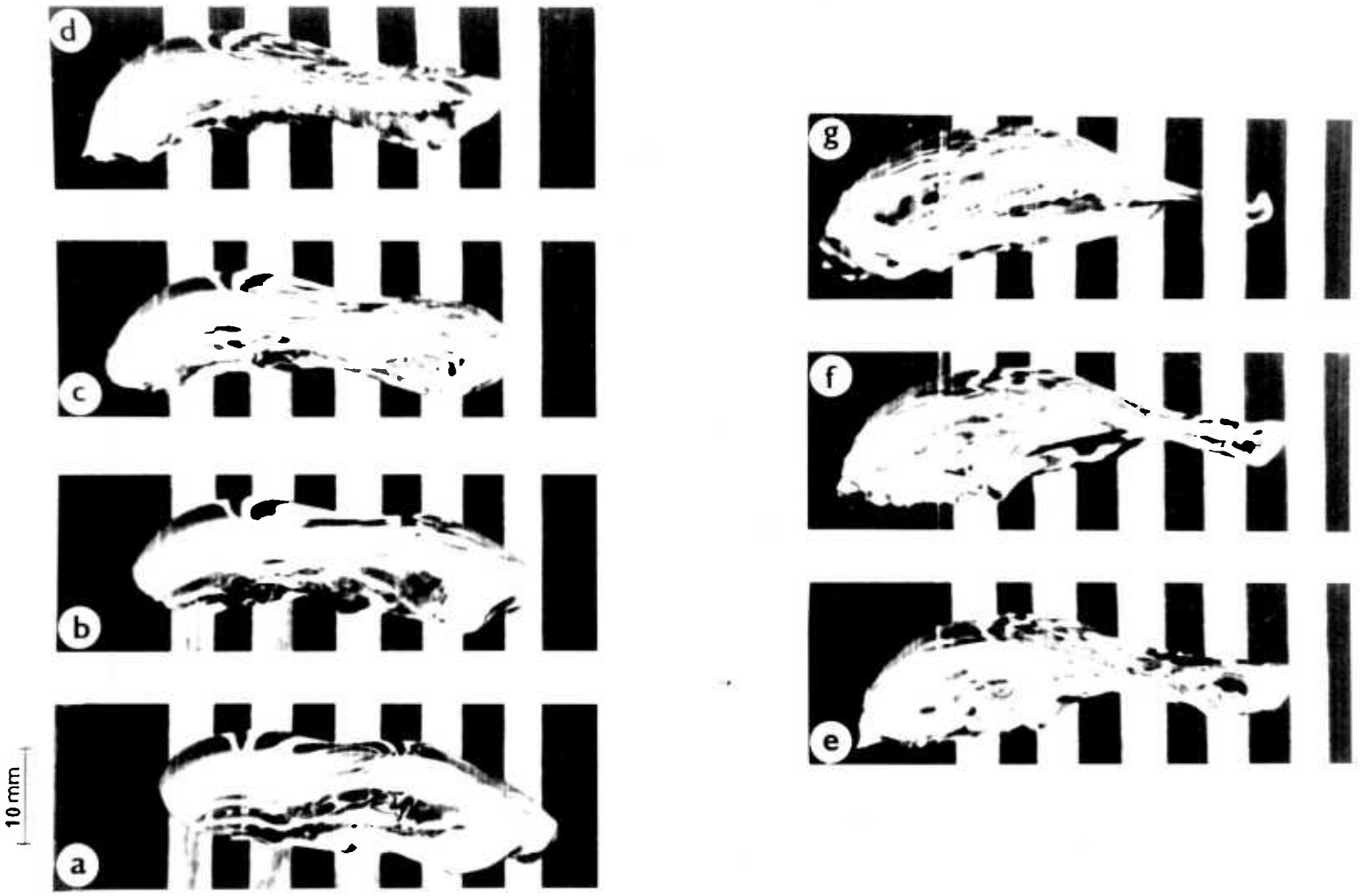

Figure 4.5(a-g): Reflections on the surface of a butane bubble rising in water during a bubble separation (Δt = 1/64 s)

In a study of the photography of droplets, Sideman (69) showed that such a technique was useful to visualise the turbulent state of the evaporating surface of a droplet at the water surface. This procedure is similar to the visualisation methods described by Werlé (88) which are used for the study of flows with free surfaces. These techniques include the use of similar backgrounds seen through the flow.

The behaviour of the stopped-evaporation droplets depended on the mass ratio of the bubble-droplet system. Three examples are given in Figures 4.6 to 4.8. When evaporation has been stopped in the early stages (Figure 4.6), the behaviour of the system was more like a droplet. The sloshing of the liquid and oscillation of the system was not significant. At higher mass ratios (Figures 4.7 to 4.8), liquid sloshing was more obvious. Figures 4.7(f-h) are shots showing the bubble-droplet in short time intervals, which give an idea of how fast the sloshing occurs. Also, the shape of the bubble part can be compared according to different positions of the liquid part. In Figure 4.8, three consecutive shots, (f), (g) and (h), again indicate the degree of the liquid movement. As the bubble part tries to keep its regular shape, the liquid part does not appear to have any specific shape. Considering the shape variations of non-evaporating bubble-droplets, it is suggested that two-dimensional photography is not adequate to obtain the true shape of the system.

4.2 RESULTS

The experimental results are divided into three parts. These are: non-evaporating, evaporating, and stopped-evaporation droplets. In the first part, the parameter of interest was the rise velocity for the sake of comparison with those of evaporating and stopped-evaporation droplets at very low mass ratios. In the case of evaporating droplets, the

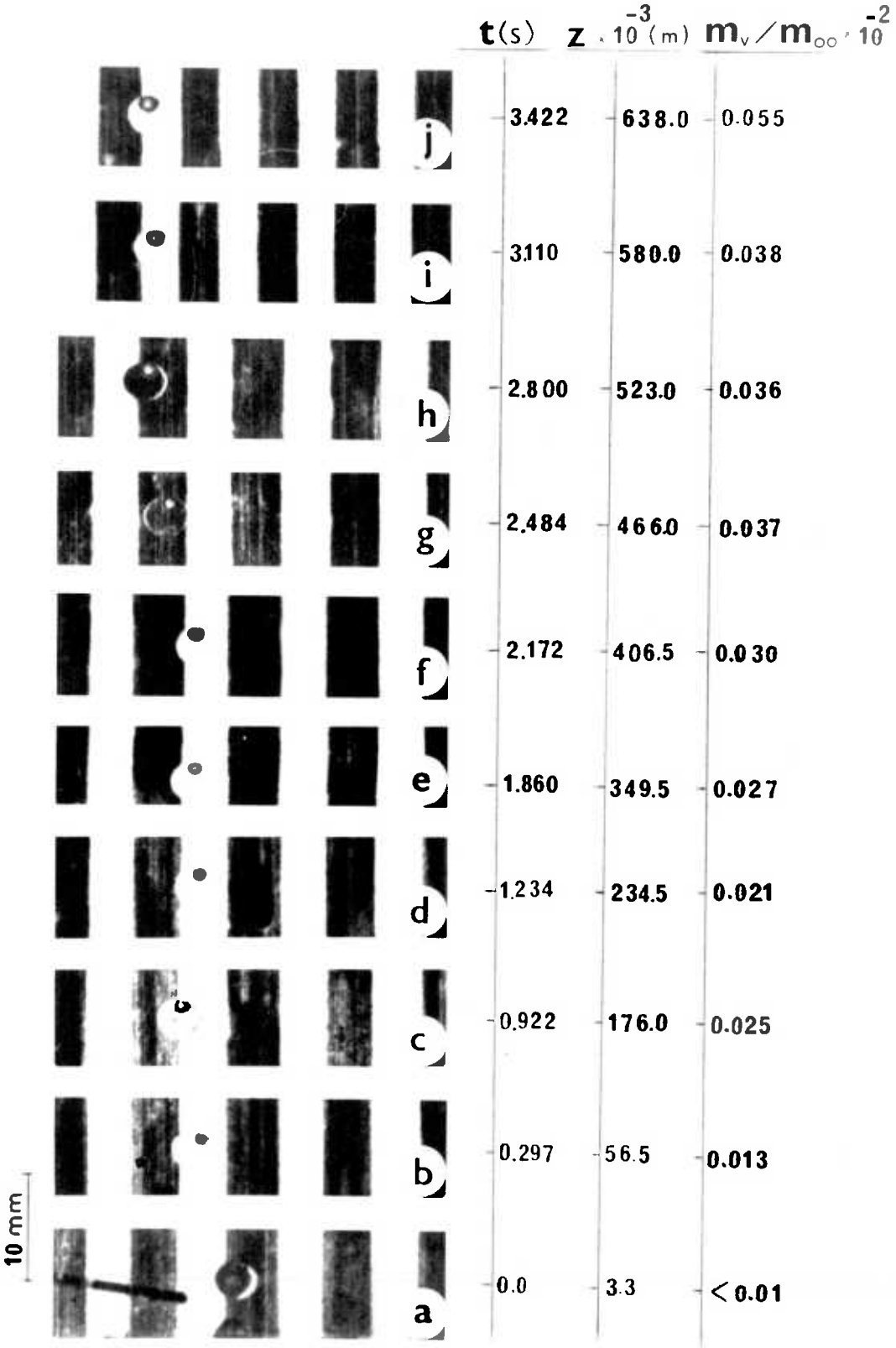

Figure 4.6(a-j): Configurations of a stopped-evaporation butane bubble-droplet rising in water

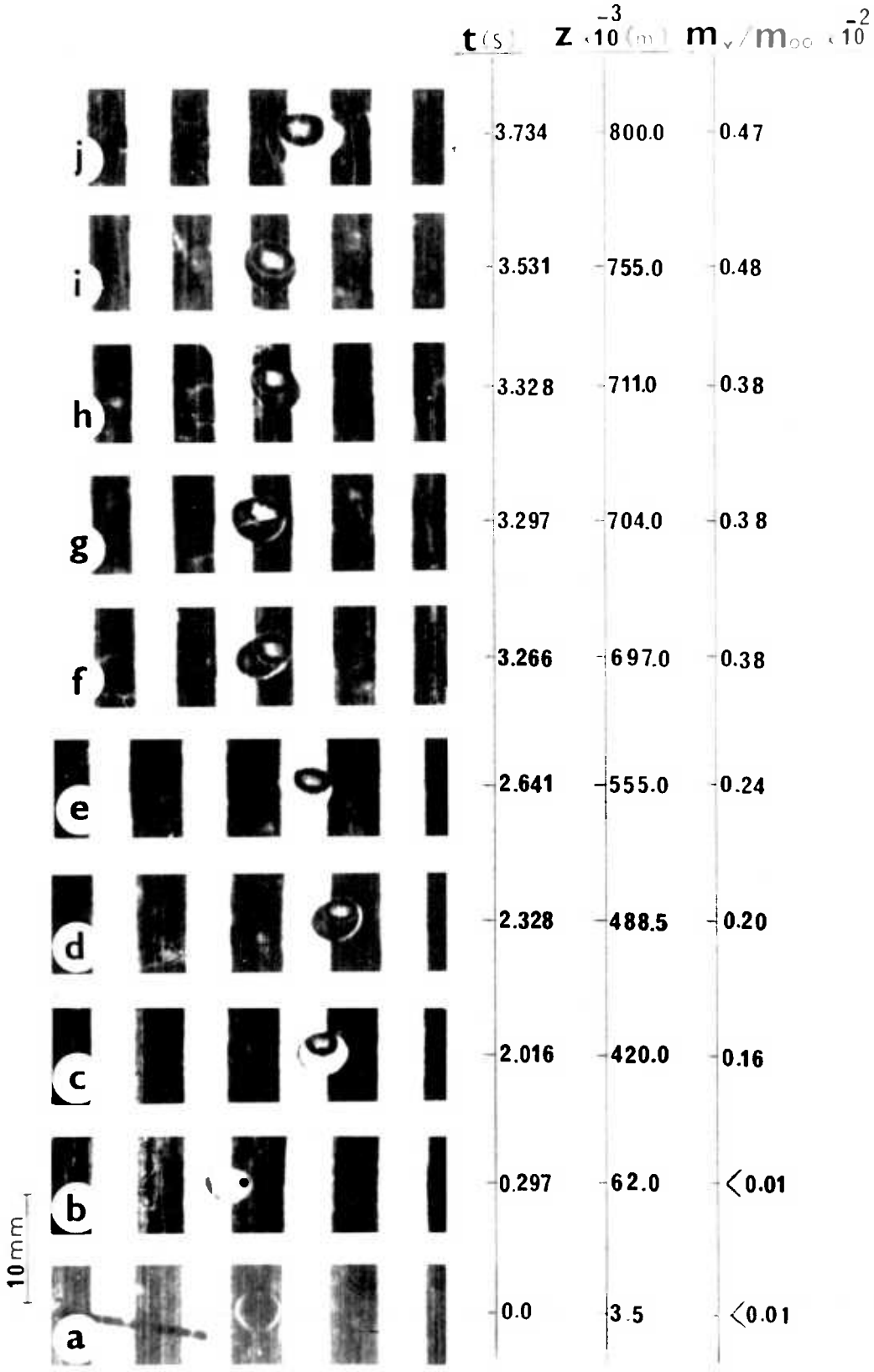

Figure 4.7(a-j): Configurations of a stopped-evaporation butane bubble-droplet rising in water

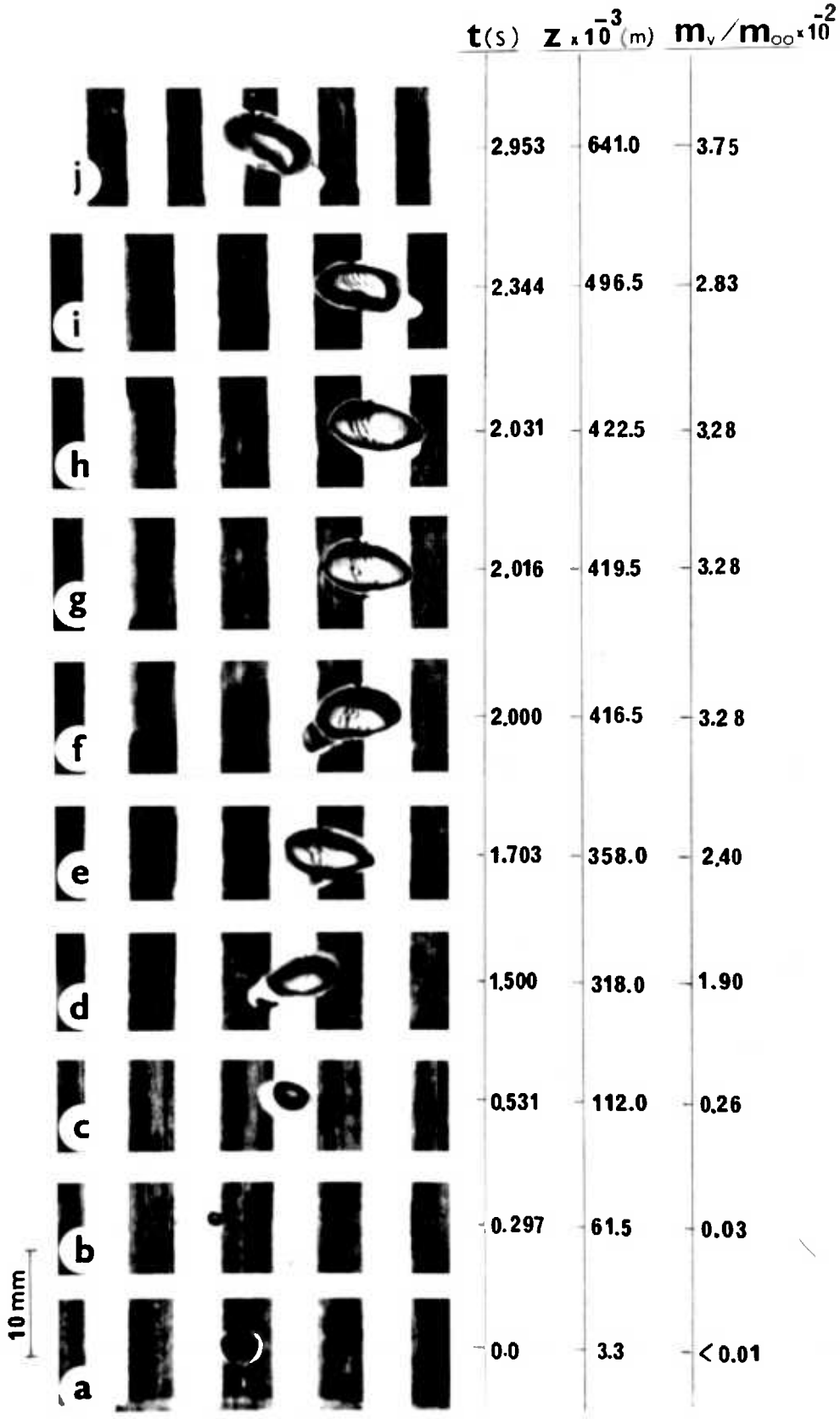

Figure 4.8(a-j): Configurations of a stopped-evaporation butane bubble-droplet rising in water

parameters studied were the growth, growth rate, acceleration of the bubble boundary (referred to the equivalent spherical radius), rise velocity and heat transfer to the droplet. For stopped-evaporation droplets, the rise velocity at mass ratios below 10% was investigated. The results are presented in the plotted form in Figures 4.9 to 4.30 and the corresponding tables are given in Appendix A, Tables A.1 to A.30. In the figures which show the variation of rise velocity of evaporating droplets against mass ratio, the latter was obtained using the fitted curves to V_v versus t' data.

4.2.1 Non-Evaporating Droplets

Two examples of the rise velocity of non-evaporating droplets are given in Figure 4.9. After the initial period, the velocity remains more or less constant around an average value. The slight variation of the velocity during the rise is due to the droplet motion on a helical path.

4.2.2 Evaporating Droplets

4.2.2.1 Growth

Examples of the variation of vapour volume against time are shown in Figures 4.10(a) and 4.11(a). Also included in the figures are the fitted curves to each set of data, which was explained in section 3.8.8. Coefficients of the polynomials are given in Table 4.1. In processing the data, time zero ($t' = 0$) was taken as the time related to the first available frame after the droplet was released from the nozzle. Droplets travelled a distance before clear signs of evaporation could be realised. This distance varied according to the experimental conditions, mainly the initial droplet temperature and water temperature.

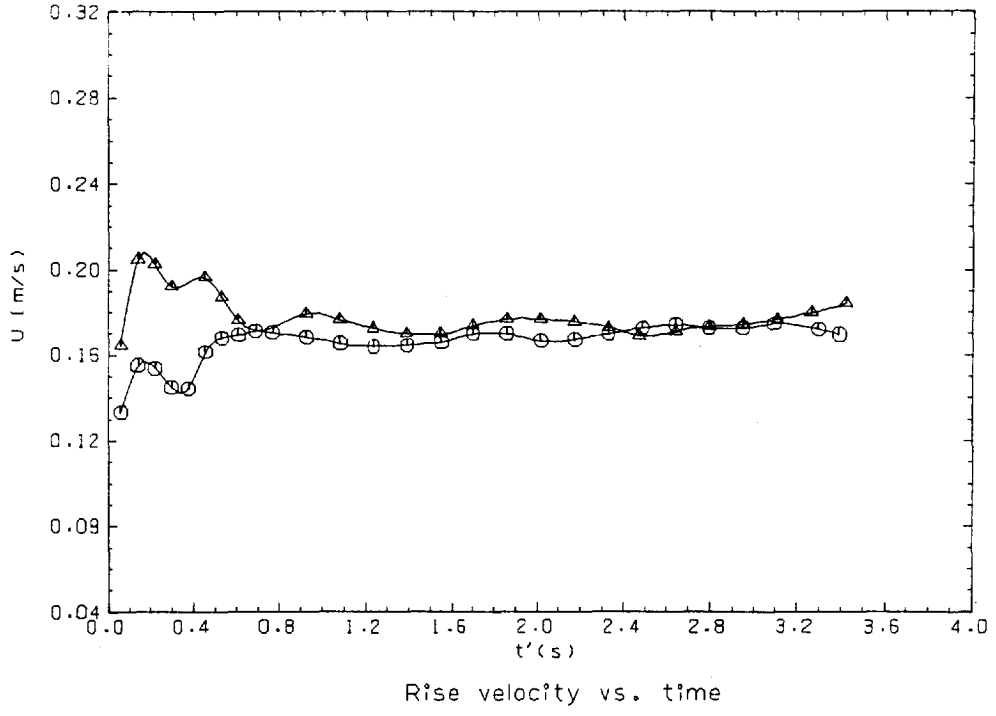

Figure 4.9: Variation of rise velocity of non-evaporating butane droplets in distilled water

Key to the figure

Symbol	Set	Run	$d \times 10^{-3}$ (m)	T_c (°C)
⊙	10	1	4.0	3.7
△	10	2	3.85	3.7

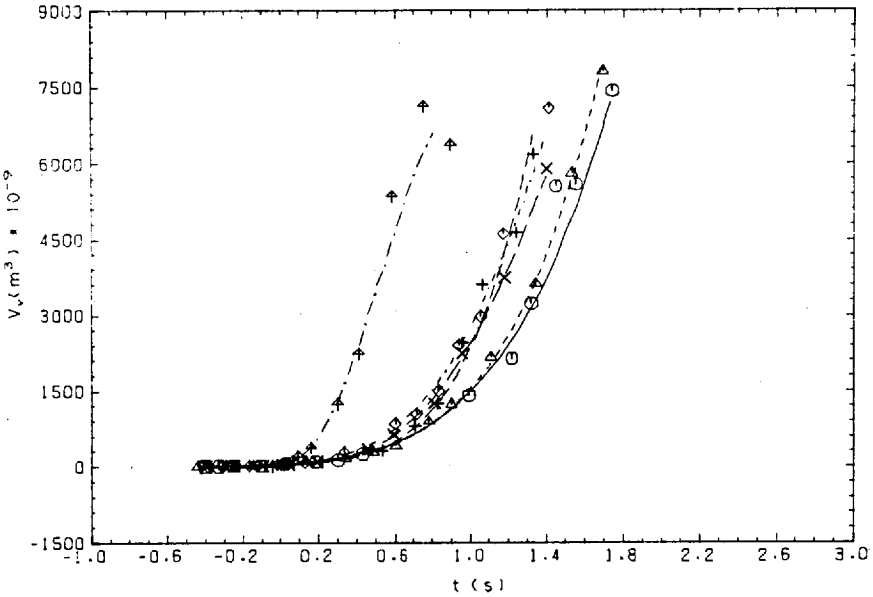

(a) Vapour volume vs. time

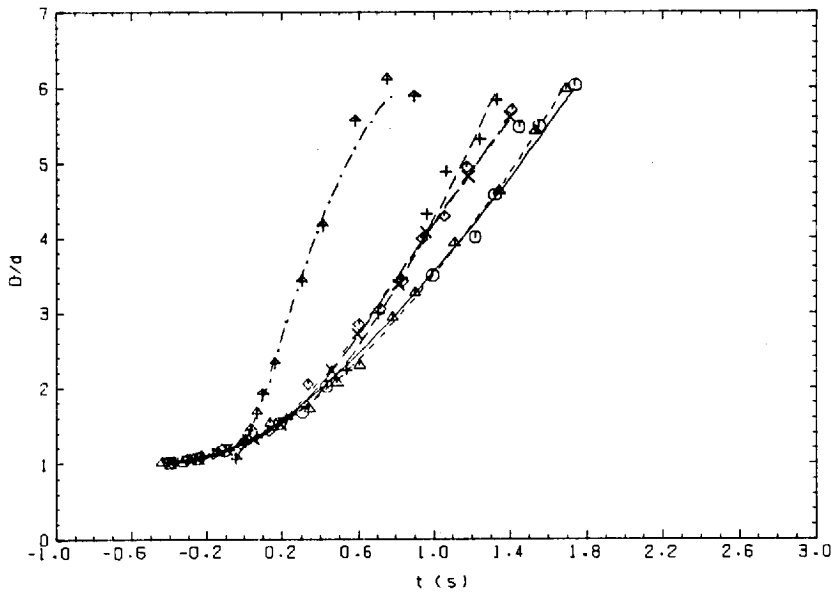

(b) Diameter ratio vs. time

Figure 4.10(a,b): Variation of vapour volume and diameter ratio of evaporating butane droplets in distilled water

Key to the figures*

Symbol	Set	Run	$d \times 10^{-3}$ (m)	ΔT_0 (°C)
⊙———	4	8	4.0	2.5
△------	4	10	4.1	2.5
+----	5	25	3.9	4.0
X— — —	5	26	4.0	4.0
◇-·-·-·-	5	28	4.2	4.0
⋔—·—·—	7	15	3.9	10.0

*In Figure 4.10(a), lines are fitted curves to the experimental data
*In Figure 4.10(b), lines are based on the fitted curves to V_v versus t' data

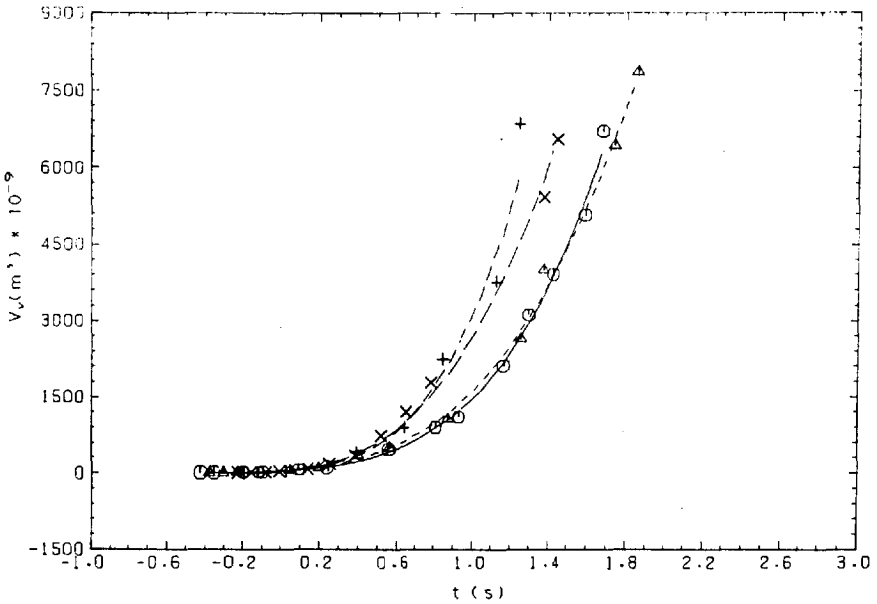

(a) Vapour volume vs. time

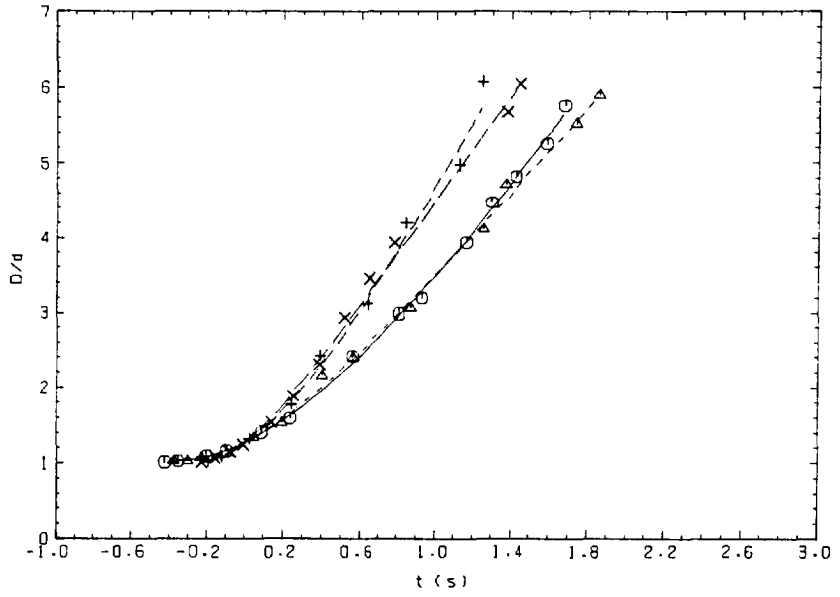

(b) Diameter ratio vs. time

Figure 4.11(a,b): Variation of vapour volume and diameter ratio of evaporating butane droplets in distilled water

Key to the figures*

Symbol	Set	Run	$d \times 10^{-3}$ (m)	ΔT_o (°C)
⊙——	4	11	4.05	2.6
△------	4	12	4.20	2.5
+- - - -	5	15	3.9	4.5
×— — —	5	16	3.85	4.6

*In Figure 4.11(a), lines are fitted curves to the experimental data

*In Figure 4.11(b), lines are based on the fitted curves to V_v versus t' data

TABLE 4.1

Coefficients of the Polynomials Fitted to the Vapour Volume/Time Data of Evaporating Butane Droplets in Distilled Water, and the Values of t''

$$V_v\ (m^3) \times 10^{-9} = a_1 + a_2\, t' + a_3\, t'^2 + a_4\, t'^3 + a_5\, t'^4 + a_6\, t'^5 \qquad (4.1)$$

where: $t'_{min} < t' < t'_{max}$

Set	Run	a_1	a_2	a_3	a_4	a_5	a_6	t'' (s)	t'_{min} (s)	t'_{max} (s)
4	8	0.07437	1.57964	-13.688	19.558	68.7994	45.4079	0.757	0.01	2.5
4	10	0.3489	-7.5110	49.0513	48.3436	-11.7092	107.2306	0.644	0.06	2.34
4	11	0.02998	0.61197	-9.39513	16.75285	57.58796	45.46845	0.779	0.28	2.46
4	12	0.2130	-7.9732	63.9678	-154.053	356.3796	-43.306	0.658	0.21	2.52
5	15	26.389	-773.12	2483.44	-3653.72	2726.51	-431.623	0.550	0.28	1.79
5	16	0.0850	11.000	-132.7864	360.80	664.769	-157.827	0.436	0.00	1.88
5	25	1.6795	11.3608	-226.1421	864.365	-1056.662	514.7664	0.731	0.35	2.06
5	26	34.59289	-504.5192	2440.557	-4570.26	3762.064	-808.2292	0.528	0.28	1.93
5	28	0.67165	-22.8474	612.3426	-1721.5857	2262.7381	-503.4206	0.445	0.02	1.85
7	15	-55.555	1575.3	-13763.0	71488.7	-75949.3	23738.3	0.106	0.06	1.44
7	32	0.1642	-6.4582	263.068	-319.7468	2087.99	-656.522	0.326	0.02	1.70
7	34	-2.004	42.426	-226.17	586.3	-508.89	195.39	0.760	0.09	2.03
10	4	39.791	-357.827	1012.428	-959.09	449.6271	3.7295	0.501	0.37	2.28
10	8	-21.9748	175.092	-491.4872	604.321	-278.2258	64.7524	0.904	0.29	2.87
11	1	9.2930	-116.7664	489.4465	-767.5412	648.8618	-119.7774	0.656	0.22	2.67
11	3	38.1704	-228.5176	512.1065	-472.391	243.7447	-31.804	0.745	0.37	2.92
11	5	23.274	-240.095	852.109	-1198.848	845.1978	-149.1885	0.635	0.22	2.92
11	12	-3.5110	35.3442	-114.881	170.07	-105.128	31.883	1.154	0.22	3.29

In order to reduce the effect of this initial period on the total time, it was decided to assume time zero (t = 0) as the time when evaporation has proceeded up to 0.5%. In this respect, the values of t'' ($t'' = t' - t$) were obtained and are given in Table 4.1. This made it easier to compare the growth of evaporating droplets at different operating conditions ($d, \Delta T_0$).

In Figures 4.10(b) and 4.11(b), the variation of the equivalent spherical diameter ratio against time is given. Figure 4.12 shows the variation of mass ratio versus time. As it was explained, all the curves pass through the point t = 0 which corresponds to the mass ratio 0.005. As can be seen, all the runs show the same trend. Evaporation time is decreased with increase of temperature difference.

Comparing different runs showed that, in some cases, droplets evaporating in nearly the same operating conditions ($d, \Delta T_0$) had different evaporation times. Examples are given in Figures 4.13(a,b). It should be noted that some of the runs presented in Figure 4.13 were carried out under different water heads above the nozzle (see the corresponding tables). As a result, for the same temperature difference, saturation and water temperature were slightly higher in the runs with higher water heads. Prolonged evaporation seemed to have been due to the comparatively higher degree of subcool of the initial droplet temperature. The fact that in some of these runs the initial droplet temperature was below the water freezing point by three or four degrees raises the possibility of freezing of the water layer adjoining the droplet as it was mentioned by Sideman et al (68). However, the mechanism of such phenomenon, if it exists, and its effect on the evaporation process is not known. Finally, the reason may be partly attributed to the slight difference in the experimental conditions at different execution times.

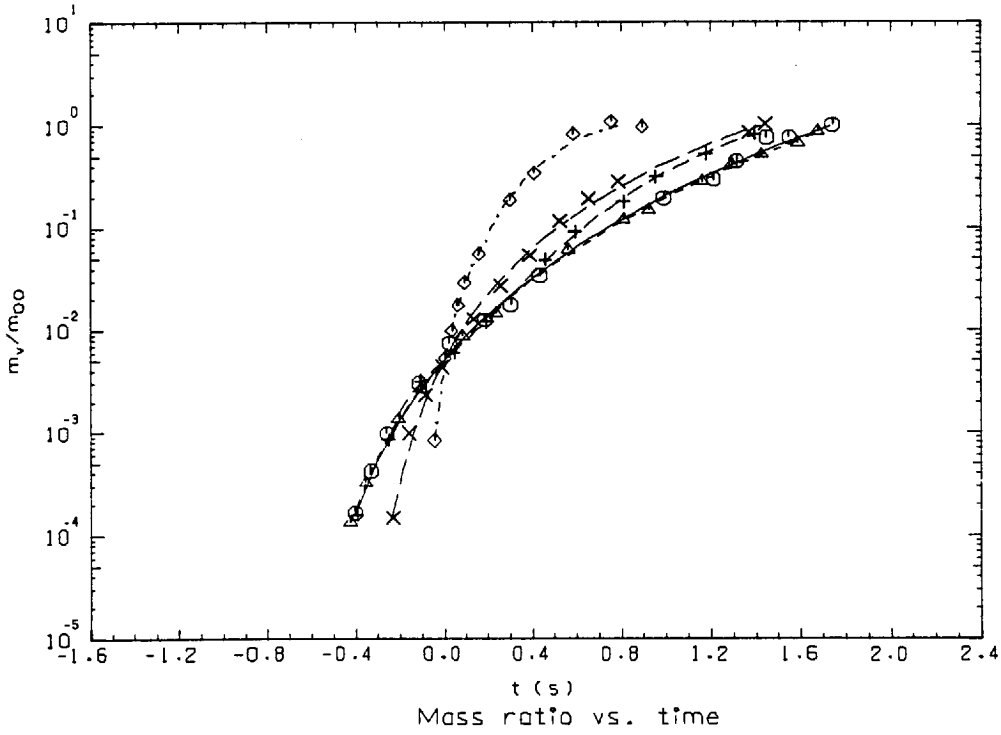

Figure 4.12: Variation of mass ratio of evaporating butane droplets in distilled water

Key to the figure*

Symbol	Set	Run	$d \times 10^{-3}$ (m)	ΔT_o (°C)
⊙———	4	8	4.0	2.5
△------	4	11	4.05	2.6
+----	5	26	4.0	4.0
x— — —	5	16	3.85	4.6
◇-·-·-·	7	15	3.90	10.0

*Lines are based on the fitted curves to V_v versus t' data

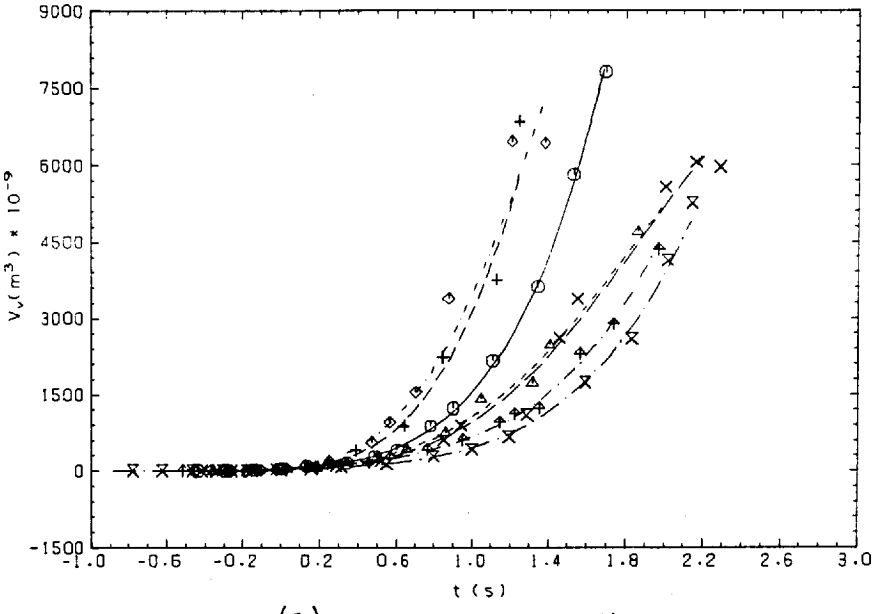

(a) Vapour volume vs. time

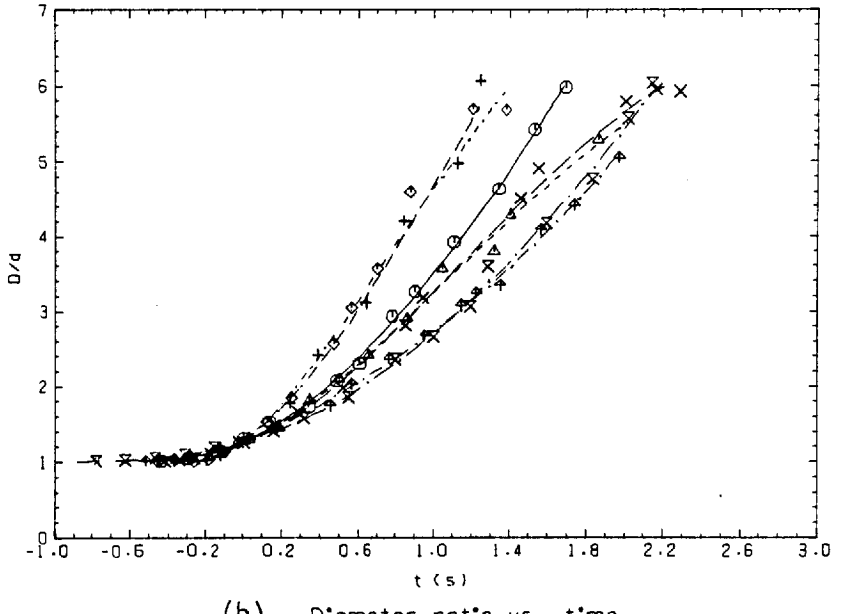

(b) Diameter ratio vs. time

Figure 4.13(a,b): Variation of vapour volume and diameter ratio of evaporating butane droplets in distilled water

Key to the figures*

Symbol	Set	Run	$d \times 10^{-3}$ (m)	ΔT_0 (°C)
⊙———	4	10	4.1	2.5
△-------	11	1	3.95	2.6
+-----	5	15	3.9	4.5
×— — —	11	5	3.8	2.8
◇--------	7	32	4.05	5.2
⊹—·—·—	10	8	4.0	2.3
⊠—·——·-	11	12	3.6	2.2

*In Figure 4.13(a), lines are fitted curves to the experimental data
*In Figure 4.13(b), lines are based on the fitted curves to V_v versus t´data

4.2.2.2 Rise velocity

Figures 4.14(a,b) show the results of the variation of rise velocity for the total of fifteen runs. Velocity increases up to about 1% evaporation and then shows a slight decrease and then increase up to the end of evaporation. Figure 4.15 shows that the Reynolds number based on water properties increases throughout the evaporation, which is quicker in the later stages of evaporation. The drop of velocity near 1% evaporation was observed in the majority of runs, and it was more distinguishable in low temperature differences. Examples are shown in Figures 4.16(a,b) to 4.19(a,b). For each run, the rise velocity is plotted against time and mass ratio. The result of superimposing all four cases is shown in Figure 4.20. Examination of this evaporation range on the ciné film indicated that this drop in velocity coincided with the increased deformation and serious movement of the liquid at the bottom of the bubble-droplet which seemed to be responsible for the increased drag force and as a result velocity decreased. At this stage, the size of the resisting force seems to be comparable with the buoyancy force and thus the effect is clear, while in the later stages the buoyancy force due to the size of the bubble becomes dominant and thus velocity continues to increase.

4.2.2.3 Instantaneous heat transfer coefficient

Since the calculation of heat transfer coefficient is based on the variation of the vapour volume against time, the direct use of experimental measurements resulted in a considerable scattering of the heat transfer coefficients. Thus it was decided to fit a curve to every set of data which comprised a few runs having nearly the same operating conditions. For two sets, shown in Figures 4.21(a,b), polynomials of degree 5

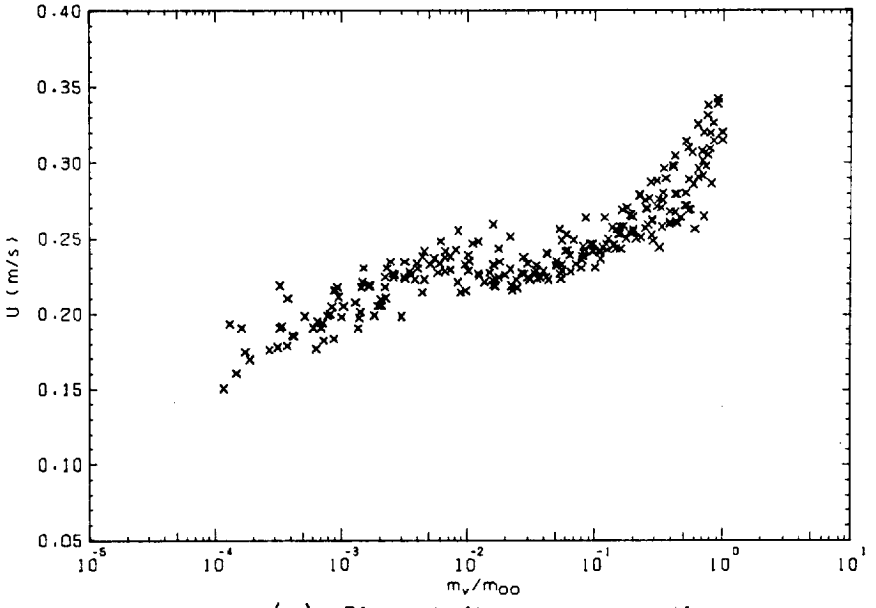

(a) Rise velocity vs. mass ratio

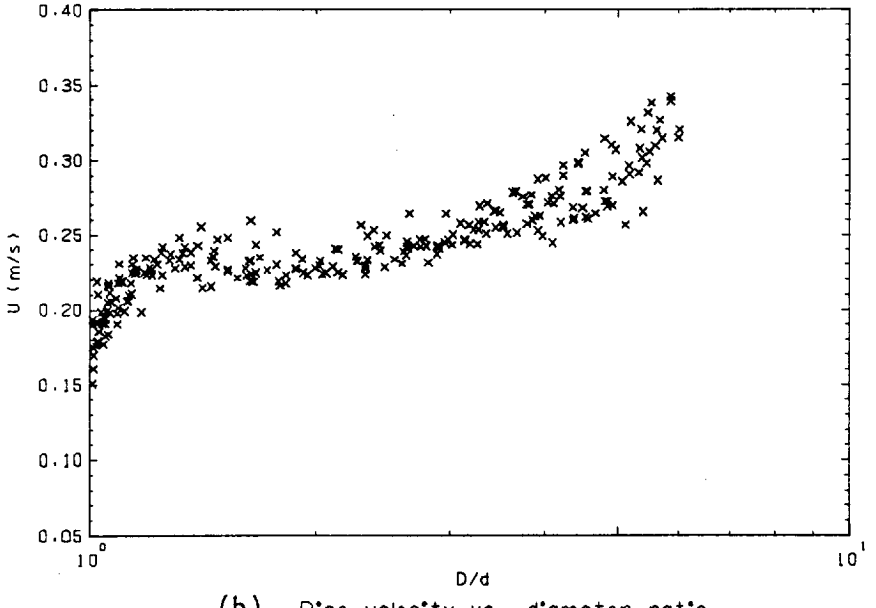

(b) Rise velocity vs. diameter ratio

Figure 4.14(a,b): Variation of rise velocity of evaporating butane droplets in distilled water

$$\left[\begin{array}{l} d = 3.6\text{-}4.2 \times 10^{-3} \text{ (m)} \\ \Delta T_0 = 1.9\text{-}4.6 \text{ (°C)} \\ T_c = 3.5\text{-}5.8 \text{ (°C)} \end{array}\right]$$

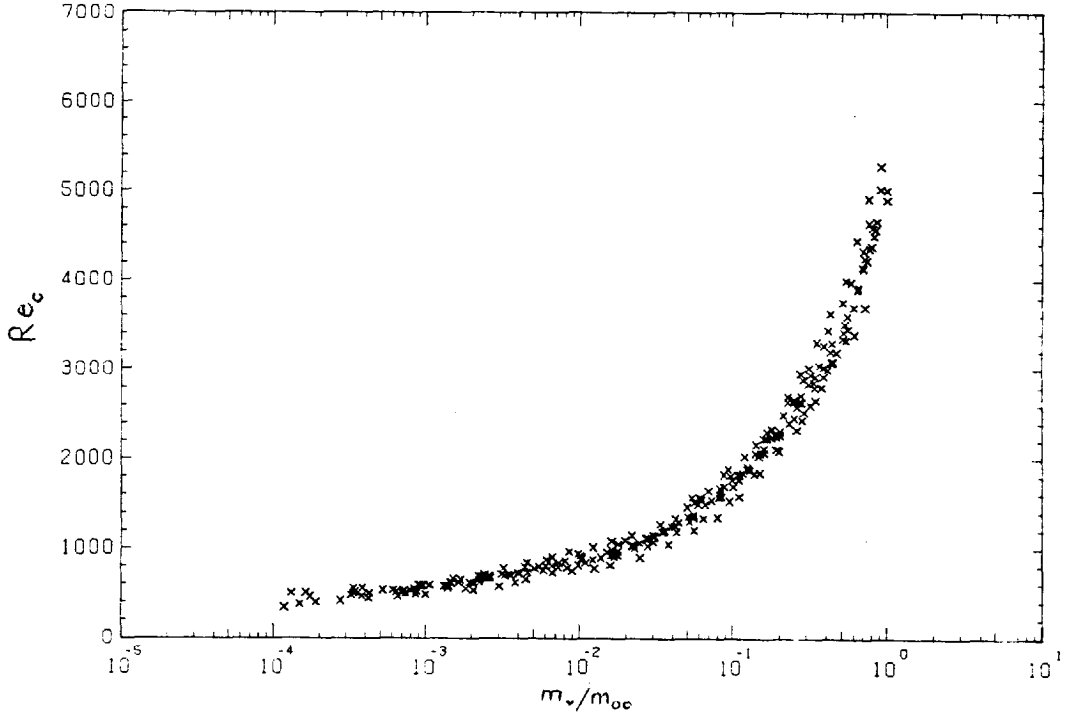

Figure 4.15: Variation of Reynolds number of evaporating butane droplets in distilled water

$$\left[\begin{array}{l} d = 3.6\text{-}4.2 \times 10^{-3}\ (\text{m}) \\ \Delta T_o = 1.9\text{-}4.6\ (^{\circ}\text{C}) \\ T_c = 3.5\text{-}5.8\ (^{\circ}\text{C}) \end{array}\right]$$

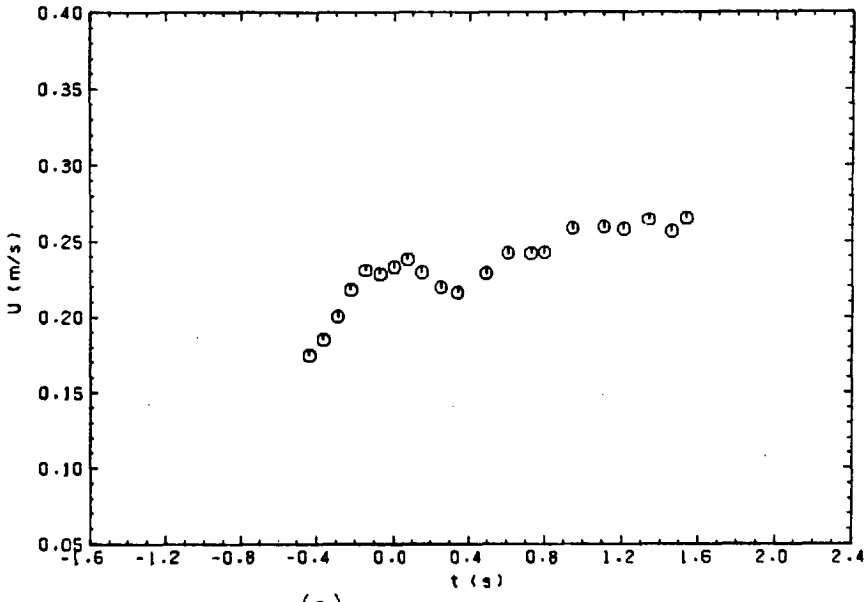

(a) Rise velocity vs. time

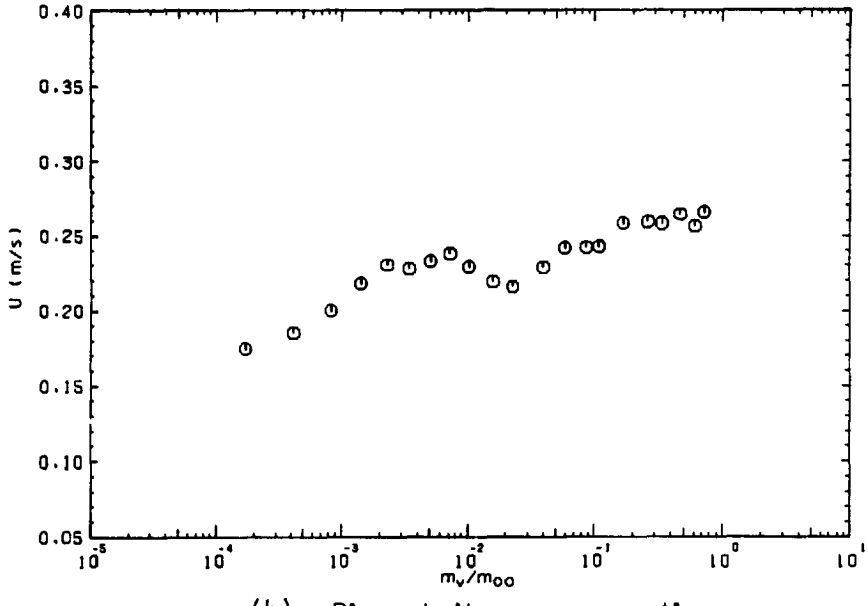

(b) Rise velocity vs. mass ratio

Figure 4.16(a,b): Variation of rise velocity of an evaporating butane droplet in distilled water

$$\begin{bmatrix} \text{Set 4, Run 10} \\ d = 4.1 \times 10^{-3} \text{ (m)} \\ \Delta T_o = 2.5 \text{ (°C)} \end{bmatrix}$$

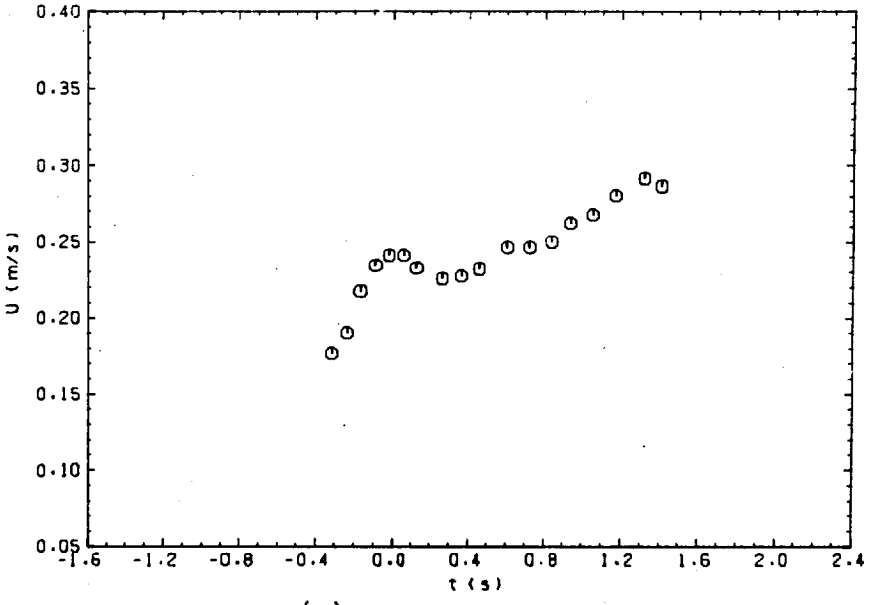

(a) Rise velocity vs. time

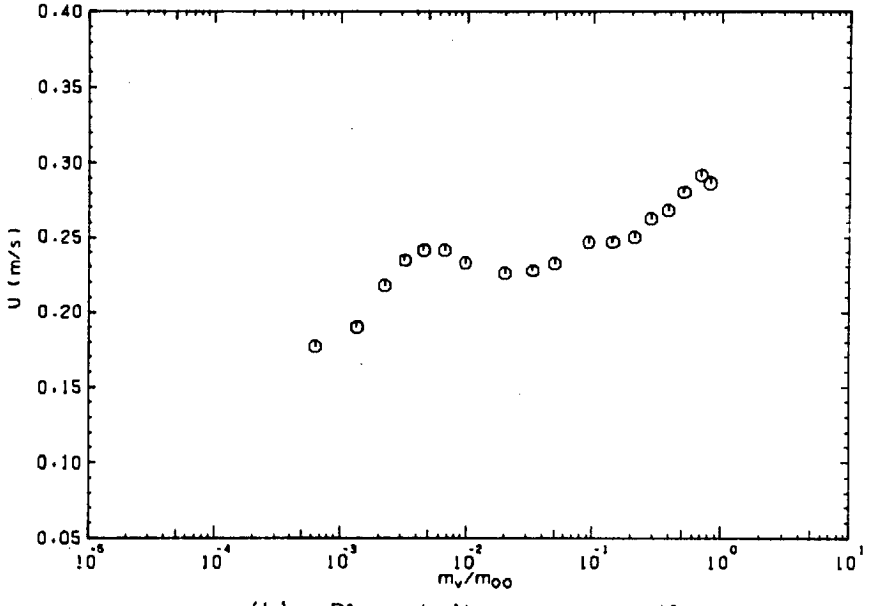

(b) Rise velocity vs. mass ratio

Figure 4.17(a,b): Variation of rise velocity of an evaporating butane droplet in distilled water

$$\left[\begin{array}{l} \text{Set 5, Run 28} \\ d = 4.2 \times 10^{-3}\ \text{(m)} \\ \Delta T_o = 4.0\ (^{\circ}\text{C}) \end{array}\right]$$

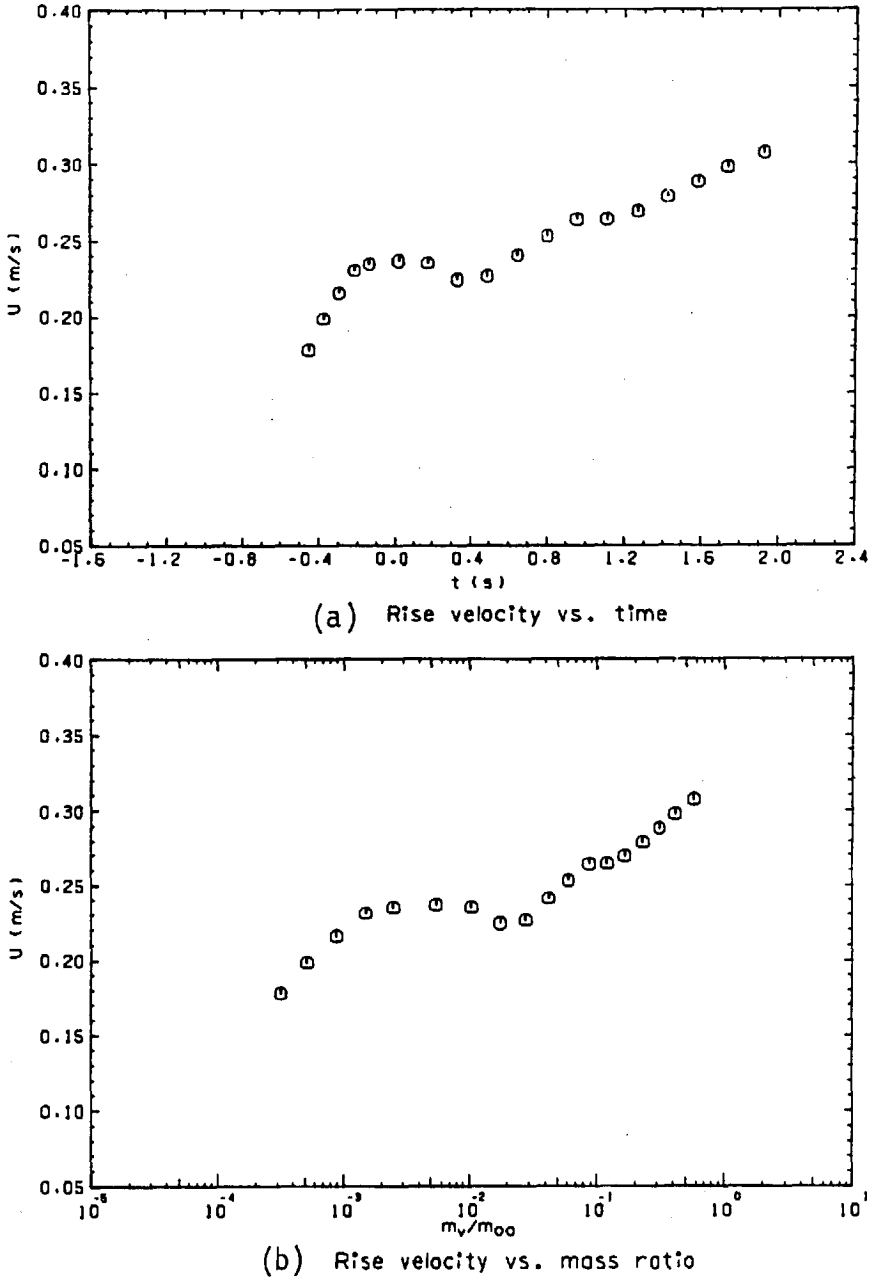

Figure 4.18(a,b): Variation of rise velocity of an evaporating butane droplet in distilled water

$$\left[\begin{array}{l} \text{Set 10, Run 8} \\ d = 4.0 \times 10^{-3}\ (\text{m}) \\ \Delta T_o = 2.3\ (^{\circ}\text{C}) \end{array}\right]$$

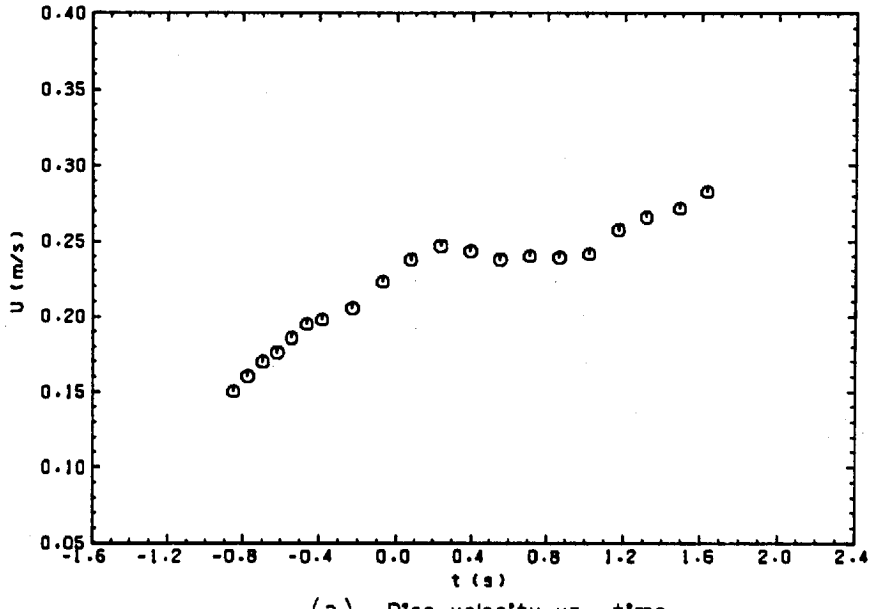

(a) Rise velocity vs. time

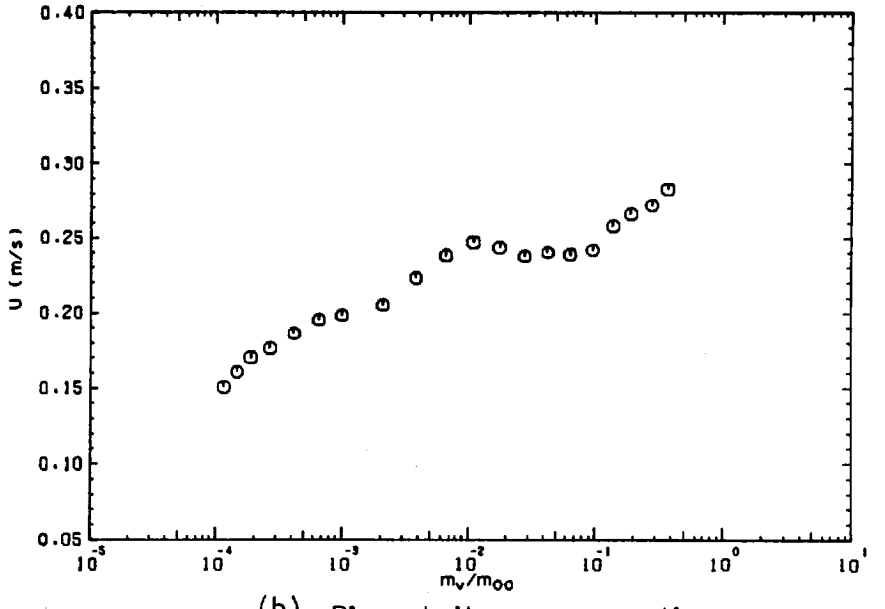

(b) Rise velocity vs. mass ratio

Figure 4.19(a,b): Variation of rise velocity of an evaporating butane droplet in distilled water

$$\left[\begin{array}{l} \text{Set 11, Run 12} \\ d = 3.6 \times 10^{-3}\ \text{(m)} \\ \Delta T_0 = 2.2\ (^{\circ}\text{C}) \end{array}\right]$$

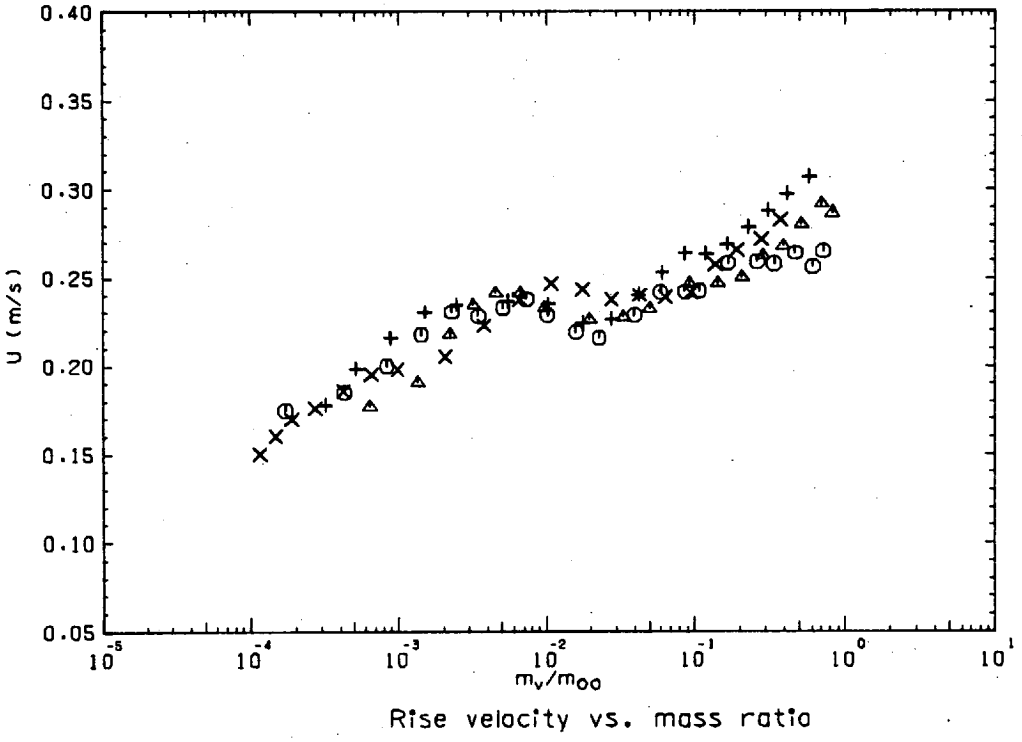

Figure 4.20: Variation of rise velocity of evaporating butane droplets in distilled water

Key to the figure

Symbol	Set	Run	$d \times 10^{-3}$ (m)	ΔT_o (°C)
⊙	4	10	4.1	2.5
△	5	28	4.2	4.0
+	10	8	4.0	2.3
×	11	12	3.6	2.2

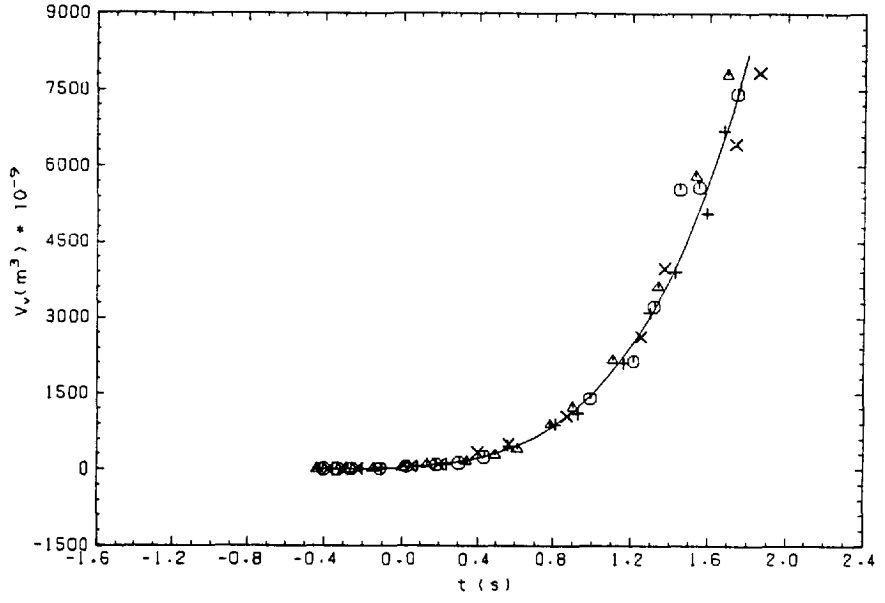

(a) Vapour volume vs. time

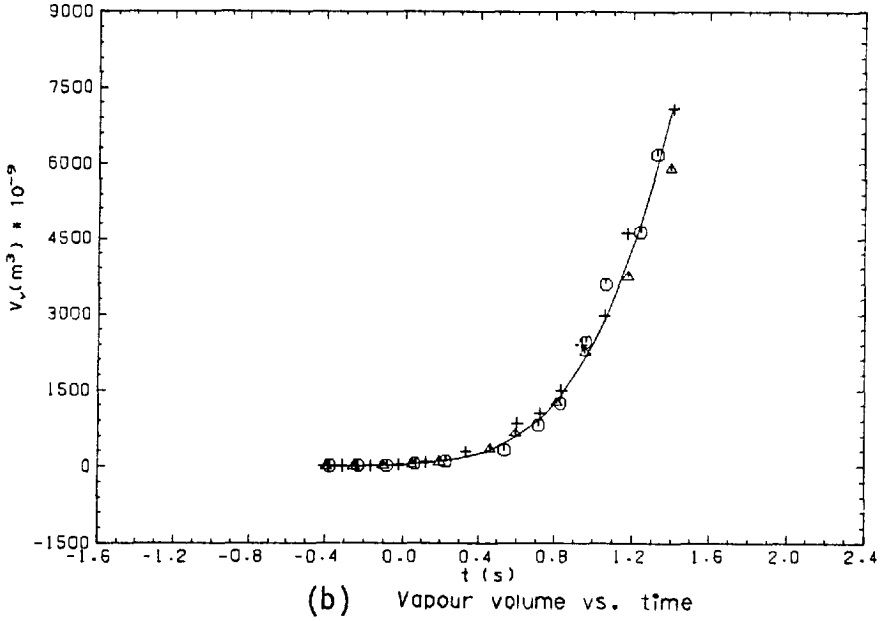

(b) Vapour volume vs. time

Figure 4.21(a,b): Variation of vapour volume of evaporating butane droplets in distilled water

Key to Figure 4.21(a)*

Symbol	Set	Run	$d \times 10^{-3}$ (m)	ΔT (°C)0
⊙	4	8	4.0	2.5
△	4	10	4.1	2.5
+	4	11	4.05	2.6
×	4	12	4.2	2.5

Key to Figure 4.21(b)*

Symbol	Set	Run	$d \times 10^{-3}$	ΔT (°C)0
⊙	5	25	3.9	4.0
△	5	26	4.0	4.0
+	5	28	4.2	4.0

*Solid line is the fitted curve to the experimental data

are fitted and included in these figures. The coefficients of these polynomials are given in Table 4.2. For every run in each set, these curves were used to obtain the instantaneous heat transfer coefficient. For each set, such results were then correlated by curve fitting. The results are shown in Figure 4.22(b), where this parameter is plotted against diameter ratio, and the corresponding correlations are given in Table 4.3. In Figure 4.22(a), the heat transfer coefficients are shown as a function of mass ratio.

4.2.2.4 Bubble growth rate and acceleration

The variation of bubble growth rate (related to the equivalent spherical radius) for set 1 and set 2 are shown in Figure 4.23(a). Growth rate increases throughout the evaporation. The values of acceleration are shown in Figure 4.23(b). It shows a maximum value at the early stages and, while remaining positive, decreases subsequently.

4.2.3 Stopped-Evaporation Droplets

4.2.3.1 Rise velocity

The droplets under study travelled a distance before the application of pressure. During this time, evaporation proceeded and the bubble-droplet grew accordingly. In the majority of cases after evaporation had been slowed down, due to the gradual decrease of hydrostatic pressure on the bubble-droplet, it continued to grow very gradually but much slower than if it had been left to evaporate under normal conditions. The rise velocity increased during an initial period, and then remained more or less constant around an average value or increased very gradually due to very gradual growth of the bubble. The results of four runs are shown in Figures 4.24(a,b) to 4.27(a,b). In these figures, mass ratios are related to the time after the application of pressure,

TABLE 4.2

Coefficients of the Polynomials Fitted to the Vapour Volume/Time Data of Evaporating Butane Droplets in Distilled Water

$$V_v \ (m^3) \times 10^{-9} = a_1 + a_2 t + a_3 t^2 + a_4 t^3 + a_5 t^4 + a_6 t^5 \qquad (4.2)$$

where: $t\ (s) = t' - t''$ (4.3)

and: $t_{min} < t < t_{max}$

Set	Run	a_1	a_2	a_3	a_4	a_5	a_6	t_{min} (s)	t_{max} (s)
1	8,10 11,12	38.6305	206.0950	417.3095	471.8838	336.9060	7.37069	-0.43	1.85
2	25,26 28	34.1642	170.8925	425.3220	856.062	874.0958	51.8299	-0.40	1.40

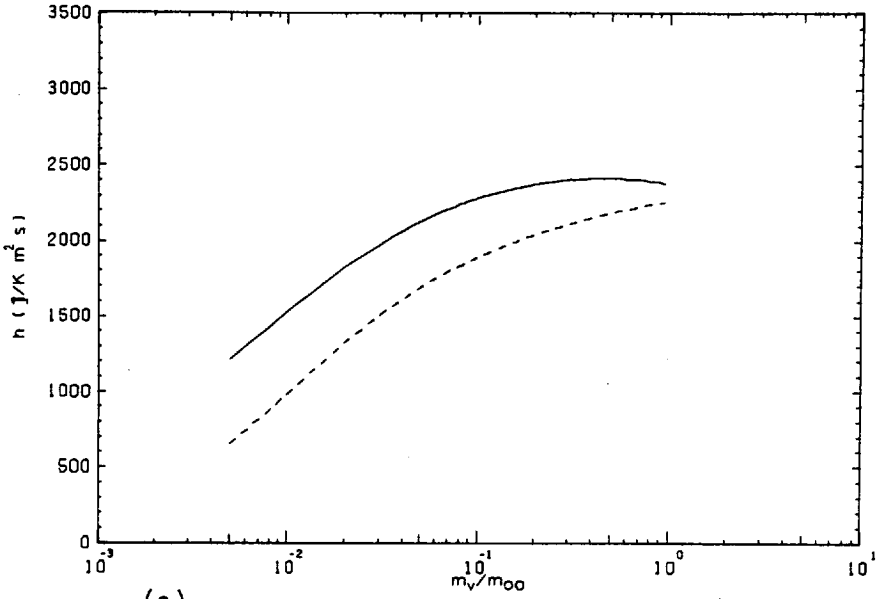

(a) Heat transfer coefficient vs. mass ratio

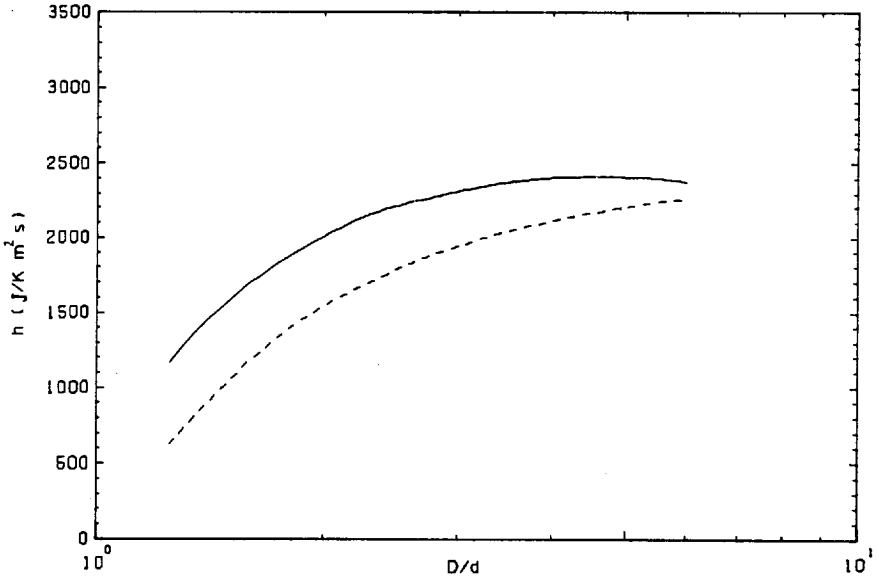

(b) Heat transfer coefficient vs. diameter ratio

Figure 4.22(a,b): Variation of heat transfer coefficient of evaporating butane droplets in distilled water.
(——— ΔT_o = 2.5°C, ----- ΔT_o = 4.0°C)

TABLE 4.3

Coefficients of the Polynomials Fitted to the Heat Transfer Coefficient/Diameter Ratio Data of Evaporating Butane Droplets in Distilled Water

$$h\ (J/Km^2s) \times 10^3 = a_1 + a_2 \left(\frac{D}{d}\right) + a_3 \left(\frac{D}{d}\right)^2 + a_4 \left(\frac{D}{d}\right)^3 + a_5 \left(\frac{D}{d}\right)^4 \qquad (4.4)$$

Set	a_1	a_2	a_3	a_4	a_5	Application
1	-9.08886	18.45024	-12.25104	3.81301	-0.45669	$D/d < 2.5$
	0.10874	1.68139	-0.46644	0.058975	-0.00291	$D/d > 2.5$
2	-3.29086	3.85454	-0.02023	-0.61393	0.13220	$D/d < 2.5$
	-0.63239	1.89194	-0.51351	0.06610	-0.00328	$D/d > 2.5$

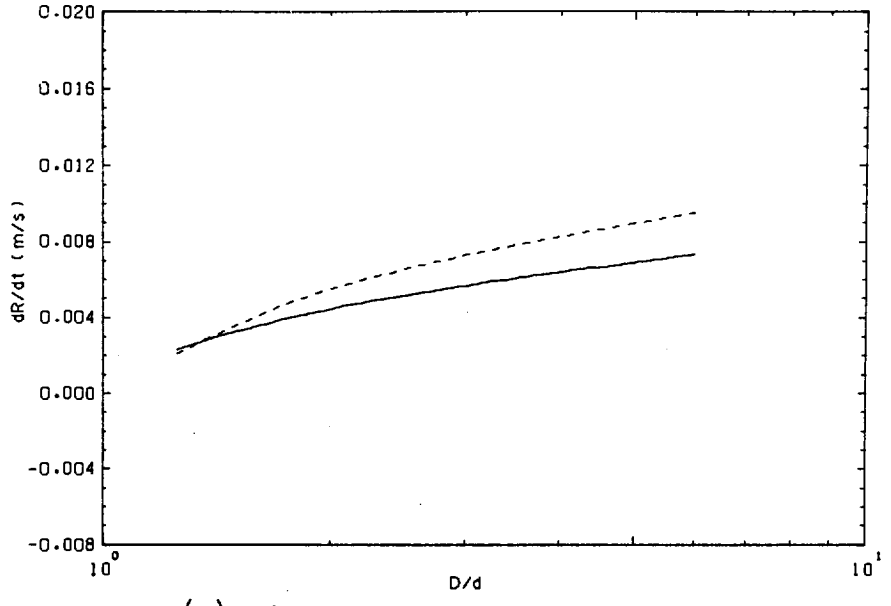

(a) Growth rate vs. diameter ratio

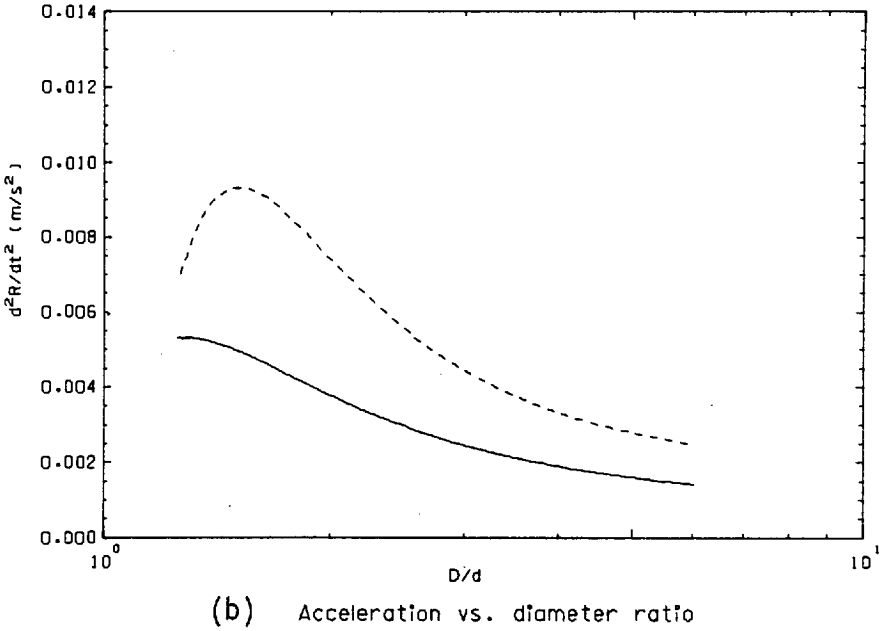

(b) Acceleration vs. diameter ratio

Figure 4.23(a,b): Variation of growth rate and boundary acceleration (related to the equivalent spherical radius) of evaporating butane droplets in distilled water. (—— ΔT_0 = 2.5°C, ----- ΔT_0 = 4.0°C)

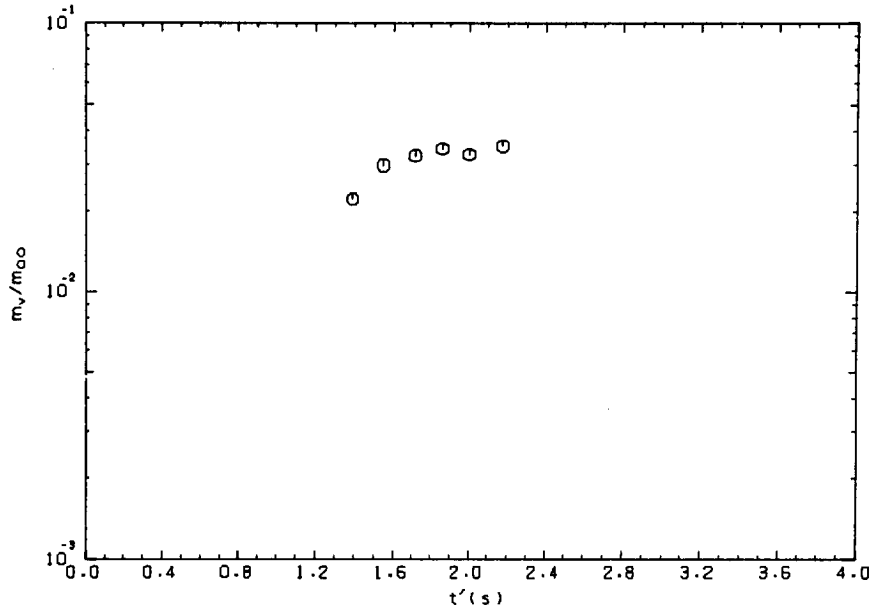

(a) Mass ratio vs. time

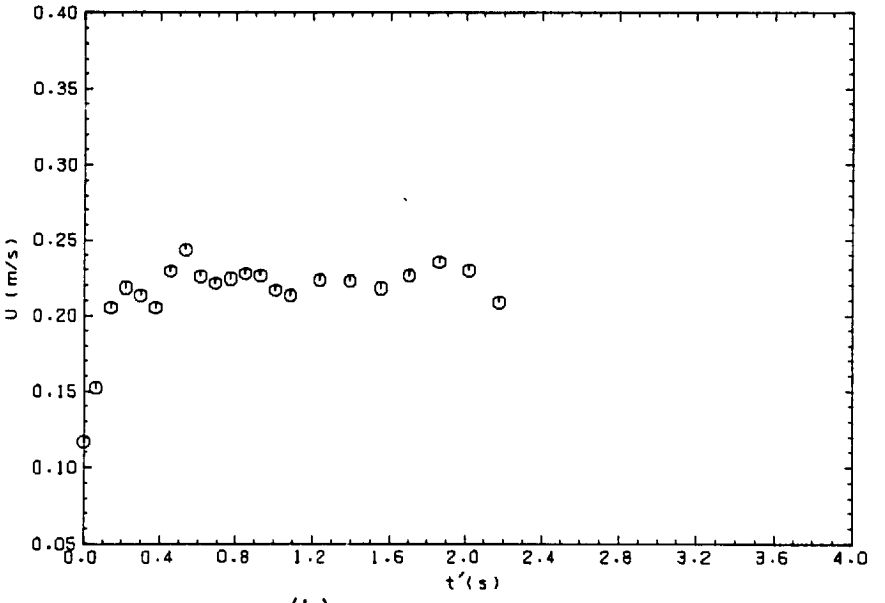

(b) Rise velocity vs. time

Figure 4.24(a,b): Variation of rise velocity and mass ratio of a stopped-evaporation butane droplet in distilled water

$$\left[\begin{array}{l} \text{Set 8, Run 7} \\ d = 4.15 \times 10^{-3} \text{ (m)} \\ T_c = 5.3 \text{ (°C)} \end{array}\right]$$

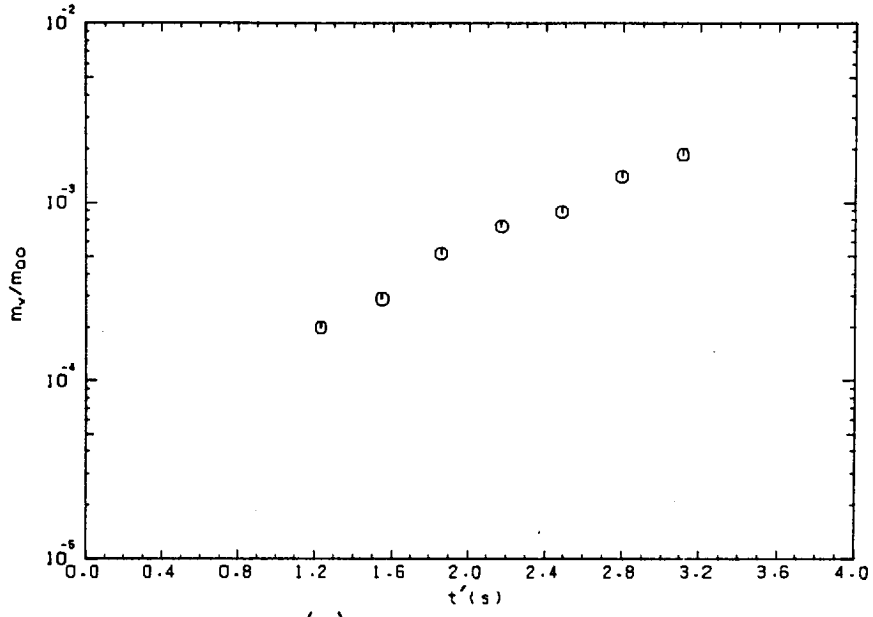

(a) Mass ratio vs. time

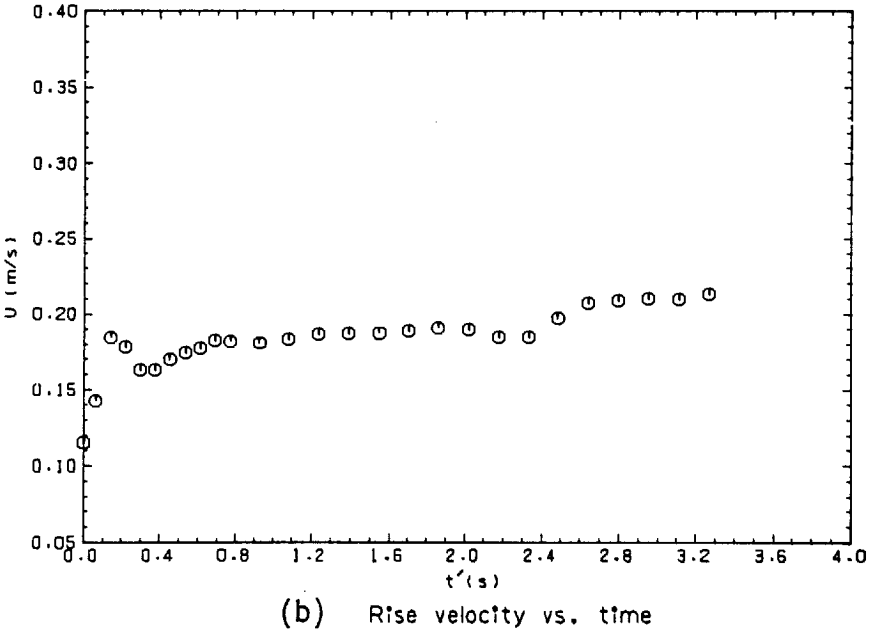

(b) Rise velocity vs. time

Figure 4.25(a,b): Variation of rise velocity and mass ratio of a stopped-evaporation butane droplet in distilled water

$$\left[\begin{array}{l} \text{Set 8, Run 17} \\ d = 4.0 \times 10^{-3}\ \text{(m)} \\ T_e = 5.4\ (^{\circ}\text{C}) \end{array}\right]$$

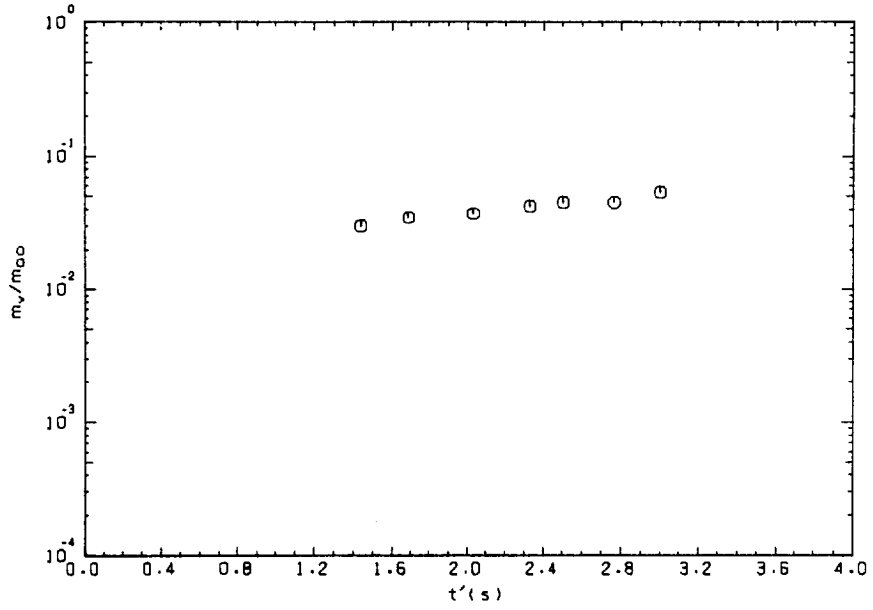

(a) Mass ratio vs. time

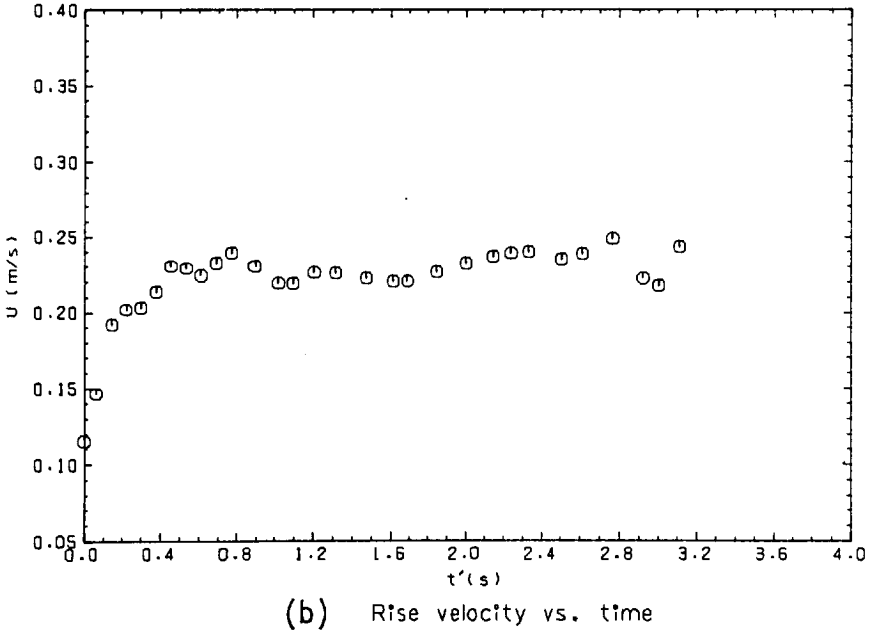

(b) Rise velocity vs. time

Figure 4.26(a,b): Variation of rise velocity and mass ratio of a stopped-evaporation butane droplet in distilled water

$$\left[\begin{array}{l} \text{Set 12, Run 3} \\ d = 3.8 \times 10^{-3}\ \text{(m)} \\ T_e = 4.6\ (^{\circ}\text{C}) \end{array}\right]$$

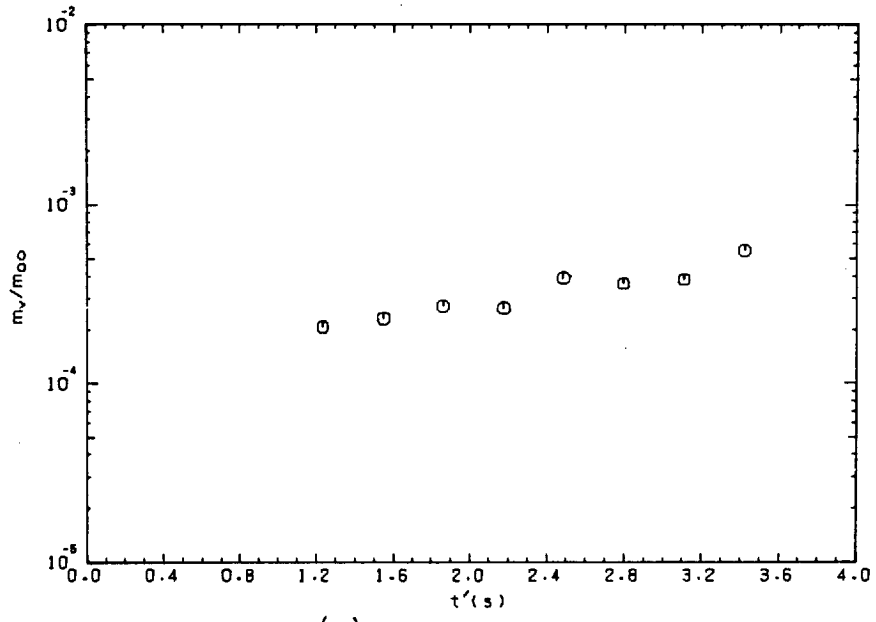

(a) Mass ratio vs. time

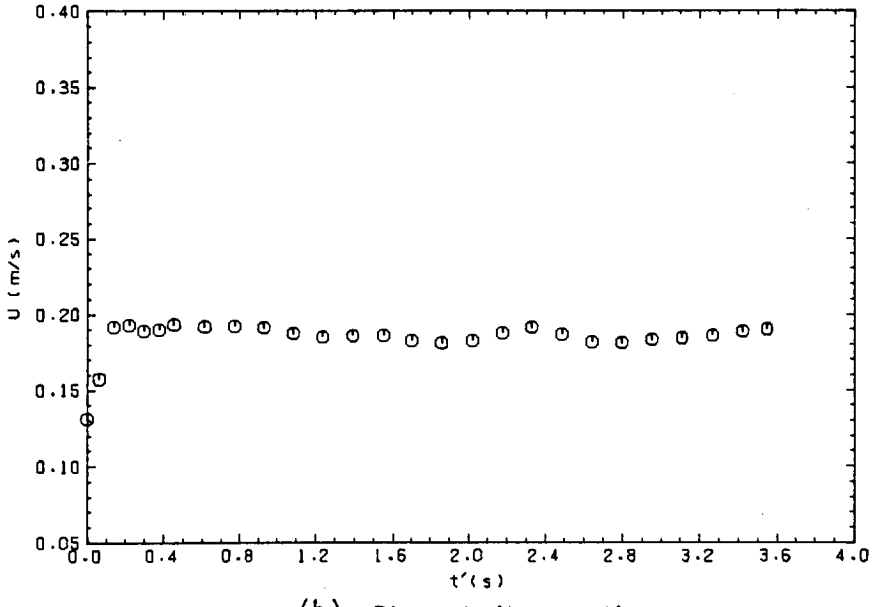

(b) Rise velocity vs. time

Figure 4.27(a,b): Variation of rise velocity and mass ratio of a stopped-evaporation butane droplet in distilled water

$$\left[\begin{array}{l} \text{Set 12, Run 15} \\ d = 3.85 \times 10^{-3}\ \text{(m)} \\ T_e = 4.2\ (^{\circ}\text{C}) \end{array}\right]$$

while the velocities cover the whole period of the droplet rise. Examples of the nearly complete stoppage of evaporation can be seen in Figures 4.24, 4.26 and 4.27, and examples of considerable slow evaporation can be seen in Figure 4.25. In some cases due to the application of a pressure greater than the saturation pressure of the liquid droplet, some of the vapour was actually condensed and the bubble-droplet size decreased. In cases where evaporation has been stopped and thus the size of the system remained constant, still some variation in the instantaneous velocity can be seen. Similar behaviour was observed for one-phase non-evaporating droplets. The reason for this is due to the nature of the movement of the bubble-droplet, such as helical motion, which depends on the initial size, mass ratio and other parameters like the liquid properties.

By studying each individual droplet, the region in which evaporation had been stopped was specified and the corresponding instantaneous values of parameters, such as mass ratio, diameter ratio and instantaneous velocity, were noted and then the average of the above values for each region was obtained. The results of the total of twenty five runs are given in Figures 4.28(a,b), where the average values of rise velocity and Reynolds number based on water properties are plotted against mass ratio.

4.2.4 Comparison Between Rise Velocity of Evaporating and Stopped-Evaporation Bubble-Droplets

Considering an evaporating bubble-droplet, one expects a resisting force on the system due to the growth and acceleration of the system. In order to verify the effect of omission of these terms, comparisons were made between the rise velocity of evaporating droplets and those of stopped-evaporation droplets at the same diameter ratio or

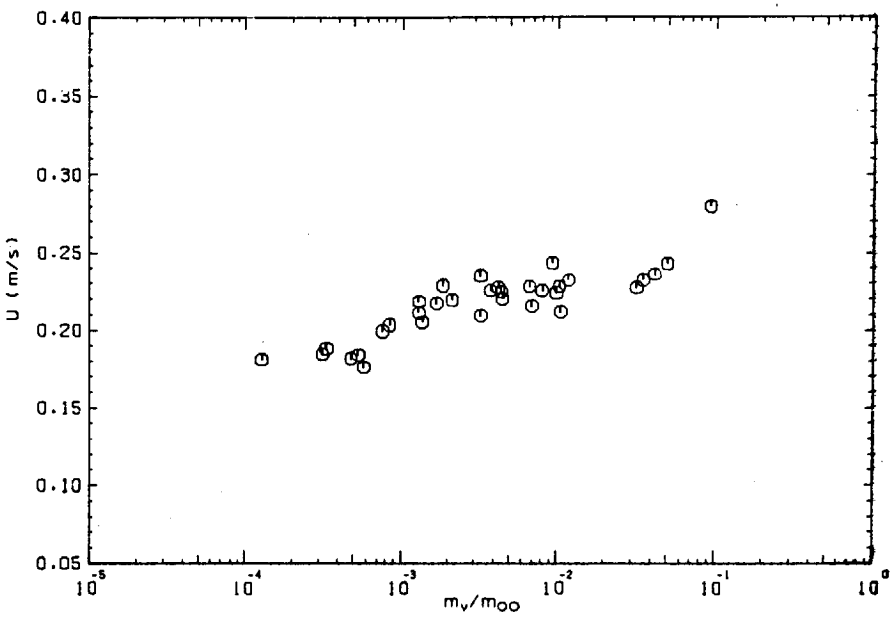

(a) Rise velocity vs. mass ratio

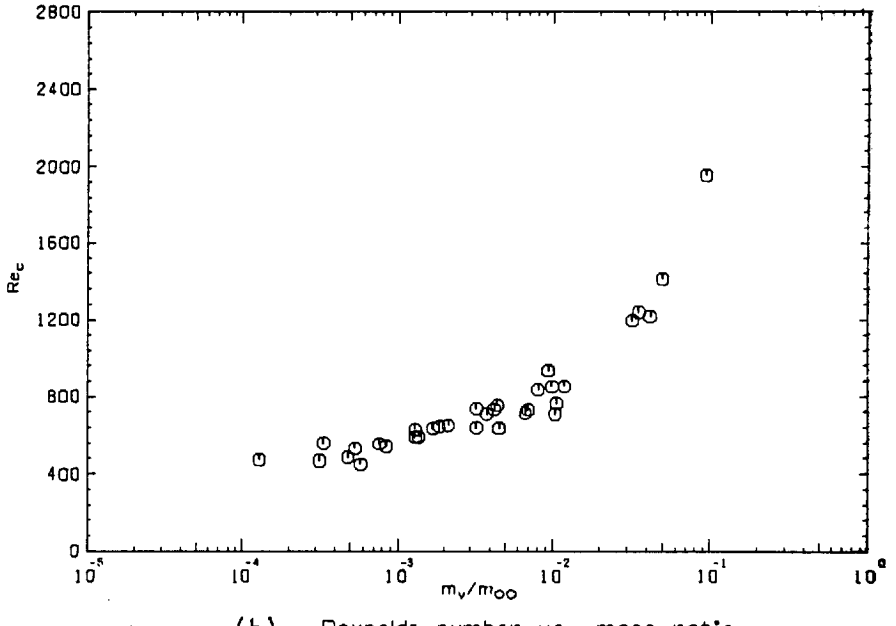

(b) Reynolds number vs. mass ratio

Figure 4.28(a,b): Variation of rise velocity and Reynolds number of stopped-evaporation butane droplets in distilled water

$$\left[\begin{array}{l} d = 3.8\text{-}4.2 \times 10^{-3} \text{ (m)} \\ T_e = 3.5\text{-}6.5 \text{ (°C)} \end{array}\right]$$

mass ratio. However, if the temperature difference (ΔT) is low, the effect is expected to be small. To get more pronounced effects, the tests had to be carried out in high values of ΔT. But testing in such conditions caused some difficulties. For example, due to quicker evaporation, a shorter time was available for the application of pressure. Therefore, the present tests were mainly conducted in low temperature differences. Comparisons are made in Figures 4.29(a,b), where the velocities are compared for droplets having nearly the same initial sizes and rising in water with nearly the same conditions. In these figures, the data of stopped-evaporation droplets are the instantaneous values, such as those shown in Figures 4.24 to 4.27. It should be noted that, when considering a stopped-evaporation and an evaporating droplet (with the same initial size) due to the difference between vapour densities, when they are at the same mass ratio they have different sizes, and when they have the same sizes they are at different mass ratios. Thus, in any case, such systems have a slightly different physical condition which should be kept in mind when their behaviours are compared. However, two systems with the same sizes are more alike and thus in Figures 4.29(a,b) the velocities are plotted against diameter ratio. Figures 4.29(a,b) show that stopped-evaporation droplets tend to show lower velocities than those of the evaporating droplets. This tendency, provided the effect of slight difference in the droplet sizes and water temperatures is small, indicates that, although growth and acceleration are omitted, still the drag force on the stopped-evaporation bubble-droplet is higher than those of evaporating droplets. More comparisons are made in Figures 4.30(a,b), in which the average values of rise velocity, mass ratio and diameter ratio of stopped-evaporation droplets (in the range where evaporation is stopped) are compared with those of the instantaneous values of evaporating

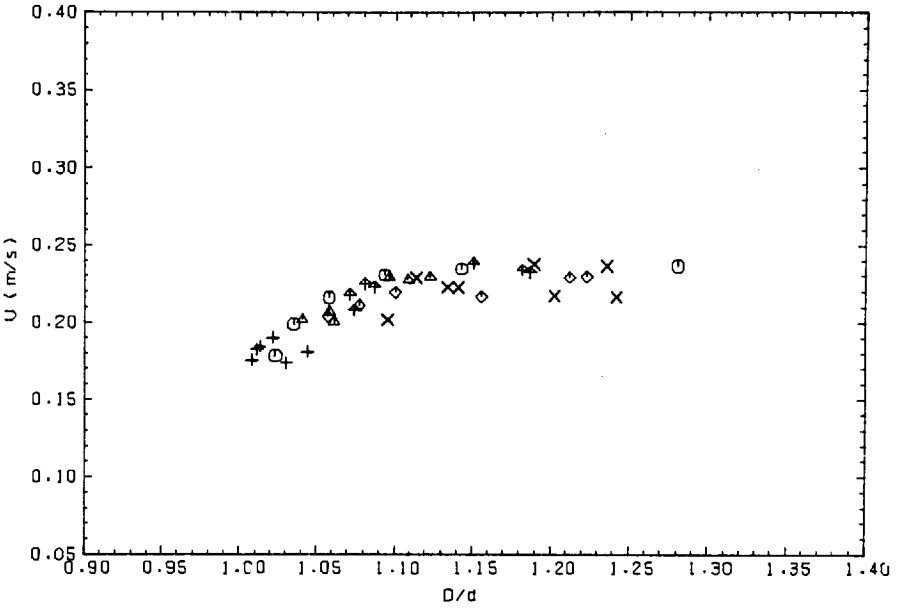

(a) Rise velocity vs. diameter ratio

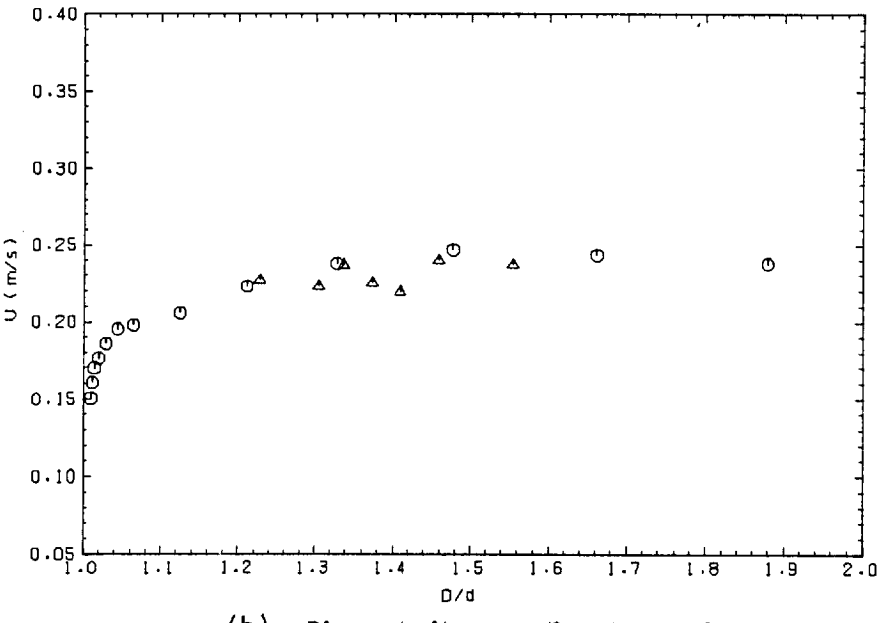

(b) Rise velocity vs. diameter ratio

Figure 4.29(a,b): Comparison between the rise velocity of evaporating and stopped-evaporation butane droplets in distilled water

Key to Figure 4.29(a)

Symbol	Set	Run	$d \times 10^{-3}$	T_c	ΔT_o	
⊙	10	8	4.0	4.5	2.3	E
△	10	6	4.0	4.0	-	S
+	10	7	4.0	4.3	-	S
×	10	9	4.1	4.5	-	S
◇	10	10	4.0	4.7	-	S
⟡	10	11	4.05	4.8	-	S

Key to Figure 4.29(b)

Symbol	Set	Run	$d \times 10^{-3}$	T_c	ΔT_o	
⊙	11	12	3.6	4.2	2.2	E
△	11	13	3.8	4.7	-	S

E ≡ evaporating droplet; S ≡ stopped-evaporation droplet

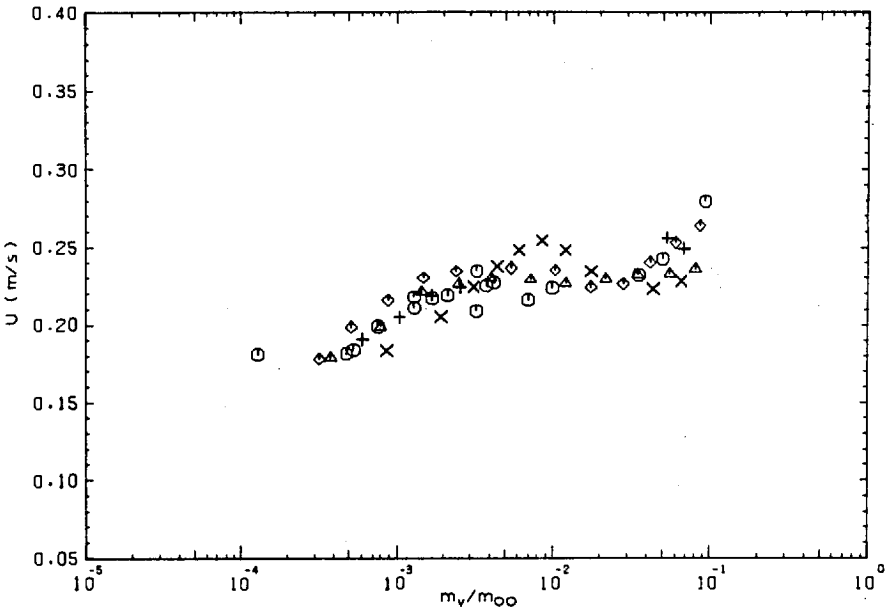

(a) Rise velocity vs. mass ratio

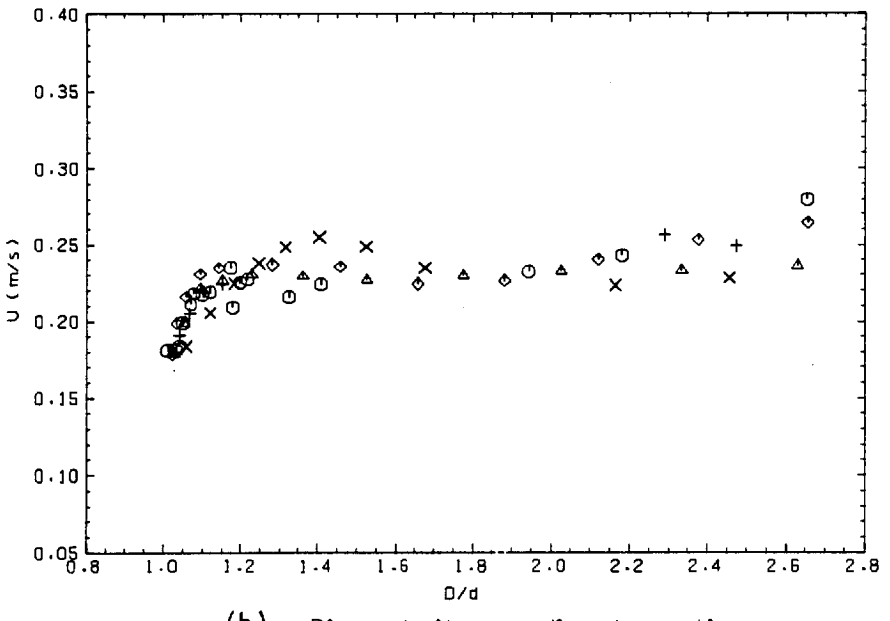

(b) Rise velocity vs. diameter ratio

Figure 4.30(a,b): Comparison between the rise velocity of evaporating and stopped-evaporation butane droplets in distilled water

Key to the figure

Symbol	Set	Run	$d \times 10^{-3}$ (m)	T_c (°C)	ΔT_o (°C)	
⊙	-	-	4.0-4.1	4.5-6.2	-	S
△	4	8	4.0	3.5	2.5	E
+	7	34	4.1	4.6	2.4	E
×	5	26	4.0	5.4	4.0	E
◇	10	8	4.0	4.5	2.3	E

E ≡ evaporating droplet; S ≡ stopped-evaporation droplet

droplets. In this case, droplets have nearly the same initial diameters but ascend in water with slightly different temperatures. No significant difference can be realised between the two velocities.

4.3 DISCUSSION AND COMPARISON WITH RESULTS OF THE PREVIOUS INVESTIGATORS

Among the previous workers, a butane/water combination was adopted by Sideman et al (68), Simpson et al (77) and Nene et al (55). More detailed information was given by Nazir (53). Sideman's results on a butane/water combination were not presented in their paper, since these results were completely different from those obtained for the other combinations, namely, butane/sea water, pentane/distilled water and sea water. The reason was attributed to the possible ice formation on the droplet surface when it entered the column at a temperature below the freezing point of water. In the following, the rise velocity of evaporating droplets are compared with those obtained by Nazir at the same mass ratio and also with the velocities of one-phase bubbles or droplets having the same size. The heat transfer coefficients are compared with the correlation given by Simpson et al (78) and Sideman's et al (68) results for two other combinations.

4.3.1 Rise Velocity of Evaporating Droplets

Considering a bubble-droplet system at different mass ratios, we divide the whole evaporation range into four regions (Figure 4.31). In region I, the bubble-droplet is more similar to a droplet than a bubble. This corresponds to the evaporation ratio below 0.1%. The shape of the system is close to a sphere. During this time, the rise velocity increases due to the gradual growth. At 0.1% evaporation, the bubble volume has occupied about 18% of the total volume. After 0.1% and

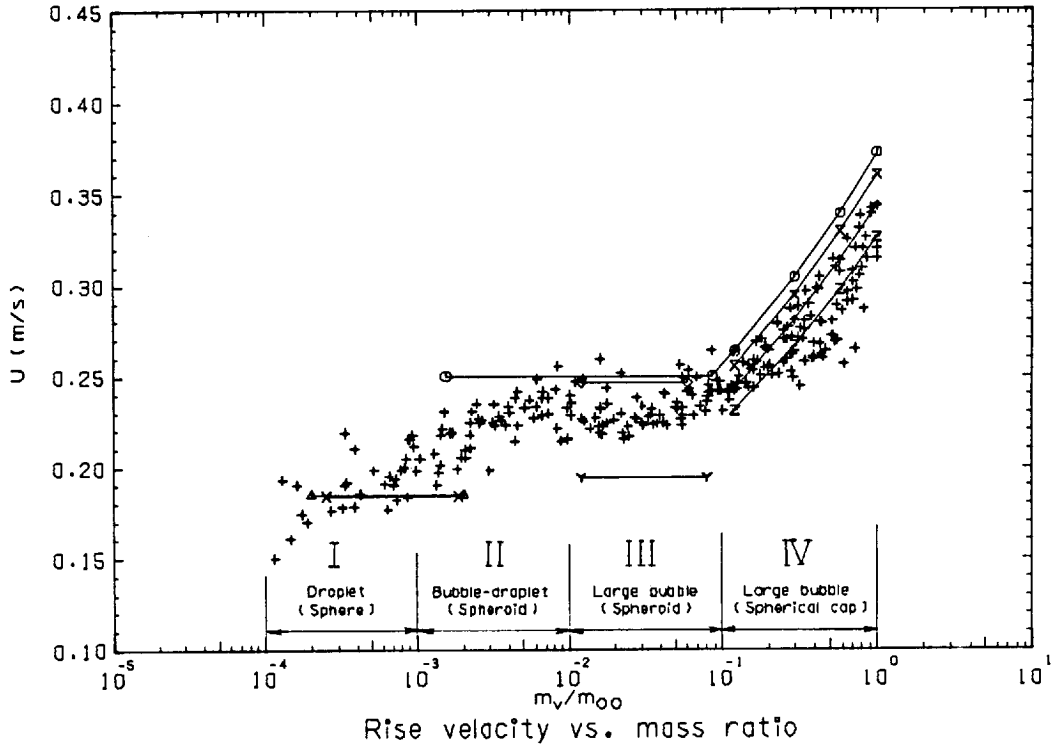

Figure 4.31: Comparison between the rise velocity of evaporating butane droplets in distilled water and other investigators' results

Key to the figure

Symbol	Description
+	Evaporating droplets, present work, $d_{av} = 4.0 \times 10^{-3}$ (m)
⊙	Evaporating droplets, Nazir (53), $d_{av} = 3.75 \times 10^{-3}$ (m)
△	Droplets, Harmathy (25)
×	Droplets, Klee et al (35)
◇	Large bubbles, Harmathy (25)
Y	Large bubbles, Peebles (56)
⧖	Spherical cap bubbles, Fr = 1.05, Wegener (87)
Z	Spherical cap bubbles, Fr = 0.95, Wegener (87)
↑	Spherical cap bubbles, Wallis (86)

up to about 1% evaporation (region II), when the vapour volume is about 70% of the total volume, the bubble-droplet system is neither behaves as a bubble nor a droplet and the volumes occupied by the two phases and liquid-liquid and liquid-vapour interface areas are comparable in size. The characteristics of the system in this region may be least predictable by the use of the existing theoretical and experimental models on one-phase bubbles and droplets. The shape of the system in this region is spheroidal and liquid sloshing is slow. The rise velocity continues to increase until near the end, where it gradually flattens. In region III, between 1% and 10% evaporation, the vapour occupies more than 70% of the volume and may be considered as a large bubble, although in the early parts the presence of the liquid can play a prominent role. The shape of the system is close to spheroidal and becomes more irregular near the end of this region, when vapour volume is about 96% of the total volume. Liquid sloshing is significant and as it was pointed out before, there is a decrease and then an increase in velocity in this range. In region IV, the size of the bubble-droplet is more than 2.7 times of the initial size and the shape is a spherical cap. The velocity increases as the size of the system increases.

It should be noted that the above classified shapes of the system are according to the present investigation, where the initial droplet size was about 4.0 mm in diameter. For smaller droplets, for example, the time during which the system is like a sphere, or a spheroid persists longer towards the end of evaporation. Also, the classification into regions I to IV is a simplification for the purpose of study and the boundaries of each region could be extended to the others' immediate regions.

The rise velocity results were compared with those of Nazir

(53) for evaporating bubble-droplets, and correlations by Klee et al (35) for large droplets, Harmathy (25) for large bubbles and droplets and those of Peebles et al (56) for large air bubbles, and Davies et al (10), Grace (22) and Wegener (87) for spherical cap bubbles. Their results are summarised in Table 4.4. Nazir (53) experimented on butane droplets evaporating in water and 4% and 8% salt solutions, and stated that for a butane/water combination, velocity could be considered constant equal to 0.25 m/s up to a diameter ratio of 2.7 and then increased according to the following correlation:

$$U = 0.152 \left(\frac{D}{d}\right)^{0.5} \qquad (4.5)$$

Comparisons are made in Figure 4.31. Nazir's results, represented by the constant velocity region and the above correlation, are generally higher than ours, although in the same results lower velocities were also obtained. However, if a constant velocity region is considered, our results show a velocity of about 0.23 m/s, compared with 0.25 m/s obtained by Nazir. The proposed ratio of 2.7 is consistent with our results. An average of droplet sizes used by Nazir was about 3.75 mm, compared with ours which was 4.0 mm. Thus, at a given mass ratio, larger bubble-droplets were obtained by us. In the second half of region II and in region III, the effect of bubble size on velocity is not significant, but in region IV where the rise velocity increases with bubble size our results are expected to be higher. The reason, especially in regions II and III, may be partly attributed to the extra weight of heavier droplets used by us. Sideman's experiments on droplets 3.3 mm to 3.9 mm in diameter in butane/sea water and pentane/distilled water and sea water combinations showed a maximum velocity of 0.28 m/s at the end of

TABLE 4.4

Rise Velocity of Droplets and Bubbles in Liquids

Reference	Formula	Condition	Description
Peebles et al (56)	$U = 1.18\ ((g\ \sigma)/\rho_c)^{0.25}$	$3.10\ M^{-0.25} < Re_c$	Large bubbles, based on air bubbles in twenty two liquids
Klee et al (35)	$U = 17.6\ \rho_c^{-0.55}\ (\rho_c - \rho_d)^{0.28}\ \mu_c^{0.10}\ \sigma^{0.18}$ *	$D_d > 0.33\ \rho_c^{-0.14}\ (\rho_c - \rho_d)^{-0.43}\ \mu_c^{0.30}\ \sigma^{0.24}$ *	Based on rise and fall of droplets in various liquids
Harmathy (25)	$U = 1.53\ ((g\ (\rho_c - \rho_d)\ \sigma)/\rho_c^2)^{0.25}$	$Re_c > 500$, $E\theta < 13$	Large droplets or bubbles
	$U = 0.715\ ((g\ (\rho_c - \rho_d)\ D_b)/\rho_c)^{0.5}$	$E\theta > 40$	Spherical cap bubbles
Davies et al (10) Wallis (86)	$U = 1.0\ (g\ (D_b/2))^{0.5}$	$R_b \geq 2\ (\sigma/(g\ \rho_c))^{0.5}$	Spherical cap bubbles
Grace (22)	$Re_c = 0.70\ (E\theta)^{0.75}/M^{0.25}$	$Re_c \geq 100$ $E\theta \geq 40$	Spherical cap bubbles
Wegener (87)	$Fr = U/(g\ (D_b/2))^{0.5}$ = constant	$Re_c > 100$	Spherical cap bubbles

* In this correlation: $\rho \equiv$ g/cc, $\mu \equiv$ poises, $\sigma \equiv$ dynes/cm, $D \equiv$ cm, $U \equiv$ cm/s.

evaporation, which is lower than our results and much lower than Nazir's results. The difference should have been due to the wall effects. Based on the paper by Collins (9), Wallis (86) gave the following relation for the wall effects:

$$\frac{U_b}{U_\infty} = 1.13\, e^{-d/D} \quad , \quad \text{when} \quad 0.125 < \frac{d}{D} < 0.6 \tag{4.6}$$

where D is the diameter of the cylinder container, and d here is the equivalent spherical diameter of the bubble. This relation shows that the container wall reduces the bubble velocity, U_b, compared with its velocity U_∞ in an infinite medium. The wall effect is negligible when:

$$\frac{d}{D} < 0.125 \tag{4.7}$$

The wall effect should be especially significant in the later stages of evaporation. The equivalent spherical diameter of the final volume of a butane droplet when it is fully vaporised is about six times bigger than its initial value. In our case, the equivalent diameter of the container is 170 mm, and thus the bubble velocity in the fully vaporised size could have been decreased by 2%. The wall effect should have been more significant in Nazir's results since the size of the container was smaller (100 mm × 100 mm × 900 mm), and much more effective in Sideman's results where the column inside diameter was 54 mm.

The rise velocity may be compared with that of ordinary butane bubbles or droplets having the same size as that of the bubble-droplet. Klipstein (36) calculated the terminal velocity of bubbles and found that it was about 10% more than that of evaporating droplets. Greater differences were obtained for larger droplets and for viscous continuous

phases. Calculations for Figure 4.31 were made for a butane droplet of 4.0 mm initial diameter and a water temperature of 4.0°C. The physical properties are given in Appendix C. In region I, the droplet velocity was calculated from the correlation by Klee et al (35) and the equation by Harmathy (25) (Table 4.4). These relations are given for the constant velocity region (terminal velocity) away from the column end effects, while our results in region I might have been influenced by the period after release. Klee's experiments covered a wide range of the physical properties of the two phases. Close velocities are calculated from these two references and are about the average of our results. The velocities in region III are compared with those calculated from the equations given by Peebles and Harmathy. Peebles' relation predicts a much lower velocity than that calculated from Harmathy's relation, and the difference was attributed by Harmathy (25) to have been due to the wall effect. The rise velocity obtained by Harmathy's equation is very close to 0.25 m/s, which was obtained by Nazir for evaporating droplets. In this region, our results show lower velocities than those of large bubbles and the difference decreases near the end of this region. The reason for the lower velocities is expected to be due to the mass of unevaporated liquid within the system which increases the gravity force and also due to growth and serious liquid sloshing which apparently exerts an extra drag on the system. The importance of the liquid mass can be estimated from the ratio of the gravity to the buoyancy force, which is given by:

$$\frac{F_1}{F_2} = \left(\frac{d}{D}\right)^3 \frac{\rho_l}{\rho_c} \qquad (4.8)$$

where F_1 and F_2 are the gravity and the buoyancy force, respectively. For a bubble-droplet, when the diameter ratio is 2, the value of F_1 is about 7.5% of F_2, while for a bubble of the same size is about 0.3%.

In region IV, the results are compared with the velocities calculated from the relations given by Harmathy (25), Wallis (86), Grace (22) and Wegener (87) (Table 4.4). Davis et al (10) gave the following equation for the rise velocity of spherical cap shape bubbles:

$$U = \frac{2}{3}\sqrt{g\,R_b} \tag{4.9}$$

where R_b is the radius of curvature in the region of the bubble's nose. Based on this relation, Wallis (86) gave an equation (Table 4.4) which indicates that the rise velocity increases with increase of the equivalent spherical diameter of the bubble. A close relation is obtained by Harmathy. Wegener et al (87) stated that the Froude number was constant for spherical cap bubbles. They showed that the rise velocity of such bubbles in different liquids and in a wide range of physical properties fall within two lines representing Froude numbers of 0.95 and 1.05. The velocities calculated using these two limits are shown in Figure 4.31. Grace's (22) formula also results in velocities close to those of Wegener for Fr = 1.05. Generally, our results are in fair agreement with those calculated for ordinary spherical cap bubbles. Slightly lower velocities again could be attributed to the extra drag due to the growth of the system and the presence of unevaporated liquid in the system.

4.3.2 Rise Velocity of Stopped-Evaporation Droplets

The same regions as in the case of evaporating droplets can be considered for the case of stopped-evaporation droplets. However, our results only cover the first three regions. Direct comparison with others' experimental results was not possible because of the lack of such data. Similar comparisons and arguments as in the previous section can be

made between the stopped-evaporation droplets and ordinary bubbles or droplets, bearing in mind that the nature of these two are more similar, since the exclusion of the growth and acceleration phenomena. Because of the similarity to the previous section, comparisons are not repeated here.

Comparisons between the rise velocity of evaporating and stopped-evaporation droplets were made in section 4.2.4. As it was mentioned, an extra resisting force should exist due to the growth and the acceleration of the system. Higher growth rates are obtained for higher temperature differences and thus produce higher drags. Sideman et al (68) mentioned that the effect of temperature difference on the arithmetic average of the velocities at 1% and 100% evaporation was not significant in the case of droplets of 3.3 mm to 3.9 mm diameter. But the effect was apparent for smaller droplets which had quicker evaporation. Further conclusions may be made from simple calculations as follows. In Chapter 2, it was shown that for a spherical bubble-droplet system, the drag forces due to the growth and the acceleration could be approximated by:

$$F_3 = 2 \pi \rho_c U R^2 \frac{dR}{dt} \tag{4.10}$$

and:

$$F_4 = \frac{2}{3} \pi \rho_c R^3 \frac{dU}{dt} \tag{4.11}$$

where F_3 is due to growth and F_4 is due to acceleration. The buoyancy force is given by:

$$F_1 = \frac{4}{3} \pi R^3 \rho_c g \tag{4.12}$$

The degree to which F_3 and F_4 affect the rise velocity of the system can be realised by their magnitudes compared with the buoyancy force, F_1. We

obtain:

$$F_{31} = \frac{F_3}{F_1} = \frac{3}{g}(d)^{-1} U \left(\frac{D}{d}\right)^{-1} \left(\frac{dR}{dt}\right) \quad (4.13)$$

and:

$$F_{41} = \frac{F_4}{F_1} = \frac{1}{2g}\frac{dU}{dt} \quad (4.14)$$

During the time when the rise velocity is nearly constant (e.g. 1% to 10% evaporation in our results), F_{41} is negligible and during the stages when the bubble accelerates it is still small. For example, after 10% evaporation, dU/dt is about 0.1 m/s^2 and thus F_4 is about 0.5% of the buoyancy force. Below 1% evaporation, a value of about 1% is obtained. Thus, in our results ($\Delta T_0 < 4.0^0$C), the effect of bubble-droplet acceleration is small. F_{31}, however, shows higher values. This ratio is directly proportional to the growth rate and velocity, and inversely proportional to the initial droplet size and diameter ratio or, as a whole, to the bubble-droplet size. So smaller droplets should have more effect than the larger ones. When $\Delta T_0 = 4.0^0$C, and at diameter ratios of 2 and 5, the growth rate values are 0.0055 and 0.009 m/s, respectively (Figure 4.23). Considering a droplet of 4.0 mm diameter, the rise velocities at diameter ratios of 2 and 5 are about 0.23 and 0.30 m/s, respectively. Substituting these values in equation (4.13), F_{31} will be 0.05 and 0.04, respectively. Thus, the effect of growth in low temperature differences could be considered small. However, in higher temperature differences, such as 10^{0}C, the value of growth rate can reach 0.015 m/s and therefore the effect will be significant.

4.3.3 Heat Transfer to Evaporating Droplets

The mechanism of heat transfer to evaporating droplets has been studied by previous workers (e.g. (36), (68), (78)). Values of heat

transfer coefficient have been given mainly after 0.5% evaporation is reached. Measurements down to 0.1% are reported (63) to have been carried out by Nene (55) on butane droplets in water. At 0.1% evaporation, the vapour volume has occupied about 18% of the total volume and is in the range which might not be classified as a droplet. Below 0.1% evaporation, however, the mechanism of heat transfer to evaporating droplets should be close to that of one-phase droplets. Many investigators have studied (75) the process of heat and mass transfer to droplets, the majority of which refer to the average heat transfer over the period of steady movement. The overall heat transfer coefficient, h, is usually expressed in terms of the outside, h_c, and inside, h_l, heat transfer coefficients as:

$$\frac{1}{h} = \frac{1}{h_l} + \frac{1}{h_c} \tag{4.15}$$

In order to make an estimate of the heat transfer coefficients, the following correlations of the outside Nusselt number are considered (11):

$$Nu_c = 5.52 \left(\frac{\mu_c + \mu_l}{2\mu_c + 3\mu_l}\right)^{3.47} \left(\frac{D \sigma \rho_c}{\mu_c^2}\right)^{0.056} (Pe_c)^{0.5} \tag{4.16}$$

which is given for non-oscillating drops with internal circulation in Reynolds number below 1500. The internal Nusselt number may also be estimated from the following equation, which was developed for the drop circulating model combined with an assumed random radial motion (24a):

$$Nu_l = 0.00375 \frac{Pe_l}{1 + (\mu_l/\mu_c)} \tag{4.17}$$

Using equations (4.16) and (4.17) for a butane droplet of 4.0 mm in diameter rising in water at 4.5°C with a velocity of 0.17 m/s, the internal

and external Nusselt numbers are 28 and 55, respectively, and the corresponding values of heat transfer coefficients are 810 and 7900 J/Km^{2}s, respectively. Thus, the overall heat transfer coefficient is 735 J/Km^{2}s. The outside Nusselt number if calculated from the following equation:

$$Nu_c = \left(\frac{12}{\pi} Re\ Pr\right)^{0.5} \qquad (4.18)$$

which is suggested by Elzinga et al (11) for the maximum heat transfer to circulating droplets is about 137. The overall heat transfer coefficient, in this case, would be 6% higher than the previous value. Nene (63,55) obtained a value of about 700 J/Km^{2}s for the average overall heat transfer coefficient to evaporating butane droplets up to 0.1% evaporation and Sideman (68) mentions a value of about 350 J/Km^{2}s for the heat transfer coefficient to non-evaporating droplets. According to the above results, at the early stages of evaporation the main resistance to heat lies in the dispersed phase liquid. It should be mentioned that the correlations and the values given in the literature for the heat transfer to the droplets mainly refer to the period of steady rise and the heat transfer during the period of release and early rise could be higher. In the present experiments, evaporation at the early stages usually coincided with this initial period. To avoid this, experimental rigs such as those adopted by Prakash et al (59) and Tochitani et al (83) should be used. In such cases, a lower column below the main column was used and was kept at a lower temperature. After release, the droplets travelled in the lower column before entering the main column. Droplets, after release, travelled for a short time before clear signs of evaporation could be seen. In some cases, especially when the initial droplet temperature was low, this time seemed to be not long enough for the whole liquid in the droplet to raise

its temperature to the saturation point corresponding to the total pressure and three to four times higher overall heat transfer coefficient than the above estimated values would be needed. In the experimental work by Tochitani et al (82) they mentioned that pentane vapour bubbles grew in size in a pool of pentane (99% pure and saturated with water) while the bulk temperature was well below the normal boiling point. They suggested that vaporisation could proceed even under negative values of nominal temperature difference, provided nucleation occurred. Thus, in the present case, if the reason not to be attributed to higher rates of heat transfer due to the characteristics of droplet behaviour during the initial period of release and rise, other factors may be considered. These include the effect of air nucleus, presence of volatile compositions in the liquid droplet or the possibility that the saturation temperature could have been reached locally at the gas-liquid interface before all the liquid temperature has risen to that extent. If the last case is valid, the temperature is not uniform throughout the liquid, and then some of the heat transferred to the system would be spent to warm up the unevaporated liquid. The prolonged evaporation time of the liquid droplets, as shown in Figures 4.13(a,b), could have been due to the same reason. The possibility of ice formation at the droplet surface when the droplet enters the water at a temperature below the freezing point, as mentioned by Sideman (68), needs some consideration, and if that happens, it would cause an extra resistance to heat transfer.

The present heat transfer coefficient results are compared with those calculated from Simpson's correlation and those of Sideman et al (68) in Figure 4.32. While comparing these results, it should be considered that the overall temperature difference, ΔT_o, in our results is defined as the average of all the ΔT values at the intervals where the

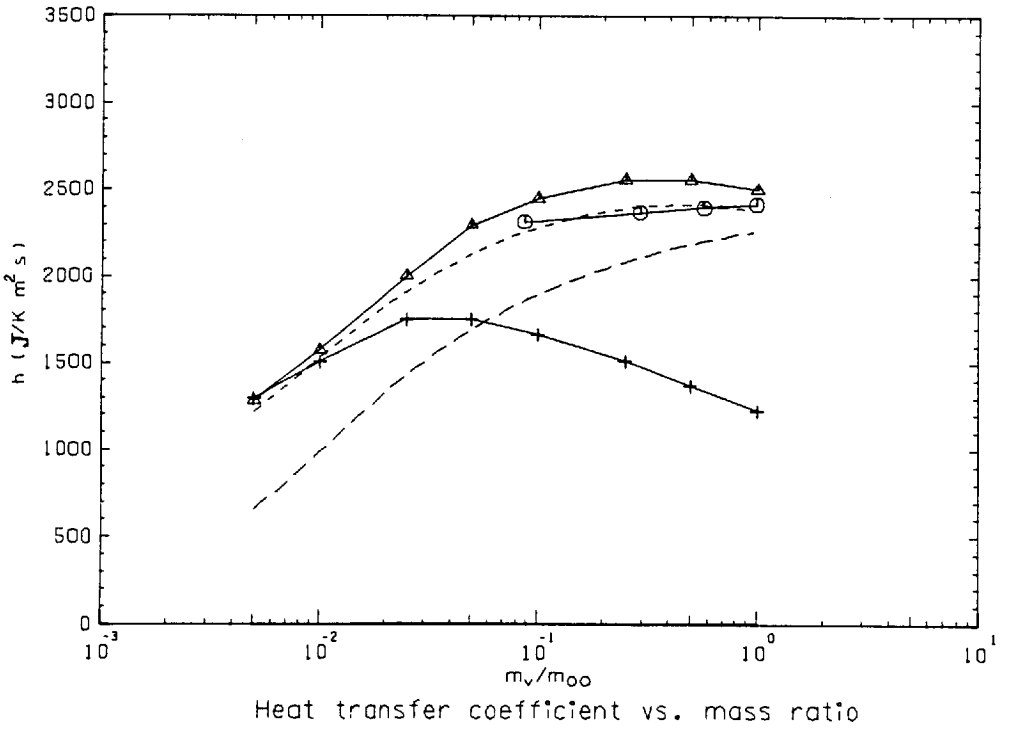

Figure 4.32: Comparison between the heat transfer coefficient of evaporating droplets in distilled water and other investigators' results

Key to the figure

Symbol	Description
-------	Present work, ΔT_0 = 2.5 (°C)
- - - - -	Present work, ΔT_0 = 4.0 (°C)
ⓘ	Simpson et al correlation (77), ΔT_0 = 2.0°C to 8°C
△	Pentane/distilled water, ΔT_0 = 2.0 (°C), Sideman et al (68)
+	Butane/sea water, ΔT_0 = 4.0 (°C), Sideman et al (68)

vapour volume was measured, while ΔT_o in Sideman's results is taken as the average of ΔT values at the top and bottom of the column. The present results and Simpson's correlation were obtained using the instantaneous equivalent spherical area of the bubble-droplet, while Sideman calculated the area by taking the entire droplet as a spheroid. Lower heat transfer coefficients are obtained for higher ΔT_o (Figure 4.32). Sideman's (68) and Nazir's (53) results show the same tendency. Tochitani et al (84) also noted that the average overall heat transfer coefficient decreased with increase of ΔT_o. However, Rice et al (63) mentioned that the average heat transfer coefficient was independent of temperature difference.

4.3.4 Effect of Water Vapour Pressure

In order to estimate the effect of water vapour pressure on the various parameters, the bubble-droplet system was assumed to be in an equilibrium state at any instant, and the vapour temperature in the system was obtained by iteration. Iteration was ended when the sum of the vapour pressures of the dispersed phase and the continuous phase liquid was equal to the total pressure (water head pressure plus atmospheric pressure) within a specified accuracy. In this case, the calculated butane partial pressure is lower than when water vapour pressure was neglected and thus the saturation temperature is lower and the temperature difference is higher. This mainly affects the heat transfer coefficients which is inversely proportional to temperature difference (equation (3.12)), but the effect on other parameters such as mass ratio and diameter ratio which were calculated using the value of vapour density is negligible. Comparisons are made in Figure 4.33. The heat transfer coefficient is

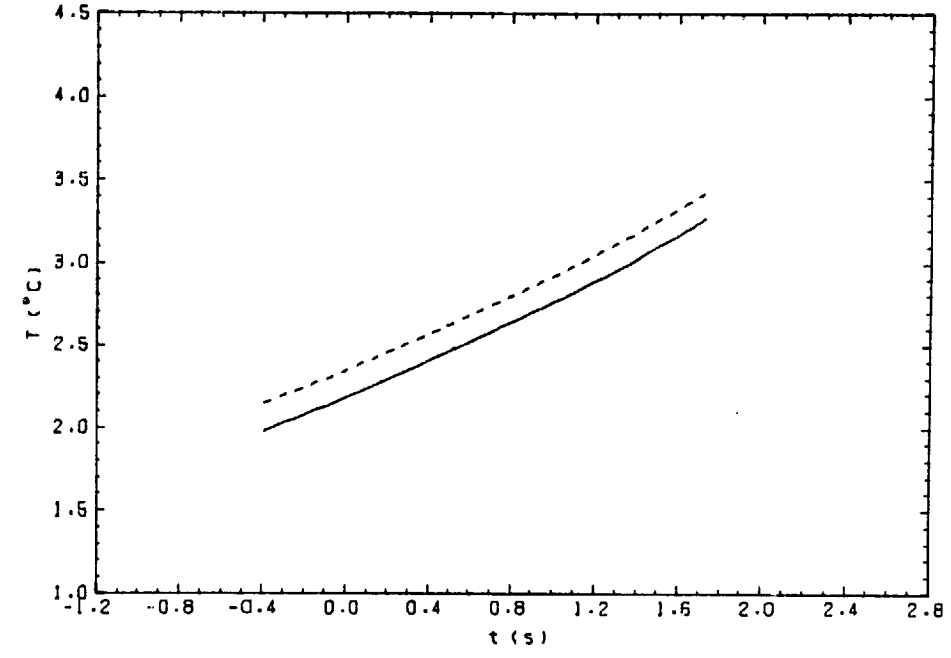

Temperature difference vs. time

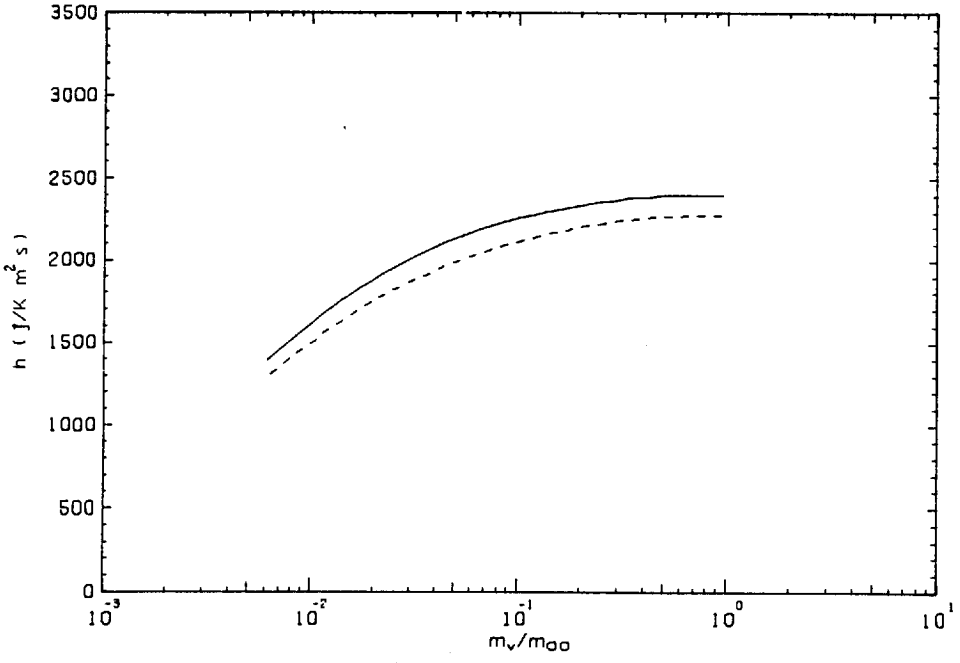

Heat transfer coefficient vs. mass ratio

Figure 4.33: Effect of water vapour pressure

(Set 4, Run 8; ΔT_0 = 2.5°C; ——— P_W = 0, ----- $P_W \neq 0$)

decreased by 7.5% at 0.5% evaporation and 5% at the end of evaporation. The percentage of difference is lower in higher temperature differences.

4.4 RECOMMENDATIONS

The execution of the experimental investigation included in Chapters 3 and 4 indicated that further studies on the following points could be useful for the progress of knowledge on the subject:

(a) The mechanism of heat transfer to evaporating droplets below 0.1% evaporation and its resemblance to that of non-evaporating droplets should be studied.

(b) The heat transfer to and dynamics of stopped-evaporation two-phase bubble-droplet systems should be studied. Similar procedures as those which have been used for the study of one-phase bubbles or droplets may be adopted.

(c) Tests should be carried out to stop the evaporation of evaporating droplets in high temperature differences, high percentages of evaporation and for small droplets, and their hydrodynamics should be compared with those of evaporating droplets.

(d) Due to the inadequacy of two-dimensional photography, a study of the shape variation of the vapour and liquid parts within stopped-evaporation bubble-droplet systems during their rise would be useful for the better understanding of the actual instantaneous shape of evaporating droplets, and also to obtain more information on the size and shape of the liquid-liquid interfacial area.

(e) The effect of the liquid-liquid interface curvature on the

apparent shape of the dispersed phase liquid-vapour interface and the size of the bubble within a bubble-droplet system in the early stages of evaporation (e.g. below 0.5% evaporation) should be examined.

(f) The possibility of ice formation at the droplet-water interface when the droplet is injected at a temperature below the freezing point of water and its effect on the evaporation process needs some consideration.

(g) In order to have better control over the initial droplet temperature and to separate the early stages of evaporation from the initial period of release and acceleration, experimental rigs similar to those used previously (59,83) are recommended. The height of such a column should be chosen according to the height needed by the droplet to reach its terminal velocity.

CHAPTER 5

COMPARISON OF THE EXPERIMENTAL RESULTS WITH THE PREDICTED VALUES

5.1 INTRODUCTION

In this chapter, the present experimental results (two sets, namely, ΔT_0 = 2.5°C and 4.0°C, $d \simeq 4.0$ mm) are compared with the predicted values. Heat transfer coefficients were calculated from the present data (Table 4.3) and also from Sideman's model (equation (1.15)) and Simpson's correlation (equation (1.11)). The present data and Sideman's model were applied from 0.5% evaporation (t = 0) to the end of evaporation, and Simpson's correlation was used from the time when the diameter ratio had already reached 2.7. The initial growth rate was calculated from equation (2.63). Other initial conditions and the operating conditions (d, T_c, ATMP) were taken as the average of the experimental values. The initial and operating conditions are given in Table 5.1.

It should be considered that the experimental results for diameter ratio and growth rate, used here for conducting the comparison, are the values which correspond to the equivalent spherical volume of the bubble-droplet.

5.2 RESULTS AND DISCUSSION

Comparison for Case 1 (ΔT_0 = 2.5°C, Table 5.1) are made in Figures 5.1(a-h). Figures 5.1(a,b) show the variation of diameter ratio and vapour volume against time. When the present data and Simpson's correlation are used, good agreement is obtained between the experimental results and the predicted ones. Longer evaporation time is predicted when Sideman's model is used. The reason is due to the values of heat

TABLE 5.1

Operating and Initial Conditions

Case	OPERATING CONDITIONS			INITIAL CONDITIONS								Equation Number Used for Calculation of h	Figure Number
	$d \times 10^{-3}$ (m)	T_c (°C)	ATMP (N/m^2)	ΔT_o (°C)	t_o (s)	$(\frac{D}{d})_o$	$Z_o \times 10^{-3}$ (m)	$X_o \times 10^{-3}$ (m/s)	U_o (m/s)	T_o (°C)	P_o (N/m^2)		
1	4.10	3.53	101341.0	2.18	0.0	1.271	152.0	2.37 5.52	0.230	1.35	108662.0	see Table 4.3 (1.15)	5.1(a-h)
				2.58	0.707	2.7	318.0	5.45	0.242	0.951	107035.0	(1.11)	
2	4.02	5.54	102281.0	3.72	0.0	1.268	143.0	2.18 9.51	0.232	1.61	109704.0	see Table 4.3 (1.15)	5.2(a-f)
				4.06	0.610	2.7	286.0	8.50	0.241	1.26	108284.0	(1.11)	

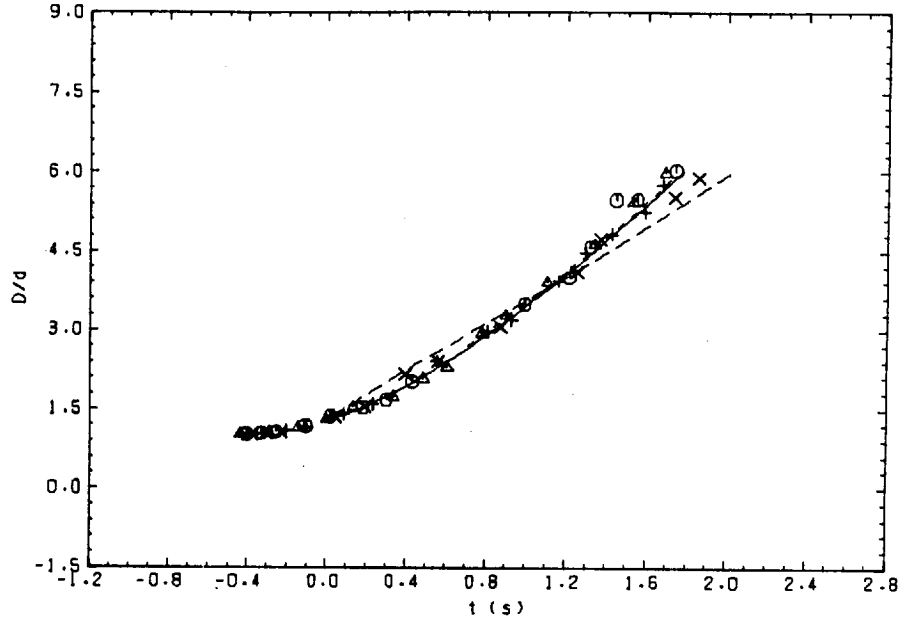

(a) Diameter ratio vs. time

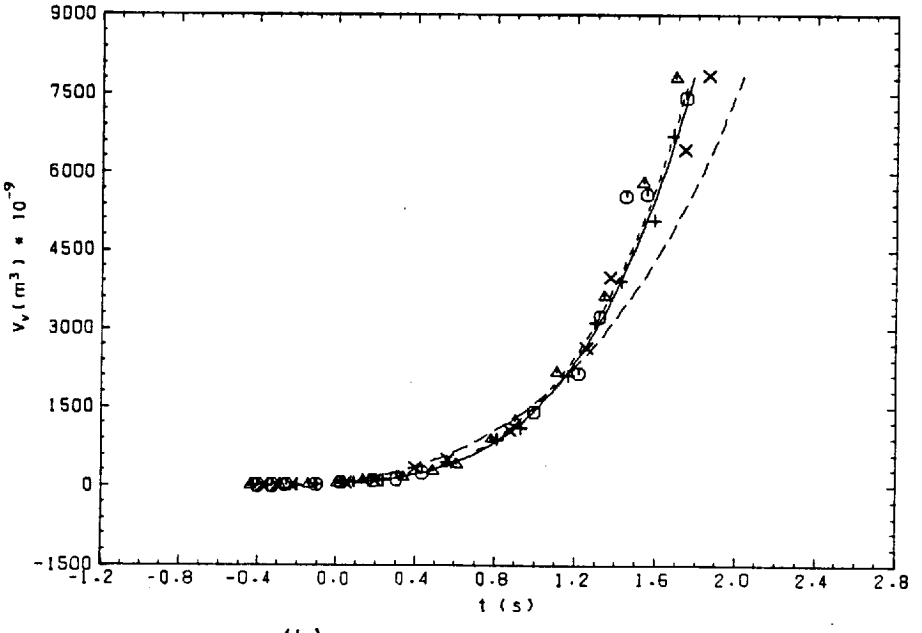

(b) Vapour volume vs. time

Figure 5.1(a-h): Comparison of the experimental results with prediction

Key to the figures

EXPERIMENT				
Symbol	Set	Run	$d \times 10^{-3}$ (m)	ΔT_o (°C)
⏲	4	8	4.0	2.5
△	4	10	4.1	2.5
+	4	11	4.05	2.6
×	4	12	4.20	2.5

PREDICTION	
Symbol	h Obtained From
———	Present results
- - - - - -	Simpson's correlation
— — — —	Sideman's model

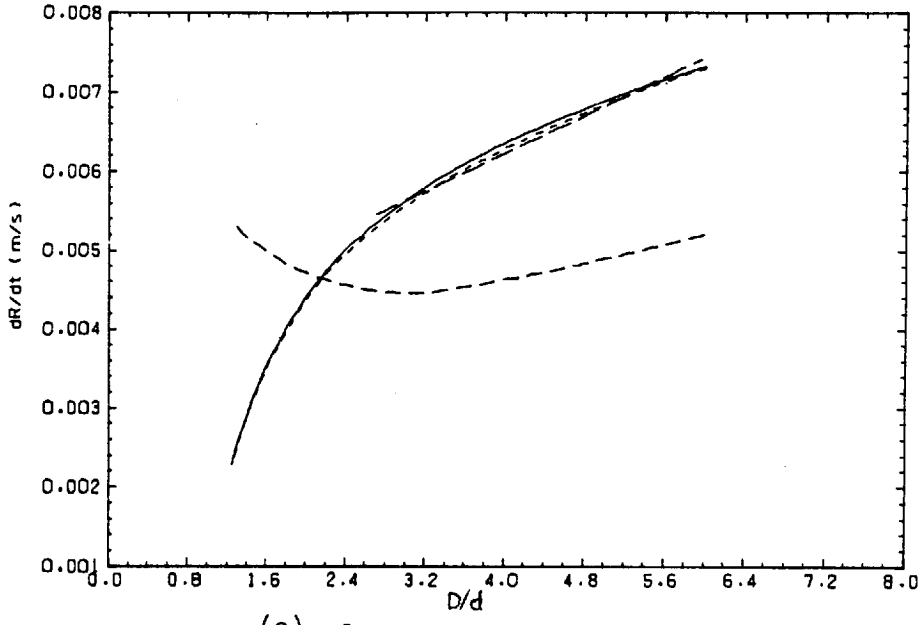

(c) Growth rate vs. diameter ratio

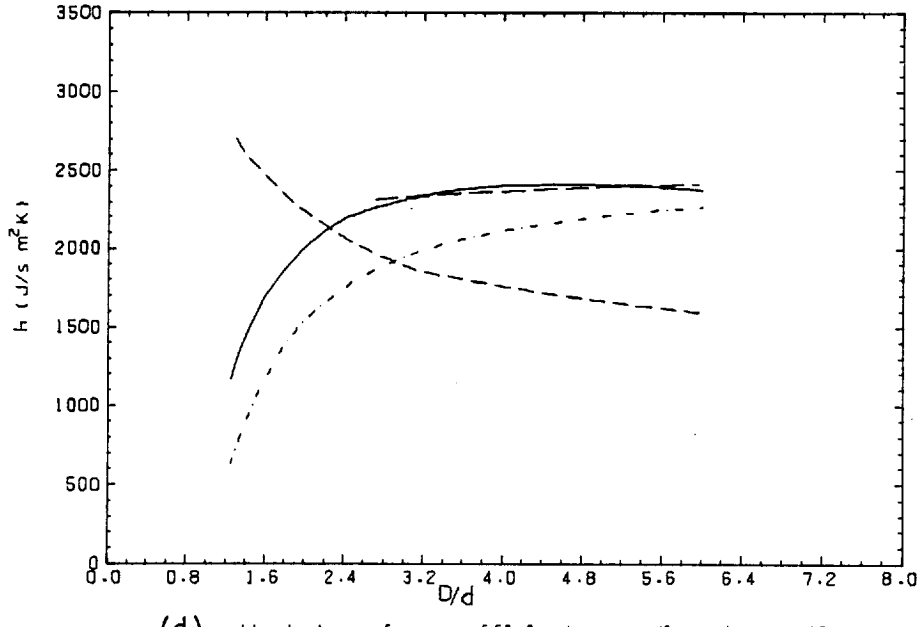

(d) Heat transfer coefficient vs. diameter ratio

Figure 5.1(a-h) (continued)

Key to Figure 5.1(c)

PREDICTION	
Symbol	h Obtained From
-------	Present results
— — — —	Simpson's correlation
- - - - -	Sideman's model
EXPERIMENT	
———	Present results, ΔT_o = 2.5°C

Key to Figure 5.1(d)

Symbol	Model
———	Present results, ΔT_o = 2.5°C
— · — · —	Present results, ΔT_o = 4.0°C
— — · — —	Simpson's correlation
- - - - -	Sideman's model

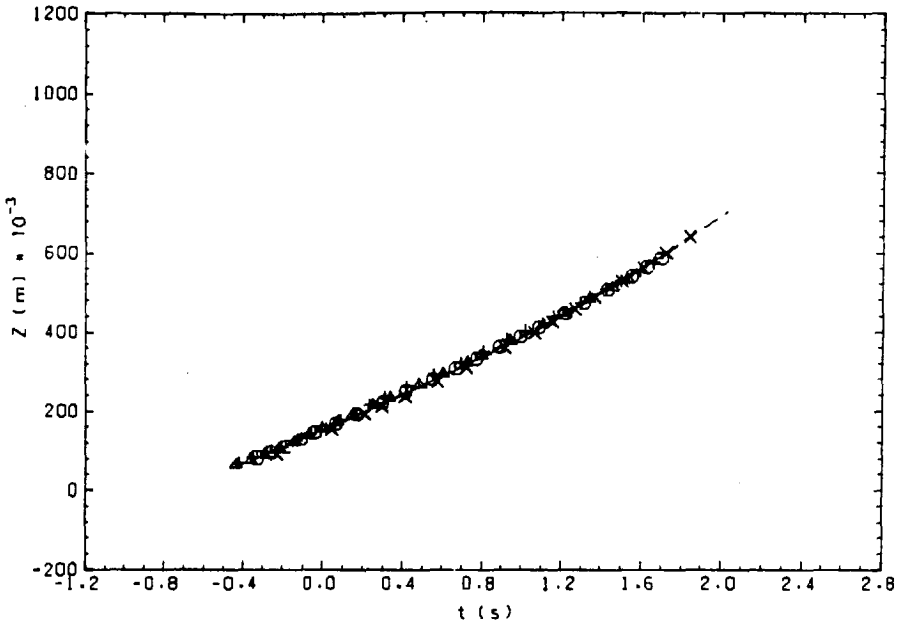

(e) Height vs. time

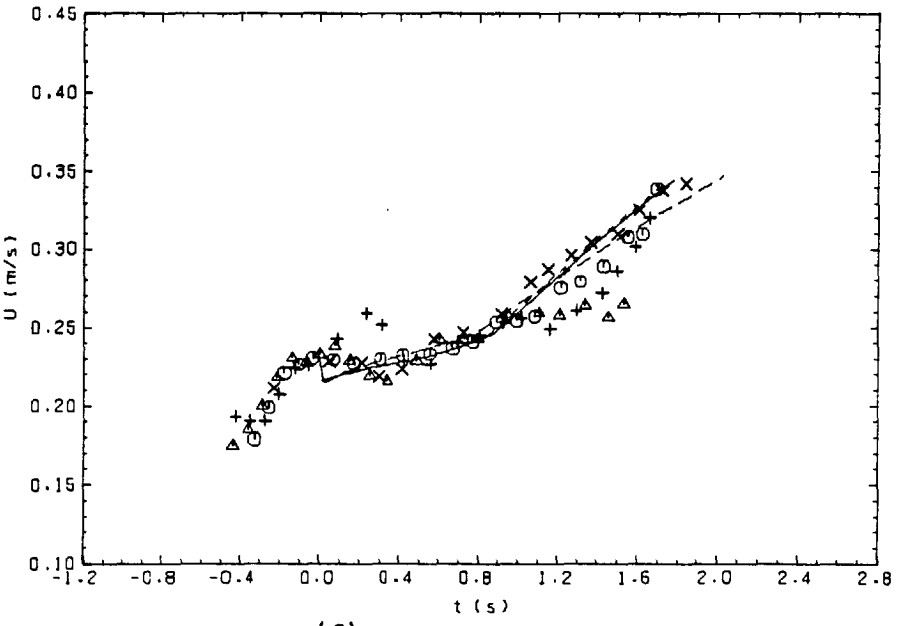

(f) Rise velocity vs. time

Figure 5.1(a-h) (continued)

(Key to the figures as in Figure 5.1(a,b))

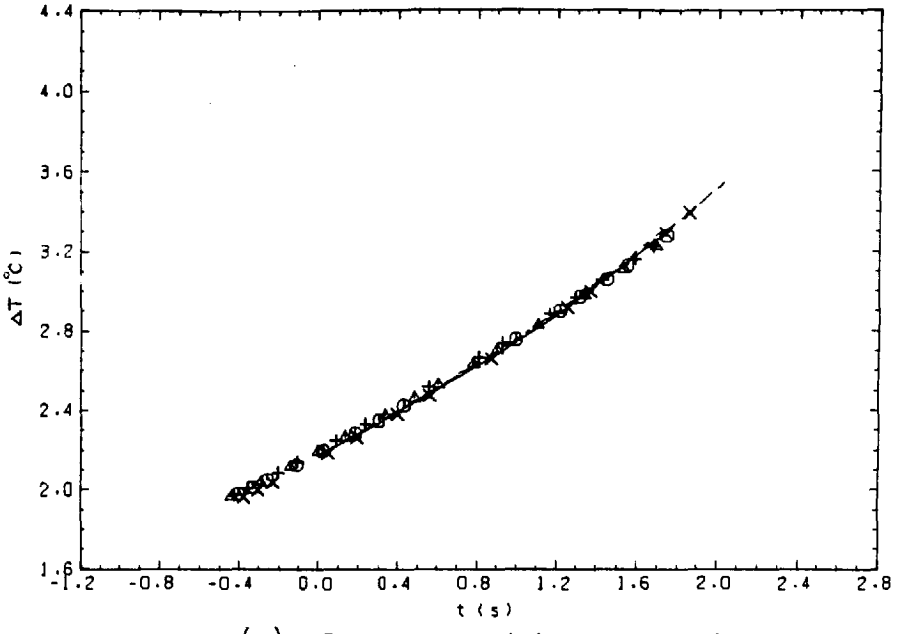

(g) Temperature difference vs. time

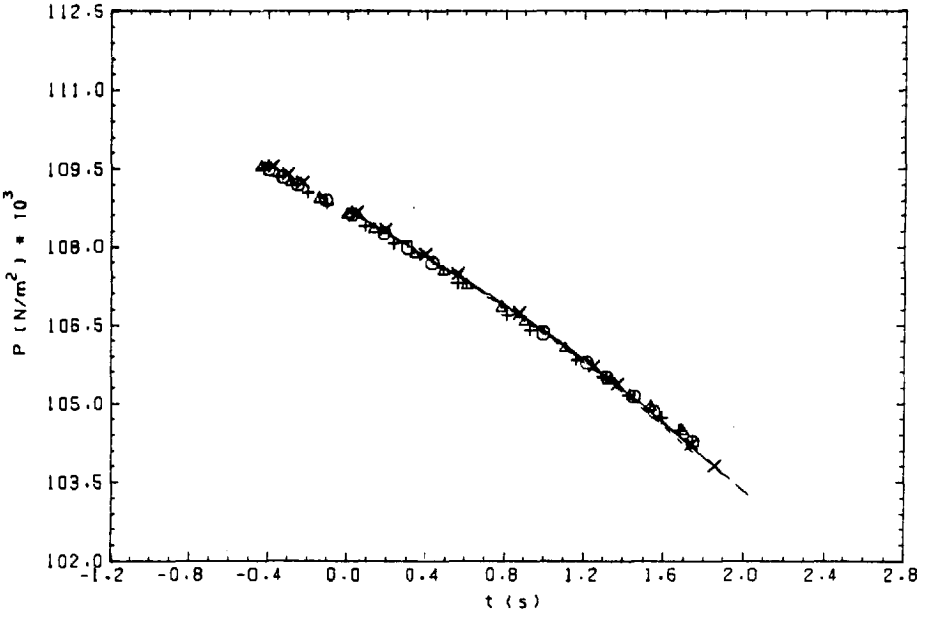

(h) Pressure vs. time

Figure 5.1(a-h) (continued)

(Key to the figures as in Figure 5.1(a,b))

transfer coefficients. These are shown in Figure 5.1(d), which includes the results for Case 2 (ΔT_0 = 4.0°C). Sideman's model, as mentioned before, predicts higher values at the early stages of evaporation due to the neglect of the inside resistance to heat. The faster evaporation during the early stages is later compensated by the slower evaporation at the later stages when the heat transfer coefficient falls below those predicted by the two other correlations. Variation of the growth rate against diameter ratio is shown in Figure 5.1(c). Nearly the same trends as in Figure 5.1(d) are obtained, except that since the growth rate is a function of the temperature difference (equation (2.63)) and this factor increases with time, the growth rate values increase faster than the heat transfer coefficients (Figure 5.1(d)). When Sideman's model is used, growth rate values decrease at first and then increase gradually, while the heat transfer coefficient decreases continuously.

The variation of height against time is shown in Figure 5.1(e). Close agreement is obtained. The rise velocity is shown in Figure 5.1(f). The same trends are found. At the early stages, predicted velocities are lower than the experimental values; thus, starting from a high initial velocity, it falls quickly to the predicted values. The reason could be due to the values of the drag coefficients. It was found that if, at this stage, the drag coefficients were calculated 10% lower than the ones used, the initial decrease would be eliminated and the velocity would increase gradually. In the later stages of evaporation, the predicted values are closer to the upper limit of the experimental results.

The variation of temperature difference and pressure is shown in Figures 5.1(g,h). Good agreement is obtained between the predicted and the experimental results.

Comparisons for Case 2 (ΔT_0 = 4.0°C, Table 5.1) are made in Figures

5.2(a-f). The heat transfer coefficients are shown in Figure 5.1(d). As can be seen, the present data for this case are lower than the previous case (ΔT_o = 2.5°C). As a result, shorter evaporation time is calculated when Sideman's model or Simpson's correlation was used. Variations of mass ratio and height versus time, and growth rate versus diameter ratio, are shown in Figures 5.2(c,d,f). Rise velocity is plotted against time in Figure 5.2(e). The agreement with the experimental results is poorer than in Case 1 (Figure 5.1(f)). In the later stages of evaporation, as in the previous case, the predicted velocities are closer to the upper limit of the experimental values. The reason could be attributed to the higher drag due to the shape variation and movement of the growing bubble in the actual experimental conditions.

Comparison of the predicted results with Sideman's (68) and Nazir's (53) experimental results were made in the joint paper by the author (47). However, conducting the present experiments showed that more detailed information on the previous experimental conditions were needed before an appropriate comparison could be made. In the above mentioned paper (47), the agreement between experiment and theory was poorer than the agreement achieved here between our own results. The reason was due to the lack of more accurate knowledge on the initial and experimental conditions, but mainly due to the misinterpretation of the initial temperature difference (ΔT_o) and also over-esimation of the heat transfer coefficient in the early stages of evaporation by extrapolation of equation (1.11) to lower diameter ratios than 2.7. In tabulating his results, Nazir (53) defined the temperature difference as the difference between the water temperature and butane normal boiling temperature (-0.5°C), while in this model the boiling point of butane at the local pressure is considered. Therefore, the initial temperature difference should be less than 2.0°C, which was

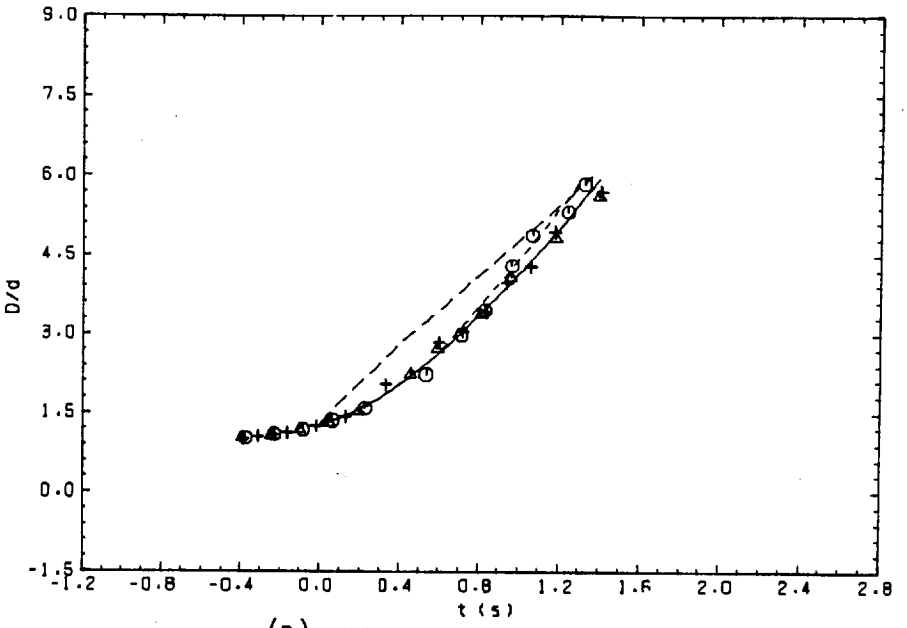

(a) Diameter ratio vs. time

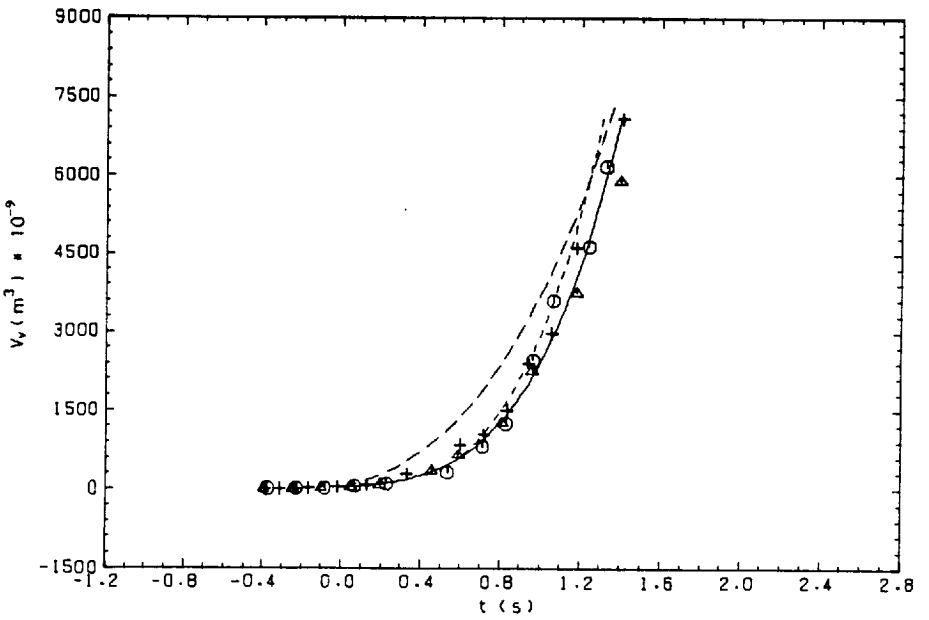

(b) Vapour volume vs. time

Figure 5.2(a-f): Comparison of the experimental results with prediction

Key to the figures

EXPERIMENT				
Symbol	Set	Run	$d \times 10^{-3}$ (m)	ΔT_o (°C)
○	5	25	3.9	4.0
△	5	26	4.0	4.0
+	5	28	4.2	4.0

PREDICTION	
Symbol	h Obtained From
———	Present results
- - - - - - -	Simpson's correlation
— — — —	Sideman's model

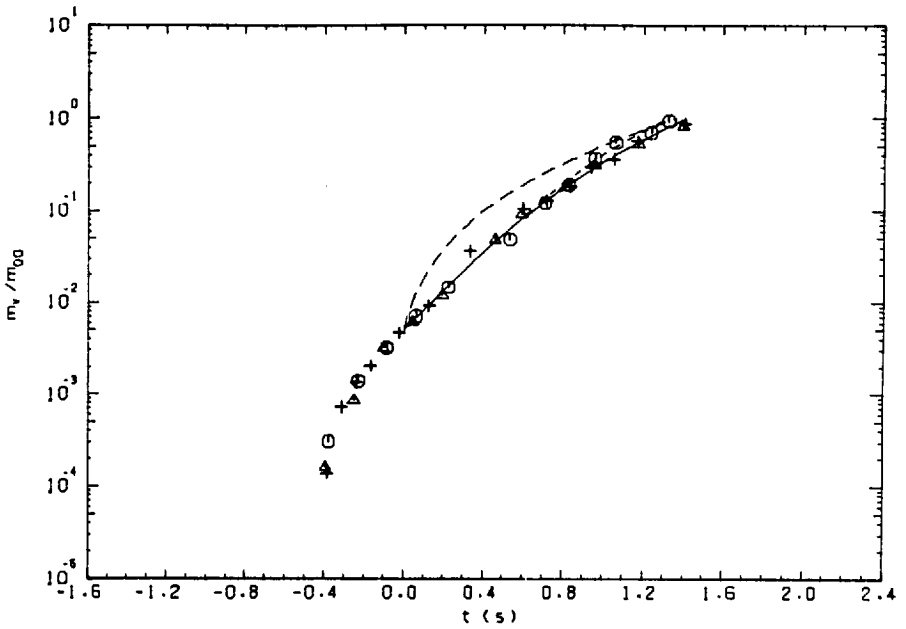

(c) Mass ratio vs. time

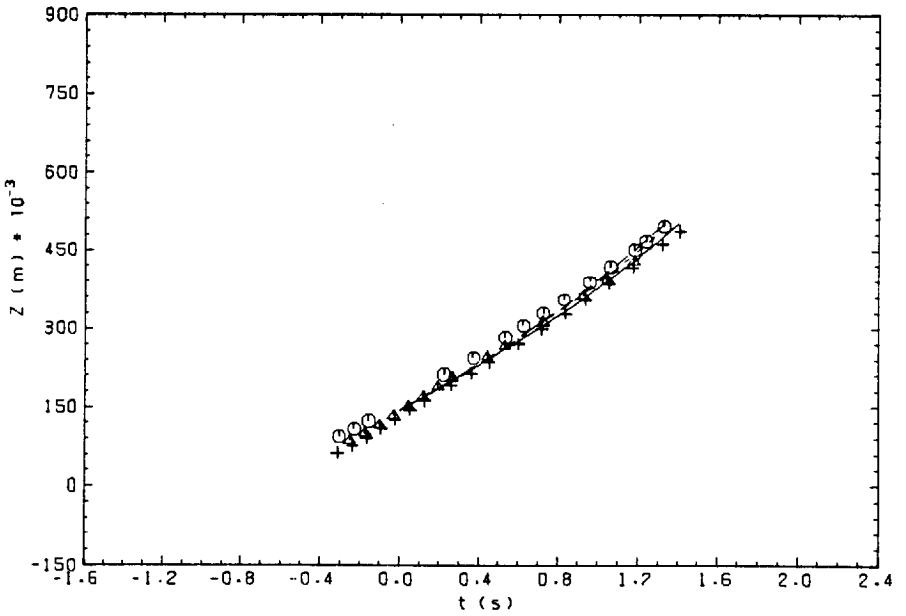

(d) Height vs. time

Figure 5.2(a-f) (continued)

(Key to the figures as in Figure 5.2(a,b))

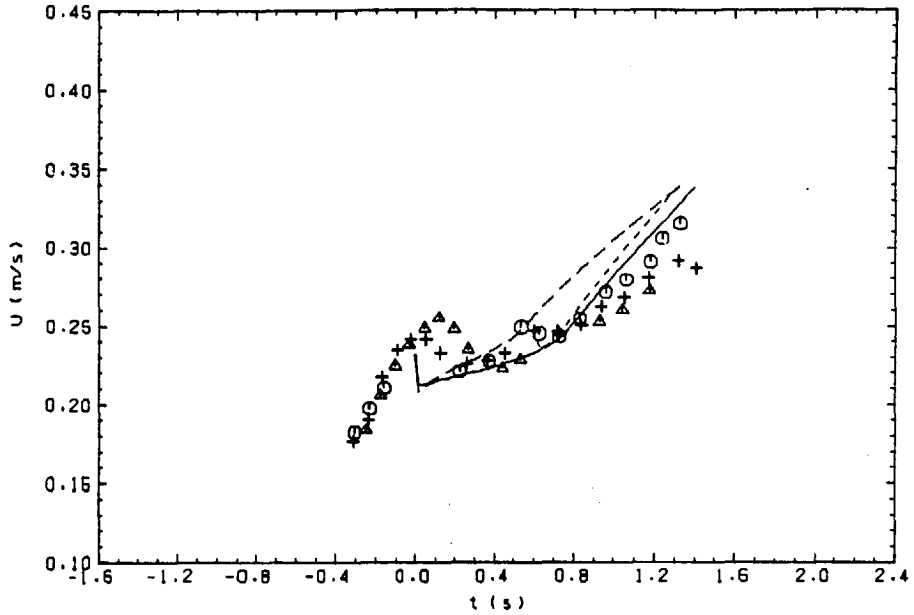

(e) Rise velocity vs. time

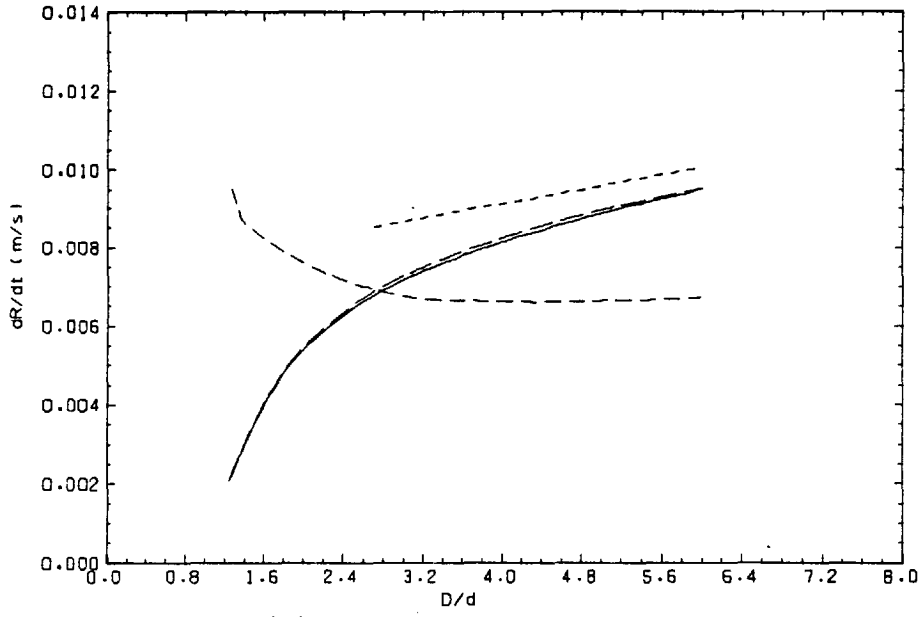

(f) Growth rate vs. diameter ratio

Figure 5.2(a-f) (continued)
(Key to Figure 5.2(e) as in Figure 5.2(a,b))

Key to Figure 5.2(f):

PREDICTION	
Symbol	h Obtained From
———	Present results
- - - - - - -	Simpson's correlation
– – – – –	Sideman's model
EXPERIMENT	
– – – –	Present results, ΔT_0 = 4.0°C

assumed when comparisons were made with Nazir's results. Thus, a better agreement would be obtained than that which was shown in the previous results (47). A similar argument holds for the case when comparison was made with the experimental results of Sideman et al (68). Sideman et al defined the temperature difference as the difference between the water temperature and the average of the butane boiling point at the top and bottom of the column. In this case, the actual initial temperature difference would be again lower than the one assumed; but the effect is smaller than Nazir's case.

CHAPTER 6

EXPERIMENTAL INVESTIGATION OF THE MOVEMENT OF BUBBLES AND BUBBLE-DROPLETS IN IMMISCIBLE LIQUIDS*

6.1 INTRODUCTION

The motion of bubbles in various liquids has been under considerable study. Rosenburg (65) studied the movement of air bubbles in water and classified their shapes and paths according to their sizes or Reynolds numbers, as given in Table 6.1. In this and similar studies, the cine photography has been the usual procedure used to study the shape and path of bubbles or droplets. Aybers et al (4,5) studied the shape and motion of air bubbles in water and used a photographic technique similar to ours to record the path of bubbles.

The method presented here uses still photography which makes it easier to study the movement of the bubbles. Data can be obtained, such as path, velocity, variation of size like growth and collapse, and indications of the surface instabilities. Results are presented for rising small and medium size air bubbles, evaporating butane droplets, condensing butane bubbles, and spherical cap shape butane bubbles in distilled water.

6.2 EXPERIMENTAL TECHNIQUE

The main features of the rig were described in Chapter 3. Photography was performed in a dark environment and the only projected light on the column was from one or both of the light sources which were

---

* A paper entitled "Motion of Bubbles and Bubble-Droplets in an Immiscible Liquid", published in Wärme und Stoffübertragung (48), was based on the work presented in this chapter.

TABLE 6.1 (65)

Description of Motion and Shape of Air Bubbles in Water as a Function of the Bubble Size

R_e (cm)	Re	Description
< 0.062	< 400	Spherical bubbles travelling in rectilinear paths
0.062-0.077	400-500	Oblate spheroid; rectilinear motion
0.077-0.24	500-1100	Oblate spheroid; helical motion
0.24-0.35	1100-1600	Oblate spheroid, essentially, but shape becomes increasingly irregular with increasing Re; motion is almost rectilinear
0.35-0.88	1600-5000	Transition - oblate spheroid to spherical caps; shape is very irregular and fluctuates continuously; motion is almost rectilinear
> 0.88	> 5000	Spherical caps; rectilinear motion

transferred through the slit. The slit was an essential part of this method. It allowed a slab of light to shine along the centre of the column, where the bubbles ascended.

The method utilises the reflections from the light sources on the bubbles. Figures 6.1(a), (b) and (c) show an air bubble resting at the nozzle. In Figure 6.1(a), the lower light source is used; the reflection points are indicated by A, B and C. In Figure 6.1(b), where both light sources are used, and shows another similar point to A on the bubble. In order to specify the position of the reflections relative to the bubble surface, back lighting was used in a part of the exposure time, thus giving a clear outline of the bubble surface. As can be seen, the reflection points are slightly away from the actual bubble boundary and, consequently, the distance between the points A and C is smaller than the diameter of the bubble. When photography was performed in a dark environment, traces of the reflection points were photographed continuously during the exposure time. The aperture of the camera was left open during the time when the bubble was passing in front of the camera, except in the case of velocity measurement when it was set to a specific time. Use of a robust stand for the camera and also a cable release made it possible to eliminate movement of the camera during the long exposure time. Specifications of the still camera and the lenses were described in Section 3.2.1 of Chapter 3.

6.3 RESULTS

6.3.1 Path of Medium Size Bubbles

Medium size air bubbles (about 3.15 mm in diameter) were injected from a nozzle 1.0 mm in diameter into a column of quiescent distilled water at $20^{o}C$. Configurations of a bubble after release and

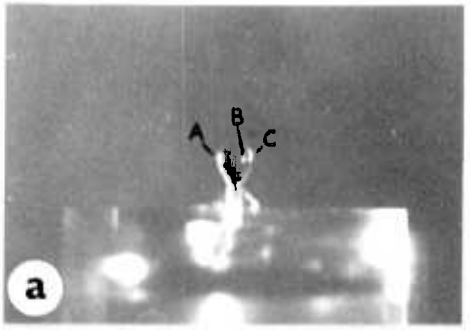

Figure 6.1(a-c): Light reflections on a bubble attached to the nozzle

during its rise further up in the column were recorded by the ciné camera and are shown in Figures 6.2(a) and (b), respectively. The paths of such bubbles are shown in Figures 6.3(a) and (b). We observed a spiral movement; however, it appeared on the photograph as a sinusoidal path which had constant amplitude and wavelength. A difference was realised between the path during the initial period of rise and during the time when it had reached its steady movement. In the former case, the edges of the path were not smooth, which was due to the bubble deformation and its turbulent movement; while, in the latter, the edges were clearly smoother due to the stabilised motion. These can be better seen in the close-up of the path shown in Figures 6.4 and 6.5. When both sources of light were used, the two reflection points showed two different traces. These are shown in Figures 6.6(a) and (b) (at the earlier stages of rise) and in Figure 6.7 (in the later stages of rise). The roughness of the path increased with the rate of bubble formation, due to the increased deformation and turbulent movement of the bubbles. An example is shown in Figure 6.8, in which f = 1.6 bubble/s, compared with Figure 6.6 where f = 0.7 bubble/s.

6.3.2 Path of Small Bubbles

Small air bubbles were formed by a stainless steel tubing in distilled water at 20°C. The path of a bubble 0.66 mm in diameter is shown in Figure 6.9. The shape of the bubble was spherical and the path was rectilinear.

6.3.3 Path of Condensing Bubbles

Butane bubbles were used for this purpose. Water was cooled down to a temperature below the butane saturation temperature at the nozzle

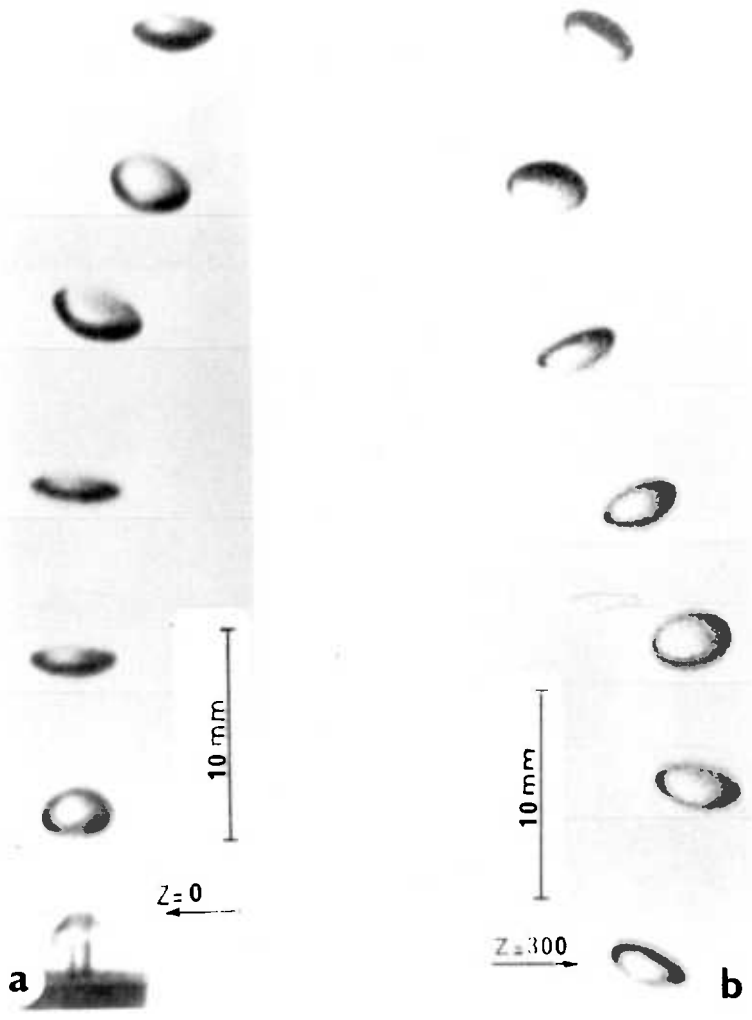

Figure 6.2(a,b): Configurations of an air bubble in water taken by a ciné camera (Δt = 1/32 s)

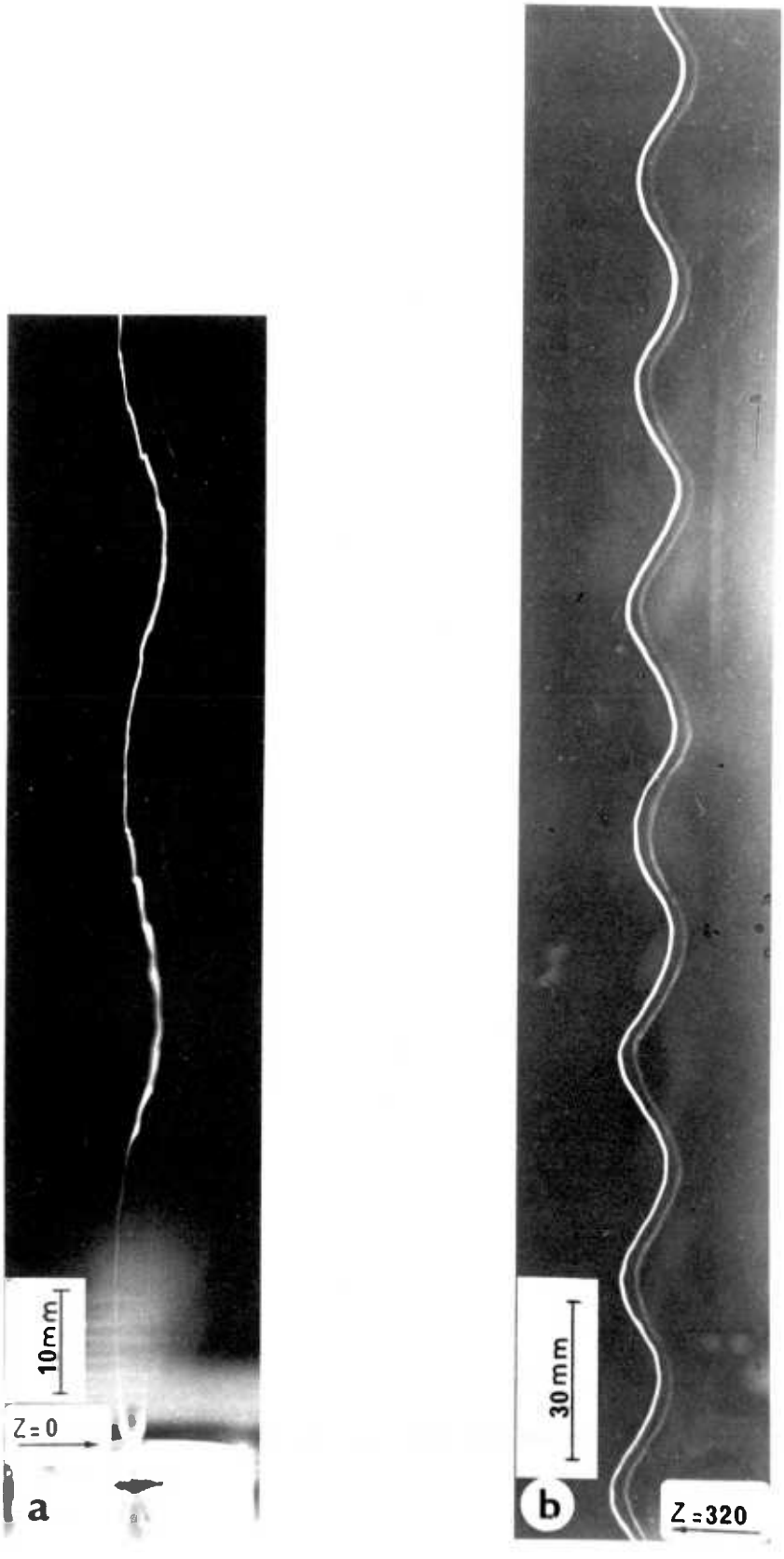

Figure 6.3(a,b): The path of air bubbles in water

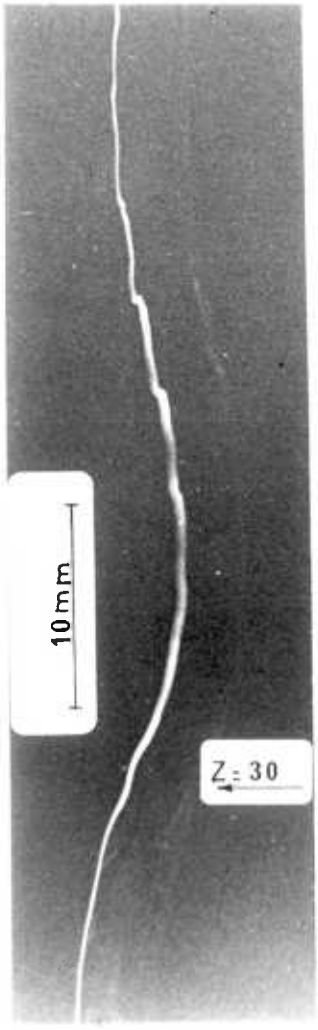

Figure 6.4: The path of an air bubble in water at the earlier stage of its rise

Figure 6.5: The path of an air bubble in water at the later stage of its rise

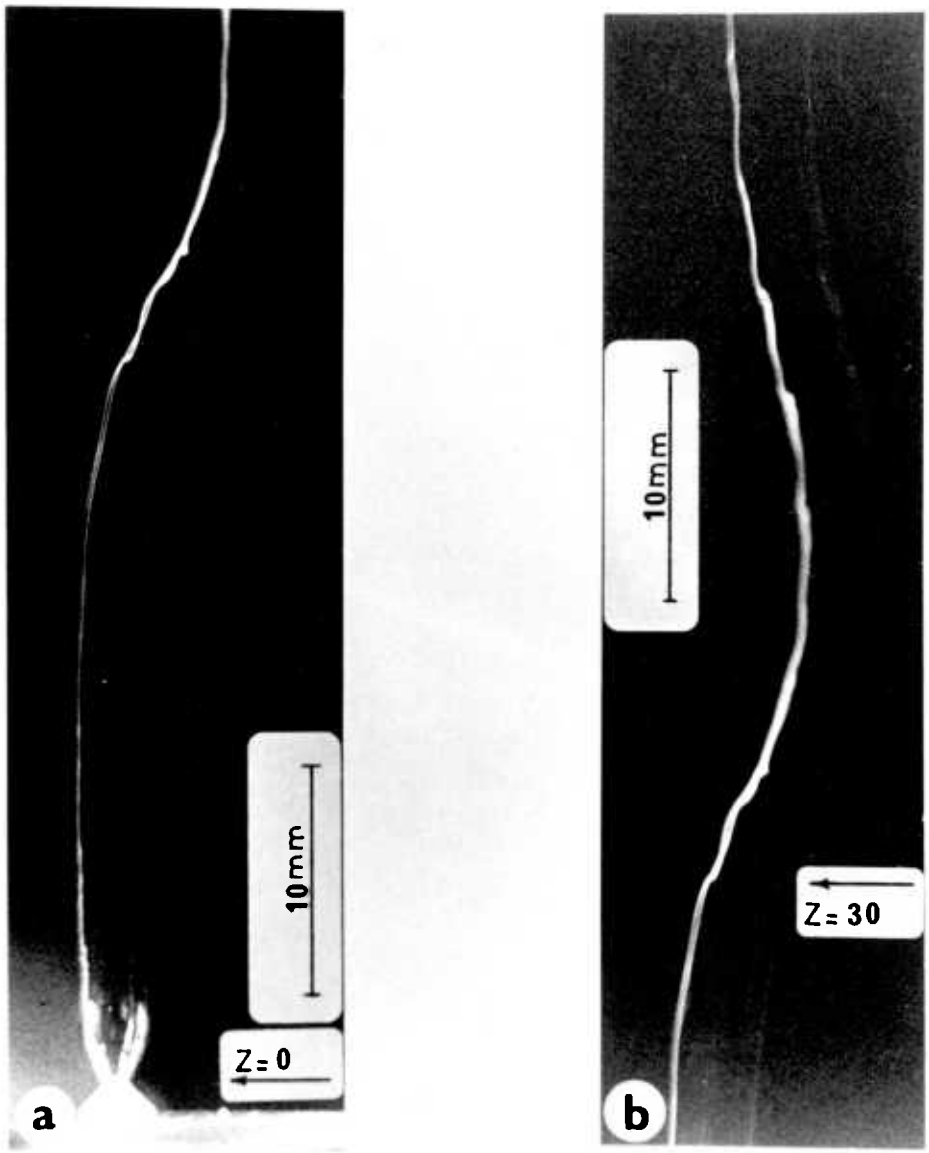

Figure 6.6(a,b): The path of air bubbles in water shown by two reflection points (at the earlier stage of its rise, f = 0.7)

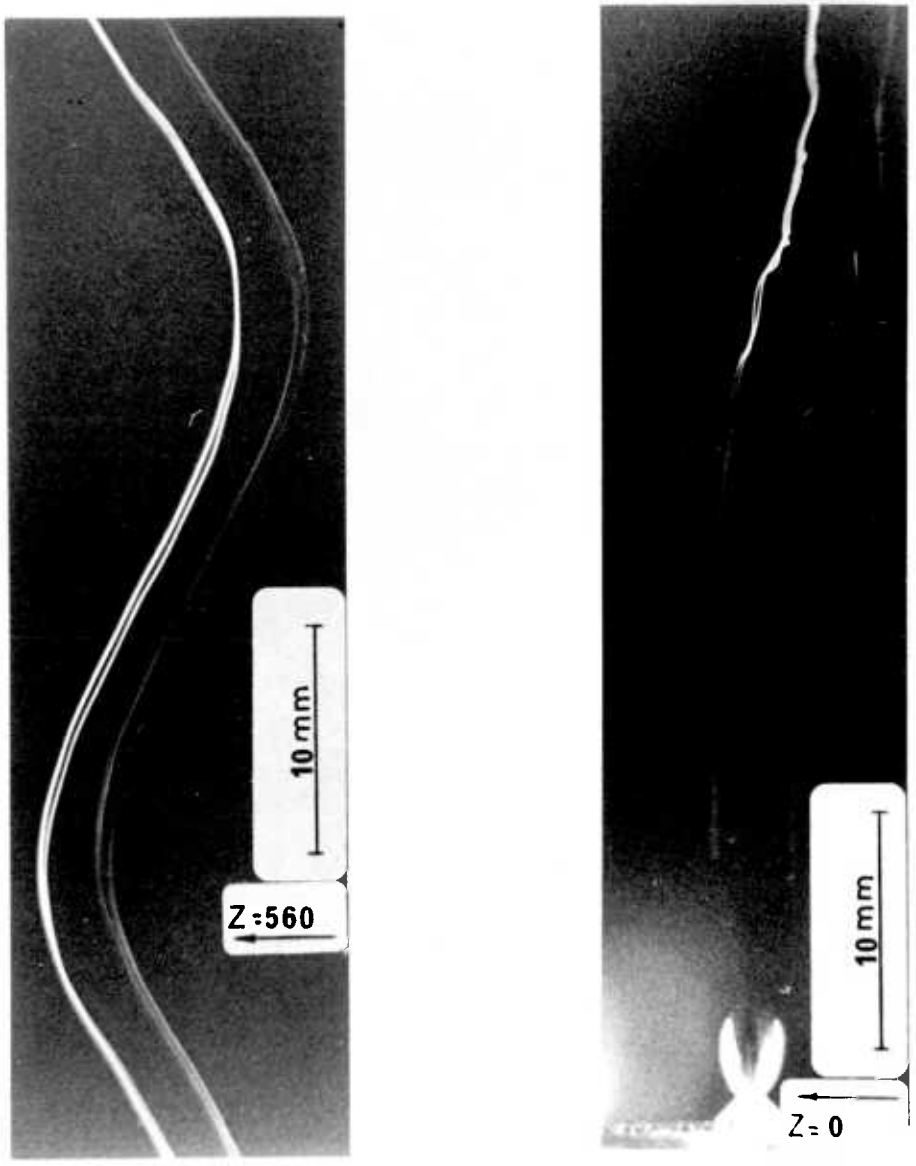

Figure 6.7: The path of an air bubble in water shown by two reflection points (at the later stage of its rise)

Figure 6.8: The path of an air bubble in water shown by two reflection points (at the earlier stage of its rise, f = 1.6)

Figure 6.9: The path of a small air bubble in water

level. A Chromel-Alumel thermocouple (Gulton, insulated thermocouple, type E, 1 mm diameter) was placed in the nozzle assembly passage to measure the temperature of the flowing butane gas. Experimental conditions were:

Atmospheric pressure	=	766.6 mm Hg
Water temperature	=	$0.64^{o}C$
Gas temperature in the nozzle assembly	=	$13.5^{o}C$
Butane saturation temperature at the nozzle level	=	$1.93^{o}C$
Water column height	=	900 mm
Number of bubbles/s	=	0.5 bubble/s
Nozzle diameter	=	1.0 mm

Configurations of a condensing butane bubble are shown in Figure 6.10. Examples of the path are given in Figures 6.11(a), (b) and (c). The bubble, after release, moved in a vertical straight line for a short time and then changed its direction of movement significantly. Considerable deformation occurred at this stage. The bubble followed a short helical path and then continued to rise in a vertical straight line. At this stage, the bubble shape was nearly spherical. The path at the region where it deviates from the straight line is very rough compared to the other sections of the path, due to the erratic movement of the bubble. The turning of the path could be in any direction, such as that shown in Figure 6.11(c), which was towards the camera, and thus the path appears to be straight. After the bubble path became straight again, its size did not decrease significantly, indicating that the condensation was not complete. Thus, most of the condensation occurred during the initial period of rise after separation. In the later stages of rise, due to a decrease of pressure and also a slight increase of water temperature, the

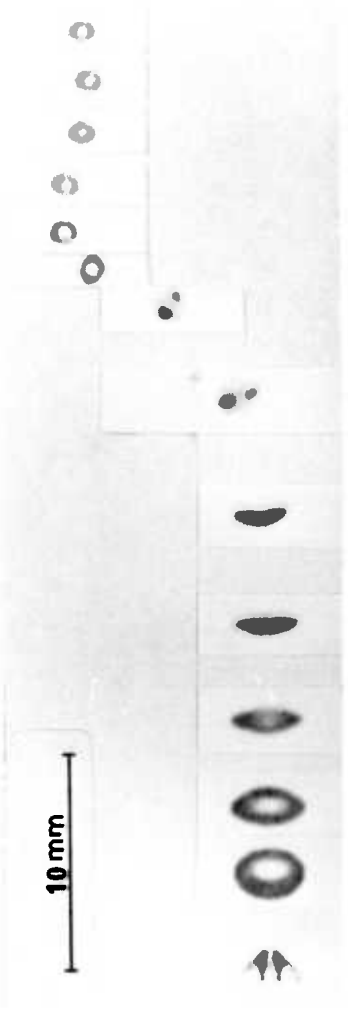

Figure 6.10: Configurations of a condensing butane bubble in water taken by a ciné camera (t = 1/64 s)

Figure 6.11(a-c): The path of condensing butane bubbles in water

condensed vapour gradually re-evaporated and the bubble size increased. Because of this, straight motion was gradually turned to helical movement as expected for a bubble of that size. During the bubble formation, some condensation took place. This was realised from the size of the bubble near the water surface. At this stage, because the water temperature was higher than the saturation temperature of butane, evaporation took place and the size of the resulting bubble became larger than the size of the bubble just after its release from the nozzle.

6.3.4 Path of Evaporating Droplets

The configuration of an evaporating butane droplet in water was shown in Figure 4.2. The path of such evaporating droplets are shown in Figures 6.12(a), (b) and (c) at various levels in the column. The slow growth is due to the low temperature difference which, at the nozzle level, was 2.0°C. The path of a droplet when ΔT = 5.5°C is shown in Figure 6.13(a), in which quicker growth can be seen. The edge of the paths are smooth while the droplet is in the early stages of evaporation due to the small size of the bubble. They become rough when the bubble size increases and becomes irregular and unstable. The bubble-droplet motion could be considered to be rectilinear when droplet formation was slow and the turbulence in water was small (Figure 6.13(a)). Deviations from the straight line increased when the number of evaporating drops and the movement within the water increased (Figure 6.13(b)).

6.3.5 Path of Spherical Cap Bubbles

Spherical cap bubbles were those which generated from the complete evaporation of butane droplets in water. The typical shape of spherical cap bubbles was shown in Figure 4.3. Two examples of the path

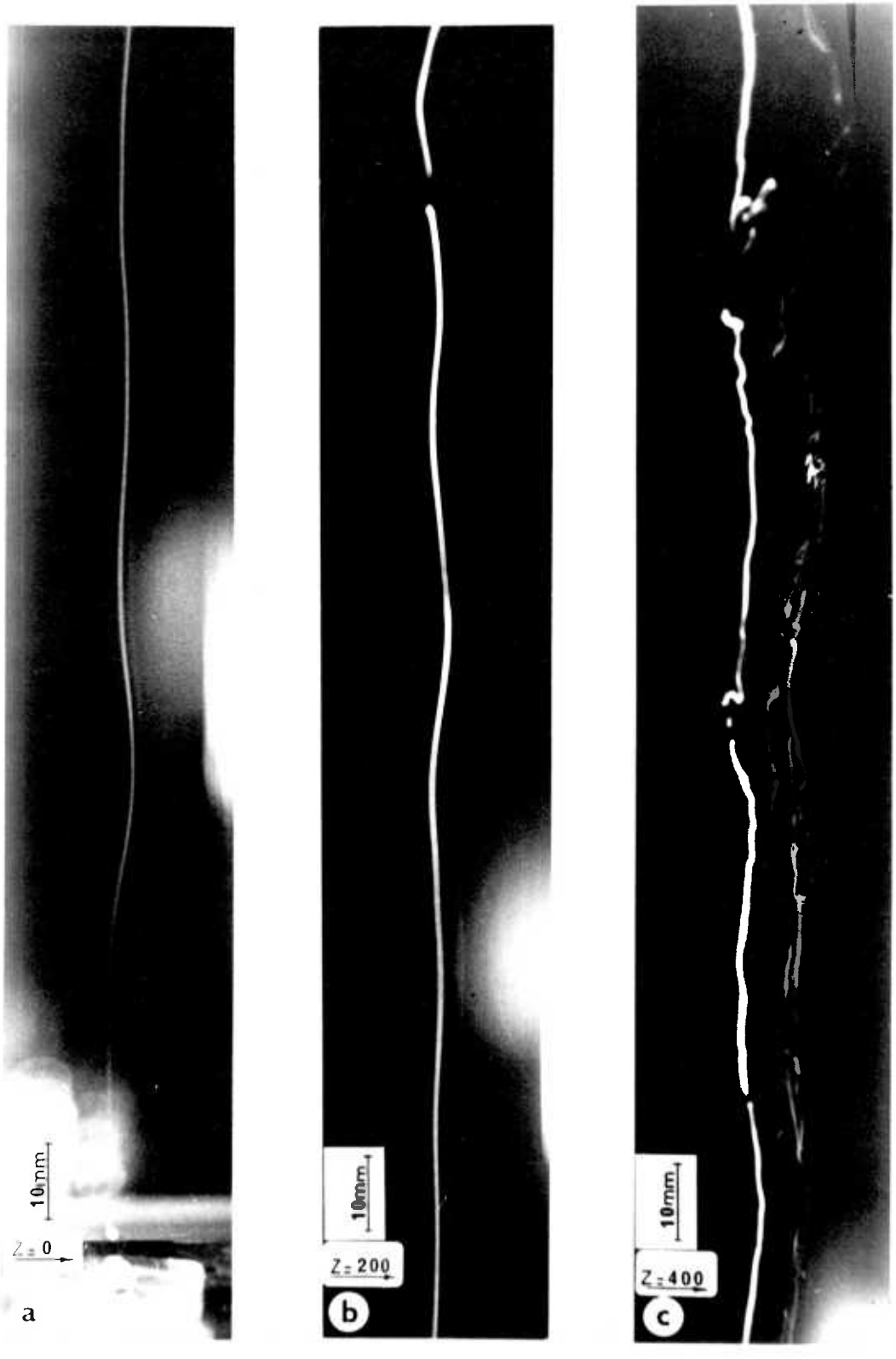

Figure 6.12(a-c): The path of evaporating butane droplets in water

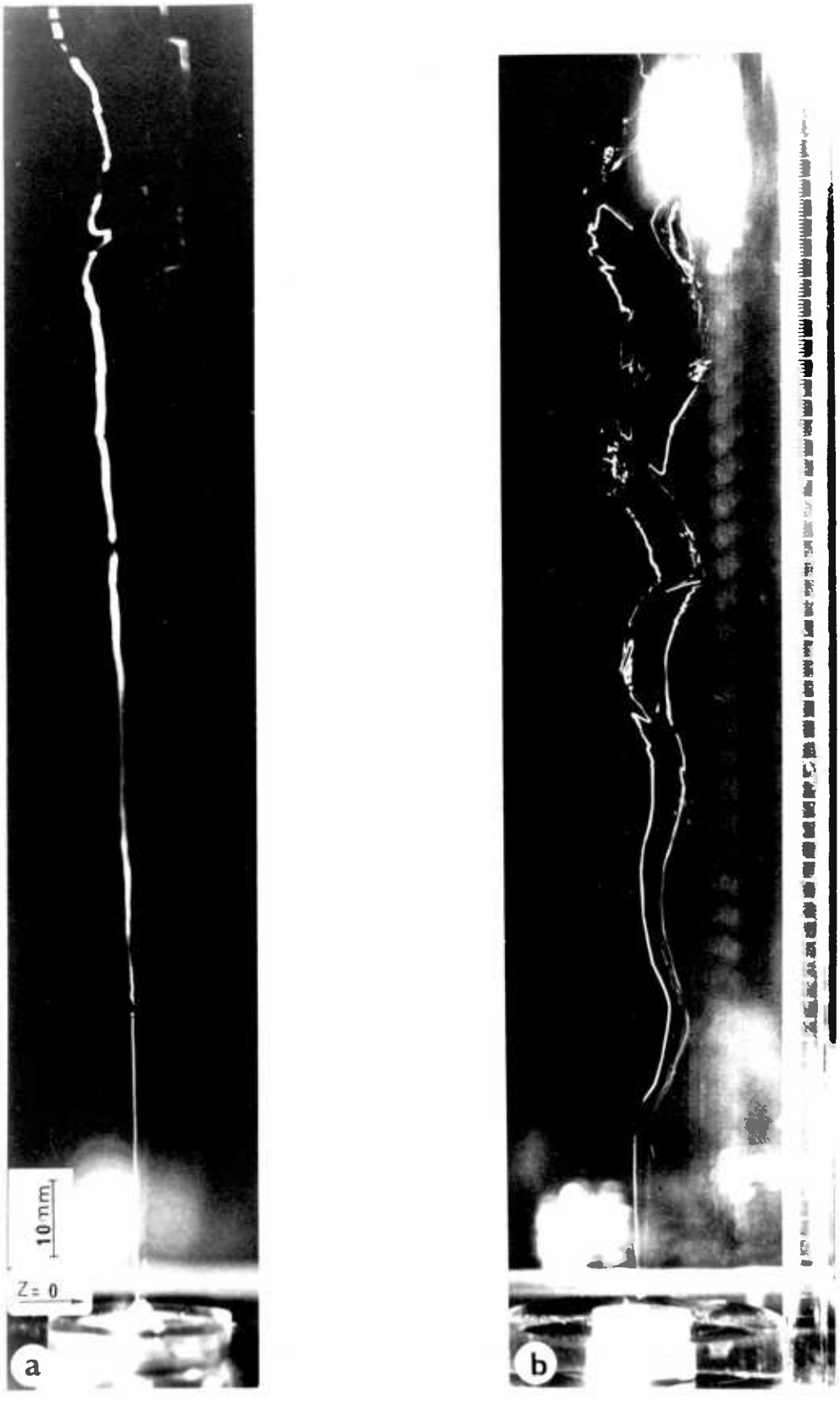

Figure 6.13(a,b): The path of evaporating butane droplets in water

are shown in Figures 6.14(a) and (b). The path was rectilinear. The very rough and irregular edges of the path is due to the unstable surface of the bubble and its erratic movement.

Spherical cap shape bubbles are generally assumed to be axisymmetric and as a part of a sphere. However, observations from the top of the column showed that deviations from this assumption might exist. Attempts were made to photograph the bubble from the top by use of the slit. For doing so, the slit was placed horizontally with respect to the vertical column. In such a position, the slab of light illuminated only a cross-section of the column, the width of which was about 20 mm. The camera was placed at the top of the column. The bubble crossed this section during its rise and was illuminated; thus, an overall shape of the outline of the bubble during the time the bubble passed through the illuminated section was recorded on the photograph. This time, assuming a bubble velocity of about 0.30 m/s, would be about 0.07 seconds. Examples of the results are shown in Figures 6.15(a), (b), (c) and (d). Unstable conditions and the turbulent nature of the bubble during this short period can be realised from these photographs. However, on the average, the bubble shape may be considered to be axisymmetric.

6.3.6 Velocity Measurement

If the exposure time is set to a certain value (e.g. 1/8, 1/30 second), the velocity of the bubble is calculated by dividing the length of the path by the exposure time. By using this method, the velocity of several bubbles can be measured simultaneously. Examples for the medium size air bubbles (about 3.15 mm diameter) in water are shown in Figure 6.16 for one bubble and Figure 6.17 for several bubbles. In Figure 6.18, the velocity of a small bubble, 0.75 mm in diameter, in a train of bubbles of about the same size, is measured to be 104 mm/s.

Figure 6.14(a,b): The path of spherical cap shape butane bubbles in water

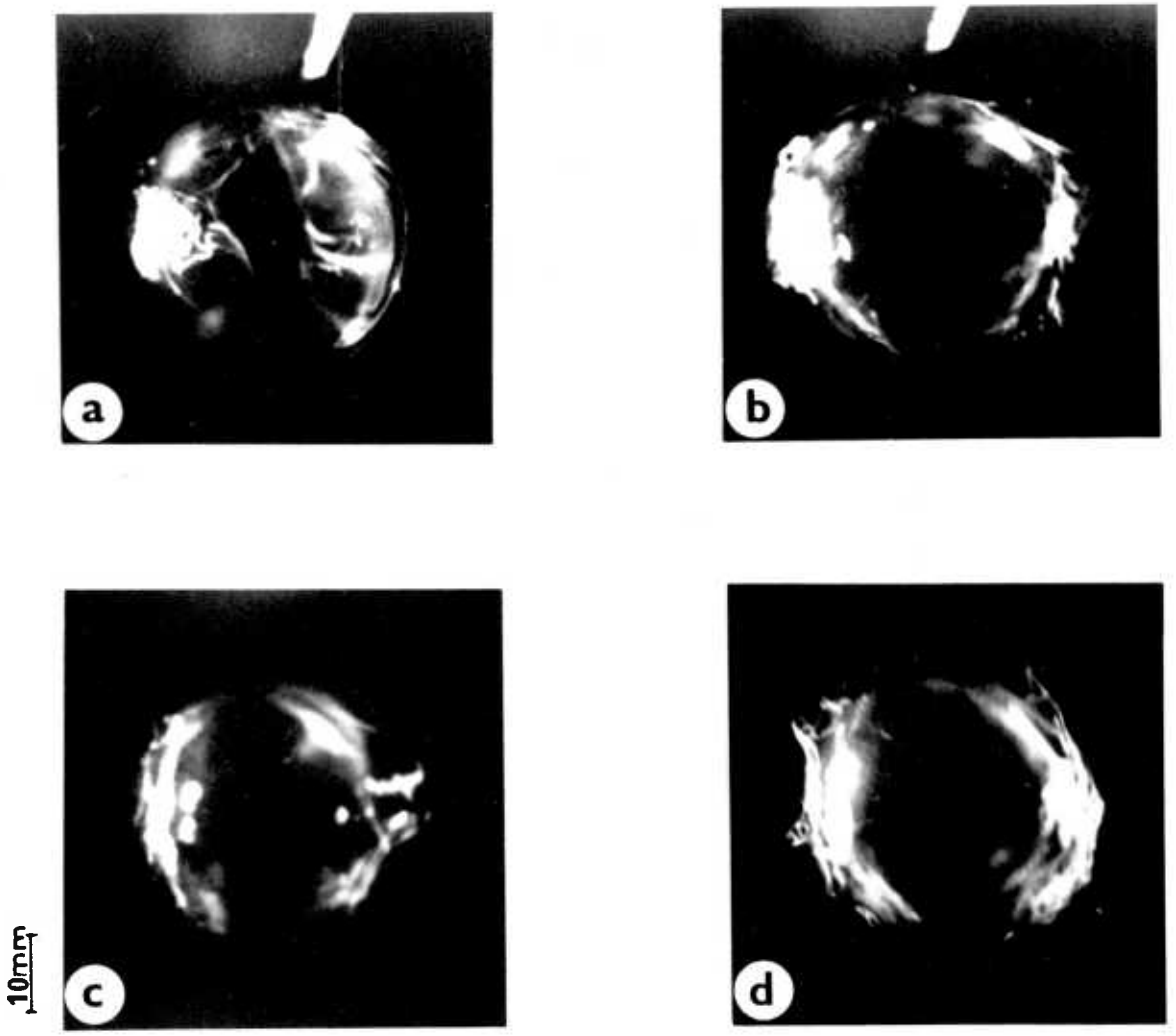

Figure 6.15(a-d): "View from top" of spherical cap shape butane bubbles rising in water

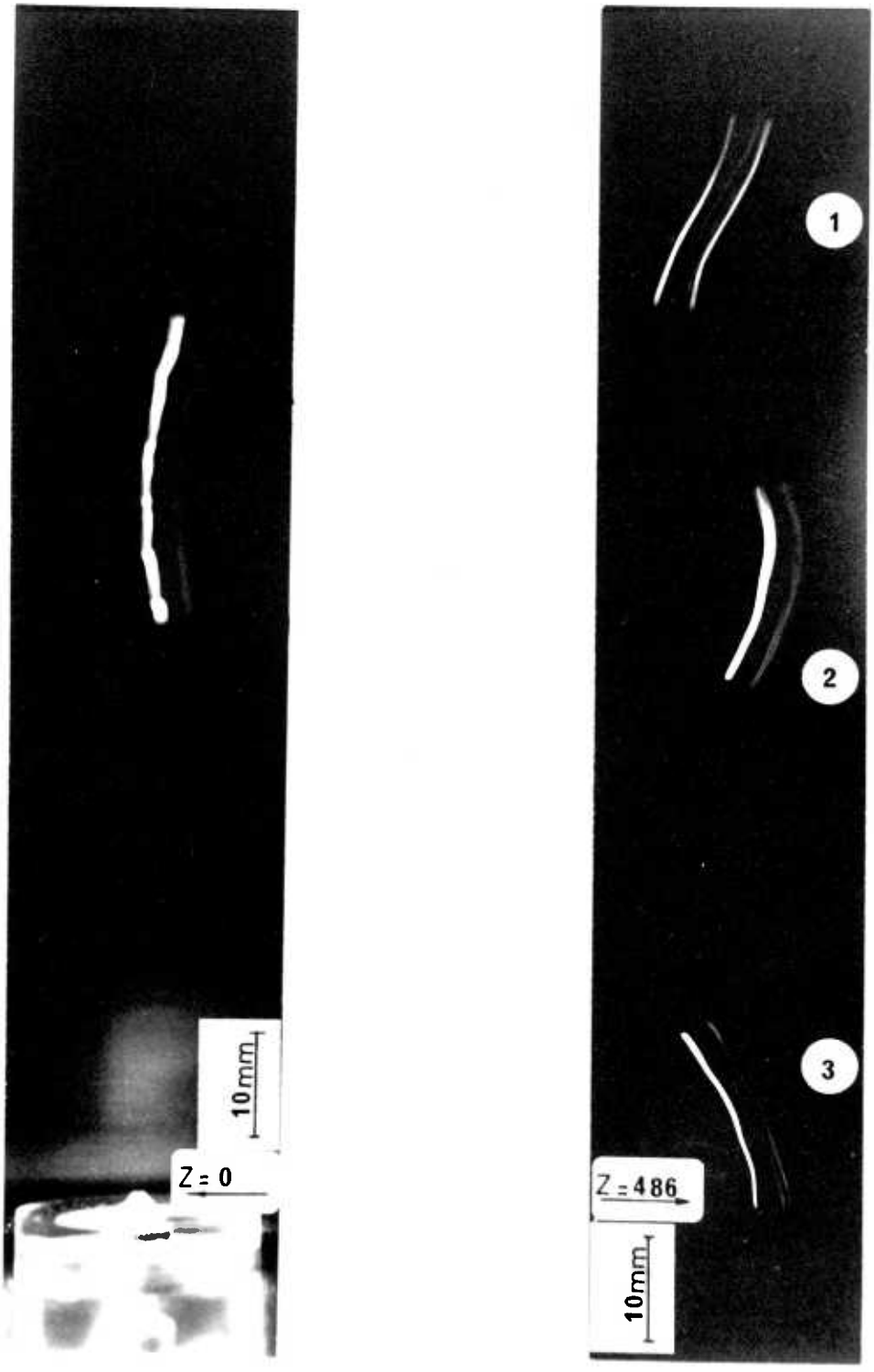

Figure 6.16: Velocity measurement of an air bubble in water (U = 240 mm/s)

Figure 6.17: Velocity measurement of three air bubbles in water (simultaneously) (U_1 = 282, U_2 = 286, U_3 = 266 mm/s)

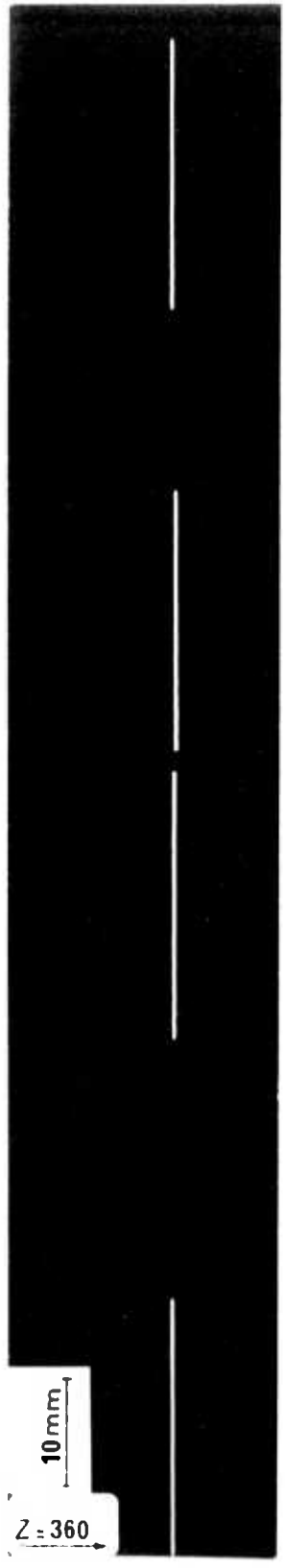

Figure 6.18: Velocity measurement of small air bubbles in water (simultaneously)

6.4 DISCUSSION AND SUGGESTIONS FOR FUTURE WORK

The path recorded by this method is the projected path of the bubble on the plane parallel to the camera. Thus, the velocity measurement by this method would be more accurate when the bubble moves mostly along this plane. For example, for small bubbles which move in a straight line, accurate measurement can be achieved. The advantage that this method has over the ciné photography method is that it is applicable for the study of the movement of several bubbles simultaneously, since, in the ciné photography method, the identity of the bubbles may be lost, especially when the bubbles are the same size.

The inadequacy of this method is that no information can be achieved from the recorded path about the actual size and shape of the bubble. This is especially important when a bubble grows or collapses. Also, this procedure is not directly useful for the study of the path of liquid droplets, since no strong reflection on the droplet was seen. This is especially a disadvantage when evaporating droplets are under study. In this case, the amount of the unvaporised liquid and thus the mass ratio is not known. To overcome this problem, a technique should be developed to record the shape of the bubble or evaporating droplet in time intervals on the path. However, in order to obtain the path of non-evaporating droplets, a small bubble can be injected into the droplet. In such a case, the reflections on the bubble will leave a trace which would indicate the path of the droplet.

Developing a technique to include the picture of the bubble on the path at time intervals and the study of the path of non-evaporating droplets and stopped-evaporation droplets were left for future work.

CHAPTER 7

COMPUTER PROGRAMS

7.1 INTRODUCTION

Computer programs were developed to perform the calculations involved in the theoretical model (Program TEREZ1) and to process the experimental data (Program EXREZ1 and Program EXREZ2). The programs were written in FORTRAN IV language and were used on a CDC 6400 computer. The main task of TEREZ1 is to solve the differential equations which are mentioned in Chapter 2 by using the initial and operating conditions and other required information, such as the heat transfer coefficient, vapour pressure, etc. EXREZ1 was developed to process the experimental data concerning the evaporating droplets, and EXREZ2, which is similar to EXREZ1, was developed to deal with the data of stopped-evaporation droplets. Each program calls a number of subroutines which perform a specific task. These programs and subroutines are explained in more detail in the following sections. A number of smaller programs were written to do the minor tasks which are not mentioned here.

7.2 GENERAL DESCRIPTION OF THE PROGRAMS

7.2.1. Program TEREZ1

This program was developed to perform the calculations involved in the prediction model of an evaporating droplet in an immiscible liquid. It calls the subroutine DØ2AEF which solves the set of differential equations. Basic information on the process is given within this program. Its task is also to set the initial conditions and to process the results of integration. The final results are then printed out or stored on tapes for further processing or plotting. Setting the operating

conditions and the calculation of the continuous phase and dispersed phase properties and drag coefficient are carried out by calling ENTRY points within subroutine PROPETY.

Computation ends when the whole liquid mass of bubble-droplet is evaporated or it has reached the water surface before the evaporation is completed. The flow chart of Program TEREZ1 is shown in Figure 7.1. Details of the subroutines which are used in TEREZ1 are as follows:

(a) Subroutine DØ2AEF: This subroutine is a NAG library program which is available at the Imperial College Computer Centre (ICCC). The number of equations, initial conditions, error bounds, step length and the length over which integration is required are the input data to this subroutine. The output is the result of the integration which can be used as the new initial values for integration over the next step. The subroutine terminates the computation if an error (for example, an unsuccessful iteration) is detected. Further explanations on the procedure of integration has been mentioned in Section 2.3. DØ2AEF calls subroutine AUX.

i) Subroutine AUX: The differential equations are specified within this subroutine. ENTRY VAPOUR and ENTRY DRAG are called within this subroutine.

(b) Subroutine PROPETY: This subroutine mainly deals with the calculation of the physical properties of the phases involved in the process. It includes a number of ENTRY points which are as follows:

i) ENTRY CONST: Some of the chemical constants of the dispersed phase (Appendix C.1) are specified here.

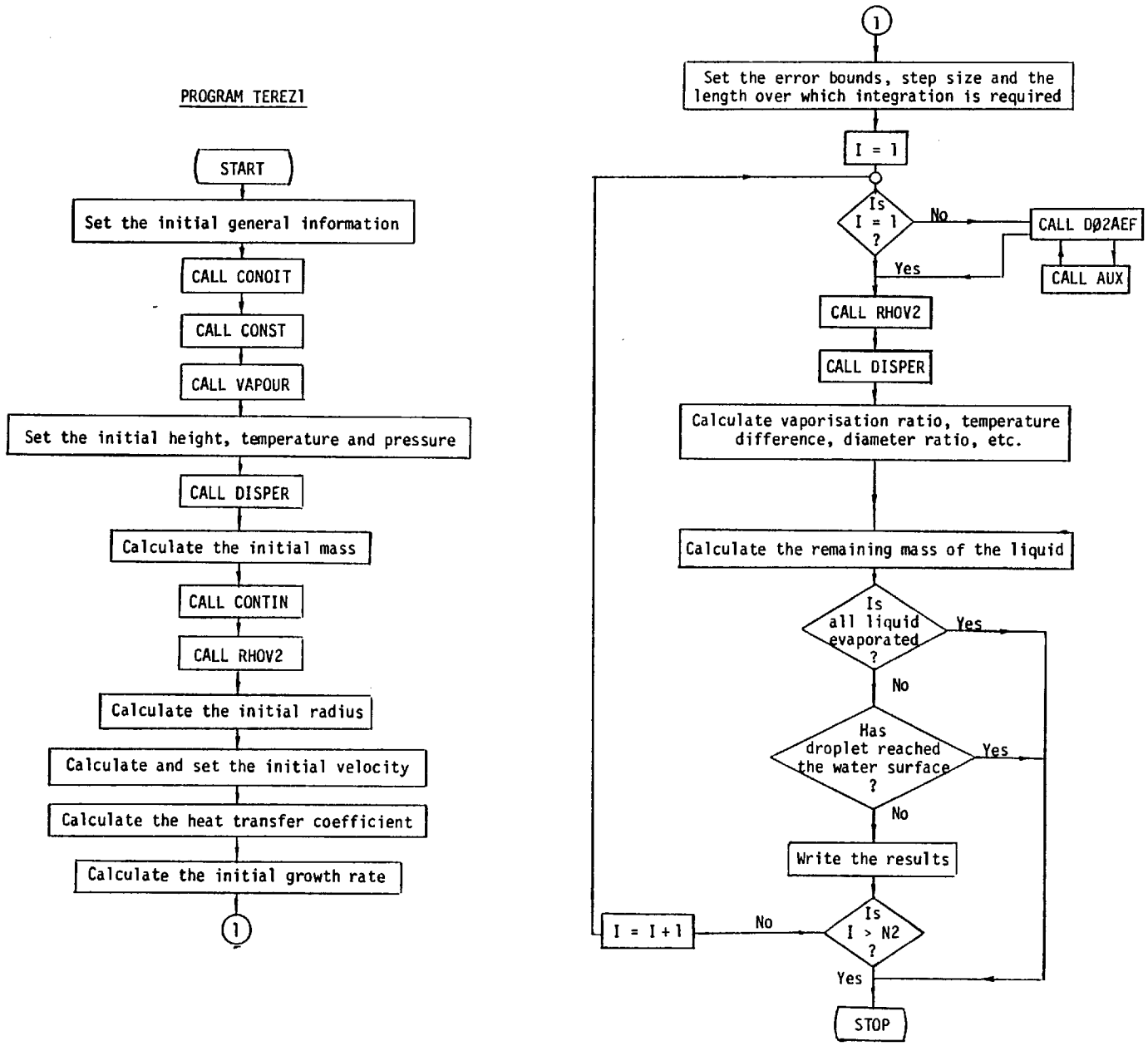

Figure 7.1: Flow chart of program TEREZ1

ii) ENTRY CONTIN: Some of the physical properties of the continuous phase, such as density, viscosity and specific heat, are calculated using the available correlations (Appendix C.3).

iii) ENTRY DISPER: Some of the physical properties of the dispersed phase, such as density, viscosity and heat of conductivity, are obtained using the available correlations (Appendix C.2).

iv) ENTRY RHOV2: This calculates the vapour density of the dispersed phase, using a procedure which is explained in Appendix B.

v) ENTRY VAPOUR: The vapour pressure of the dispersed phase and its derivative with time is obtained at this point.

vi) ENTRY DRAG: The drag coefficient is calculated here.

vii) ENTRY CONDIT: At this point, the operating conditions (atmospheric pressure, initial droplet size and initial temperature difference) are specified.

7.2.2 Program EXREZ1

This program was developed to process the experimental data concerning the evaporation of butane droplets in distilled water. The input data to the program are the experimental data, including frame number, height, vapour volume, droplet size, water temperature, etc. The input data also includes the coefficients of the polynomials which were fitted separately to the vapour volume versus time data. Data are processed within the program and the results of the process include time,

rise velocity, vaporisation ratio, diameter ratio, heat transfer coefficient, temperature difference, growth rate and bubble-droplet boundary acceleration. Rise velocities are obtained using a numerical differentiation method by calling subroutine DGT3. For the calculation of the growth rate and the boundary acceleration, differentiation is carried out using DGT3 and the equations of the fitted curves to the vapour volume versus time data. Polynomials of the fourth degree are fitted to the data of height versus time by calling subroutine EØ2ACF. These polynomials are used to determine the height at a required time.

The flow chart of this program is shown in Figure 7.2. Details of the subroutines which are used in EXREZ1 are as follows:

(a) Subroutine VEL1: In this subroutine, the data concerning the height measurement are read and then the main task is to calculate the velocity at any point by using DGT3. Subroutine EØ2ACF is called here for the fitting process.

(b) Subroutine HEAT1: The vapour volume data are read and some calculations concerning this parameter, such as the growth rate of vapour bubbles, are carried out. It also repeats the calculations at smaller time intervals (e.g. 0.01 seconds) by using the fitted curves.

(c) Subroutine CAL1: This subroutine is mainly used to calculate the parameters, such as diameter ratio, vaporisation ratio, heat transfer coefficient, growth rate, etc.

(d) Subroutine EØ2ACF: This is a NAG library program which is available in ICCC. Its task is to fit a polynomial of the specified degree to a set of data points.

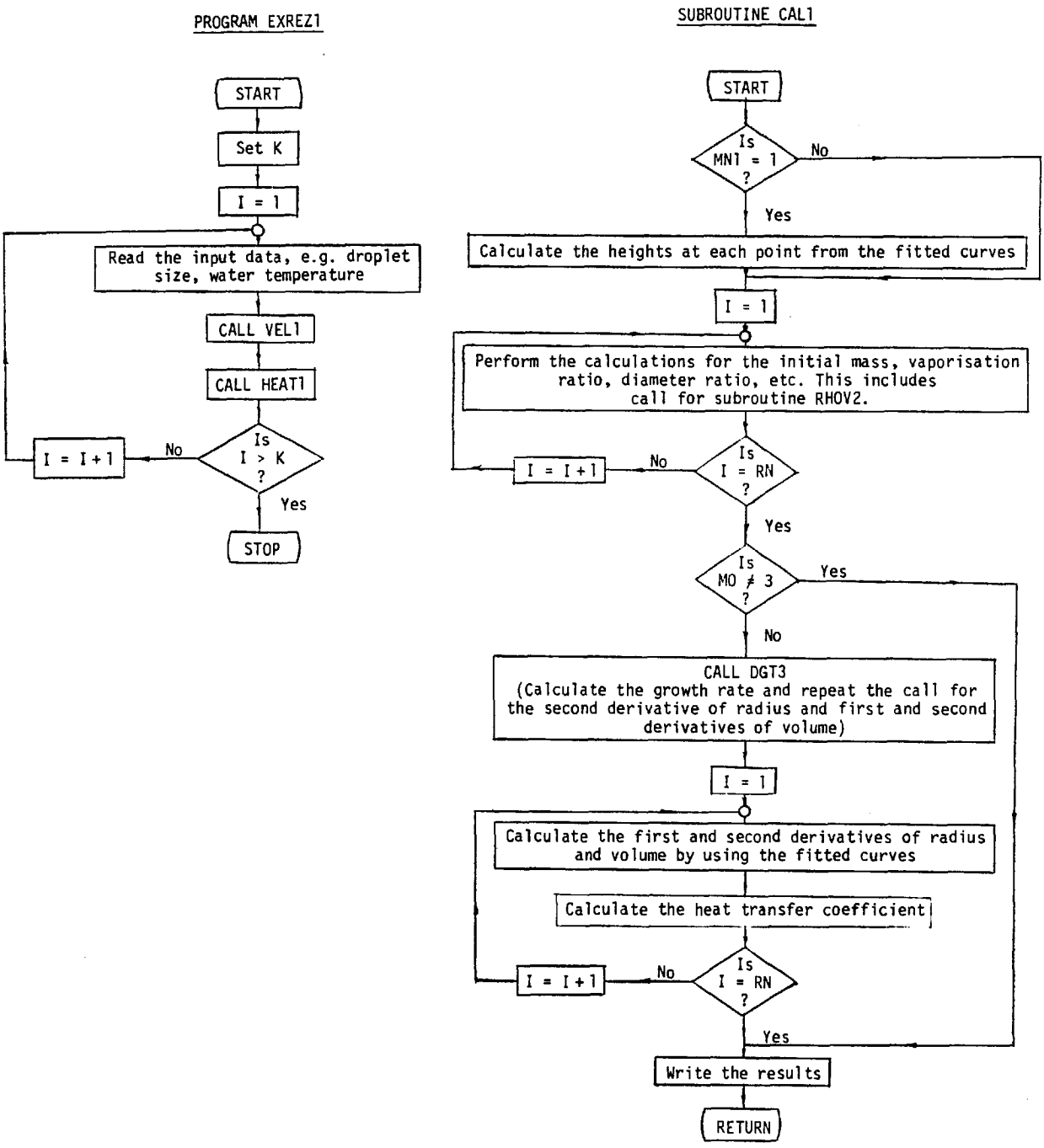

Figure 7.2: Flow chart of program EXREZ1

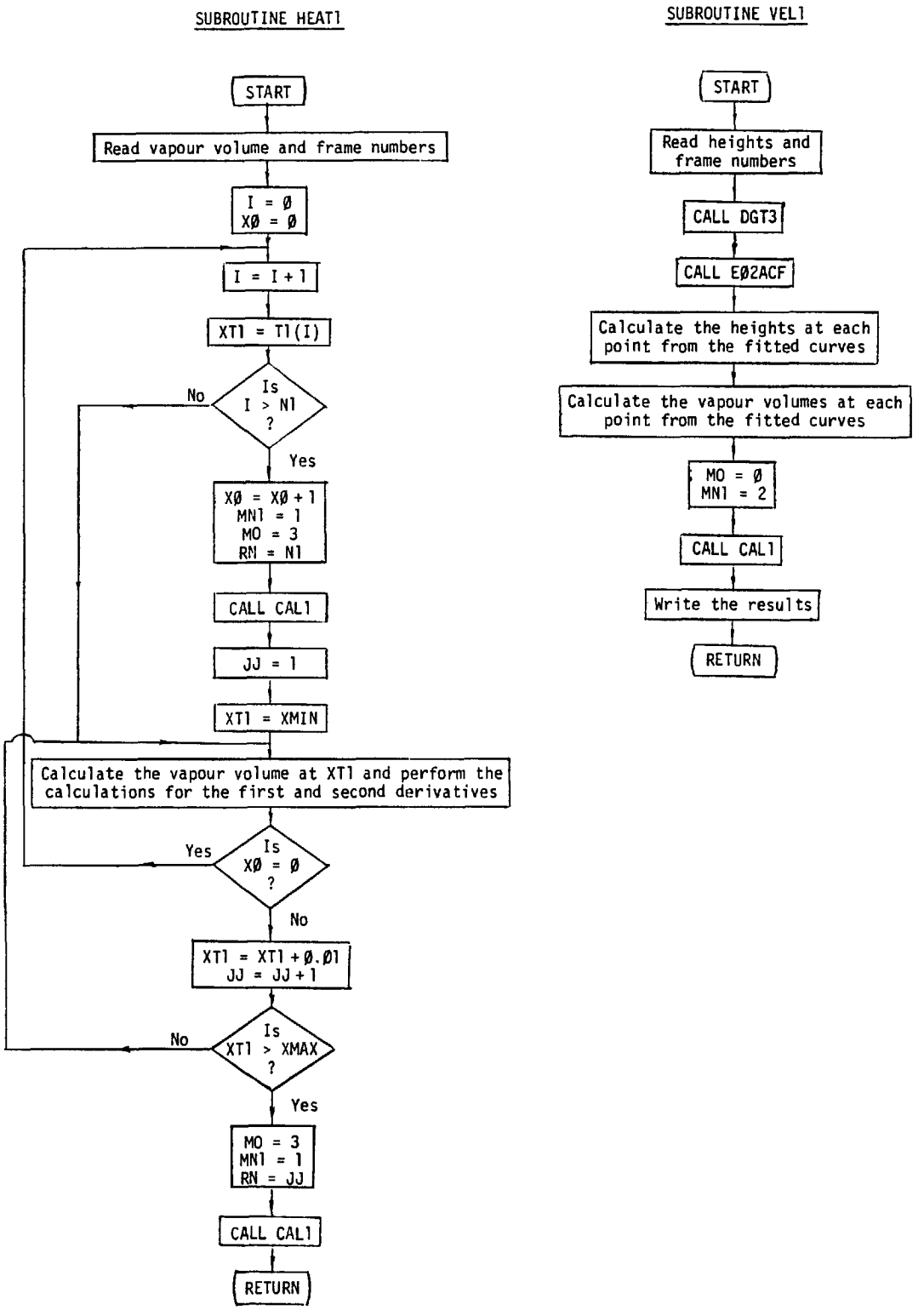

Figure 7.2: (continued)

(e) Subroutine DGT3: This subroutine carries out the numerical differentiation for a set of data points (Appendix E.1).

(f) Subroutine RHOV2: This subroutine is the same as ENTRY RHOV2 which was described in Section 7.2.1 (part b(iv)).

7.2.3 Program EXREZ2

EXREZ2 was developed to process the data of the stopped-evaporation droplets. It is basically similar to EXREZ1 but excludes the calculations of heat transfer coefficient and growth rate and those which were related to the fitted curves to the vapour volume data.

The flow chart of Program EXREZ2 is shown in Figure 7.3. Details of the subroutines which are called by EXREZ2 are as follows:

(a) Subroutine VEL2: The main task of VEL2 is to read the data of the height measurement and to calculate the velocities by using DGT3, and to fit polynomials to the data.

(b) Subroutine HEAT2: The data of vapour volume measurement are read and calculations on these values are carried out.

(c) Subroutine CAL2: Calculations for the determination of the vaporisation ratio and diameter ratio are done within this subroutine.

(d) Subroutine VAPOUR: This subroutine is similar to ENTRY VAPOUR, which was mentioned in Section 7.2.2 (part b(v)), but does not include the calculation for the first derivative of vapour pressure.

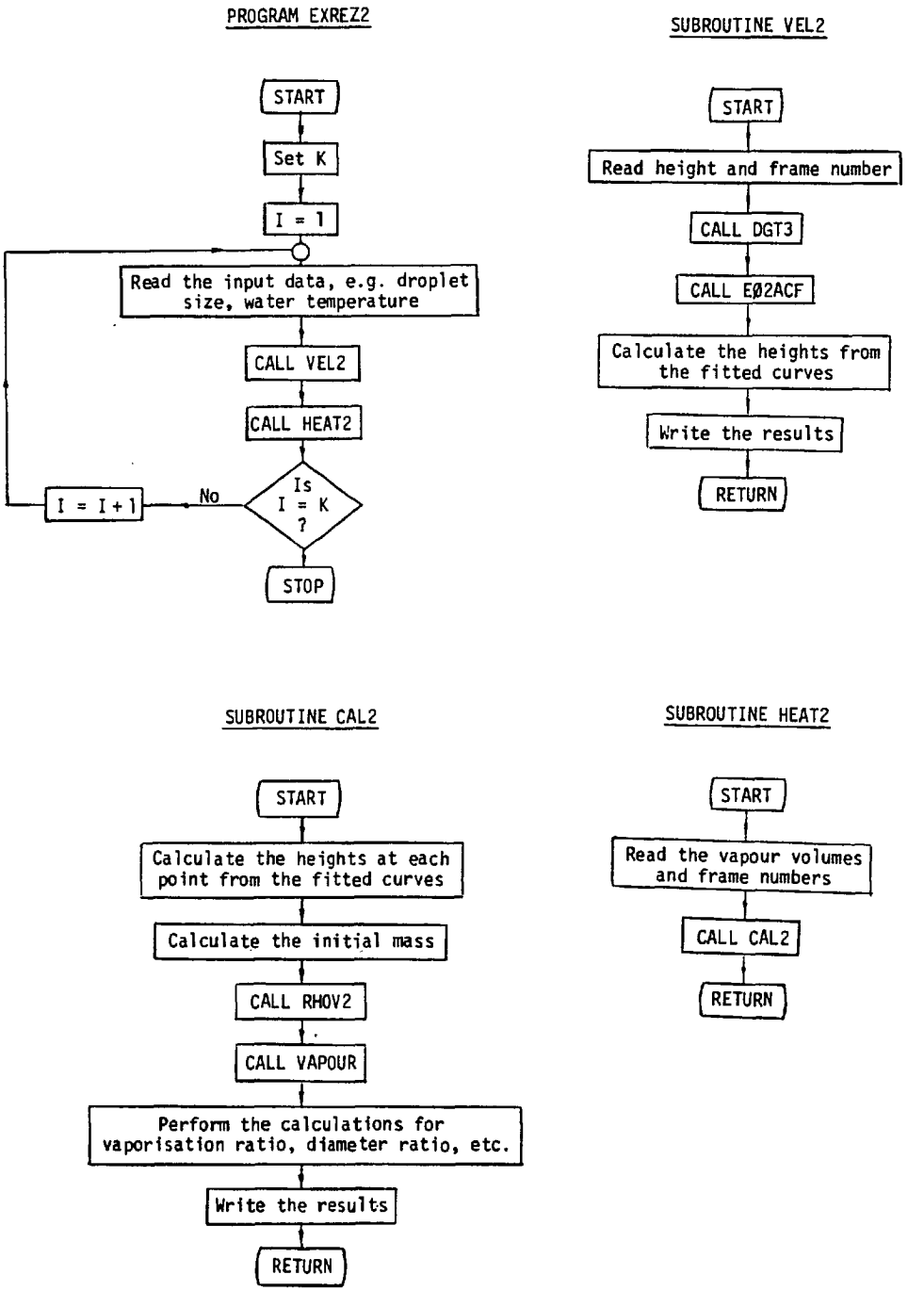

Figure 7.3: Flow chart of program EXREZ2

(e) Subroutines DGT3, RHOV2 and EØ2ACF: These subroutines are the same as the ones which were described in Section 7.2.2.

7.3 FLOW CHARTS

Flow charts of Programs TEREZ1, EXREZ1 and EXREZ2, and the related subroutines, are shown in Figures 7.1, 7.2 and 7.3, respectively.

The key to the flow charts is as follows:

K	:	the number of experimental runs under study
N1	:	the number of data points
N2	:	the number of steps for which the integration is required
MO,MN1	:	indicator
XMIN,XMAX	:	the extreme ends of calculation
T1	:	experimental time data
XT1	:	time

CHAPTER 8

CONCLUSIONS

The main objectives of the present work (section 1.3.1) within the existing limitations were achieved.

As for the theoretical study, a model of an evaporating droplet in an immiscible liquid was presented. This model predicted the variation of the bubble-droplet radius, height, rise velocity, temperature and pressure against time. Therefore, the total evaporation time and the distance taken for complete evaporation were obtained. In the range considered, the results showed that the initial velocity and initial temperature were not decisive factors. On the whole, good agreement was obtained between the theoretical prediction and the present experimental results.

The present experimental rig and the use of ciné photography provided the basic means necessary for the study.

The results obtained from the experimental study of evaporating butane droplets in water were within the range of the results of previous investigators. For the droplet sizes studied, the whole evaporation range was classified into four regions, in which the evaporating bubble-droplet behaved mainly as a spherical droplet, a spheroidal bubble-droplet, a large spheroidal bubble and a spherical cap bubble. The main features of the variation of rise velocity of the evaporating droplets were consistent with the results previously obtained on the butane/water combination (77), but lower velocities were obtained. A drop in velocity was usually observed around 1% evaporation and it coincided with the time of increased deformation and serious sloshing of the liquid at the bottom of the bubble-droplet system. After 1% evaporation, the rise velocity of

evaporating droplets was mainly lower than those of bubbles due to the weight of unevaporated liquid, growth and acceleration. Heat transfer coefficient results showed that it varied rapidly in the early stages of evaporation and then varied gradually. Lower heat transfer coefficients were obtained for higher temperature differences.

The evaporation of the butane droplets was slowed down considerably and a study of the resulting non-evaporating two-phase bubble-droplets, which is useful if the better understanding of the parameters involved, is believed to be a novel step in the subject. The general features of the variation of rise velocity of stopped-evaporation droplets (versus mass ratio up to 10% evaporation) were the same as those of evaporating droplets, and rise velocities of evaporating droplets at low temperature differences were not significantly different from those of stopped-evaporation droplets at the same diameter ratio.

The experimental procedure described in Chapter 6 was successful in recording the path of the bubbles and bubble-droplets, and other information, such as velocity, variation of size like growth and collapse, and indications of surface instabilities, was obtained.

APPENDIX A

TABLES OF THE EXPERIMENTAL DATA

TABLE A.1

Evaporating Butane Droplet in Distilled Water

Set 4 : Run 8

$d = 4.0 \times 10^{-3}$ (m); $T_c = 3.5$ (^{o}C); $\Delta T_o = 2.5$ (^{o}C);

ATMP = 101341.0 (N/m^2); $H = 0.90$ (m)

t' (s)	D/d*	ξ*	Z (m) $\times 10^{-3}$
0.4265	1.027	0.00038	82.3
0.5000	1.053	0.00079	95.5
0.5735	1.094	0.00146	111.5
0.6471	1.152	0.00250	128.0
0.7206	1.227	0.00402	145.0
0.8235	1.362	0.00723	169.0
0.9265	1.527	0.01211	192.0
1.0588	1.775	0.02172	222.0
1.1765	2.025	0.03447	249.5
1.3088	2.334	0.05508	280.0
1.4265	2.628	0.08051	307.5
1.5294	2.900	0.10957	332.0
1.6471	3.226	0.15220	361.0
1.7500	3.523	0.19929	387.5
1.8382	3.787	0.24817	409.5
1.9706	4.198	0.33859	445.0
2.0735	4.529	0.42534	474.0
2.1912	4.920	0.54495	507.0
2.3088	5.323	0.68946	542.0
2.3824	5.582	0.79399	565.0
2.4559	5.845	0.91067	587.5

t' (s)	D/d	ξ	V_v (m^3) $\times 10^{-9}$
0.3529	1.013	0.00016	1.167
0.4265	1.030	0.00042	2.979
0.5000	1.065	0.00098	6.953
0.6471	1.176	0.00297	21.220
0.7794	1.366	0.00736	52.740
0.9412	1.533	0.01231	88.510
1.0588	1.674	0.01743	125.570
1.1912	2.015	0.03387	244.680
1.7500	3.487	0.19305	1410.790
1.9706	3.996	0.29127	2139.140
2.0735	4.573	0.43788	3223.610
2.2059	5.471	0.75064	5543.910
2.3088	5.482	0.75344	5579.000
2.5000	6.026	0.99697	7419.800

* Calculated using the fitted curves to the vapour volume/time data

TABLE A.2

Evaporating Butane Droplet in Distilled Water

Set 4 : Run 10

$d = 4.1 \times 10^{-3}$ (m); $T_c = 3.5$ (^{o}C); $\Delta T_o = 2.5$ (^{o}C);

ATMP = 101341.0 (N/m^2); $H = 0.90$ (m)

t' (s)	D/d*	ξ*	Z (m) $\times 10^{-3}$
0.2059	1.013	0.00017	63.8
0.2794	1.030	0.00042	77.0
0.3529	1.056	0.00083	91.0
0.4265	1.092	0.00142	106.5
0.5000	1.140	0.00228	123.0
0.5735	1.201	0.00346	140.5
0.6471	1.275	0.00509	156.5
0.7206	1.363	0.00727	174.5
0.7941	1.466	0.01018	191.5
0.8971	1.632	0.01583	214.5
0.9853	1.795	0.02258	233.5
1.1324	2.105	0.03922	265.5
1.2500	2.385	0.05903	293.5
1.3676	2.690	0.08662	322.5
1.4412	2.894	0.10878	340.0
1.5882	3.328	0.16732	376.5
1.7500	3.844	0.25945	420.0
1.8529	4.193	0.33727	446.0
1.9853	4.663	0.46433	481.0
2.1029	5.101	0.60771	512.0
2.1765	5.384	0.71432	530.5

t' (s)	D/d	ξ	V_v (m^3) $\times 10^{-3}$
0.2059	1.012	0.00015	1.161
0.3529	1.050	0.00074	5.673
0.5000	1.146	0.00239	18.350
0.6471	1.303	0.00575	44.350
0.7794	1.530	0.01223	94.580
0.9853	1.723	0.01941	150.720
1.1324	2.068	0.03695	287.710
1.2500	2.299	0.05242	409.140
1.4265	2.929	0.11299	885.090
1.5441	3.257	0.15671	1230.570
1.7500	3.915	0.27444	2164.600
1.9853	4.631	0.45487	3606.600
2.1765	5.419	0.72815	5799.600
2.3382	5.978	0.97543	7800.900

* See footnote for Table A.1

TABLE A.3

Evaporating Butane Droplet in Distilled Water

Set 4 : Run 11

$d = 4.05 \times 10^{-3}$ (m); $T_c = 3.5$ (^{o}C); $\Delta T_o = 2.6$ (^{o}C);

ATMP = 101341.0 (N/m^2); $H = 0.90$ (m)

t' (s)	D/d*	ξ*	Z (m) $\times 10^{-3}$
0.3529	1.010	0.00013	68.0
0.4265	1.024	0.00033	82.0
0.5000	1.047	0.00069	96.0
0.5735	1.084	0.00129	110.0
0.6471	1.136	0.00221	126.5
0.7206	1.205	0.00355	143.0
0.8676	1.391	0.00802	176.5
1.0147	1.635	0.01594	214.5
1.0882	1.775	0.02168	233.5
1.2059	2.019	0.03408	261.5
1.3382	2.321	0.05404	290.5
1.4706	2.646	0.08217	321.5
1.5882	2.953	0.11582	350.4
1.7059	3.277	0.15948	379.0
1.7941	3.529	0.19998	402.0
1.9412	3.967	0.28517	438.5
2.0735	4.380	0.38424	471.5
2.2059	4.809	0.50856	507.5
2.2794	5.054	0.59021	527.5
2.3676	5.355	0.70133	554.0
2.4412	5.612	0.80602	576.5

t' (s)	D/d	ξ	V_v (m^3) $\times 10^{-3}$
0.3529	1.010	0.00013	0.967
0.4265	1.023	0.00032	2.371
0.5735	1.087	0.00134	9.841
0.6765	1.157	0.00260	19.217
0.8676	1.413	0.00862	63.830
1.0147	1.599	0.01461	108.510
1.3382	2.408	0.06095	455.730
1.5882	2.978	0.11884	893.190
1.7059	3.186	0.14622	1101.700
1.9412	3.933	0.27783	2104.000
2.0735	4.468	0.40825	3100.700
2.2059	4.822	0.51259	3904.900
2.3676	5.254	0.66194	5062.000
2.4559	5.764	0.87365	6695.700

* See footnote for Table A.1

TABLE A.4

Evaporating Butane Droplet in Distilled Water

Set 4 : Run 12

$d = 4.2 \times 10^{-3}$ (m); $T_e = 3.5$ (^{o}C); $\Delta T_o = 2.5$ (^{o}C);

ATMP = 101341.0 (N/m^2); $H = 0.90$ (m)

t' (s)	D/d^*	ξ^*	Z (m) $\times 10^{-3}$
0.4265	1.064	0.00096	90.2
0.7059	1.336	0.00658	154.0
0.8676	1.609	0.01499	191.0
0.9559	1.784	0.02211	211.0
1.0735	2.037	0.03521	235.5
1.2353	2.415	0.06162	275.0
1.3824	2.780	0.09617	310.5
1.5735	3.277	0.15973	359.0
1.7206	3.671	0.22573	397.5
1.8088	3.911	0.27344	423.0
1.9265	4.235	0.34752	456.5
2.0294	4.522	0.42283	488.0
2.1618	4.894	0.53528	528.0
2.2647	5.185	0.63559	560.5
2.3824	5.519	0.76473	600.0
2.5000	5.853	0.91015	640.0

t' (s)	D/d	ξ	V_v (m^3) $\times 10^{-9}$
0.2794	1.023	0.00032	2.592
0.3529	1.030	0.00043	3.426
0.4265	1.061	0.00092	7.380
0.7059	1.341	0.00669	54.010
0.8529	1.538	0.01249	101.180
1.0588	2.153	0.04244	345.170
1.2206	2.398	0.06021	491.240
1.5294	3.057	0.12903	1059.600
1.9118	4.110	0.31729	2628.800
2.0294	4.713	0.47941	3983.800
2.3971	5.523	0.76633	6433.500
2.5147	5.899	0.93154	7849.200

* See footnote for Table A.1

TABLE A.5

Evaporating Butane Droplet in Distilled Water

Set 5 : Run 15

$d = 3.9 \times 10^{-3}$ (m); $T_c = 5.6$ (^{o}C); $\Delta T_o = 4.5$ (^{o}C);

ATMP = 101221.0 (N/m^2); $H = 0.90$ (m)

t' (s)	D/d^*	ξ^*	Z (m) $\times 10^{-3}$
0.3529	1.024	0.00034	67.5
0.4265	1.091	0.00141	81.2
0.5000	1.190	0.00325	97.0
0.5735	1.314	0.00602	114.0
0.6471	1.461	0.01008	131.5
0.7206	1.633	0.01593	149.0
0.7941	1.828	0.02422	165.5
0.8971	2.136	0.04142	188.5
1.0147	2.532	0.07196	215.0
1.0882	2.798	0.09868	232.5
1.1912	3.191	0.14837	258.0
1.3382	3.785	0.24983	293.0
1.4118	4.092	0.31640	314.0
1.5147	4.530	0.43018	341.0
1.6029	4.913	0.54872	364.0
1.7206	5.428	0.73981	397.0

t' (s)	D/d	ξ	V_v (m^3) $\times 10^{-9}$
0.3529	1.024	0.00034	2.183
0.4265	1.091	0.00142	9.111
0.5735	1.317	0.00611	39.390
0.7941	1.781	0.02206	142.800
0.9412	2.423	0.06255	406.100
1.1912	3.109	0.13681	892.600
1.3971	4.192	0.34063	2232.000
1.6765	4.975	0.56897	3752.000
1.7941	6.072	1.03552	6849.000

* See footnote for Table A.1

TABLE A.6

Evaporating Butane Droplet in Distilled Water

Set 5 : Run 16

$d = 3.85 \times 10^{-3}$ (m); $T_c = 5.8$ (^{o}C); $\Delta T_o = 4.6$ (^{o}C);

ATMP = 101281.0 (N/m^2); $H = 0.90$ (m)

t' (s)	D/d*	ξ*	Z (m) $\times 10^{-3}$
0.2059	1.012	0.00016	36.5
0.2794	1.049	0.00072	50.7
0.3529	1.127	0.00205	65.0
0.4265	1.251	0.00456	81.5
0.5147	1.449	0.00973	101.0
0.5882	1.644	0.01641	116.5
0.6912	1.948	0.03039	140.0
0.8088	2.322	0.05467	165.5
0.9559	2.813	0.10070	199.5
1.0882	3.270	0.16035	230.0
1.2059	3.681	0.23033	260.0
1.3235	4.096	0.31832	289.0
1.4559	4.564	0.44095	321.0
1.7794	5.698	0.85524	419.5
1.8676	6.002	0.99772	447.5

t' (s)	D/d	ξ	V_v (m^3) $\times 10^{-9}$
0.2059	1.011	0.00015	0.920
0.2794	1.065	0.00098	6.102
0.3529	1.142	0.00232	14.440
0.4265	1.239	0.00429	26.720
0.5735	1.543	0.01273	79.510
0.6912	1.886	0.02714	169.840
0.8235	2.304	0.05334	334.590
0.9559	2.937	0.11524	724.780
1.0882	3.452	0.18962	1195.700
1.2206	3.929	0.28103	1777.000
1.8088	5.675	0.84423	5414.000
1.8824	6.044	1.01847	6545.000

* See footnote for Table A.1

TABLE A.7

Evaporating Butane Droplet in Distilled Water

Set 5 : Run 25

$d = 3.9 \times 10^{-3}$ (m); $T_c = 5.2$ (^{o}C); $\Delta T_o = 4.0$ (^{o}C);

ATMP = 102281.0 (N/m^2); $H = 0.90$ (m)

t' (s)	D/d^*	ξ^*	Z (m) $\times 10^{-3}$
0.4265	1.050	0.00073	94.0
0.5000	1.088	0.00137	107.8
0.5735	1.137	0.00223	123.0
0.9559	1.570	0.01368	211.0
1.1029	1.878	0.02674	243.0
1.2647	2.333	0.05550	281.5
1.3529	2.631	0.08144	304.0
1.4559	3.017	0.12506	328.0
1.5588	3.443	0.18777	354.0
1.6912	4.044	0.30621	388.0
1.7941	4.549	0.43681	417.0
1.9118	5.165	0.63950	449.5
1.9706	5.487	0.76657	467.0
2.0588	5.987	0.99514	495.0

t' (s)	D/d	ξ	V_v (m^3) $\times 10^{-9}$
0.3529	1.022	0.00030	1.945
0.5000	1.089	0.00139	8.984
0.6471	1.186	0.00319	20.770
0.7941	1.349	0.00694	45.260
0.9559	1.592	0.01446	94.550
1.2647	2.232	0.04797	315.540
1.4412	2.989	0.12145	801.870
1.5588	3.450	0.18877	1249.700
1.6912	4.301	0.36924	2452.000
1.7941	4.879	0.53973	3592.800
1.9706	5.307	0.69301	4632.400
2.0588	5.836	0.92115	6170.000

* See footnote for Table A.1

TABLE A.8

Evaporating Butane Droplet in Distilled Water

Set 5 : Run 26

$d = 4.0 \times 10^{-3}$ (m); $T_c = 5.4$ (^{o}C); $\Delta T_o = 4.0$ (^{o}C);

ATMP = 102281.0 (N/m^2); $H = 0.90$ (m)

t' (s)	D/d*	ξ*	Z (m) $\times 10^{-3}$
0.2794	1.058	0.00086	84.8
0.3529	1.120	0.00194	99.0
0.4265	1.182	0.00312	115.0
0.5000	1.244	0.00443	132.0
0.5735	1.315	0.00609	150.0
0.6471	1.405	0.00848	168.5
0.7206	1.525	0.01215	187.5
0.7941	1.678	0.01775	205.0
0.9706	2.165	0.04349	245.0
1.0588	2.455	0.06550	264.5
1.2500	3.141	0.14184	311.0
1.4559	3.914	0.27778	362.0
1.5735	4.354	0.38307	392.0
1.7059	4.835	0.52482	427.0

t' (s)	D/d	ξ	V_v (m^3) $\times 10^{-9}$
0.1324	1.012	0.00016	1.096
0.2794	1.057	0.00086	6.000
0.4265	1.185	0.00317	22.210
0.5735	1.313	0.00604	42.390
0.7206	1.518	0.01192	83.940
0.9853	2.228	0.04781	338.380
1.1176	2.714	0.09012	639.600
1.3382	3.369	0.17591	1254.200
1.4853	4.071	0.31287	2237.500
1.7059	4.822	0.52068	3740.500
1.9265	5.604	0.81639	5891.100

* See footnote for Table A.1

TABLE A.9

Evaporating Butane Droplet in Distilled Water

Set 5 : Run 28

$d = 4.2 \times 10^{-3}$ (m); $T_e = 5.4$ (^{o}C); $\Delta T_o = 4.0$ (^{o}C);

ATMP = 102281.0 (N/m^2); $H = 0.90$ (m)

t' (s)	D/d^*	ξ^*	Z (m) $\times 10^{-3}$
0.1324	1.043	0.00064	63.0
0.2059	1.087	0.00135	76.0
0.2794	1.134	0.00219	91.0
0.3529	1.186	0.00320	108.0
0.4265	1.250	0.00457	125.5
0.5000	1.335	0.00660	143.5
0.5735	1.447	0.00970	161.0
0.7059	1.722	0.01962	190.5
0.8088	1.994	0.03302	214.0
0.8971	2.257	0.04995	234.0
1.0441	2.737	0.09260	269.5
1.1618	3.146	0.14272	299.0
1.2794	3.567	0.20974	327.5
1.3824	3.941	0.28382	354.0
1.5000	4.369	0.38747	385.5
1.6176	4.795	0.51220	417.0
1.7647	5.316	0.69737	460.5
1.8529	5.621	0.82337	486.0

t' (s)	D/d	ξ	V_v (m^3) $\times 10^{-9}$
0.0588	1.011	0.00014	1.085
0.1324	1.049	0.00073	5.770
0.2059	1.087	0.00136	10.810
0.2794	1.125	0.00203	16.190
0.4265	1.254	0.00465	37.180
0.5735	1.426	0.00909	72.860
0.7794	2.044	0.03599	289.670
1.0441	2.839	0.10392	841.000
1.1618	3.040	0.12836	1041.300
1.2794	3.416	0.18351	1492.400
1.3824	3.988	0.29422	2398.000
1.5000	4.279	0.36358	2971.000
1.6176	4.943	0.56166	4601.800
1.8529	5.701	0.85932	7081.000

* See footnote for Table A.1

TABLE A.10

Evaporating Butane Droplet in Distilled Water

Set 7 : Run 15

$d = 3.9 \times 10^{-3}$ (m); $T_c = 11.6$ (^{o}C); $\Delta T_o = 10.0$ (^{o}C);

ATMP = 101408.0 (N/m^2); $H = 0.90$ (m)

t' (s)	D/d*	ξ*	Z (m) $\times 10^{-3}$
0.1406	1.450	0.00983	28.5
0.2188	1.992	0.03316	43.0
0.2969	2.622	0.08163	60.0
0.4531	3.832	0.26426	96.0
0.6094	4.823	0.53016	135.0
0.7656	5.543	0.80374	180.5

t' (s)	D/d	ξ	V_v (m^3) $\times 10^{-9}$
0.0625	1.056	0.00084	5.467
0.1094	1.279	0.00524	34.220
0.1406	1.449	0.00980	63.970
0.1719	1.663	0.01729	112.930
0.2031	1.915	0.02894	189.070
0.2656	2.321	0.05518	360.870
0.4063	3.422	0.18711	1227.000
0.5156	4.156	0.33799	2222.000
0.6875	5.554	0.81017	5349.000
0.8594	6.107	1.07361	7120.200
1.0000	5.881	0.95474	6355.000

* See footnote for Table A.1

TABLE A.11

Evaporating Butane Droplet in Distilled Water

Set 7 : Run 32

$d = 4.05 \times 10^{-3}$ (m); $T_c = 6.9$ (^{o}C); $\Delta T_o = 5.2$ (^{o}C);

ATMP = 103194.0 (N/m^2); $H = 0.90$ (m)

t' (s)	D/d*	ξ*	Z (m) $\times 10^{-3}$
0.2188	1.107	0.00172	58.0
0.2969	1.215	0.00384	74.2
0.3750	1.366	0.00749	91.5
0.4531	1.555	0.01336	110.5
0.5313	1.775	0.02222	129.5
0.6094	2.019	0.03492	148.3
0.7656	2.553	0.07536	187.0
0.8906	3.008	0.12602	216.5
1.0459	3.593	0.21739	253.5
1.5156	5.314	0.70660	384.5

t' (s)	D/d	ξ	V_v (m^3) $\times 10^{-9}$
0.0625	1.009	0.00011	0.777
0.1406	1.035	0.00051	3.651
0.2188	1.136	0.00224	16.230
0.2969	1.257	0.00477	34.550
0.4531	1.533	0.01259	91.390
0.5781	1.854	0.02595	188.870
0.7969	2.562	0.07617	556.830
0.8906	3.039	0.13007	952.640
1.0313	3.561	0.21154	1554.000
1.2031	4.597	0.45918	3386.000
1.5313	5.691	0.86854	6454.500
1.7031	5.682	0.86042	6422.500

* See footnote for Table A.1

TABLE A.12

Evaporating Butane Droplet in Distilled Water

Set 7 : Run 34

$d = 4.1 \times 10^{-3}$ (m); $T_e = 4.6$ (^{o}C); $\Delta T_o = 2.4$ (^{o}C);

ATMP = 101515.0 (N/m^2); $H = 1.3$ (m)

t' (s)	D/d^*	ξ^*	Z (m) $\times 10^{-3}$
0.3750	1.041	0.00060	91.5
0.4531	1.067	0.00104	106.8
0.5313	1.104	0.00169	123.5
0.6094	1.151	0.00257	141.0
1.4688	2.290	0.05343	335.0
1.5469	2.472	0.06838	355.0
1.7031	2.883	0.11092	391.0
1.8594	3.352	0.17660	429.0
2.0156	3.876	0.27481	469.0

t' (s)	D/d	ξ	V_v (m^3) $\times 10^{-9}$
0.1250	1.009	0.00010	0.760
0.1719	1.012	0.00016	1.155
0.2188	1.016	0.00022	1.590
0.2969	1.023	0.00033	2.370
0.3750	1.042	0.00063	4.580
0.4531	1.072	0.00113	8.220
0.5313	1.100	0.00161	11.800
0.6094	1.146	0.00247	18.080
1.4531	2.312	0.05512	409.890
1.5313	2.416	0.06346	472.630
1.7656	2.995	0.12474	933.360
1.9063	3.531	0.20702	1553.350
2.0313	3.953	0.29168	2194.080

* See footnote for Table A.1

TABLE A.13

Evaporating Butane Droplet in Distilled Water

Set 10 : Run 4

$d = 3.5 \times 10^{-3}$ (m); $T_c = 5.2$ (^{o}C); $\Delta T_0 = 2.8$ (^{o}C):

ATMP = 102341.0 (N/m^2); $H = 1.37$ (m)

t' (s)	D/d*	ξ*	Z (m) $\times 10^{-3}$
0.6094	1.427	0.00950	125.0
0.6875	1.551	0.01362	142.0
0.7656	1.679	0.01860	160.0
0.9219	1.955	0.03213	197.3
1.0781	2.271	0.05303	230.5
1.2344	2.636	0.08557	268.3
1.3906	3.055	0.13547	308.5
1.5469	3.524	0.20994	344.5
1.7031	4.038	0.31738	384.0
1.8594	4.593	0.46764	425.0
2.0313	5.244	0.69564	473.0
2.1719	5.805	0.94233	513.0

t' (s)	D/d	ξ	V_v (m^3) $\times 10^{-9}$
0.2344	1.010	0.00012	0.550
0.3750	1.094	0.00152	6.860
0.4531	1.169	0.00296	13.350
0.6094	1.444	0.01002	45.320
0.7188	1.598	0.01535	69.550
0.9063	2.027	0.03638	165.400
1.0625	2.386	0.06238	284.440
1.2031	2.609	0.08282	378.630
1.3594	2.601	0.08180	375.120
1.5000	3.514	0.20833	958.020
1.6250	3.990	0.30654	1413.240
1.7031	4.626	0.47961	2214.840
1.8281	4.580	0.46400	2148.500
1.9375	5.230	0.69158	3210.100
2.0469	5.666	0.87840	4087.440
2.1406	5.460	0.78401	3656.260
2.2813	5.955	1.01514	4750.200

* See footnote for Table A.1

TABLE A.14

Evaporating Butane Droplet in Distilled Water

Set 10 : Run 8

$d = 4.0 \times 10^{-3}$ (m); $T_c = 4.5$ (^{o}C); $\Delta T_o = 2.3$ (^{o}C);

ATMP = 101988.0 (N/m^2); $H = 1.37$ (m)

t' (s)	D/d^*	ξ^*	Z (m) $\times 10^{-3}$
0.4531	1.023	0.00032	90.5
0.5313	1.035	0.00052	105.3
0.6094	1.058	0.00088	121.5
0.6875	1.093	0.00150	139.0
0.7656	1.143	0.00243	157.5
0.9219	1.281	0.00543	193.5
1.0781	1.457	0.01033	231.5
1.2344	1.660	0.01757	267.0
1.3906	1.881	0.02775	301.5
1.5469	2.119	0.04170	337.5
1.7031	2.376	0.06061	376.5
1.8594	2.654	0.08607	416.5
2.0156	2.955	0.12023	459.0
2.1719	3.281	0.16590	499.0
2.3281	3.635	0.22649	543.0
2.4844	4.017	0.30635	586.0
2.6406	4.429	0.41051	633.0
2.8281	4.962	0.57644	688.0

t' (s)	D/d	ξ	V_v (m^3) $\times 10^{-9}$
0.3906	1.017	0.00023	1.561
0.4531	1.024	0.00035	2.363
0.5313	1.031	0.00045	3.090
0.6094	1.063	0.00097	6.612
0.7656	1.151	0.00257	17.640
0.9375	1.303	0.00598	41.140
1.0781	1.461	0.01043	71.950
1.3594	1.749	0.02135	148.010
1.4688	2.035	0.03641	252.980
1.6719	2.370	0.06011	419.380
1.8594	2.675	0.08830	618.400
2.0469	3.071	0.13551	952.800
2.1250	3.242	0.16002	1127.070
2.2500	3.341	0.17505	1236.300
2.4688	4.089	0.32336	2295.240
2.6406	4.408	0.40461	2883.800
2.8750	5.047	0.60617	4346.000

* See footnote for Table A.1

TABLE A.15

Evaporating Butane Droplet in Distilled Water

Set 11 : Run 1

$d = 3.95 \times 10^{-3}$ (m); $T_c = 4.6$ (^{o}C); $\Delta T_o = 2.6$ (^{o}C);

ATMP = 100868.0 (N/m^2); $H = 1.37$ (m)

t' (s)	D/d^*	ξ^*	Z (m) $\times 10^{-3}$
0.2969	1.027	0.00038	58.5
0.3750	1.059	0.00090	75.3
0.4531	1.101	0.00164	92.2
0.5313	1.154	0.00262	109.5
0.6094	1.218	0.00397	127.5
0.6875	1.297	0.00580	146.0
0.7656	1.391	0.00830	163.0
0.9219	1.626	0.01619	198.5
1.0781	1.917	0.02956	235.5
1.2344	2.249	0.05057	271.5
1.3906	2.607	0.08130	309.0
1.5469	2.982	0.12366	346.0
1.7031	3.363	0.17906	386.0
1.8594	3.746	0.24827	430.5
2.0156	4.123	0.33143	472.0
2.1719	4.488	0.42745	515.0
2.3281	4.836	0.53430	555.5
2.4844	5.162	0.64825	599.0
2.6406	5.458	0.76397	648.0

t' (s)	D/d	ξ	V_v (m^3) $\times 10^{-9}$
0.2969	1.027	0.00039	2.500
0.3750	1.056	0.00085	5.490
0.5313	1.166	0.00286	18.470
0.6875	1.305	0.00600	38.790
0.8438	1.452	0.01009	65.480
1.0000	1.821	0.02469	160.640
1.1563	2.098	0.04021	262.390
1.3125	2.416	0.06385	417.920
1.5156	2.911	0.11485	754.880
1.7031	3.560	0.21310	1406.130
1.9688	3.803	0.25939	1721.400
2.0625	4.282	0.37151	2470.660
2.5156	5.289	0.69719	4686.400

* See footnote for Table A.1

TABLE A.16

Evaporating Butane Droplet in Distilled Water

Set 11 : Run 3

$d = 3.6 \times 10^{-3}$ (m); $T_c = 3.7$ (^{o}C); $\Delta T_0 = 1.9$ (^{o}C);

ATMP = 100061.0 (N/m^2); $H = 1.37$ (m)

t' (s)	D/d^*	ξ^*	Z (m) $\times 10^{-3}$
0.3750	1.056	0.00085	67.5
1.0000	1.525	0.01237	208.0
1.0781	1.618	0.01573	225.5
1.2344	1.826	0.02465	259.5
1.3906	2.059	0.03737	293.5
1.5469	2.316	0.05503	329.5
1.7031	2.591	0.07884	365.0
1.8594	2.882	0.10996	401.5
2.0156	3.184	0.14943	440.5
2.1719	3.493	0.19815	481.5
2.3281	3.806	0.25682	523.0
2.5156	4.182	0.34082	574.5
2.6406	4.431	0.40504	610.0
2.8281	4.798	0.51284	670.0

t' (s)	D/d	ξ	V_v (m^3) $\times 10^{-9}$
0.3750	1.056	0.00085	4.170
0.5313	1.107	0.00173	8.480
0.6875	1.216	0.00388	19.130
0.8438	1.382	0.00798	39.410
1.0000	1.500	0.01154	57.180
1.1250	1.633	0.01627	80.800
1.2344	1.918	0.02938	146.200
1.3438	2.011	0.03451	172.100
1.5625	2.311	0.05466	273.700
1.7656	2.659	0.08548	429.700
1.8750	2.963	0.11984	603.700
1.9844	3.207	0.15291	772.000
2.3281	3.725	0.24056	1223.400
2.6250	4.346	0.38218	1957.600
2.7344	4.697	0.48216	2477.000
2.9219	4.983	0.57351	2962.700

* See footnote for Table A.1

TABLE A.17

Evaporating Butane Droplet in Distilled Water

Set 11 : Run 5

$d = 3.8 \times 10^{-3}$ (m); $T_c = 4.6$ (^{o}C); $\Delta T_o = 2.8$ (^{o}C);

ATMP = 100061.0 (N/m^2); $H = 1.37$ (m)

t' (s)	D/d*	ξ*	Z (m) $\times 10^{-3}$
0.2969	1.024	0.00033	60.5
0.3750	1.061	0.00093	77.5
0.4531	1.112	0.00182	94.5
0.5313	1.172	0.00297	108.5
0.6094	1.241	0.00444	125.5
0.7656	1.411	0.00882	158.3
0.9219	1.638	0.01655	192.5
1.0781	1.926	0.02984	228.0
1.2344	2.262	0.05126	262.5
1.3906	2.633	0.08343	300.5
1.5469	3.027	0.12877	338.0
1.7031	3.431	0.18917	378.5
1.8594	3.838	0.26577	421.0
2.0156	4.240	0.35866	465.0
2.4844	5.346	0.71494	611.0
2.6406	5.657	0.84439	661.5

t' (s)	D/d	ξ	V_v (m^3) $\times 10^{-9}$
0.2188	1.011	0.00014	0.827
0.2969	1.026	0.00038	2.204
0.3750	1.052	0.00078	4.587
0.4531	1.114	0.00187	10.950
0.6094	1.265	0.00501	29.480
0.7969	1.485	0.01111	65.620
0.9219	1.664	0.01758	104.040
1.1563	1.977	0.03264	194.080
1.4844	2.804	0.10150	607.280
1.5781	3.178	0.14968	897.230
2.0938	4.502	0.42959	2605.000
2.1875	4.904	0.55534	3375.600
2.6406	5.788	0.90396	5569.000
2.7969	5.953	0.97817	6060.000
2.9219	5.920	0.95741	5960.800

* See footnote for Table A.1

TABLE A.18

Evaporating Butane Droplet in Distilled Water

Set 11 : Run 12

$d = 3.6 \times 10^{-3}$ (m); $T_c = 4.2$ (^{o}C); $\Delta T_o = 2.2$ (^{o}C);

ATMP = 101649.0 (N/m^2); $H = 1.37$ (m)

t' (s)	D/d^*	ξ^*	Z (m) $\times 10^{-3}$
0.2969	1.010	0.00012	54.4
0.3750	1.012	0.00015	66.5
0.4531	1.014	0.00019	79.5
0.5313	1.020	0.00027	93.0
0.6094	1.029	0.00042	107.0
0.6875	1.044	0.00065	122.0
0.7656	1.064	0.00099	137.5
0.9219	1.124	0.00205	168.3
1.0781	1.211	0.00380	201.7
1.2344	1.328	0.00658	238.0
1.3906	1.477	0.01088	276.0
1.5469	1.660	0.01748	315.0
1.7031	1.879	0.02748	352.0
1.8594	2.134	0.04237	389.3
2.0156	2.423	0.06411	427.0
2.1719	2.745	0.09517	464.0
2.3281	3.099	0.13860	502.5
2.4688	3.443	0.19127	540.0
2.6406	3.895	0.27798	585.5
2.7813	4.289	0.37157	624.5

t' (s)	D/d	ξ	V_v (m^3) $\times 10^{-9}$
0.3750	1.012	0.00015	0.709
0.5313	1.020	0.00027	1.326
0.6875	1.046	0.00069	3.337
0.8438	1.081	0.00127	6.193
1.0000	1.189	0.00334	16.303
1.1563	1.260	0.00491	24.020
1.3125	1.396	0.00842	41.360
1.4688	1.583	0.01451	71.480
1.7031	1.854	0.02622	129.720
1.9531	2.353	0.05835	290.150
2.1563	2.659	0.08604	429.640
2.3438	3.052	0.13205	661.900
2.4375	3.590	0.21754	1092.560
2.7500	4.167	0.34081	1722.780
2.9844	4.763	0.50867	2583.760
3.1719	5.561	0.80956	4128.000
3.2969	6.026	1.02847	5257.700

*

TABLE A.19

Stopped-Evaporation Butane Droplet in Distilled Water

Set 8 : Run 7

$d = 4.15 \times 10^{-3}$ (m); $T_c = 5.3$ (^{o}C)

ATMP = 101515.0 (N/m^2); $H = 1.3$ (m)

t' (s)	Z (m) $\times 10^{-3}$
0.0	3.5
0.0625	10.7
0.1406	26.0
0.2188	42.7
0.2969	60.0
0.3750	76.0
0.4531	92.0
0.5313	111.8
0.6094	130.0
0.6875	147.0
0.7656	164.5
0.8438	182.0
0.9219	200.0
1.0000	217.3
1.0781	233.8
1.2344	267.5
1.3906	303.5
1.5469	337.0
1.7031	371.5
1.8594	407.5
2.0156	445.0
2.1719	479.2

t' (s)	D/d	ξ	V_v (m^3) $\times 10^{-9}$
1.3906	1.719	0.02218	151.950
1.5469	1.861	0.02962	202.900
1.7188	1.904	0.03215	220.200
1.8594	1.938	0.03419	234.200
2.0000	1.911	0.03256	223.000
2.1719	1.954	0.03517	240.900

TABLE A.20

Stopped-Evaporation Butane Droplet in Distilled Water

Set 8 : Run 17

$d = 4.0 \times 10^{-3}$ (m); $T_c = 5.4$ (^{o}C);

ATMP = 101861.0 (N/m^2); $H = 1.3$ (m)

t' (s)	Z (m) $\times 10^{-3}$
0.0	4.0
0.0625	11.2
0.1406	25.0
0.2188	40.0
0.2969	52.8
0.3750	65.5
0.4531	78.3
0.5313	92.0
0.6094	105.5
0.6875	119.7
0.7656	134.0
0.9219	162.0
1.0781	190.5
1.2344	219.0
1.3906	248.5
1.5469	277.5
1.7031	307.0
1.8594	336.3
2.0156	366.5
2.1719	395.5
2.3281	424.0
2.4844	453.0
2.6406	485.5
2.7969	517.5
2.9531	550.5
3.1094	583.0
3.2656	616.0

t' (s)	D/d	ξ	V_v (m^3) $\times 10^{-9}$
1.2344	1.015	0.00020	1.210
1.5469	1.020	0.00029	1.750
1.8594	1.034	0.00052	3.166
2.1719	1.046	0.00073	4.480
2.4844	1.054	0.00089	5.420
2.7969	1.082	0.00141	8.630
3.1094	1.104	0.00184	11.290

TABLE A.21

Stopped-Evaporation Butane Droplet in Distilled Water

Set 9 : Run 6

$d = 4.1 \times 10^{-3}$ (m); $T_c = 4.4$ (^{o}C);

ATMP = 102614.0 (N/m^2); $H = 1.37$ (m)

t' (s)	Z (m) $\times 10^{-3}$
0.0	12.3
0.0625	24.7
0.1406	42.2
0.2188	58.3
0.2969	73.7
0.3750	88.7
0.4531	104.5
0.5313	121.0
0.9531	217.5
1.0781	247.5
1.2344	283.5
1.3438	311.0
1.4688	341.5
1.6563	388.5
1.8438	437.0
2.0469	490.0
2.1875	528.5
2.3125	560.0
2.4688	602.5
2.6250	644.5
2.7813	691.0
2.9531	740.0
3.0781	774.0

t' (s)	D/d	ξ	V_v (m^3) $\times 10^{-9}$
1.5469	2.407	0.06843	470.260
1.8438	2.510	0.07826	537.800
2.5313	2.618	0.08955	615.400
2.7656	2.755	0.10524	723.200
2.9531	2.698	0.09851	677.000

TABLE A.22

Stopped-Evaporation Butane Droplet in Distilled Water

Set 9 : Run 7

$d = 4.2 \times 10^{-3}$ (m); $T_c = 4.8$ (^{o}C);

ATMP = 102614.0 (N/m^2); $H = 1.37$ (m)

t' (s)	Z (m) $\times 10^{-3}$
0.0	2.9
0.0625	10.9
0.1406	27.0
0.2188	44.3
0.2969	60.3
0.3750	76.3
0.4531	93.0
0.5938	122.5
0.6875	144.0
0.9219	195.3
1.0781	229.7
1.1719	251.0
1.2656	270.8
1.3750	295.0
1.5000	322.5
1.6563	359.2
1.7656	382.2
1.9219	419.7
2.0781	455.4
2.2344	492.4
2.3438	518.0
2.5000	555.0
2.6406	590.0

t' (s)	D/d	ξ	V_v (m^3) $\times 10^{-9}$
1.2656	1.182	0.00345	24.710
1.5000	1.193	0.00369	26.430
1.7656	1.239	0.00480	34.410
2.0718	1.275	0.00572	40.980
2.3438	1.354	0.00791	56.640
2.6406	1.442	0.01067	76.460

TABLE A.23

Stopped-Evaporation Butane Droplet in Distilled Water

Set 10 : Run 6

$d = 4.0 \times 10^{-3}$ (m); $T_c = 4.0$ (^{o}C);

ATMP = 101988.0 (N/m^2); $H = 1.37$ (m)

t' (s)	Z (m) $\times 10^{-3}$
0.0	3.7
0.0625	12.9
0.1406	28.9
0.2188	46.3
0.2969	60.2
0.3750	75.0
0.4531	90.5
0.5313	106.5
0.6094	122.5
0.6875	138.5
0.7656	154.1
0.9219	186.5
1.0781	219.0
1.2344	250.2
1.3906	282.0
1.5469	314.9
1.7031	346.5
1.8594	378.5
2.0156	409.0
2.1719	436.5
2.3281	468.0
2.4844	502.5
2.6406	539.4
2.7969	574.5
2.9531	610.4
3.1094	645.3
3.2656	682.0

t' (s)	D/d	ξ	V_v (m^3) $\times 10^{-9}$
1.2344	1.041	0.00062	3.940
1.5469	1.058	0.00093	5.870
1.8594	1.061	0.00097	6.140
2.1719	1.077	0.00127	8.000
2.4844	1.096	0.00161	10.160
2.7969	1.109	0.00186	11.740
3.1094	1.123	0.00212	13.400

TABLE A.24

Stopped-Evaporation Butane Droplet in Distilled Water

Set 10 : Run 7

$d = 4.0 \times 10^{-3}$ (m); $T_c = 4.3$ (^{o}C);

ATMP = 101988.0 (N/m^2); $H = 1.37$ (m)

t' (s)	Z (m) $\times 10^{-3}$
0.0	3.1
0.0625	11.0
0.1406	25.5
0.2188	42.7
0.2969	60.0
0.4531	88.5
0.5313	103.0
0.6094	117.5
0.6875	131.5
0.7656	145.3
0.9219	174.0
1.0781	203.0
1.2344	233.0
1.3906	260.0
1.5469	285.0
1.7031	310.7
1.8594	338.1
2.0156	365.5
2.1719	393.5
2.3281	422.5
2.4844	451.5
2.6406	480.0
2.7969	509.2
2.9531	540.0
3.1094	570.5
3.2656	599.3
3.4219	626.0
3.5781	653.5
3.7344	680.0
3.8906	710.0

t' (s)	D/d	ξ	V_v (m^3) $\times 10^{-9}$
2.1719	1.011	0.00014	0.872
2.4844	1.013	0.00016	1.040
2.7969	1.016	0.00022	1.390
3.1094	1.021	0.00030	1.930
3.4219	1.030	0.00045	2.860
3.7344	1.044	0.00069	4.380
4.0469	1.050	0.00079	5.030

TABLE A.25

Stopped-Evaporation Butane Droplet in Distilled Water

Set 10 : Run 9

$d = 4.1 \times 10^{-3}$ (m); $T_c = 4.5$ (^{o}C);

ATMP = 101988.0 (N/m^2); $H = 1.37$ (m)

t' (s)	Z (m) $\times 10^{-3}$
0.0	3.5
0.0625	12.1
0.1406	28.0
0.2188	45.0
0.2969	61.9
0.3750	77.0
0.4531	92.0
0.5313	107.0
0.6094	122.5
0.6875	139.5
0.7656	156.0
0.8906	184.0
1.6719	353.5
1.7813	375.0
1.8594	389.7
2.0156	420.0
2.1719	452.6
2.3281	488.5
2.4531	517.0
2.5469	535.8
2.6563	559.0
2.7656	584.5
2.8438	602.0
3.0781	652.9
3.1875	680.0
3.3125	707.5
3.4219	731.0
3.5313	755.0
3.6250	775.0
3.7344	800.0

t' (s)	D/d	ξ	V_v (m^3) $\times 10^{-9}$
1.6719	1.071	0.00117	7.910
2.0156	1.095	0.00162	10.940
2.3281	1.114	0.00199	13.390
2.6406	1.134	0.00238	16.060
2.8438	1.141	0.00254	17.100
3.0781	1.189	0.00357	24.080
3.3125	1.202	0.00386	26.000
3.5313	1.242	0.00482	32.520
3.7344	1.236	0.00467	31.520

TABLE A.26

Stopped-Evaporation Butane Droplet in Distilled Water

Set 10 : Run 10

$d = 4.0 \times 10^{-3}$ (m); $T_c = 4.7$ (^{o}C);

ATMP = 101988.0 (N/m^2); $H = 1.37$ (m)

t' (s)	Z (m) $\times 10^{-3}$
0.0	3.5
0.0625	12.3
0.1406	27.7
0.2188	44.9
0.2969	61.5
0.3750	76.9
0.4531	92.8
0.5313	106.7
0.6094	121.0
0.6875	136.5
0.7656	151.0
0.9219	182.3
1.0781	214.7
1.2344	245.5
1.3906	278.2
1.5469	312.0
1.7031	344.0
1.8594	377.5
2.0156	412.5
2.1719	449.5
2.2969	476.6
2.4375	507.0
2.5469	530.7
2.6406	550.6
2.7344	572.4
2.8438	597.5
2.9375	619.0

t' (s)	D/d	ξ	V_v (m^3) $\times 10^{-9}$
1.2344	1.057	0.00093	5.950
1.5469	1.077	0.00128	8.210
1.8594	1.100	0.00173	11.080
2.1719	1.122	0.00215	13.820
2.4375	1.156	0.00286	18.320
2.8438	1.223	0.00438	28.070
2.9375	1.212	0.00411	26.380

TABLE A.27

Stopped-Evaporation Butane Droplet in Distilled Water

Set 10 : Run 11

d = 4.05 × 10^{-3} (m); T_c = 4.8 (^{o}C)

ATMP = 101988.0 (N/m^2); H = 1.37 (m)

t' (s)	Z (m) × 10^{-3}
0.0	3.5
0.0625	12.0
0.1406	27.5
0.2188	44.5
0.2969	61.6
0.3750	76.5
0.4531	92.7
0.5313	105.7
0.6094	120.9
0.6875	136.2
0.7656	152.9
0.8438	169.9
0.9219	186.5
1.0781	219.2
1.2344	251.2
1.3906	284.0
1.5469	317.1
1.7031	352.0
1.8594	387.3
2.0156	421.5
2.1719	456.5
2.3281	492.0
2.4844	529.5
2.6406	566.5
2.7969	602.6
2.9531	639.0

t' (s)	D/d	ξ	V_v (m^3) × 10^{-9}
1.2344	1.074	0.00124	8.190
1.5469	1.071	0.00117	7.750
1.7031	1.081	0.00136	8.990
1.8594	1.087	0.00148	9.770
2.1719	1.114	0.00201	13.320
2.4844	1.151	0.00277	18.320
2.7969	1.187	0.00356	23.570
2.9531	1.182	0.00344	22.800

TABLE A.28

Stopped-Evaporation Butane Droplet in Distilled Water

Set 11 : Run 13

$d = 3.8 \times 10^{-3}$ (m); $T_c = 4.7$ (^{o}C);

ATMP = 101648.0 (N/m^2); $H = 1.37$ (m)

t' (s)	Z (m) $\times 10^{-3}$
0.0	2.8
0.0625	10.6
0.1406	22.5
0.2188	35.1
0.2969	46.5
0.3750	58.9
0.4531	72.0
0.5313	86.5
0.6094	102.0
0.7656	133.5
0.9219	165.8
1.0781	199.0
1.2344	232.0
1.3906	264.2
1.5469	299.0
1.7031	335.0
1.8594	367.8
2.0156	404.5
2.1719	441.5
2.3281	478.5
2.4688	508.6
2.5625	529.5
2.6875	558.0
2.7813	581.0
2.8906	606.5
2.9688	623.5
3.0625	644.5
3.1563	668.0
3.2656	695.2

t' (s)	D/d	ξ	V_v (m^3) $\times 10^{-9}$
1.5469	1.227	0.00450	24.280
1.8594	1.304	0.00648	34.980
2.1719	1.336	0.00736	39.750
2.3281	1.373	0.00846	45.690
2.4844	1.409	0.00957	51.680
2.7813	1.459	0.01122	60.590
3.0625	1.553	0.01463	79.020
3.2656	1.672	0.01961	105.900

TABLE A.29

Stopped-Evaporation Butane Droplet in Distilled Water

Set 12 : Run 3

$d = 3.8 \times 10^{-3}$ (m); $T_c = 4.6$ (^{o}C);

ATMP = 100428.0 (N/m^2); $H = 1.37$ (m)

t' (s)	Z (m) $\times 10^{-3}$
0.0	2.5
0.0625	9.7
0.1406	24.2
0.2188	39.7
0.2969	55.7
0.3750	71.5
0.4531	89.1
0.5313	107.5
0.6094	124.9
0.6875	142.5
0.7656	161.3
0.8906	191.0
1.0156	218.9
1.0938	235.8
1.2031	260.1
1.3125	285.3
1.4688	319.5
1.6094	351.2
1.6875	368.2
1.8438	403.5
2.0000	439.0
2.1406	472.2
2.2344	494.5
2.3281	517.0
2.5000	558.0
2.6094	583.4
2.7656	622.0
2.9219	661.0
3.0000	677.3
3.1094	702.5

t' (s)	D/d	ξ	V_v (m^3) $\times 10^{-9}$
1.4375	1.889	0.03050	168.170
1.6875	1.958	0.03459	190.700
2.0313	2.000	0.03722	205.200
2.3281	2.071	0.04193	231.200
2.5000	2.115	0.04500	248.100
2.7656	2.116	0.04504	248.350
3.0000	2.234	0.05394	297.400

TABLE A.30

Stopped-Evaporation Butane Droplet in Distilled Water

Set 12 : Run 15

$d = 3.85 \times 10^{-3}$ (m); $T_c = 4.2$ (^{o}C)

ATMP = 100428.0 (N/m^2); $H = 1.37$ (m)

t' (s)	Z (m) $\times 10^{-3}$
0.0	3.3
0.0625	11.5
0.1406	26.4
0.2188	41.5
0.2969	56.5
0.3750	71.0
0.4531	86.1
0.6094	116.1
0.7656	146.0
0.9219	176.1
1.0781	205.7
1.2344	234.5
1.3906	263.5
1.5469	292.5
1.7031	321.5
1.8594	349.5
2.0156	378.0
2.1719	406.5
2.3281	436.5
2.4844	466.2
2.6406	494.7
2.7969	522.9
2.9531	551.2
3.1094	580.0
3.2656	608.7
3.4219	638.0
3.5469	661.6

t' (s)	D/d	ξ	V_v (m^3) $\times 10^{-9}$
1.2344	1.015	0.00021	1.170
1.5469	1.017	0.00023	1.310
1.8594	1.019	0.00027	1.530
2.1719	1.019	0.00026	1.500
2.4844	1.027	0.00039	2.200
2.7969	1.025	0.00036	2.050
3.1094	1.026	0.00038	2.160
3.4219	1.036	0.00056	3.150

APPENDIX B

A METHOD FOR THE CALCULATION OF THE DENSITY OF PURE HYDROCARBONS AND NON-POLAR GASES (2)

The following equation is given when T_r, $\rho_r \leq 1$:

$$P_r = T_r \left[- W_1(T_r)\ \rho_r^2 - W_2(T_r)\ \rho_r^3 + g(\rho_r) \right] \qquad (B.1)$$

where: P_r = reduced pressure, P/P_c

P = pressure, lbf/in^2

P_c = critical pressure, lbf/in^2

T_r = reduced temperature, T/T_c

T_c = critical temperature, ^{o}R

T = temperature, ^{o}R

$W_1(T_r) = 5.5\ T_r^{-1} + (\beta - 5.5)\ T_r^{-2}$

$W_2(T_r) = 0.5\ (-4.5 - \alpha_k + 2\beta)(1 - T_r^{-2})$

β = tabular function of Z_c given in Table C.1

Z_c = critical compressibility factor

α_k = Riedel parameter = 5.811 + 4.919 ω

ω = acentric factor

$$g(\rho_r) = \frac{(1+\beta)^3\ \rho_r}{\beta\ (3\beta - 1) - (3\beta^2 - 6\beta - 1)\ \rho_r + \beta\ (\beta - 3)\ \rho_r^2}$$

ρ_r = reduced density, $\rho/\rho_c = V_c/V$

ρ = density, in pound-moles per cubic foot

ρ_c = critical density, in pound-moles per cubic foot

V = molar volume, in cubic feet per pound-mole

V_c = critical volume, in cubic feet per pound-mole

The values of the above constants are given in Table C.1 of Appendix C.

At a given pressure and temperature, an initial value for density is chosen and P_r is calculated from the above equation. If this value and the known value of P_r agree within an arbitrary limit, the chosen density is the desired value. Otherwise, another value for density should be chosen and the step is repeated. It is suggested that the next value of density may be obtained from the following equation:

$$\rho_{r,(i+1)} = \rho_{r,i} + \frac{P_r - P_i}{(\partial P_r / \partial \rho_r)_{T_r}} \tag{B.2}$$

APPENDIX C

SOME CHEMICAL CONSTANTS AND PHYSICAL PROPERTIES OF n-BUTANE, n-PENTANE AND WATER

C.1 CHEMICAL CONSTANTS OF n-BUTANE AND n-PENTANE

TABLE C.1*

Some Chemical Constants of n-Butane and n-Pentane

	n-butane	n-pentane
P_c (psi)	550.7 (16)	489.0 (18)
T_c (^oC)	152.0 (16)	196.6 (18)
V_c (ml/gr)	4.386 (16)	4.098 (18)
Z_c (2)	0.274	0.262
β (2)	6.97	7.53
ω (2)	0.2010	0.2539

* For the notation, see Appendix B.

C.2 PHYSICAL PROPERTIES OF n-BUTANE AND n-PENTANE

TABLE C.2

Correlations for the Physical Properties of Liquid n-Butane and Liquid n-Pentane as Fitted to the Data of Galant (16-18)

$$y = a\,x + b \qquad (C.1)$$

where: y = property

x = temperature, ^{o}C

Property (SI units)	Substance	a	b	Range (^{o}C)
$c_p \times 4.18 \times 10^3$	n-butane	0.00125	0.57	-10 to +10
	n-pentane	0.00170	0.532	+30 to +50
$h_{fg} \times 4.18 \times 10^3$	n-butane	-0.26	92.5	-20 to +20
	n-pentane	-0.21	93.3	+30 to +50
$k \times 4.18 \times 10^{-3}$	n-butane	-0.12	28.4	-10 to +10
	n-pentane	-0.0925	28.925	+30 to +50
ρ	n-butane	-0.9	603.0	-10 to +10
	n-pentane	-0.95	643.5	-40 to +50
$\mu \times 10^{-3}$	n-butane	-0.00175	0.208	-10 to +10
	n-pentane	-0.00147	0.260	+30 to +45
$\sigma \times 10^{-3}$	n-butane	-0.12	14.8	-40 to +60
	n-pentane	-0.1125	18.4	0 to +70

C.3 PHYSICAL PROPERTIES OF WATER

The following physical properties of liquid water are given as functions of temperature:

(a) Viscosity (3):

$$\log_e \mu\ (10^{-3}) = 0.030185 - 2191.6/T + 6.38605 \times 10^5/T^2 \qquad (C.2)$$

when $273 < T < 350$, T (^{o}K), and μ (Ns/m^2).

(b) Specific Heat (3):

$$C_p = 17.6611 - 0.147914\ T + 6.08619 \times 10^{-4}\ T^2 - 1.11867 \times 10^{-6}\ T^3 + 7.80297 \times 10^{-10}\ T^4 \qquad (C.3)$$

when $273 < T < 450$, T (^{o}K), and C_p (kJ/kg^{o}K).

(c) Thermal Conductivity (3):

$$k = -0.61694 + 7.17851 \times 10^{-3}\ T - 1.167 \times 10^{-5}\ T^2 + 4.70358 \times 10^{-9}\ T^3 \qquad (C.4)$$

when $273 < T < 400$, T (^{o}K), and k (J/ms^{o}K).

(d) Density:

$$\rho = 999.9 + 0.5466 \times 10^{-1}\ T - 0.7517 \times 10^{-2}\ T^2 + 0.3403 \times 10^{-4}\ T^3 \qquad (C.5)$$

when $0 < T < 50$, T (^{o}C), and ρ (kg/m^3).

(e) Surface tension: The data from reference (7) for the water surface tension against air was correlated into the following correlation:

$$\sigma = 75.598 - 0.13772\ T - 0.19145 \times 10^{-4}\ T^2 - 0.12636 \times 10^{-4}\ T^3 \qquad (C.6)$$

when $0 < T < 25$, T (^{o}C), and σ (dyne/cm).

(f) Interfacial tension: The value of interfacial tension between butane vapour and water is given by (41):

$$\sigma = \sigma_o - 2.335\ P - 0.591\ P^2 \qquad (C.7)$$

where P is the pressure in atmospheres and σ_o is the water surface tension against its own vapour at $25^{o}C$ and is equal to $\sigma_o = 71.98 \times 10^{-3}$ N/m.

Data was not found on the interfacial tension between water and pentane vapour. However, since the inclusion of a small error in the determination of the interfacial tension was not crucial, the following approximation was adopted. Considering the required conditions

between the interfacial tensions at the three-phase interface (32, 49), for which the bubble remains attached to the system, the interfacial tension at the water/pentane vapour interface was assumed to be equal to the sum of the liquid/liquid and dispersed phase liquid/vapour interfacial tensions.

APPENDIX D

THE EVALUATION OF CHEBYSHEV SERIES USED FOR THE REPRESENTATION OF VAPOUR PRESSURES (13)

D.1 NOTES ON CHEBYSHEV POLYNOMIALS

The function $y = f(x)$ defined over [-1,1] may be expressed in a Chebyshev expansion as:

$$y = \tfrac{1}{2} a_o E_o(x) + \sum_{s=1}^{n} a_s E_s(x) \qquad (-1 \leqslant x \leqslant 1) \qquad (D.1)$$

where a_o, a_1, .., a_n are the Chebyshev coefficients, and $E_s(x)$ is the Chebyshev polynomial in x of degree s which is defined as:

$$E_s(x) = \cos (s \cos^{-1} x) \qquad (D.2)$$

Since $E_s(x)$ are orthogonal polynomials, there is a three-term recurrence relation connected them as:

$$E_{s+1}(x) - 2x E_s(x) + E_{s-1} = 0 \qquad (D.3)$$

Having the values of a_s, y can be obtained for a given value of x by evaluating a sequence b_s where:

$$b_s = a_s + 2x b_{s+1} - b_{s+2} \qquad (D.4)$$

and: $b_{n+2} = b_{n+1} = 0 \qquad (0 \leqslant s \leqslant n)$

It can be shown that:

$$y = \tfrac{1}{2}(b_o - b_2) \tag{D.5}$$

D.2 THE VAPOUR PRESSURE EQUATION

The values of vapour pressure P have been generated by evaluating equations of the form:

$$T \log_{10} P = \tfrac{1}{2} a_o + \sum_{s=1}^{n} a_s E_s(x) \tag{D.6}$$

which have been fitted to the data for each compound. x is defined as:

$$x = \frac{2T - (T_{max} + T_{min})}{T_{max} - T_{min}} \tag{D.7}$$

where T_{max} and T_{min} are the temperatures just above and just below the extreme temperatures of the fitted data. T_{max}, T_{min} and the Chebyshev coefficients a_o to a_n for each compound are given in reference (13). The values for n-butane and n-pentane are given in Table D.1. The vapour pressure P can be obtained from:

$$\log_{10} P = \frac{1}{2T}(b_o - b_2) \tag{D.8}$$

where T is in degrees Kelvin and P in KN/m^2.

For temperatures between -1.0^{o}C and 8.0^{o}C, n-butane vapour pressures were obtained using the above method and were fitted by the following correlations:

$$T = -40.985 + 0.58175 \times 10^{-3} P - 0.22119 \times 10^{-8} P^2 + 0.4084 \times 10^{-4} P^3 \quad (D.9)$$

where T is in degrees centigrade and P is in N/m^2.

TABLE D.1

Constants in Equations (D.6) and (D.7) for n-Butane and n-Pentane

Substance	T_{min}	T_{max}	a_o	a_1	a_2	a_3	a_4	a_5
n-butane	170	426	1393.923	838.384	-14.240	6.324	-0.547	0.440
n-pentane	147	470	1171.153	1093.595	-30.010	9.705	-0.092	-

APPENDIX E

MATHEMATICAL PROCEDURES

E.1 NUMERICAL DIFFERENTIATION

A subroutine (subroutine DGT3) was used for numerical differentiation. The subroutine computes an array $Z = (z_1, .., z_n)$ of derivative values, given the argument values $X = (x_1, .., x_n)$ and the corresponding function values $Y = (y_1, .., y_n)$. Except at the end points x_1 and x_n, z_i is the derivative at x_i of a polynomial of degree 2 relevant to the three successive points (x_{i-1},y_{i-1}), (x_i,y_i) and (x_{i+1},y_{i+1}).

For $i = 1, .., n-2$, we must find a_i, b_i and c_i such that:

$$\bar{y}_i(x) = a_i x^2 + b_i x + c_i \qquad \text{(E.1.1)}$$

and passes through (x_i,y_i), (x_{i+1},y_{i+1}) and (x_{i+2},y_{i+2}). The derivative values z_i for $i = 2, .., n-1$ and the end points are given by:

$$z_1 = 2a_1 x_1 + b_1 \qquad \text{(E.1.2)}$$

$$z_i = 2a_{i-1} x_i + b_{i-1} \qquad (i = 2, .., n-1) \qquad \text{(E.1.3)}$$

$$z_n = 2a_{n-2} x_n + b_{n-2} \qquad \text{(E.1.4)}$$

a_i and b_i can be calculated by using the values of x_i and y_i for three successive points in equation (E.1.1), and then by substitution in equations (E.1.2) to (E.1.4) we get:

$$z_1 = \frac{y_2 - y_1}{x_2 - x_1} + \frac{y_3 - y_1}{x_3 - x_1} - \frac{y_3 - y_2}{x_3 - y_2} \qquad \text{(E.1.5)}$$

$$z_i = \frac{y_i - y_{i-1}}{x_i - x_{i-1}} + \frac{y_{i+1} - y_i}{x_{i+1} - x_i} - \frac{y_{i+1} - y_{i-1}}{x_{i+1} - x_{i-1}} \qquad (i = 2, .., n-1) \qquad \text{(E.1.6)}$$

$$z_n = \frac{y_n - y_{n-1}}{x_n - x_{n-1}} + \frac{y_n - y_{n-2}}{x_n - x_{n-2}} - \frac{y_{n-1} - y_{n-2}}{x_{n-1} - x_{n-2}} \qquad \text{(E.1.7)}$$

E.2 CURVE FITTING

A NAG library program (subroutine EØ2ABF, available in ICCC) was used for curve fitting. The routine calculates a weighted least-squares polynomial approximation to a set of data points by Forsythe's method (15) using orthogonal polynomials.

If the given points are (x_i, f_i), $i = 1, 2, .., M$ and each point has a positive weight w_i associated with it, the routine computes the coefficients of the polynomial $p(x)$ of degree N which minimises the expression:

$$\sum_{i=1}^{M} w_i \, (p(x_i) - f_i)^2 \qquad \text{(E.2.1)}$$

over the set of polynomials of degree N. The maximum value of N is 50 and $N < M-1$.

REFERENCES

1. ADAMS, A.E.S., & PINDER, K.L.
"Average heat transfer coefficient during the direct evaporation of a liquid drop",
Can. J. Chem. Engng., 50, pp. 707-713 (1972).

2. AMERICAN PETROLEUM INSTITUTE
Technical Data Book: Petroleum Refining (1970).

3. AMERICAN SOCIETY OF HEATING, REFRIGERATING AND AIR-CONDITIONING ENGINEERS, INC.
Thermophysical Properties of Refrigerants (1973).

4. AYBERS, N.M., & TAPUCU, A.
"The motion of gas bubbles rising through stagnant liquid",
Wärme- und Stoffübertragung, 2, pp. 118-128 (1969).

5. AYBERS, N.M., & TAPUCU, A.
"Studies on the drag and shape of gas bubbles rising through a stagnant liquid",
Wärme- und Stoffübertragung, 2, pp. 171-177 (1969).

6. BIRD, R.B., STEWART, W.E., & LIGHTFOOT, E.N.
Transport Phenomena,
John Wiley & Sons (1960).

7. CHEMICAL RUBBER COMPANY
CRC Handbook of Chemistry and Physics,
56th edition, CRC Press (1975-1976).

8. COLE, R.
"Boiling nucleation",
Adv. in Heat Transfer, 10, pp. 85-186 (1974).

9. COLLINS, R.

"The effect of a containing cylindrical boundary on the velocity of a large bubble in a liquid",

J. Fluid Mechanics, 28(1), pp. 97-112 (1967).

10. DAVIES, R.M., & TAYLOR, S.F.

"The mechanics of large bubbles rising through extended liquids and through liquids in tubes",

Proc. R. Soc. Lond., pp. 375-390 (1950).

11. ELZINGA, E.R., Jr., & BANCHERO, J.T.

"Film coefficients for heat transfer to liquid drops",

Chem. Engng. Progr., Symp. Ser. 55, pp. 149-161 (1959).

12. ELZINGA, E.R., Jr., & BANCHERO, J.T.

"Some observations on the mechanics of drops in liquid-liquid systems",

A.I.Ch.E. Jl., 7(3), pp. 394-399 (1961).

13. ENGINEERING SCIENCES DATA

"The evaluation of Chebyshev Series used for the representation of vapour pressure", Physical Data: Vapour Pressure, 5a, Item No. PDI, Engineering Sciences Data Unit (1972).

14. FILATKIN, V.N., & DOLOTOV, A.G.

"Heat transfer during the boiling of single drops of a hydrocarbon mixture during direct contact with water", (in Russian)
in Tr. Vses. Nauch.-Tekh. Konf. Termodin, Sb. Dokl. Sekts, Termodin Fazouykh Perekhodov, Potoka Neobratimykh Protsessou, pp. 321-329, Teplofiz. Svoistva Veshchestv. Leningrad.Teckhnol. Inst. Khlod. Prom.: Leningrad, USSR (1970).

15. FORSYTHE, G.E.

"Generation and use of orthogonal polynomials for data-fitting with a digital computer",

S.I.A.M. Jnl., (1957).

16. GALLANT, R.W.

"Physical properties of hydrocarbons. Part 1: Methane, ethane, propane, butane",

Hydrocarb. Process., 44(7), pp. 95-103 (1965).

17. GALLANT, R.W.

"Physical properties of hydrocarbons. Part 9: Thermal conductivity of C1 to C4 hydrocarbons",

Hydrocarb. Process., 45(12), pp. 113-121 (1966).

18. GALLANT, R.W.

"Physical properties of hydrocarbons. Part 15: C_5 - C_8 alkanes",

Hydrocarb. Process., 46(7), pp. 121-129 (1967).

19. GARNER, F.H., & HAMERTON, D.

"Circulation inside gas bubbles",

Chem. Engng. Sci., 3(1), (1954).

20. GARNER, F.H., JENSON, V.G., & KEEY, R.B.

"Flow pattern around spheres and the Reynolds analogy",

Trans. Inst. Chem. Engrs., 37, pp. 191-197 (1959).

21. GEAR, C.W.

Numerical initial value problems in ordinary differential equations, Prentice-Hall (1971).

22. GRACE, J.R.

"Shapes and velocities of bubbles rising in infinite liquids",

Trans. Inst. Chem. Engrs., 51, pp. 116-120 (1973).

23. GRADON, L., & SELECKI, A.

"Evaporation of a liquid drop immersed in another immiscible liquid. The case of $\sigma_c < \sigma_d$",

Int. J. Heat & Mass Transfer, 20, pp. 459-466 (1977).

24. HABERMAN, W.L., & MORTON, R.K.
"An experimental study of bubbles moving in liquids",
Trans. Am. Soc. Civ. Engrs., 121, pp. 227-252 (1956).

24a. HANDLOS, A.E., & BARON, T.
"Mass and heat transfer from drops in liquid-liquid extraction",
A.I.Ch.E. Jnl., 3(1), pp. 127-136 (1957).

25. HARMATHY, T.Z.
"Velocity of large drops and bubbles in media of infinite or restricted extent",
A.I.Ch.E. Jnl., 6(2), pp. 281-288 (1960).

26. HARPER, J.F.
"The motion of bubbles and drops through liquids",
Adv. in Applied Mechanics, 12, pp. 59-129 (1972).

27. HARRIOT, P., & WIEGANDT, H.
"Counter current heat exchangers with vaporising immiscible transfer agent",
A.I.Ch.E. Jnl., 10(5), pp. 755-758 (1964).

28. HOWE, E.D.
Fundamentals of Water Desalination,
Marcel Dekker, Inc., New York (1974).

29. HUBBARD, D.S., LEINROTH, J.P., WIEGANDT, H.F., et al.
"Spray freezing of brine with an immiscible refrigerant",
Office of Saline Water, R&D No. 312 (1968).

30. ISENBERG, J., MOALEM, D., & SIDEMAN, S.
"Direct-contact heat transfer with change of phase: Bubble collapse with translatory motion in single and two-component systems",
Heat Transfer, 5, Boiling Sessions, B1-B5, B2.5 (1970).

31. ISENBERG, J., & SIDEMAN, S.
"Direct contact heat transfer with change of phase: Bubble condensation in immiscible liquids",
Int. J. Heat & Mass Transfer, 13, pp. 997-1011 (1970).

32. JARVIS, T.J., DONOHUE, M.D., & KATZ, J.L.
"Bubble nucleation mechanisms of liquid droplets superheated in other liquids",
J. Colloid Interface Sci., 50(2), pp. 359-368 (1975).

33. KENNING, D.B.R.
"Two-phase flow with non-uniform surface tension",
Applied Mechanics Reviews, 21(11), pp. 1101-1111 (1968).

34. KINTER, R.C.
"Drop phenomena affecting liquid extraction",
Adv. in Chem. Engng., 4, pp. 51-92 (1963).

35. KLEE, A.J., & TREYBAL, R.E.
"Rate of rise or fall of liquid drops",
A.I.Ch.E. Jnl., 2(4), pp. 444-447 (1956).

36. KLIPSTEIN, D.H.
"Heat transfer to a vaporising immiscible drop",
D.Sc. Thesis, Massachusetts Institute of Technology (1963).

37. KNAPP, R.T.
Cavitation,
McGraw-Hill, New York (1970).

38. KUMAR, R., & KULOOR, N.R.
"The formation of bubbles and drops",
Adv. in Chem. Engng., 8, pp. 255-368 (1970).

39. L'ECUYER, M.R., & MURTHY, S.N.B.
"Energy transfer from a liquid to gas bubbles forming at a submerged orifice",
NASA TN-D 2547 (1965).

40. LEVICH, V.G., & KRYLOV, V.S.
"Surface-tension-driven phenomena",
Annual Review of Fluid Mechanics, 1, pp. 293-316 (1969).

41. MASSOUDI, R., & KING, A.D., Jr.
"Effect of pressure on the surface tension of water. Adsorption of low molecular gases on water at 25°C",
J. Phys. Chem., 78(22), pp. 2262-2266 (1974).

42. MIKIC, B.B., ROHSENOW, W.M., & GRIFFITH, P.
"On bubble growth rate",
Int. J. Heat & Mass Transfer, 13, pp. 657-666 (1970).

43. MISSIRLIS, J.
"Heat transfer to evaporation drops",
Office of Saline Water, R&D No. 658, pp. 40-43 (1971).

44. MOALEM, D., & SIDEMAN, S.
"Bubble condensation with non-homogeneous distribution of non-condensables",
Int. J. Heat & Mass Transfer, 14, pp. 2152-2156 (1971).

45. MOALEM, D., SIDEMAN, S., ORELL, A., & HESTRONI, G.
"Direct contact heat transfer with change of phase: Condensation of a bubble train",
Int. J. Heat & Mass Transfer, 16, pp. 2305-2319 (1973).

46. MOALEM, D., & SIDEMAN, S.
"The effect of motion on bubble collapse",
Int. J. Heat & Mass Transfer, 16, pp. 2321-2329 (1973).

47. MOKHTARZADEH, M.R., & EL-SHIRBINI, A.A.
"A theoretical analysis of evaporating droplets in an immiscible liquid",
Int. J. Heat & Mass Transfer, 22, pp. 27-38 (1979).

48. MOKHTARZADEH, M.R., & EL-SHIRBINI, A.A.
"Motion of bubbles and bubble-droplets in an immiscible liquid",
Wärme- und Stoffübertragung, 12, pp. 25-33 (1979).

49. MOORE, G.R.
"Vaporisation of superheated drops in liquids",
A.I.Ch.E. Jnl., 5(4), pp. 458-466 (1959).

50. MORI, Y., HIJIKATA, K., & NAGATANI, T.
"Fundamental study of bubble dissolution in liquid",
Int. J. Heat & Mass Transfer, 20, pp. 41-50 (1977).

51. MORI, Y.H., & KOMOTORI, K.
"Boiling of single superheated drops in an immiscible liquid",
Heat Transfer, Japanese Res., 5, pp. 75-95 (1976).

52. MORI, Y.H., & KOMOTORI, K.
"Boiling modes of volatile liquid drops in an immiscible liquid, depending on degree of superheat",
ASME Pub. 76-HT-13 (1976).

53. NAZIR, M.
"Direct contact heat transfer, evaporation of butane drops in brine",
Ph.D. Thesis, University of Strathclyde, Glasgow (1972).

54. NENE, R.
"Heat transfer to evaporating drops",
Office of Saline Water, R&D No. 823, pp. 16-20 (1972).

55. NENE, R.

"Direct contact heat transfer to an evaporating butane drop suspended in a stream of water during the initial stages of evaporation", M.Sc. Thesis, Department of Chemical Engineering & Materials Science, Syracuse University (1973).

56. PEEBLES, F.N., & GARBER, H.J.

"Studies on the motion of gas bubbles in liquids", *Chem. Eng. Prog.*, 2(49), pp. 88-97 (1953).

57. PLESSET, M.S., & ZWICK, S.A.

"The growth of vapour bubbles in superheated liquids", *J. Appl. Phys.*, 25(4), pp. 493-500 (1954).

58. PRAKASH, C.B., & PINDER, K.L.

"Direct contact heat transfer between two immiscible liquids during vaporisation. Part I: Measurement of heat transfer coefficient", *Can. J. Chem. Engng.*, 45, pp. 210-214 (1967).

59. PRAKASH, C.B., & PINDER, K.L.

"Direct contact heat transfer between two immiscible liquids during vaporisation. Part II: Total evaporation time", *Can. J. Chem. Engng.*, 45, pp. 215-220 (1967).

60. PUGH, O.

"Desalination - its widening rôle", *Atom*, 189, pp. 131-142 (1972).

61. RAYLEIGH, L.

"Pressure due to collapse of bubbles", *Phil. Mag.*, pp. 94-98 (1917).

62. RICE, P.A., GALE, R.P., & BARDUHN, A.J.

"Solubility of butane in water and salt solutions at low temperatures", *J. Chem. Engng. Data*, 21(2), pp. 204-206 (1976).

63. RICE, P.A., NENE, R.G., & BARDUHN, A.J.
"Prediction of the heat transfer rates in crystallisers",
5th Int. Symp. on Fresh Water from the Sea, 3, pp. 285-291 (1976).

64. ROHSENOW, W.M.
"Boiling",
Annual Rev. Fluid Mech., 3, pp. 211-236 (1971).

65. ROSENBERG, B.
"The drag and shape of air bubbles moving in liquids",
The David W. Taylor Model Basin, Report 727 (1950).

66. SELECKI, A., & GRADON, L.
"Über den Verdampfungs mechanismus eines sich in einer nicht mischbaren Flüssigkeit bewegenden Flüssigkeits tropfens", (in German)
Chemie. Ing. Techn., 44(18), pp. 1077-1081 (1972).

67. SELECKI, A., & GRADON, L.
"Equation of motion of an expanding vapour drop in an immiscible liquid medium",
Int. J. Heat & Mass Transfer, 19, pp. 925-929 (1976).

68. SIDEMAN, S., & TAITEL, Y.
"Direct-contact heat transfer with change of phase: Evaporation of drops in an immiscible liquid medium",
Int. J. Heat & Mass Transfer, 7, pp. 1273-1289 (1964).

69. SIDEMAN, S.
"Photography of drops in liquid media",
Chem. Engng. Sci., 19, p. 426 (1964).

70. SIDEMAN, S., & HIRSH, G.
"Direct-contact heat transfer with change of phase. III: Analysis of the transfer mechanism of drops evaporating in immiscible liquid media",
Israel J. Technol., 2(2), pp. 234-241 (1964).

71. SIDEMAN, S., & BARSKY, Z.
"Turbulence effect on direct-contact heat transfer with change of phase: Effect of mixing on heat transfer between an evaporating volatile liquid in direct contact with an immiscible liquid medium", *A.I.Ch.E. Jl.*, 11(3), pp. 539-545 (1965).

72. SIDEMAN, S., & GAT, Y.
"Direct-contact heat transfer with change of phase: Spray-column studies of a three-phase heat exchanger", *A.I.Ch.E. Jl.*, 12(2), pp. 296-303 (1965).

73. SIDEMAN, S. HIRSH, G., & GAT, Y.
"Direct-contact heat transfer with change of phase: Effect of the initial drop size in three-phase heat exchangers", *A.I.Ch.E. Jl.*, 11(6), pp. 1081-1087 (1965).

74. SIDEMAN, S., & HIRSH, G.
"Direct-contact heat transfer with change of phase: Condensation of single vapour bubbles in an immiscible liquid medium - Preliminary studies", *A.I.Ch.E. Jl.*, 11(6), pp. 1019-1025 (1965).

75. SIDEMAN, S.
"Direct-contact heat transfer between immiscible liquids", *Adv. Chem. Engng.*, 6, pp. 207-286 (1966).

76. SIDEMAN, S., & ISENBERG, J.
"Direct-contact heat transfer with change of phase: Bubble growth in three-phase systems", *Desalination*, 2, pp. 207-214 (1967).

77. SIMPSON, H.C., BEGGS, G.C., & NAZIR, M.
"Evaporation of butane drops in brine", *Desalination*, 15, pp. 11-23 (1974).

78. SIMPSON, H.C., BEGGS, G.C., & NAZIR, M.
"Evaporation of a droplet of one liquid rising through a second immiscible liquid. A new theory of the heat transfer process",
Heat Transfer, Proc. 5th Int. Heat Transfer Conf., 5, pp. 59-63 (1974).

79. SIMPSON, H.C., BEGGS, G.C., & SOHAL, M.S.
"Nucleation of butane drops in flowing water",
6th Int. Heat Transfer Conf., 4 (1978).

80. SPIEGLER, K.S.
Principles of Desalination,
Academic Press, New York (1966).

81. THORSEN, G., STORDALEN, R.M., & TERJESEN, S.G.
"On the terminal velocity of circulating and oscillating liquid drops",
Chem. Engng. Sci., 23, pp. 413-426 (1966).

82. TOCHITANI, Y., MORI, Y.H., & KOMOTORI, K.
"Vaporisation of a liquid injected into an immiscible liquid through a single nozzle",
Wärme- und Stoffübertragung, 8, pp. 249-259 (1975).

83. TOCHITANI, Y., MORI, Y.H., & KOMOTORI, K.
"Vaporisation of single liquid drops in an immiscible liquid. Part I: Forms and motions of vaporising drops",
Wärme- und Stoffübertragung, 10, pp. 51-59 (1977).

84. TOCHITANI, Y., MORI, Y.H., & KOMOTORI, K.
"Vaporisation of single liquid drops in an immiscible liquid. Part II: Heat transfer characteristics",
Wärme- und Stoffübertragung, 10, pp. 71-79 (1977).

85. UNITED STATES DEPARTMENT OF THE INTERIOR
Office of Saline Water, Saline Water Conversion Report (1967).

86. WALLIS, G.B.

One-Dimensional Two-Phase Flow,

McGraw-Hill Company (1969).

87. WEGENER, P.P., & PARLANGE, J.Y.

"Spherical cap bubbles",

Annual Rev. Fluid Mech., 5, pp. 79-100 (1973).

88. WERLÉ, H.

"Hydrodynamic flow visualisation",

Annual Rev. Fluid Mech., 5, pp. 361-382 (1973).

89. WINNIKOW, S., & CHAO, B.T.

"Droplet motion in purified systems",

Phys. Fluids, 9, pp. 50-61 (1966).